A Multiomics Approach to Evaluate Advances in Liver Transplantation

Anders William Ohman

B.A., Biology
Clark University, 2010

M.A., Biology
Clark University, 2011

A Dissertation Submitted in Partial Fulfillment of the Requirements for the Degree of Doctor of Philosophy in the Division of Biology and Medicine at Brown University

Providence, Rhode Island
February 2023

Signature Page

This dissertation by Anders William Ohman is accepted in its present form by the Pathobiology Graduate Program as satisfying the dissertation requirement for the degree of Doctor of Philosophy.

Date: _____ _____

Jennifer A. Sanders, Ph.D.
Advisor

Recommended to the Graduate Council

Date: _____ _____

Nikos Tapinos, M.D., Ph.D.
Committee Chair

Date: _____ _____

Jonathan S. Reichner, Ph.D.
Reader

Date: _____ _____

Richard N. Freiman, Ph.D.
Reader

Date: _____ _____

M. Korkut Uygun, Ph.D.
Outside Reader

Approved by the Graduate Council

Date: _____ _____

Thomas A. Lewis, Ph.D.
Dean of the Graduate School

Curriculum Vitae

Anders William Ohman

I. EDUCATION

Brown University — Providence, RI
Doctor of Philosophy, Pathobiology — Expected Feb 2023
Advisor: Jennifer A. Sanders, Ph.D.
Thesis: *"A Multiomics Approach to Evaluate Advances in Liver Transplantation"*

Harvard University Extension School — Cambridge, MA
Continuing Education Courses, Biology — Fall 2015 & 2016

Clark University — Worcester, MA
Master of Arts, Biology — May 2011
Advisor: David S. Hibbett, Ph.D.
Thesis: *"Automated Clustering of Fungal ITS Sequences"*
Bachelor of Arts, Biology, *cum laude* — May 2010

II. RESEARCH EXPERIENCE

Brown University, Rhode Island Hospital — Providence, RI
Pre-doctoral Research Trainee, *Laboratory of Jennifer A. Sanders, Ph.D.* — 2017 – Present

Harvard Medical School, Brigham and Women's Hospital — Boston, MA
Senior Technical Research Assistant, *Laboratory of Daniela M. Dinulescu, Ph.D.* — 2016 – 2017
Technical Research Assistant II, *Laboratory of Daniela M. Dinulescu, Ph.D.* — 2013 – 2016

Clark University — Worcester, MA
Accelerated Degree Program Research Assistant, *Laboratory of David S. Hibbett, Ph.D.* — 2009 – 2011

III. PUBLICATIONS

Raigani S., Santiago J., **Ohman A.W.**, Heaney M., Baptista S., Coe T.M., De Vries R.J., Rosales I.A., Shih A., Markmann J.F., Gruppuso P., Uygun K., Sanders J., Yeh H. (2022). Pan-caspase inhibition during normothermic machine perfusion of discarded livers mitigates ischemia-reperfusion injury. *Frontiers in Immunology, 13*. doi:10.3389/fimmu.2022.940094

Ohman A.W.*, Raigani S.*, Santiago J.C., Heaney M.G., Boylan J.M., Parry N, Carroll C., Baptista S.G., Uygun K., Gruppuso P.A., Sanders J.A., & Yeh H. (2021). Activation of autophagy during normothermic machine perfusion of discarded livers is associated with improved hepatocellular function. *American Journal of Physiology-Gastrointestinal and Liver Physiology, 322(1), G21–G33.* doi:10.1152/ajpgi.00266.2021

Dejene S.B., **Ohman A.W.**, Du W., et al. (2019). Defining fallopian-tube derived miRNA cancer signatures. *Cancer Medicine, 00:1–8.* doi:10.1002/cam4.2416

Baldwin P.E., **Ohman A.W.**, et al. (2019). Nanoformulation of Talazoparib Delays Tumor Progression and Ascites Formation in a Late Stage Cancer Model. *Frontiers in Oncology, 9.* doi:10.3389/fonc.2019.00353

Ohman A.W.*, Baldwin P.E.*, Tangutoori S., Dinulescu D.M., & Sridhar S. (2018). Intraperitoneal Delivery of NanoOlaparib for Disseminated Late Stage Cancer Treatment. *International Journal of Nanomedicine, 2018:13, 8063-8074.* doi:10.2147/IJN.S186881

Tucker D.W., Getchell C.R., McCarthy E.T., **Ohman A.W.**, Sasamoto N., Xu S., Ko J.Y., Gupta M., Shafrir A., Medina J.E., Lee J.J., MacDonald L.A., Malik A., Hasselblatt K.T., Li W., Zhang H., Kaplan S.J., Murphy G.F., Hirsch M.S., Liu J.F., Matulonis U.A., Terry K.L., Lian C.G., & Dinulescu, D. M. (2017). Epigenetic Reprogramming Strategies to Reverse Global Loss of 5-Hydroxymethylcytosine, a Prognostic Factor for Poor Survival in High-grade Serous Ovarian Cancer. *Clinical Cancer Research, 24(6), 1389-1401.* doi:10.1158/1078-0432.ccr-17-1958

Ohman A.W.*, Hasan N.*, & Dinulescu D.M. (2015). The promise and challenge of ovarian cancer models. *Translational Cancer Research, 4(1), 14-28.* doi:10.3978/j.issn.2218-676X.2015.01.02

Ohman A.W.*, Hasan N.*, & Dinulescu D.M. (2014). Advances in Tumor Screening, Imaging, and Avatar Technologies for High-Grade Serous Ovarian Cancer. *Frontiers in Oncology, 4.* doi:10.3389/fonc.2014.00322

Perets R., Wyant G., Muto K., Bijron J., Poole B., Chin K., Chen J.Y.H., **Ohman A.W.**, Stepule C.D., Kwak S., Karst A.M., Hirsch M.S., Setlur S.R., Crum C.P., Dinulescu D.M., & Drapkin, R. (2013). Transformation of the Fallopian Tube Secretory Epithelium Leads to High-Grade Serous Ovarian Cancer in Brca;Tp53;Pten Models. *Cancer Cell*, *24(6), 751-765.* doi:10.1016/j.ccr.2013.10.013

Hibbett D.S., **Ohman A.**, Glotzer D., Nuhn M., Kirk P., & Nilsson R.H. (2011). Progress in molecular and morphological taxon discovery in Fungi and options for formal classification of environmental sequences. *Fungal Biology Reviews*, *25(1), 38-47.* doi:10.1016/j.fbr.2011.01.001

Hibbett D.S., **Ohman A.**, & Kirk P.M. (2009). Fungal ecology catches fire. *New Phytologist*, *184(2), 279-282.* doi:10.1111/j.1469-8137.2009.03042.x

** These authors contributed equally to this work.*

IV. HONORS & AWARDS

NIH, National Institute of Environmental Health Sciences (NIEHS) 2018 – 2022
Brown University Training in Environmental Pathology Award (T32)
Project: 5T32ES007272, PI: Jennifer Sanders, Ph.D.

American Society of Investigative Pathology Apr 2021 & 2022
Trainee Scholar Award for Outstanding Research in Experimental Pathology

Brown University Graduate Program in Pathobiology Sept 2021
Flash Talk Award

Brown University Graduate Student Council 2020, 2021, & 2022
Conference and External Travel Award

American Association for the Study of Liver Disease Nov 2020
Liver Transplant & Hepatobiliary Surgery Fellow Award *(Contributing Author)*
"Best of the Liver Meeting" Presentation *(Contributing Author)*

American Society of Investigative Pathology Nov 2020
Monga-Hans Trainee Scholar Award for Excellence in Liver Pathobiology Research

Keystone Symposia Oct 2020
Student Scholarship Award

Clark University Fall 2006, 2007, 2008
Dean's List

V. ORAL PRESENTATIONS

Pathobiology for Investigators, Students, and Academicians Young Investigators May 2022, Webinar
"Improving Alternatives to Orthotopic Liver Transplantation"

Experimental Biology Apr 2022, Philadelphia, PA
"Regulation of Transplanted Fetal Hepatocyte Proliferation by Histone Post-Translational Modifications"

Providence Area Aging Research Forum Oct 2021, Providence, RI
"Durable Persistence of the Fetal Hepatocyte Phenotype After Liver Cell Transplantation"

Pathobiology for Investigators, Students, and Academicians Young Investigators Oct 2021, Webinar
"Durable Persistence of the Fetal Hepatocyte Phenotype After Liver Cell Transplantation"

Brown University 31st Annual Pathobiology Graduate Program Retreat Sept 2021, Webinar
"Durable Persistence of the Fetal Hepatocyte Phenotype After Liver Cell Transplantation"

Women and Infants Hospital Pediatric Research Colloquium May 2021, Webinar
"Long-Term Persistence of Fetal Hepatocyte Gene Signature Following Transplantation to Adult Liver"

Brown University Pathobiology Graduate Program Recruitment Jan 2021, Webinar
"Harnessing the Fetal Hepatocyte Phenotype to Improve Liver Cell Transplantation"

Brown University Pathobiology Graduate Program Data Club Nov 2020, Webinar
"Ongoing Thesis Project: Understanding the Fetal Hepatocyte Growth Phenotype"

The Liver Meeting Digital Experience Nov 2020, Webinar
"Normothermic machine perfusion of discarded human livers alleviates ischemia-reperfusion injury and promotes regenerative pathways" *(Contributing Author)*

Pathobiology for Investigators, Students, and Academicians Young Investigators Oct 2021, Webinar
"Harnessing the Fetal Hepatocyte Phenotype to Improve Liver Cell Transplantation"

Brown University 30th Annual Pathobiology Graduate Program Retreat Sept 2020, Webinar
"Flash Talk: Harnessing the Fetal Hepatocyte Phenotype to Improve Liver Cell Transplantation"

Brown University Pathology and Laboratory Medicine Summer Intern Research Talks Jul 2019, Prov, RI
"Engineering Transplantable Hepatocytes via Epigenomics"

Brown University Pathobiology Data Club Apr 2019, Providence, RI
"PARPi Nanoparticles in a Model of BRCA-Deficient Ovarian Cancer"

VI. POSTER PRESENTATIONS

Rhode Island Hospital Annual Celebration of Pediatric Scholarship Oct 2022, Providence, RI
"Long-Term Persistence of Fetal Hepatocyte Gene Signature Following Transplantation to Adult Liver"

Experimental Biology Apr 2022, Philadelphia, PA
"Long-Term Persistence of Fetal Hepatocyte Gene Signature Following Transplantation to Adult Liver"

Experimental Biology Apr 2021, Webinar
"Long-Term Persistence of Fetal Hepatocyte Gene Signature Following Transplantation to Adult Liver"

Pathobiology for Investigators, Students, and Academicians Young Investigators Nov 2020, Webinar
"Harnessing the Fetal Hepatocyte Phenotype to Improve Liver Cell Transplantation"

Keystone eSymposia - Tissue Plasticity: Preservation and Alteration of Cellular Identity Oct 2020, Web
"Harnessing the fetal hepatocyte proliferative phenotype to improve liver cell transplantation"

Brown University 29th Annual Pathobiology Graduate Program Retreat Aug 2019, Providence, RI
"Methods Development for Utilizing Omics Technologies to Characterize Fetal Hepatocyte Plasticity"

Rhode Island Hospital Annual Celebration of Pediatric Scholarship Oct 2019, Providence, RI
"Methods Development for Utilizing Omics Technologies to Characterize Fetal Hepatocyte Plasticity"

Brown University 28th Annual Pathobiology Graduate Program Retreat Aug 2018, Providence, RI
"Using a Breast Epithelial Reporter Cell Line to Evaluate EMT Phenotypes and Cell-Cell Interactions"

Clark University Fall Fest Oct 2010, Worcester, MA
"Automated fungal DNA sequence comparison"

VII. TEACHING EXPERIENCE

Brown University Division of Biology and Medicine Providence, RI
Biology of the Eukaryotic Cell (BIOL 2050) Graduate Teaching Assistant Fall 2018
Course Directors: Kenneth R. Miller, Ph.D. & Susan A. Gerbi, Ph.D.

Brown University Harriet W. Sheridan Center for Teaching and Learning Providence, RI
Teaching Certificate I: Reflective Teaching Practices Fall 2018

VIII. LEADERSHIP EXPERIENCE & COMMUNITY INVOLVEMENT

Graduate Student Council of Brown University Providence, RI
Chair of Technology 2020 – 2022
Departmental Representative 2019 – 2020

Brown University Providence, RI
Graduate School Orientation Campus Tour Guide Aug 2021
Pathobiology Graduate Program Peer Mentor 2019 – 2020

Brown University, Rhode Island Hospital Providence, RI

Undergraduate and Graduate Student Mentorship

Sierra Madden, Undergraduate Student	2022
Beatrice Campilan, Undergraduate Student	2022
Sarah Wong, Undergraduate Student	2022
Emily Kim, Undergraduate Student	2021 – 2022
Alexandra Burgess, Undergraduate Student	2020 – 2022
Jacob Abraham, Undergraduate Student	2020 – 2021
Angella Nakasagga, Undergraduate Student	2019
Lindsey Carlsen, Graduate Student	2019
Kelsey Huntington, Graduate Student	2019
Maryam Bonakdar, Graduate Student	2018
Layra Cintrón-Rivera, Graduate Student	2018

Harvard Medical School, Brigham and Women's Hospital Boston, MA

Undergraduate Student Mentorship and Technician Training

Eric McCarthy, Research Technician	2017
Morgan Krush, Undergraduate Student	2016 – 2017
Samuel Kaplan, Undergraduate Student	2015
Jeremy Thong, Undergraduate Student	2015
Jenny Zhu, Research Technician	2015
Douglass Tucker, Research Technician	2014
Christopher Getchell, Research Technician	2014

Bridgewater State University Bridgewater, MA

South Shore Regional Science Fair Biology Judge 2014

IX. PROFESSIONAL ASSOCIATIONS

American Association for Cancer Research, Associate Membership	2019 – Present
American Chemical Society, Student Membership	2019 – Present
American Association for the Study of Liver Diseases, Student Membership	2020 – 2022
American Society for Investigative Pathology, Pre-Doctoral Trainee Membership	2019 – 2022
American Association for the Advancement of Science, Student Membership	2019 – 2022

Preface

The work presented in this thesis was performed in the laboratory of Dr. Jennifer Sanders at Rhode Island Hospital. I performed all of the experiments reported with the following exceptions:

Chapter 2 – Jennifer Sanders performed the rodent surgeries used for the laser capture microdissection samples. Jennifer Sanders and Megan Heaney assisted me with collecting the hepatocyte cellular isolations. Virginia Hovanesian at Rhode Island Hospital assisted with the ImageJ analysis pipeline to calculate tissue volume from laser captured samples. GENEWIZ performed RNA library preparation and sequencing as fee-for-service. Jeannie Camarillo performed the histone extraction and mass spectrometry quantitation of histone marks.

Chapter 3 – Siavash Raigani performed the normothermic perfusion and measured functional perfusate metrics; generated the heatmaps in Figures 3D, 8A, and 11A; and cowrote the original draft of the manuscript. John Santiago worked collaboratively on data analysis and scripting; generated the visualizations in Figure 3A-B, 10B, and Supplemental Figure S3. The scoring of all histopathology was performed by Nicola Parry. Joan Boylan and Megan Heaney performed the Western blots in Figure 10C and 11B.

Chapter 4 – Siavash Raigani performed the normothermic perfusion and measured functional perfusate metrics. John Santiago performed the bioinformatics analyses and visualizations in Figure 3, and Supplemental Figure 2. The scoring of all histopathology was performed by Nicola Parry. Megan Heaney performed the Western blots featured in Figure 6 and Supplementary Figure 8.

Dedication and Acknowledgements

This dissertation is dedicated to the memory of my grandfather, Arthur Carin.

By teaching me the wonder of science through discovery and inquiry, you made all this possible.

I want to start by thanking my advisor, Jennifer Sanders, for taking a chance on me as a graduate student. You were one of the first people I met in my graduate school interviews, and I feel very fortunate to have been able to complete my studies under your mentorship. Your support, wisdom, and patience have made my graduate career at Brown able to flourish – there are not enough PIs in academia like you. You also cultivated a fantastic laboratory: Philip Gruppuso, Joan Boylan, Valerie Zabala, John Santiago, and Megan Heaney have been an incredible network of brilliant scientists who made every project a team effort and a learning experience. Thank you to my committee members Nikos Tapinos, Richard Freiman, and Jonathan Reichner for your academic and at times personal mentorship over the years, as well as to Korkut Uygun for agreeing to be my outside reader and for trusting me about the Cauliflower 65 at Kabob & Curry. I also appreciate Michele Welindt and the entire Pathobiology Graduate Program for coordinating the logistics of my time in the program going all the way back to my incredible interview day.

I have been so grateful to have had the support of my friends from Brown University like my amazing peer mentor Jenna Wurster, Megan Gura, and Mai Huynh, who have taken time away from their research to hike mountains, run races, or serve in student governments with me, and have helped to keep me together through grad school and especially during the challenges of the COVID-19 pandemic. Some of my closest friendships at Brown have been from my Pathobiology cohort, Shannon Martin and Swathi Penumutchu, whom since the first weeks of Fall 2017 have consistently provided me with not only reliable study buddies but also sometimes warm soup or invaluable life advice when I desperately needed it. Some of my

fondest moments during the program were in your company, whether undergoing shared hardships, celebrating milestones (academic or personal), or just spending hours talking. I can't wait to be attending your own defenses!

To my friends from before Brown, from childhood and Clark University, thank you for inexplicably being there for me ever since. Ethan Hansen and Sarah Scherer, I've cherished our friendships for as long as I can remember and am grateful that you invited me to be involved in your (respective) beautiful weddings. AJ and Chandra Singh-Cades, we've all come a long way since our primary pastime was tooling around the Natick Mall. To those I met through "B3" – Aaron Crootof, Chris Skoglund, Sunewan and Samuel Paneto – I'm glad that despite all of our changes since Worcester, our friendships (and strange senses of humor) have endured. David Glancy, who has the honor of first introducing me to the Brown University graduate community – I have been so glad to see our friendship grow and develop to what it is now, and it has been a joy to get to know Brittany Mayweather as well. Thank you for all the times you've hosted or visited me, as well as for involving me in your wedding (and so much more of your life).

To my sister Rebecca Ohman, you are brilliant and wise beyond your years, and I am so proud of the person you are. I've been lucky to grow up with someone for so much of my life who understands me so well (även när jag talar svenska). Your empathy and thoughtfulness improves the lives of everyone around you, and seeing your successes brings me incredible joy. I love you and I'll always have your back in any way that I can.

And finally, I could not have made it even partway through graduate school without the constant and endless love and support of my fiancée, Prapti Pokharel. You have been there through some of the most difficult moments and helped make everything seem solvable. I have loved traveling the world with you, broadening my culinary horizons, and the home we've built together. I can't thank you enough for everything you've done for me, so all I can do to show my appreciation is to marry you and give you back the same daily kindness you've given me.

Table of Contents

List of Tables and Figures

Chapter 1:
Introduction

The Liver

The liver is a critical organ for the functioning of the vertebrate body. Its primary function is as the major site for metabolic homeostasis, whereby it regulates the content of the blood and synthesizes useful proteins. [1] To do this, it performs an array of specific functions to reprocess nutrients from food into more usable forms for the body and into primary molecular components. These products of the liver include critical compounds for the blood such as: albumin, which regulates fluid pressure and carries hormones through the body; coagulation factors, which enable clotting in the case of injury to stop bleeding; cholesterol, a component of hormones and cell membranes; and circulating innate immunity proteins, which directly and indirectly combat bacterial infection. [2] The liver also produces and secretes digestive bile through ducts to the gallbladder and eventually into the intestine, which helps break down and absorb fats. It produces enzymes of the cytochrome P450 (CYP) family, some of which metabolize and detoxify ingested foreign chemicals, including poisons and pharmaceuticals. [3] The liver collects and breaks down waste products from the body, including bilirubin and ammonia, and also has a critical role in energy storage, converting and storing glucose in the form of glycogen to balance blood sugar levels in the time periods between feeding and fasting.

These myriad functions are carried out by multiple cell types, organized in a hexagonal lobule architecture at the microscopic level (Figure 1A). These include hepatic stellate cells, which produce the extracellular matrix and store vitamin A; Kupffer cells, which are tissue resident macrophages and perform immune surveillance of the liver; endothelial cells, a fenestrated layer lining the sinusoids where blood mixes, and cholangiocytes, which are epithelial cells that line the bile duct and control the flow rate and pH of bile. [2] The parenchymal cell type of the liver are the hepatocytes, which make up about 80% of the liver's mass, 60% of its total cell count, and perform the majority of the liver's functions, such as detoxification as well

as synthesis of proteins and lipids. As a result of these activities, it is essential for the body to retain healthy and active hepatocytes in the right proportion to its overall mass.

Liver Regeneration

The liver is routinely exposed to harmful foreign agents, such as consumed chemicals and bacteria, so damage to the organ is a routine occurrence. The body relies on consistent liver function, and liver failure eventually leads to hepatic encephalopathy, where toxins migrate to and enflame the brain, causing cognitive impairment and eventually coma. Regeneration of hepatocytes allows the liver to tolerate and recover from damage it incurs by replacing injured cells. Hepatocytes have uniquely prodigious regenerative abilities following damage when compared with most somatic cells, [4] which allow the liver to regenerate from injury (Figure 1B). This attribute is a highly conserved process in evolutionary history and is present even in fish livers. While a complex series of molecular events carry out this regenerative process, the phenomenon has been recognized by human society for thousands of years. The ancient Greek myths of Prometheus and Tityus involve birds of prey feasting on the titular figures' livers as a form of eternal torture, as the regrowth of their livers allows for a perpetual prolonging of their punishments. [5] A full scientific understanding of the molecular mechanisms underlying liver regeneration took several additional millennia, and is still under active investigation today.

Liver regeneration has primarily been studied *in situ* using a technique called partial hepatectomy (PH), whereby a large portion of the liver is surgically excised and is observed to quickly regenerate. [6,7] Up to 2/3rds of a rodent liver's mass can be removed and is then able to regenerate to within 1% of the original mass in under 2 weeks (Figure 1C). This process occurs by way of compensatory growth, during which the remaining liver mass expands rather than the removed lobes regenerating as they were at the structural level. This ensures that the proper ratio of hepatocyte mass to body size is maintained to ensure metabolic homeostasis. In

humans, partial hepatectomy can also be used clinically to remove localized hepatic tumors and regenerate healthy tissue, as well as kickstart liver recovery from areas of damage. [8,9]

Quiescent hepatocytes are poised at the G0 phase of the cell cycle and expediently progress through the G1 phase within 1-2 days after damage occurs. A number of different signaling pathways contribute to regeneration from partial hepatectomy. These include cytokines such as tumor necrosis factor (TNF) and Interleukin 6 (IL6) which enhance the activity of mitogens and prepare the cell to enter G1 from quiescence. These extracellular proteins act on the cell by way of transmembrane receptors, while growth factors such as hepatocyte growth factor (HGF) and epidermal growth factor (EGF) are direct hepatocyte mitogens that lead directly to growth and proliferation. Metabolic regulatory pathways such as the mammalian target of Rapamycin (mTOR), Wnt signaling, and Cyclin D1 mediate the duration and scale of regeneration to correspond to the amount of damage that has occurred. Some of these pathways are direct mitogens and are required for regeneration to occur, such as HGF and EGF. Other cytokines like TNF interact with and enhance mitogens but are dispensable as they can be compensated for by redundant alternative pathways. As a result, experimental disruption of some of these individual factors delay, but do not completely prevent, regeneration. [10] While the factors that initiate regeneration in the adult liver are well-characterized, what stops regeneration at the right time is still unclear. There are a number of theories related to the concentration of the Yap protein as controlled by the Hippo pathway, sensing of bile acid levels and interaction with FGF15, as well as the maintenance of hepatocyte number through a kind of quorum or oxygen sensing, which may potentially be related to lobular zonation and distance from the portal triad.

Liver Disease

Despite its regenerative ability, the liver is still susceptible to serious injuries that overwhelm its regenerative capacity, or which are biproducts of the regenerative process such

as deposition of fibrotic tissue during cycles of injury and healing. [11] These types of damage and the scope of injury are classified into multiple different kinds based on the frequency of injury as well as the severity and nature of damage to the liver. Figure 2 shows the classical model of progression from transient liver injury to hepatitis and, eventually, development of hepatocellular carcinoma. The liver can withstand some degree of acute injury and recover if the source of injury is removed. However, an overwhelming amount of acute injury can lead to acute liver failure (ALF), while repeated injury can develop into chronic liver disease (CLD).

Acute Liver Failure

ALF is caused by sudden and intense hepatocellular injury without preexisting damage such as cirrhosis or chronic sources of injury. [12] This condition is rare and is driven in the US primarily by acetaminophen or other medication overdose (including due to unintentional mixing of medications exacerbating the combinatorial harm to the liver), or by hepatitis viral infection. ALF can also be caused by medical conditions such as Wilson's Disease, in which a buildup of copper occurs in the body, and Budd-Chiari syndrome, in which hepatic veins are clogged or narrowed. A minority (30%) of ALF cases require transplantation, as acute injury can generally be managed at the symptom level once the source of injury is removed. However, a similar percentage of ALF patients die due to the condition, and part of the reason is lack of livers for transplantation.

Chronic Liver Disease

CLD occurs when repeated damage to the liver replaces the functional parenchyma with increasing amounts of nonfunctional scar tissue. This damage can be caused from a variety of sources, such as environmental damage from ingested toxins, the steatotic buildup of fat and the resulting inflammatory damage called steatohepatitis, or the deposition of fibrotic tissue resulting from the healing process after viral damage. [13] As the liver is essential for a variety of functions which maintain metabolic homeostasis, this disruption can be deadly. Over 44,000

people die from CLD annually in the US, making it a leading cause of death for ages 25-64 years. [14]

The causes of CLD can vary dramatically based on geographical area. Multiple types of viruses can cause hepatitis, most commonly the hepatitis B virus (HBV), a DNA virus of the family *Hepadnaviridae,* and hepatitis C virus (HCV), an RNA virus of the family *Flaviviridae*. HBV and HCV are spread person-to-person by exposure to infected blood or bodily fluids, including vertical transfer from mother to child. Other clades of virus also have context-dependent links to hepatitis, such as the human enteric adenovirus 41, which can cause hepatitis in immunocompromised children. [15] These and other known hepatitis-causing viruses can directly infect hepatocytes and form chronic infections that are difficult to clear, in part due to the tolerogenic environment of the liver resulting from its routine processing of exogenous compounds. [16,17] While there are some treatments for symptoms of hepatitis virus infection, many of these treatments are limited by toxicities and there are currently no durable cures. As a result, vaccination is critical for prevention and suppression. [18] Hepatitis viruses are more prevalent in areas with lower vaccination rates and higher rates of risky behaviors, such as sharing of contaminated needles for intravenous drug usage. [19] As a result, the global HBV birth dose vaccination rate of 39% in 2015 reflected an averaging of the high 70% rate of the Americas and Western Pacific with that of 10% in Africa. In countries that have made improvements in vaccinating their populations against hepatitis viruses, the primary causes of hepatitis and therefore the major divers of liver transplantation have shifted from viruses to causes linked to diet and lifestyle, such as alcoholic liver disease (ALD) and nonalcoholic fatty liver disease (NAFLD).

ALD is driven by alcohol consumption and is considered the most prevalent form of CLD. [20] ALD presents on a spectrum of severity from steatosis, steatohepatitis, fibrosis, to cirrhosis. By contrast, NAFLD has a similar clinical presentation but without a history of alcohol abuse. In

the developing world, hepatitis viral infection and aflatoxin exposure from agricultural use are leading causes, [21] while in developed nations it is more common to be the result of general poor diet and sedentary lifestyles. [22] The incidence of CLD is rising, particularly in the pediatric population, which is associated with increases in pediatric obesity. In 2018, it was estimated that about 25% of the world population has NAFLD, and a recent model has estimated that there will be a 178% increase in NAFLD-related deaths by 2030. [23,24] Nonalcoholic steatohepatitis (NASH) is the most serious form of NAFLD and has also increased dramatically in incidence. Development of NASH is associated primarily with obesity and metabolic syndromes. [25] As of 2020, NASH was the most common reason for a liver transplant in women, older patients, and those on Medicare in the United States. [26] This increasing proportion of fatty liver in the general population exacerbates existing issues in the supply of donor organs. Hepatic steatosis is now being reported in 30-51% of donor livers, [27] and this is likely to rise, leading to a situation where at the same time that more patients need liver transplants, fewer healthy donor livers are becoming available.

Hepatocellular Carcinoma

CLD and cirrhosis have a strong link to hepatocellular carcinoma (HCC), with the majority (80-90%) of HCC cases having cirrhosis as a precursor. [28] Cirrhosis triggers hepatocyte regeneration, which can lead to the formation of nodules that may become malignant. As liver cancer is the 6th most deadly cancer and HCC makes up approximately 80% of all liver cancers, [29] the total number of annual deaths ultimately related to CLD may be much larger than recorded CLD deaths alone. [30] Like many of the cancers with the highest mortality rates, HCC diagnosis is typically late-stage with significant damage to the liver and minimal restorative treatment options. However, in addition to transplantation, the ability of the patient's liver to significantly regenerate can be harnessed to surgically resect the tumor-containing areas of the liver, which can in some cases lead to recovery.

Clinical Treatments

Liver disease has several potential treatments depending on its cause, such as changing dietary or exercise habits and losing weight (referred to as lifestyle changes). This can reverse a limited degree of liver injury and help to mitigate some symptoms of liver damage that cannot be reversed (Figure 2). However, clinical treatment options are limited at the point that permanent damage and cirrhosis occurs, referred to as end-stage liver disease (ESLD).

Albumin Dialysis and Bioartificial Liver Devices

Attempts at using medical devices to supplement liver function have not been successful in the clinic. Some platforms exist to perform albumin dialysis, but this only encompasses one of the liver's diverse functions, and additionally has resulted only in temporary, inconsistent improvement of symptoms with lack of survival benefit. [31] A more ambitious goal is to create a bioartificial liver (BAL) system that can recapitulate most or all of the liver's metabolic functions, such as protein synthesis and detoxification, using living cells. While attempts at differentiation of embryonic stem cells into hepatocytes has produced populations of cells with hepatocyte-like characteristics, issues of scaling and potential immunocompatibility preclude using these cells widely. [32] Other efforts have sought to use hepatocytes derived from animals, induced pluripotent stem cells, or even hepatoblastoma lines to perform some biological functions. However, needing to separate these cell populations from patient plasma using a membrane inhibits some function, and without the maintenance of viable human hepatocytes *in vitro*, these systems cannot perform all the work of the liver. [33] This means that the only long-term curative treatment for liver disease involves transplantation to replace the damaged parenchyma.

Orthotopic Liver Transplantation

Whole-organ orthotopic transplantation is the primary curative therapeutic option available to patients with liver failure and has high 5-year survival rates. Unfortunately, livers suitable for this purpose are rare. The donor must ideally have a blood type match to the

recipient and be in geographical proximity due to limitations in preserving the organ following donation. [34] This requires the US be subdivided into 11 different transplant regions that are each 2-6 states across. [35] Due to these challenges, a long waitlist exists with less than 50% of patients on it receiving a transplant within 3 years and 20% of these patients dying prior to transplant. Patient stratification on the waitlist is determined by a calculation called the model for end-stage liver disease (MELD) Score, which uses biological criteria to assess a patient's liver function. Worse liver function and other risks of complications receive higher scores and a corresponding higher priority for available livers. It is also at the discretion of the transplant team to use extended criteria donor livers or marginal grafts, which come from deceased donors with risk factors measured via the donor risk index (DRI) that could lead to harm to the patient following transplantation, including immediate or delayed failure. This is generally used to extend the donor pool in cases where the alternative is waitlist mortality. Studies have shown that grafts from young liver donors fail at higher rates in older recipients than younger recipients, but failure rates and 5-year survival rates in older recipients are not substantially different when receiving a liver from any aged donor. [36] This means that an optimal practice to expand the liver donor pool and meet more patient need could be to accept but earmark older extended criteria donors for use exclusively in older recipients.

Split Liver Transplantation

One way to make the most out of the donor liver pool is to transplant part of a liver, leveraging its inherent regenerative abilities so that partial sections can be transplanted to different recipients. When this is done using a full adult donor organ, this allows for multiple recipients to benefit from the same liver, doubling its impact. The liver is usually split asymmetrically into the smaller left and larger right lobes. The smaller portion can be used for transplant to a pediatric patient, while the larger half can be used for an adult. It is also more common in some nations such as Japan to use partial split transplants taken from living donors,

rather than from organs procured from deceased donors, as a result of different legal norms related to organ donations as well as differing postmortem cultural considerations. [37,38] As there are health risks to the donor in this process, living donor transplantations are uncommon in the USA, making up <5% of liver transplantations. [39] The majority of US donor organs come from deceased donors after brain death (DBD), with a minority donated after cardiac death (DCD).

Donor Organ Preservation

Since the 1960s, the primary method to preserve donor organs has been static cold storage (SCS). [40] The organ is removed and placed into a solution at low temperatures to slow the metabolism of cells to minimize cellular damage while the organ removed from the oxygen and nutrients of the body. Elaborations of this technique involve covering the liver with ice slush or pumping a chilled solution into the organ prior to SCS. While this can be effective at preserving the liver for short durations, it can also result in damage over time and during transplantation, including ischemia-reperfusion injury (IRI). Because of this “shelf life”, it is not possible to distribute donor livers throughout the US, so the Organ Procurement and Transplantation Network (OPTN) has subdivided the country into 11 regions based on geographical proximity. Donor and recipient pools are matched based on these zones, which take into account the location of transplant centers and historical patient referral patterns.

Machine Perfusion

One of the first advancements to the static cold organ preservation process was the use of a hypothermic perfusion technique, where a chilled fluid is actively pumped through the organ to facilitate even cooling, instead of simply filling the liver with a chilled fluid. In addition, this active perfusion process also results in some amount of clearance of harmful liver byproducts, reducing the negative impact of SCS on the organ. This process has been continually tweaked to try and improve outcomes, such as by oxygenating the perfusion solution or adding amino acids and other substances to provide additional nutrients to the liver. A more recent

advancement is the use of normothermic machine perfusion (NMP), where instead of chilling the donor liver to slow the metabolism, it is perfused with a nutrient-containing blood-like solution at physiological temperatures in order to recapitulate the liver's natural environment, minimize disruption, and provide continuity to biological processes prior to transplantation (Figure 3). This technique is undergoing widespread clinical evaluation and may offer the ability to not only preserve functional livers but even increase the pool of usable livers. [41]

Viability Assessment

As there are more patients on the waitlist than treatable with the number of available donor livers, it is essential to maximize the use of the limited organs available for either whole or split liver transplantations. An important way to do so is by minimizing waste resulting from discard. If a donor liver is steatotic, or if it has undergone IRI, it may not meet viability criteria, meaning that it is unlikely to result in successful transplantation or positive long-term patient outcomes. [42] To avoid this, transplant surgeons use discretion at time of transplant and can decide to discard rather than transplant a marginal liver. The most common reason for discard is the presence of steatosis, and this is primarily assessed subjectively. However, this qualitative assessment may not reflect the true functional state of the liver. Thus, a more accurate quantitative set of metrics is needed in order to minimize discard of potentially-functional livers. NMP may offer a platform to provide such metrics, as the perfusate can be examined to determine the liver's metabolic effects on the solution. These measurements provide a more accurate picture of the donor liver's function for a surgeon, which could allow for a more informed decision and improve utilization of so-called marginal livers.

A potential alternative option to the many challenges that come with using whole or split liver transplantation is to circumvent the scarcity of livers suitable for transplantation by harvesting hepatocytes to perform cellular transplantation (Figure 4). The unique regenerative

attribute of hepatocytes offers the potential to harvest and transplant cells, rather than a full or split liver, to restore function to a critically damaged liver.

Hepatic Cellular Transplantation

Hepatic cell transplantation (HCT) was first used clinically in humans in the 1990s. [43,44] Isolated hepatocytes were collected from a perfused, partially resected liver, and were then injected into the spleen in 10 adult patients. This led to hepatocyte survival and patient recovery for a typical range of 1 to 6 months following the transplant, with one patient having detectable transplanted hepatocytes at 11 months. [32,33] Since then, there have been a number of similar clinical trials undertaken using adult hepatocytes in patients with inherited metabolic diseases or acute liver failure. [45–47] However, clinical improvements generally last for only a few months, as transplanted adult hepatocytes are not very proliferative and ultimately die off from the stresses of transplantation or rejection by the recipient's immune system. In addition, due to the scarcity of healthy organs for transplant, livers digested to provide cells for HCT are often suboptimal or damaged, which is potentially responsible for suboptimal grafting. Furthermore, these cells cannot be easily maintained in culture, as they rapidly de-differentiate. Because these cells only remain effective for a period of months post-transplant and do not continue to proliferate, this technique is predominantly used to bridge patients to orthotopic transplant, rather than as a curative therapy. Adult hepatocytes are therefore not suitable to fully regenerate a damaged liver or permanently cure metabolic defects.

One solution being explored is to use induced pluripotent stem cells (iPSCs) derived from a patient's own somatic cells, which would be an ideal option for availability and immune tolerance. These cells would lack any procurement concerns and could be expanded *ex vivo* at scale using established technologies. Unfortunately, the current state of the field has resulted in generating incompletely-differentiated and immature hepatocyte-like cells (HLCs) which are considered unsafe to use in a patient. [48] Concerns about genomic stability raise the potential for

tumorigenesis over time, and these iPSCs have not progressed to use in clinical trials. This field is continuing to advance, utilizing organoid models and scaffolding systems in an attempt to improve the development and differentiation process. [49,50] Current iterations of PSC-derived HLCs resemble fetal hepatocytes more than adult hepatocytes – which may be a potential benefit to that technique when considering the distinct properties of fetal hepatocytes. [51]

Fetal Hepatocyte Transplantation

In contrast to adult hepatocytes, fetal hepatocytes have been demonstrated to durably persist and proliferate in animal models and human clinical trials. [52,53] While they have a generally mature hepatic phenotype, they exhibit variable levels of expression of critical CYP enzymes, which can affect their ability to process toxins and pharmaceutical compounds. However, the recipient's own adult hepatocyte mass can be sufficient to compensate for this deficiency in transplanted cells. [54] More importantly for consistent clinical use, there are serious ethical concerns relating to their procurement, and their inability to be maintained in culture in a fetal state after isolation makes them problematic to source despite their utility. [55] This makes it important to characterize the mechanisms responsible for their growth phenotype in order to translate this advantage to adult hepatocytes or hepatocyte-like cells.

Thesis Overview

This dissertation's goal was to explore potential novel improvements to the current standard of orthotopic liver transplantation using a multiomics approach. Multiomics refers to the integration of several individual -omic techniques to study a biological system. [56] In our studies, we have utilized combinations of transcriptomic, epigenomic, and proteomic techniques in tandem to create a comprehensive profile of fetal hepatocytes before, during, and after hepatic cellular transplantation. We have also utilized transcriptomics and proteomics to study livers undergoing normothermic machine perfusion. We hope a more detailed understanding of these processes will allow for optimization of HCT and NMP techniques in the clinic.

Fetal Hepatocyte Cellular Transplantation

Our lab at Brown University and Rhode Island Hospital has long focused on studying and characterizing the molecular mechanisms which underpin the late stages of fetal liver development and comparing these pathways to those active during liver regeneration (Figure 5). We have previously compared the activation of the major signaling pathways that regulate cellular proliferation and growth in adult rat hepatocytes to fetal hepatocytes at embryonic day 19 (ED19). [57] Previous studies from our laboratory on rats have characterized multiple mitogenic signaling pathways involved in initiation of regeneration from PH in adult hepatocytes. [58–60] Intraperitoneal injection of growth factors into the adult liver triggered a series of mitogenic events, including Erk activation, PI3K/Akt signaling, and mTOR signaling. These pathways are activated in liver regeneration and are necessary drivers of recovery from PH by triggering important events for hepatocyte proliferation, including ribosomal activity and progression into the cell cycle, while inhibition of these factors delays regeneration. By contrast, when the same growth factors were injected in ED19 fetuses *in situ*, upstream signaling events were activated in the liver but we observed no activation of downstream components, demonstrating that the signaling pathways are uncoupled along intermediate relays. Proliferation of fetal hepatocytes occurred independent of the mitogenic signaling that characterizes regeneration in adult liver. It was also found that administering rapamycin to block mTOR has no suppressive effect on fetal hepatocyte proliferation, while rapamycin inhibits transcription and induces cell-cycle arrest in adult hepatocytes, [61] and also inhibited development of HCC focal lesions. [62] Our lab has previously explored the drivers of the differences between the adult and ED19 fetal signaling responses during regeneration by comparing gene expression. By performing PCR-based suppressive subtractive hybridization on total RNA from frozen liver, 13 genes were identified as overexpressed in fetal vs adult liver which may be growth-associated, with another 12 genes of unknown significance. [63] However, the drivers behind the fetal proliferative phenotype have still not been fully characterized.

In rats, ED19 is a developmental timepoint during late in gestation, only a few days before term at ED21. However, the developmental events that occur at this stage correspond to those of the human mid-gestational fetal period at approximately 16 weeks (Figure 6). This mid-gestation population has been used successfully with fetal HCT in human clinical trials, [64–67] and the same mitogenic pathways identified in the rat are found to be employed in human hepatocyte growth as well, [66,68] so what we learn from signaling in ED19 rats is relevant for translational research in humans and is informative about the most successfully-transplantable human fetal hepatocyte population. The hypothesis that the mitogen-independent growth of ED19 fetal hepatocytes would be advantageous in a hepatocyte cellular transplant scenario was tested using the dipeptidyl peptidase-4 (DPPIV)/Mitomycin-C rat model. [69] Adult hosts underwent a 2/3rd partial hepatectomy, followed by splenic injection of immunopurified fetal hepatocytes. The fetal cells migrated to and engrafted in the adult host liver and form colonies. Over 10 months, the fetal cells continued to replicate with a proliferative advantage over the remaining adult cells, eventually comprising up to 35% of a healthy, functional liver (Figure 7). This proliferation is in stark contrast to the slow, finite replication phenotype seen in transplanted adult hepatocytes.

The study conducted in Chapter 2 was designed to identify the specific mechanisms underlying the ability of these fetal hepatocytes to repopulate the adult liver and persist up to 10 months post-transplant. Our hypothesis was that retained epigenetic differences intrinsic to the transplanted fetal cells alter gene expression related to proliferation. Epigenetics refers to heritable changes in cells resulting from causes other than the DNA sequence itself and involves molecular modification of the transcription machinery to influence the rate of mRNA production at certain sites on the genome. [70,71] Epigenetics was first established in the context of its major role in driving cell differentiation and establishment of cell identity during development. [72] However, epigenetic factors are also responsible for aspects of somatic cellular

plasticity such as the response to injury, [73] and dysregulation of these systems have been indicted as potential factors in tumorigenesis. [74] In the liver specifically, hepatocyte differentiation and identity is driven by pioneer factors, which are transcription factors that affect chromatin compacting in tandem with histones. [75] Chromatin compacting helps to regulate the phenotypes of quiescent vs. regenerating hepatocytes by altering the repressive or permissive marks on proliferative genes. Different types of liver regeneration also can involve dedifferentiation of somatic hepatocytes to progenitor cells, as well as transdifferentiation of biliary cells to hepatocytes via epigenetic mechanisms. [76]

We have previously investigated one epigenetic modifier, DNA methylation, in fetal and adult human liver and found that while different patterns exist in the two populations, these did not correlate with gene expression. [77] This led us to begin exploring the role of histone post-translational modifications (hPTMs), which are known to have important roles in regulating cell identity during development. Histones are the major structural proteins of the genome and can have modifiers bound to their amino-terminal tails which alter the packing of chromatin via electrostatic charge or recruitment of additional factors. [78] Depending on the modification type and histone tail location, transcription of nearby genes can increase or decrease. PTMs can be added to or removed from a histone site by a number of specific enzymes and signaling pathways responsive to environmental signals, meaning that hPTMs contribute not only to differentiation but also cellular plasticity. [79] Recently, histone methylation has been shown to regulate hepatic metabolism and the maintenance of differentiation in human cells, with modification of methyltransferase and demethylase activity resulting in retrodifferentiation. [80] We hypothesized that hPTM regulation is responsible for maintaining the differential expression of growth-regulating genes between fetal and adult hepatocytes and aimed to quantify those relevant differences. To interrogate these factors, our study examined hPTM and gene

expression profiles of laser-captured fetal-derived post-transplant colonies and paired adult host tissue, compared to primary isolated fetal and adult hepatocytes.

Normothermic Machine Perfusion Advances

In addition to our work exploring fetal HCT in a rodent model, we also examined the use of normothermic machine perfusion in human livers. When compared to cold ischemia or hypothermic perfusion, NMP has the benefit of providing a more physiological set of conditions for the liver, including providing nutrients and clearing waste products. It also allows for the ability to measure how the liver is performing its myriad functions by measuring protein levels in the perfusate, allowing for a quantitative assessment of liver viability and thereby a more accurate prediction of transplant success. While many livers are sourced from a healthy DBD donor, other donor livers raise concerns for use in transplantation when they may have suffered damage such as IRI, or if they are steatotic as is increasingly common in the US population. There has also been an increase in the number of DCD livers, which is more likely to lead to transplantation challenges and worse 3-year survival rates. [81] Having the ability to improve liver function and gather physiological metrics prior to the transplantation process is of critical importance, but we aimed to also examine the gene expression changes underpinning the response to perfusion. Learning more about why a liver responds well or poorly to NMP may allow for improvements to the process as well as better characterization of metrics for identifying organs with different functional capacities.

To explore these mechanisms in detail, we entered into a collaboration with the Organ Reengineering Group at Massachusetts General Hospital and Harvard Medical School. This group has expertise with the NMP process as well as access to discarded human donor livers that we gathered samples from at multiple time points throughout the perfusion process. We used these samples to measure liver viability metrics over time, quantify protein levels by Western blot, and examine the transcriptome via RNA-Seq. In Chapter 3, we studied the use of

NMP on DCD lean and steatotic livers that were discarded for transplant using multiomics approaches. In Chapter 4, we strove to utilize the observations resulting from the work in Chapter 3 to meaningfully improve liver functionality during NMP. We hypothesized that the addition of the irreversible pan-caspase inhibitor emricasan to the perfusate may have the effect of mitigating pathologic apoptosis in nonfunctional livers, which may be contributing to liver injury and lower viability for transplantation. Discarded DCD donor livers, similar to untreated control livers, were perfused with the addition of emricasan and underwent similar physiological, genomic, and proteomic analysis to the analytical process described in Chapter 3.

Figures

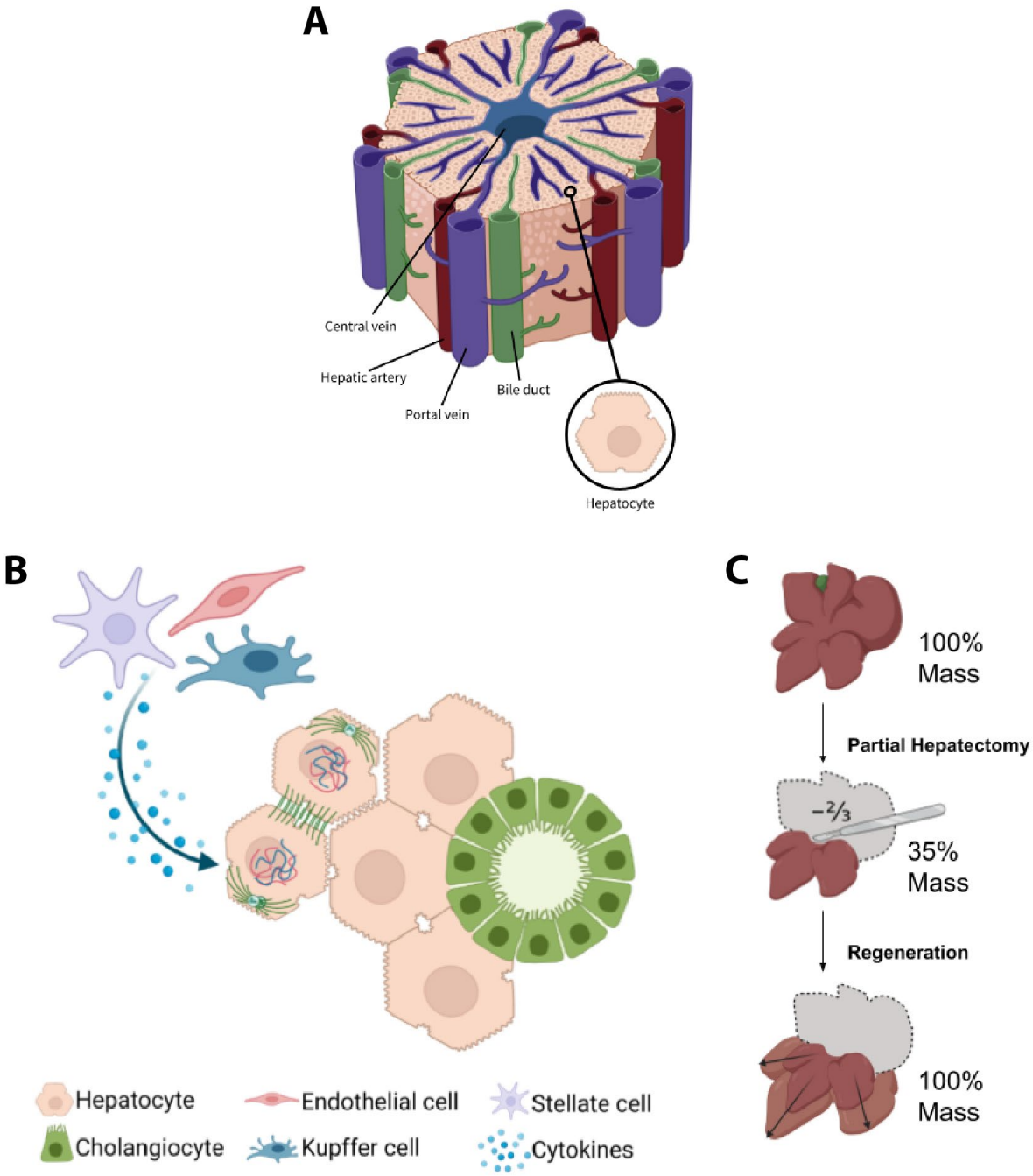

Figure 1. Anatomy of the liver and regeneration. (A) A cross-section of the basic unit of organization of the liver, a hexagonal lobule. Hepatocytes make up the majority of the organ. (B) Regeneration is induced by mitogens from the microenvironment triggering poised hepatocytes to enter the cell cycle. (C) During rodent PH, the liver mass is surgically reduced to ~30%. Hepatocyte regeneration causes expansion of the remaining liver to within 1% of the original mass in under 2 weeks. Created with BioRender.

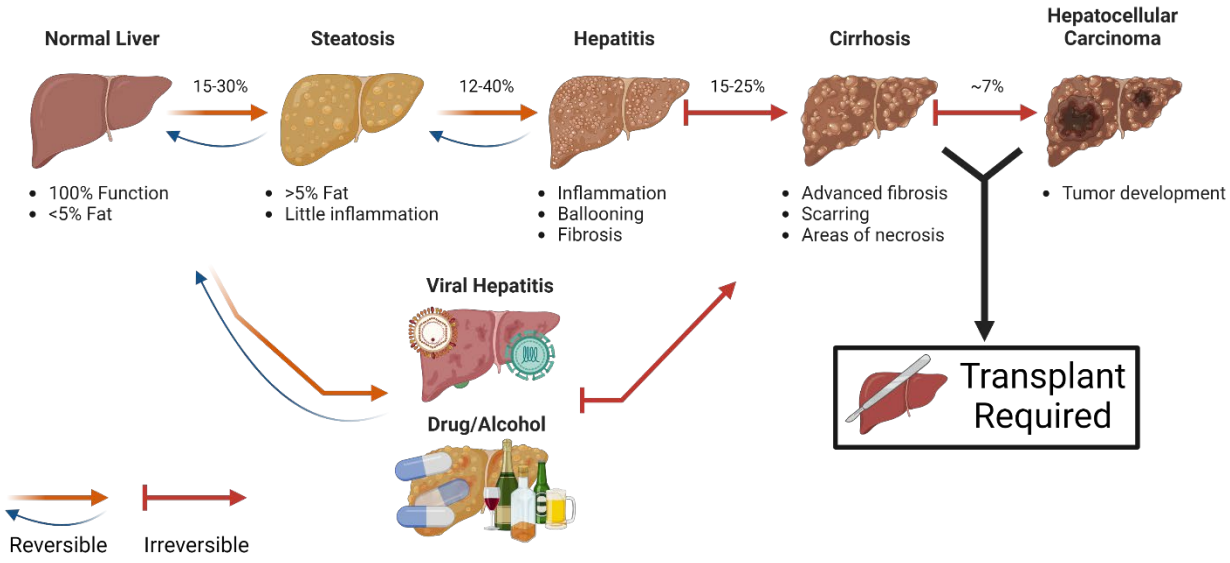

Figure 2. Progression of liver injury and clinical manifestations. A healthy liver can progress to HCC via multiple stages of accumulating reversible and irreversible injury with distinct phenotypes at each stage. Cirrhosis and HCC are generally considered irreversible and require transplantation of a replacement liver. Created with BioRender.

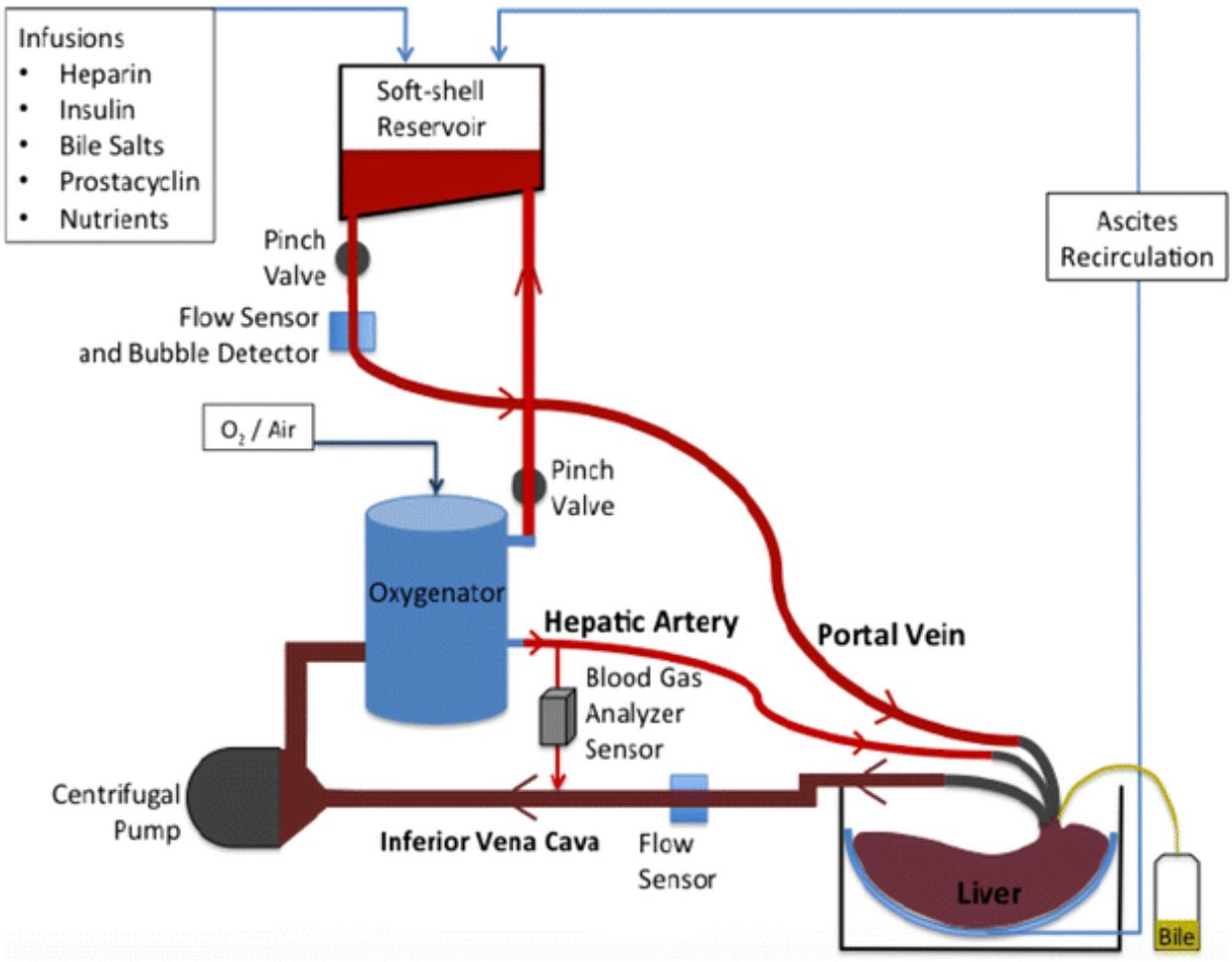

Figure 3. Schematic representation of OrganOx metra circuit.

From: Ceresa, C.D.L., Nasralla, D. & Jassem, W. Normothermic Machine Preservation of the Liver: State of the Art. *Curr Transpl Rep* **5**, 104–110 (2018). doi:10.1007/s40472-018-0186-9 [82]

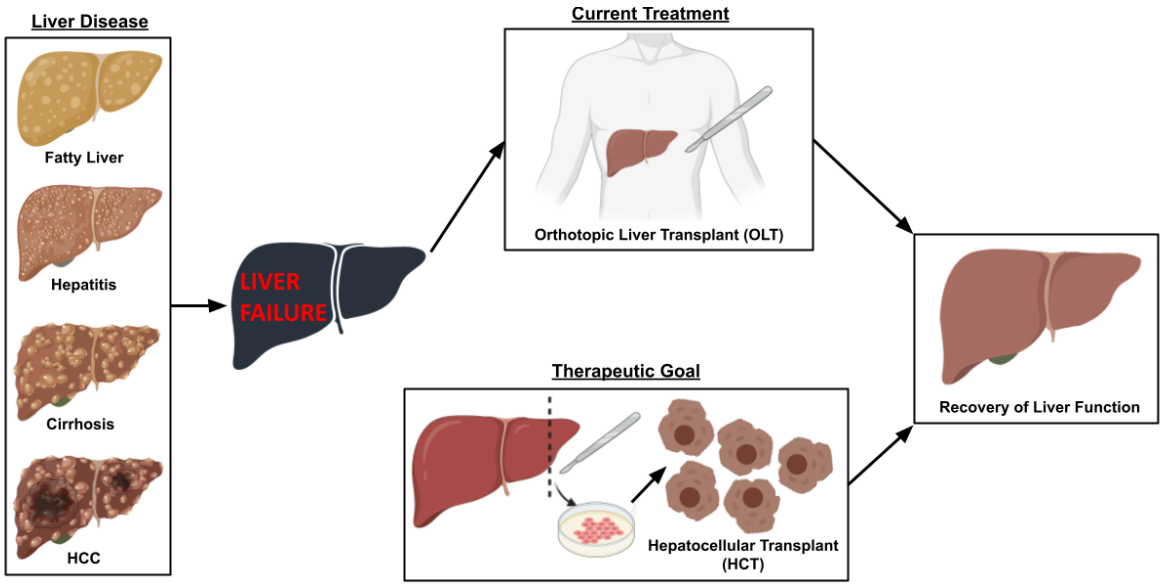

Figure 4. Overview of liver transplantation options. Current ESLD treatment consists of OLT (whole-organ or split-liver), which is limited by available functional donor organs. One alternative treatment is to culture hepatocytes for HCT, which can come from a variety of sources and may be used in multiple patients. Created with BioRender.

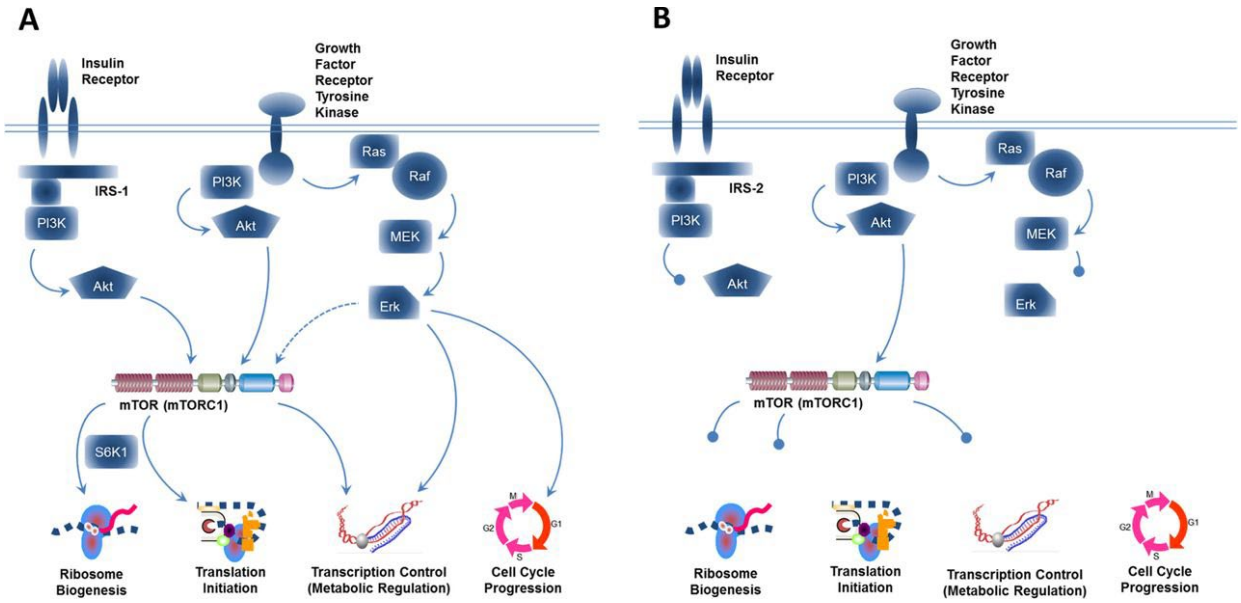

Figure 5. Hepatic insulin- and growth factor-mediated mitogenic signaling pathways in the rat. The diagrams represent a distillation of the data on mitogenic signaling in adult liver (panel A) vs late gestation fetal liver (panel B).

From: Gruppuso PA, Sanders JA. Regulation of liver development: implications for liver biology across the lifespan. *J Mol Endocrinol*. 2016;56(3):R115-R125. doi:10.1530/jme-15-0313 [83]

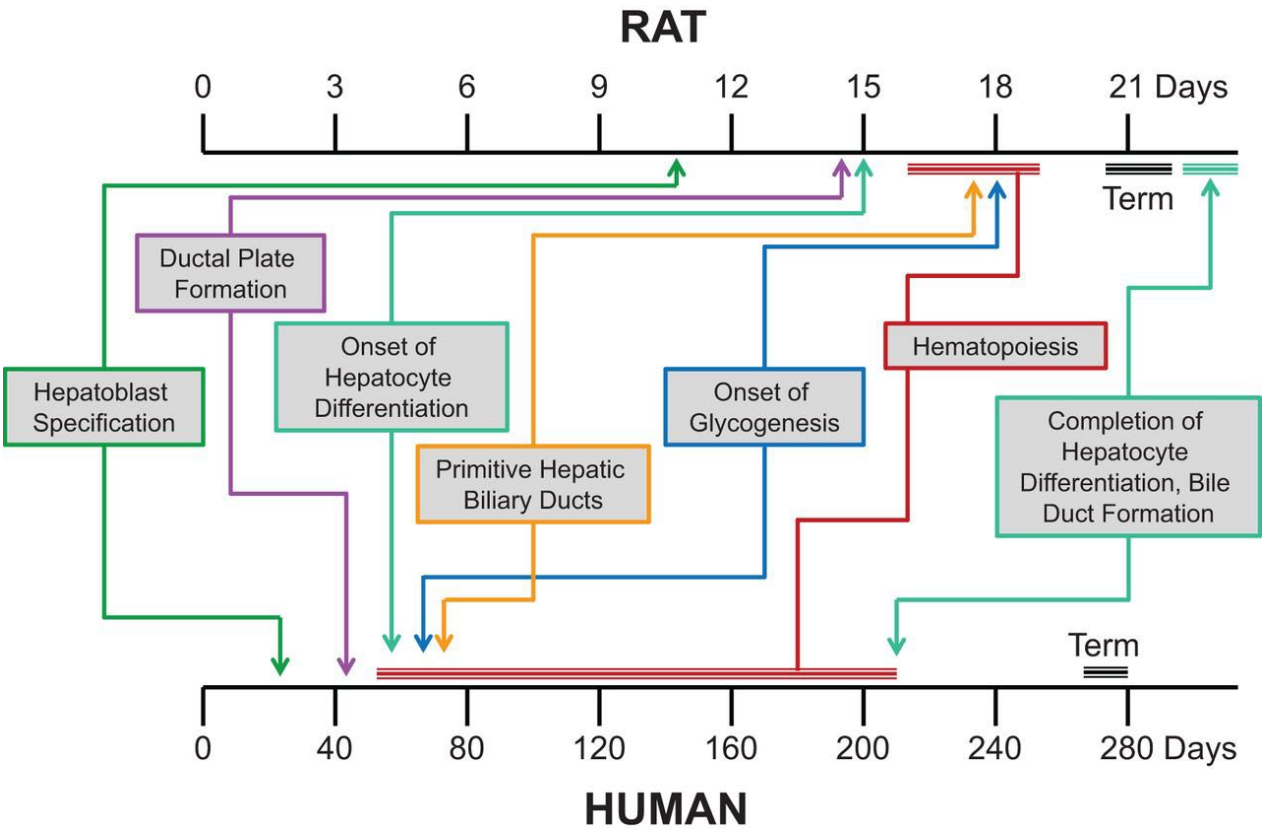

Figure 6. A timeline of liver development in the rat and human. Developmental milestones are plotted on two scales that represent the duration of gestation in rats and humans. The schematic is based on published data (Shiojiri et al. 1991, Gordillo et al. 2015). [84,85]

From: Gruppuso PA, Sanders JA. Regulation of liver development: implications for liver biology across the lifespan. *J Mol Endocrinol*. 2016;56(3):R115-R125. doi:10.1530/jme-15-0313 [83]

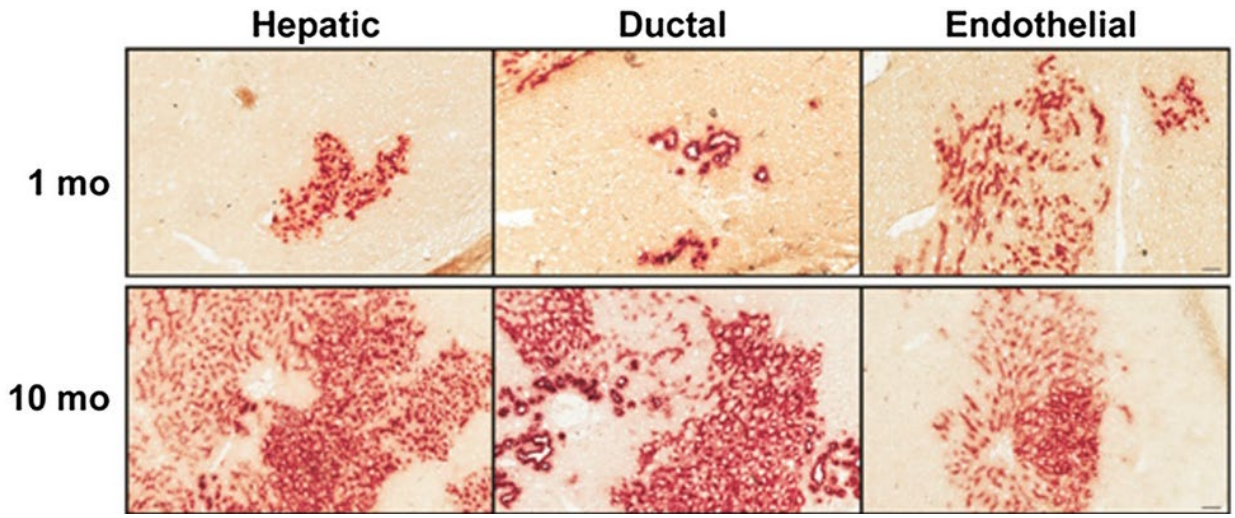

Figure 7. Liver repopulation by DPPIV+ E19 fetal LAP+ cells at 1 and 10 months after transplantation into DPPIV− adult hosts. DPPIV+ cells derived from male and female fetuses pooled from 5 to 8 litters were incubated with LAP or mock purified and sorted on an AutoMacs cell separator. Mock purified total cell isolates (unfractionated), LAP+ and LAP− fractions were transplanted via splenic injection into partial hepatectomized DPPIV− adult hosts that were pretreated with mitomycin C. Scale bar = 100 μm.

From: Boylan JM, Francois-Vaughan H, Gruppuso PA, Sanders JA. Engraftment and Repopulation Potential of Late Gestation Fetal Rat Hepatocytes. *Transplantation*. 2017;101(10):2349-2359. doi:10.1097/TP.0000000000001882 [86]

References

1. Juza RM, Pauli EM. Clinical and surgical anatomy of the liver: A review for clinicians. *Clinical Anatomy*. 2014;27(5):764-769. doi:10.1002/CA.22350

2. Godoy P, Hewitt NJ, Albrecht U, et al. Recent advances in 2D and 3D in vitro systems using primary hepatocytes, alternative hepatocyte sources and non-parenchymal liver cells and their use in investigating mechanisms of hepatotoxicity, cell signaling and ADME. *Arch Toxicol*. 2013;87(8):1315-1530. doi:10.1007/S00204-013-1078-5/TABLES/23

3. Sadler NC, Nandhikonda P, Webb-Robertson BJ, et al. Hepatic cytochrome P450 activity, abundance, and expression throughout human development. *Drug Metabolism and Disposition*. 2016;44(7):984-991. doi:10.1124/dmd.115.068593

4. Michalopoulos GK. Hepatostat: Liver regeneration and normal liver tissue maintenance. *Hepatology*. 2017;65(4):1384-1392. doi:10.1002/hep.28988

5. Tiniakos DG, Kandilis A, Geller SA. Tityus: A forgotten myth of liver regeneration. *J Hepatol*. 2010;53(2):357-361. doi:10.1016/J.JHEP.2010.02.032

6. Higgins G, Anderson M. Restoration of the liver of the white rat following partial surgical removal. In: *Experimental Pathology of the Liver*. Vol 12. ; 1931:186-202.

7. Fausto N, Campbell JS. The role of hepatocytes and oval cells in liver regeneration and repopulation. *Mech Dev*. 2003;120(1):117-130. doi:10.1016/S0925-4773(02)00338-6

8. Lu WP, Dong JH. Hepatectomy for hepatocellular carcinoma in the era of liver transplantation. *World Journal of Gastroenterology : WJG*. 2014;20(28):9237. doi:10.3748/WJG.V20.I28.9237

9. Hashavia E, Goldstein AL, Nachmany I, Shimonov A, Klausner JM, Soffer D. Definitive Repair of Injuries to the Liver During Initial Trauma Laparotomy. *https://doi.org/101177/0003134820979598*. 2020;87(8):1299-1304. doi:10.1177/0003134820979598

10. Michalopoulos GK. Hepatostat: Liver regeneration and normal liver tissue maintenance. *Hepatology*. 2017;65(4):1384-1392. doi:10.1002/hep.28988

11. Tanaka M, Miyajima A. Liver regeneration and fibrosis after inflammation. *Inflamm Regen*. 2016;36(1):1-6. doi:10.1186/S41232-016-0025-2/FIGURES/2

12. Lee WM. Acute Liver Failure. Published online 2012. doi:10.1055/s-0032-1301733

13. Asrani SK, Devarbhavi H, Eaton J, Kamath PS. Burden of liver diseases in the world. *J Hepatol*. 2019;70(1):151-171. doi:10.1016/J.JHEP.2018.09.014

14. Xu J, Murphy SL, Kochanek KD, Arias E. Deaths: Final data for 2019. *National Vital Statistics Reports*. 2021;70(8). doi:10.15620/cdc:106058

15. Baker JM, Buchfellner M, Britt W, et al. MMWR, Acute Hepatitis and Adenovirus Infection Among Children — Alabama, October 2021–February 2022. Published online 2021. doi:10.1128/CMR.5.3.262

16. Fanning GC, Zoulim F, Hou J, Bertoletti A. Therapeutic strategies for hepatitis B virus infection: towards a cure. *Nature Reviews Drug Discovery 2019 18:11*. 2019;18(11):827-844. doi:10.1038/s41573-019-0037-0

17. Gao B. Basic liver immunology. *Cell Mol Immunol*. 2016;13(3):265. doi:10.1038/CMI.2016.09

18. Tanaka J, Akita T, Ko K, Miura Y, Satake M. Countermeasures against viral hepatitis B and C in Japan: An epidemiological point of view. *Hepatology Research*. 2019;49(9):990-1002. doi:10.1111/HEPR.13417

19. Asrani SK, Devarbhavi H, Eaton J, Kamath PS. Burden of liver diseases in the world. *J Hepatol*. 2019;70(1):151-171. doi:10.1016/J.JHEP.2018.09.014

20. Seitz HK, Bataller R, Cortez-Pinto H, et al. Alcoholic liver disease. *Nature Reviews Disease Primers 2018 4:1*. 2018;4(1):1-22. doi:10.1038/s41572-018-0014-7

21. Kuniholm MH, Lesi OA, Mendy M, et al. Aflatoxin exposure and viral hepatitis in the etiology of liver cirrhosis in The Gambia, West Africa. *Environ Health Perspect*. 2008;116(11):1553-1557. doi:10.1289/EHP.11661

22. Younossi Z, Tacke F, Arrese M, et al. Global Perspectives on Nonalcoholic Fatty Liver Disease and Nonalcoholic Steatohepatitis. *Hepatology*. 2019;69(6):2672-2682. doi:10.1002/hep.30251

23. Younossi Z, Tacke F, Arrese M, et al. Global Perspectives on Nonalcoholic Fatty Liver Disease and Nonalcoholic Steatohepatitis. *Hepatology*. 2019;69(6):2672-2682. doi:10.1002/hep.30251

24. Estes C, Razavi H, Loomba R, Younossi Z, Sanyal AJ. Modeling the epidemic of nonalcoholic fatty liver disease demonstrates an exponential increase in burden of disease. *Hepatology*. 2018;67(1):123-133. doi:10.1002/HEP.29466/SUPPINFO

25. Canbay A, Sowa JP, Syn WK, Treckmann J. NASH Cirrhosis - The New Burden in Liver Transplantation: How Should It Be Managed? *Visc Med*. 2016;32(4):234-238. doi:10.1159/000446379

26. Younossi ZM, Stepanova M, Ong J, et al. Nonalcoholic Steatohepatitis Is the Most Rapidly Increasing Indication for Liver Transplantation in the United States. *Clinical Gastroenterology and Hepatology*. 2021;19(3):580-589.e5. doi:10.1016/j.cgh.2020.05.064

27. Steggerda JA, Bloom MB, Noureddin M, et al. Higher thresholds for the utilization of steatotic allografts in liver transplantation: Analysis from a U.S. national database. *PLoS One*. 2020;15(4):e0230995. doi:10.1371/JOURNAL.PONE.0230995

28. Dos Santos Marcon P, Tovo CV, Kliemann DA, Fisch P, Alves De Mattos A. Incidence of hepatocellular carcinoma in patients with chronic liver disease due to hepatitis B or C and coinfected with the human immunodeficiency virus: A retrospective cohort study. *World J Gastroenterol*. 2018;24(5):613. doi:10.3748/WJG.V24.I5.613

29. Balogh J, David Victor I, Asham EH, et al. Hepatocellular carcinoma: a review. *J Hepatocell Carcinoma*. 2016;3. doi:10.2147/JHC.S61146

30. Sanyal AJ, Yoon SK, Lencioni R. The Etiology of Hepatocellular Carcinoma and Consequences for Treatment. *Oncologist*. 2010;15(Supplement 4):14-22. doi:10.1634/theoncologist.2010-s4-14

31. Tsipotis E, Shuja A, Jaber BL. Albumin Dialysis for Liver Failure: A Systematic Review. *Adv Chronic Kidney Dis*. 2015;22(5):382-390. doi:10.1053/j.ackd.2015.05.004

32. Corbett JL, Duncan SA. iPSC-Derived Hepatocytes as a Platform for Disease Modeling and Drug Discovery. *Front Med (Lausanne)*. 2019;6(November):1-12. doi:10.3389/fmed.2019.00265

33. Iwamuro M, Shiraha H, Nakaji S, et al. A preliminary study for constructing a bioartificial liver device with induced pluripotent stem cell-derived hepatocytes. *Biomed Eng Online*. 2012;11:1-13. doi:10.1186/1475-925X-11-93

34. Ozaki CF, Katz SM, Monsour HP, Dyer CH, Wood RP. Surgical complications of liver transplantation. *Surgical Clinics of North America*. 1994;74(5):1155-1167. doi:10.21037/amj.2018.10.02

35. Duda L. National organ allocation policy: The Final Rule. *Virtual Mentor*. 2005;7(9):604-607. doi:10.1001/virtualmentor.2005.7.9.hlaw1-0509

36. Bittermann T, Goldberg DS. Quantifying the effect of transplanting older donor livers into younger recipients: the need for donor-recipient age matching. *Transplantation*. 2018;102(12):2033. doi:10.1097/TP.0000000000002341

37. Soyama A, Eguchi S, Egawa H. Liver transplantation in Japan. *Liver Transpl*. 2016;22(10):1401-1407. doi:10.1002/LT.24502

38. Zarrinpar A, Busuttil RW. Liver transplantation: past, present and future. *Nature Reviews Gastroenterology & Hepatology 2013 10:7*. 2013;10(7):434-440. doi:10.1038/nrgastro.2013.88

39. Kim PTW, Testa G. Living donor liver transplantation in the USA. *Hepatobiliary Surg Nutr*. 2016;5(2):133. doi:10.3978/J.ISSN.2304-3881.2015.06.01

40. Tchilikidi KY. Liver graft preservation methods during cold ischemia phase and normothermic machine perfusion. *World J Gastrointest Surg*. 2019;11(3):126. doi:10.4240/WJGS.V11.I3.126

41. Yeh H, Uygun K. Increasing Donor Liver Utilization Through Machine Perfusion. *Hepatology*. 2019;70(1):431-433. doi:10.1002/hep.30523

42. Mergental H, Laing RW, Kirkham AJ, et al. Transplantation of discarded livers following viability testing with normothermic machine perfusion. *Nat Commun*. 2020;11(1):1-12. doi:10.1038/s41467-020-16251-3

43. Mito M, Kusano M, Kawaura Y. Hepatocyte transplantation in man. *Transplant Proc*. 1992;24(6):3052-3053.

44. Grossman M, Rader DJ, Muller DWM, et al. A pilot study of ex vivo gene therapy for homozygous familial hypercholesterolaemia. *Nature Medicine 1995 1:11*. 1995;1(11):1148-1154. doi:10.1038/nm1195-1148

45. Fox IJ, Chowdhury JR, Kaufman SS, et al. Treatment of the Crigler–Najjar Syndrome Type I with Hepatocyte Transplantation. *New England Journal of Medicine*. 1998;338(20):1422-1427. doi:10.1056/nejm199805143382004

46. Wan Z, Zhang XG, Liu ZW, Lv Y. Therapeutic liver repopulation for metabolic liver diseases: Advances from bench to bedside. *Hepatology Research*. 2013;43(2):122-130. doi:10.1111/j.1872-034X.2012.01081.x

47. Iansante V, Mitry RR, Filippi C, Fitzpatrick E, Dhawan A. Human hepatocyte transplantation for liver disease: Current status and future perspectives. *Pediatr Res*. 2018;83(1-2):232-240. doi:10.1038/pr.2017.284

48. Palakkan AA, Nanda J, Ross JA. Pluripotent stem cells to hepatocytes, the journey so far. *Biomed Rep*. 2017;6(4):367-373. doi:10.3892/br.2017.867

49. Pettinato G, Lehoux S, Ramanathan R, et al. Generation of fully functional hepatocyte-like organoids from human induced pluripotent stem cells mixed with Endothelial Cells. *Sci Rep*. 2019;9(1). doi:10.1038/s41598-019-45514-3

50. Ng SS, Saeb-Parsy K, Blackford SJI, et al. Human iPS derived progenitors bioengineered into liver organoids using an inverted colloidal crystal poly (ethylene glycol) scaffold. *Biomaterials*. 2018;182:299-311. doi:10.1016/j.biomaterials.2018.07.043

51. Baxter M, Withey S, Harrison S, et al. Phenotypic and functional analyses show stem cell-derived hepatocyte-like cells better mimic fetal rather than adult hepatocytes. *J Hepatol*. 2015;62(3):581-589. doi:10.1016/j.jhep.2014.10.016

52. Pietrosi G, Vizzini G, Gerlach J, et al. Phases I–II matched case-control study of human fetal liver cell transplantation for treatment of chronic liver disease. *Cell Transplant*. 2015;24(8):1627-1638. doi:10.3727/096368914X682422

53. Oertel M. Fetal liver cell transplantation as a potential alternative to whole liver transplantation? *J Gastroenterol*. 2011;46(8):953-965. doi:10.1007/s00535-011-0427-5

54. Dhawan A, Puppi J, Hughes RD, Mitry RR. Human hepatocyte transplantation: Current experience and future challenges. *Nat Rev Gastroenterol Hepatol*. 2010;7(5):288-298. doi:10.1038/nrgastro.2010.44

55. Lee SY, Kim HJ, Choi D. Cell sources, liver support systems and liver tissue engineering: Alternatives to liver transplantation. *Int J Stem Cells*. 2015;8(1):36-47. doi:10.15283/ijsc.2015.8.1.36

56. Krassowski M, Das V, Sahu SK, Misra BB. State of the Field in Multi-Omics Research: From Computational Needs to Data Mining and Sharing. *Front Genet*. 2020;11:1598. doi:10.3389/FGENE.2020.610798/BIBTEX

57. Gruppuso PA, Sanders JA. Regulation of liver development: implications for liver biology across the lifespan. *J Mol Endocrinol*. 2016;56(3):R115-R125. doi:10.1530/jme-15-0313

58. J.M. B, P.A. G, Boylan JM, Gruppuso PA. Uncoupling of hepatic, epidermal growth factor-mediated mitogen- activated protein kinase activation in the fetal rat. *Journal of Biological Chemistry*. 1998;273(6):3784-3790. doi:10.1074/jbc.273.6.3784

59. Anand P, Boylan JM, Ou Y, Gruppuso PA. Insulin signaling during perinatal liver development in the rat. *Am J Physiol Endocrinol Metab*. 2002;283(4 46-4):E844-E852. doi:10.1152/ajpendo.00111.2002

60. Boylan JM, Gruppuso PA. In vitro and in vivo regulation of hepatic mitogen-activated protein kinases in fetal rats. *Am J Physiol Gastrointest Liver Physiol*. 1994;267(6 30-6):G1078-G1086. doi:10.1152/ajpgi.1994.267.6.G1078

61. Boylan JM, Sanders JA, Neretti N, Gruppuso PA. Profiling of the fetal and adult rat liver transcriptome and translatome reveals discordant regulation by the mechanistic target of rapamycin (mTOR). *American Journal of Physiology-Regulatory, Integrative and Comparative Physiology*. 2015;309(1):R22-R35. doi:10.1152/ajpregu.00114.2015

62. Francois-Vaughan H, Adebayo AO, Brilliant KE, Parry NMA, Gruppuso PA, Sanders JA. Persistent effect of mTOR inhibition on preneoplastic foci progression and gene expression in a rat model of hepatocellular carcinoma. *Carcinogenesis*. 2015;37(4):408-419. doi:10.1093/carcin/bgw016

63. Gruppuso PA, Boylan JM, Vaslet CA. Identification of candidate growth-regulating genes that are overexpressed in late gestation fetal liver in the rat. *Biochimica et Biophysica Acta - Gene Structure and Expression*. 2000;1494(3):242-247. doi:10.1016/S0167-4781(00)00244-X

64. Semeraro R, Cardinale V, Carpino G, et al. The fetal liver as cell source for the regenerative medicine of liver and pancreas. *Ann Transl Med*. 2013;1(2). doi:10.3978/j.issn.2305-5839.2012.10.02

65. Pietrosi G, Chinnici C. Report on liver cell transplantation using human fetal liver cells. In: *Methods in Molecular Biology*. Vol 1506. Humana Press Inc.; 2017:283-294. doi:10.1007/978-1-4939-6506-9_20

66. Oertel M. Fetal liver cell transplantation as a potential alternative to whole liver transplantation? *J Gastroenterol*. 2011;46(8):953-965. doi:10.1007/s00535-011-0427-5

67. Tolosa L, Pareja-Ibars E, Teresa Donato M, et al. Neonatal livers: A source for the isolation of good-performing hepatocytes for cell transplantation. *Cell Transplant*. 2014;23(10):1229-1242. doi:10.3727/096368913X669743

68. Guégan JP, Frémin C, Baffet G. The MAPK MEK1/2-ERK1/2 Pathway and Its Implication in Hepatocyte Cell Cycle Control. *Int J Hepatol*. 2012;2012:1-13. doi:10.1155/2012/328372

69. Boylan JM, Francois-Vaughan H, Gruppuso PA, Sanders JA. Engraftment and Repopulation Potential of Late Gestation Fetal Rat Hepatocytes. *Transplantation*. 2017;101(10):2349-2359. doi:10.1097/TP.0000000000001882

70. Haig D. The (Dual) Origin of Epigenetics. *Cold Spring Harb Symp Quant Biol*. 2004;LXIX:1-4. doi:0-87969-729-6/04

71. Noble D. Conrad Waddington and the origin of epigenetics. *Journal of Experimental Biology*. 2015;218(6):816-818. doi:10.1242/jeb.120071

72. Basu A, Tiwari VK. Epigenetic reprogramming of cell identity: lessons from development for regenerative medicine. *Clinical Epigenetics 2021 13:1*. 2021;13(1):1-11. doi:10.1186/S13148-021-01131-4

73. Paksa A, Rajagopal J. The epigenetic basis of cellular plasticity. *Curr Opin Cell Biol*. 2017;49:116. doi:10.1016/J.CEB.2018.01.003

74. Flavahan WA, Gaskell E, Bernstein BE. Epigenetic plasticity and the hallmarks of cancer. *Science (1979)*. 2017;357(6348). doi:10.1126/SCIENCE.AAL2380/ASSET/2FF35D44-7C85-4DB2-A8B2-7DDCFE75DAF1/ASSETS/GRAPHIC/357_AAL2380_F4.JPEG

75. Macchi F, Sadler KC. Unraveling the Epigenetic Basis of Liver Development, Regeneration and Disease. *Trends in Genetics*. 2020;36(8):587-597. doi:10.1016/J.TIG.2020.05.002

76. Li W, Li L, Hui L. Cell Plasticity in Liver Regeneration. *Trends Cell Biol*. 2020;30(4):329-338. doi:10.1016/J.TCB.2020.01.007

77. Huse SM, Gruppuso PA, Boekelheide K, Sanders JA. Patterns of gene expression and DNA methylation in human fetal and adult liver. *BMC Genomics*. 2015;16(1):1-14. doi:10.1186/s12864-015-2066-3

78. Saksouk N, Simboeck E, Déjardin J. Constitutive heterochromatin formation and transcription in mammals. *Epigenetics Chromatin*. 2015;8(1):1-17. doi:10.1186/1756-8935-8-3

79. Gruppuso PA, Boylan JM, Zabala V, et al. Stability of histone post-translational modifications in samples derived from liver tissue and primary hepatic cells. *PLoS One*. 2018;13(9):1-14. doi:10.1371/journal.pone.0203351

80. Pediconi N, Salerno D, Lupacchini L, et al. EZH2, JMJD3, and UTX epigenetically regulate hepatic plasticity inducing retro-differentiation and proliferation of liver cells. doi:10.1038/s41419-019-1755-2

81. Haque O, Yuan Q, Uygun K, Markmann JF. Evolving utilization of donation after circulatory death livers in liver transplantation: The day of DCD has come. *Clin Transplant*. 2021;35(3):e14211. doi:10.1111/CTR.14211

82. Ceresa CDL, Nasralla D, Jassem W. Normothermic Machine Preservation of the Liver: State of the Art. *Curr Transplant Rep*. 2018;5(1):104-110. doi:10.1007/S40472-018-0186-9/FIGURES/1

83. Gruppuso PA, Sanders JA. Regulation of liver development: implications for liver biology across the lifespan. *J Mol Endocrinol*. 2016;56(3):R115-R125. doi:10.1530/jme-15-0313

84. Gordillo M, Evans T, Gouon-Evans V. Orchestrating liver development. *Development*. 2015;142(12):2094-2108. doi:10.1242/DEV.114215

85. Shiojiri N, Lemire JM, Fausto N. Cell Lineages and Oval Cell Progenitors in Rat Liver Development. *Cancer Res*. 1991;51(10):2611-2620. Accessed November 16, 2022.

https://aacrjournals-org.revproxy.brown.edu/cancerres/article/51/10/2611/496566/Cell-Lineages-and-Oval-Cell-Progenitors-in-Rat

86. Boylan JM, Francois-Vaughan H, Gruppuso PA, Sanders JA. Engraftment and Repopulation Potential of Late Gestation Fetal Rat Hepatocytes. *Transplantation*. 2017;101(10):2349-2359. doi:10.1097/TP.0000000000001882

Chapter 2:
Long-Term Persistence of Fetal Hepatocyte Gene Expression and Histone Modification Signatures Following Transplantation to Adult Liver

Long-Term Persistence of Fetal Hepatocyte Gene Expression and Histone Modification Signatures Following Transplantation to Adult Liver

Anders W. Ohman [1], Megan G. Heaney [2], Joan M. Boylan [2], John C. Santiago [1], Juliette A. Morris [3], Jeannie M. Camarillo [3], Neil L. Kelleher [3], Philip A. Gruppuso [1,2], Jennifer A. Sanders [1,2]

[1] Brown University, Division of Biology and Medicine, Providence, RI, USA
[2] Rhode Island Hospital, Department of Pediatrics, Providence, RI, USA
[3] Northwestern University, National Resource for Translational and Developmental Proteomics, Chicago, IL, USA

Introduction

Hepatic cell transplantation (HCT) offers a potential alternative to whole-organ liver transplantation. Unfortunately, adult cells only remain functionally effective for a period of months post-transplant and do not continue to proliferate, thus relegating this approach to use as a bridge to orthotopic transplant rather than a curative therapy itself. [1] By contrast, fetal hepatocytes have been demonstrated to durably persist and proliferate in animal models and in human clinical trials. [2,3] Previous work in the dipeptidyl peptidase-4 (DPPIV)/Mitomycin-C rat model has demonstrated that transplanted embryonic day 14 (ED14) hepatocytes are able to reconstitute a liver that has undergone partial hepatectomy (PH). [4] Douglas Hixson's group has further shown that ED16 fetal liver cells sorted for cholangiocyte markers were able to reconstitute a PH liver in the same model. [5] These cells lost ductal markers and gained hepatocyte markers, proliferating increasingly over 1 year to make up 70% of the host rat liver. We have previously compared activation of the major signaling pathways that regulate cellular proliferation and growth in adult rat hepatocytes to fetal rat hepatocytes at ED19. [6] These studies led to the conclusion that late gestation fetal hepatocyte proliferation is largely independent of mitogenic signaling pathways, which was demonstrated to lead to a proliferative competitive growth advantage in the DPPIV rat model. [7] We observed that transplanted ED19 cells sorted for hepatic lineage markers continued to replicate for at least 10 months with a proliferative advantage over the remaining adult hepatocytes that resulted in their eventually comprising up to 35% of a healthy, functional liver.

The present study was aimed at characterizing the phenotype of the transplanted fetal colonies at 10 months to gain a preliminary understanding of the mechanisms underlying the ability of fetal hepatocytes to competitively repopulate an adult liver. We hypothesized that epigenetic mechanisms drive the retention of the fetal hepatocyte phenotype, thus conferring a growth advantage to the fetal cells. By utilizing laser-capture microdissection (LCM), we

characterized the transcriptome and histone post-translational modification (hPTM) signatures of fetal-derived colony or adult host liver tissue from our transplant model 10 months following fetal hepatocyte transplantation. These results were compared to parallel analyses performed on hepatocytes isolated from adult and ED19 fetal liver.

Materials and Methods

Animals

ED19 fetal hepatocytes and adult hepatocytes were isolated as previously described from American and German Fischer 344 (F344) rats, respectively. [8,9] The male and female fetuses harvested from American F344 rats express wild type dipeptidyl peptidase-4 (DDPIV+). Using monoclonal antibodies directed against leucine aminopeptidase (LAP), a hepatic cell surface marker, and OC.2, a hepatic oval cell and ductal cell surface marker, immunopurified subpopulations of fetal cells were obtained. [7] The three populations, LAP+ (no OC.2 selection), LAP+/OC.2+, and LAP+/OC.2− were verified by immunofluorescence staining.

The LAP+ fetal hepatocytes were transplanted, as previously described, via splenic injection into partial hepatectomized male German F344 rats that express an inactive form of DPPIV (DPPIV−) (Figure 1A). [7] Ten months following fetal cell transplantation, animals were euthanized and livers flash-frozen in a hexane-acetone bath before being stored at −80°C. Cryopreserved blocks from 5 biological replicates of 10-month post-transplant rat liver tissue were cut into 8μm sections by cryostat (Leica Biosystems, Wetzlar, DE, USA) and placed onto Arcturus PEN Membrane slides (Applied Biosystems, Waltham, MA, USA). Slides were stored at −80°C with desiccant pellets (W A Hammond Drierite Co., Xenia, OH, USA).

All animals were housed under standard conditions with access to food and water *ad libitum* and euthanized by exsanguination under isoflurane anesthesia. Studies were performed

in accordance with the guidelines of the National Institutes of Health and the Rhode Island Hospital Institutional Animal Care and Use Committee.

Laser Capture Microdissection

Slides were removed from −80°C storage and thawed under sodium phosphate buffer (0.1M). Tissue was encircled using a hydrophobic immunopen and incubated at room temperature for 15 minutes with fresh stain (1.5 mg Gly-Pro 4-methoxy-β-naphthylamide hydrochloride, 5 mg Fast Blue BB Salt, 500 µL Dimethylformamide, 0.1M sodium phosphate buffer). Stain was decanted and slides were dipped into DEPC water to rinse and then air dried, after which they were quickly transferred in small batches to the laser capture instrument. When being prepared for RNA-Seq, buffer and stain were prepared with 200 units/mL of RNasin Ribonuclease Inhibitor (Promega Corporation, Madison, WI, USA). Slides were assessed for the presence of stained colonies via ArcturusXT (Applied Biosystems). Colonies with hepatocyte morphology were cut and bound onto Arcturus CapSure Macro caps (Applied Biosystems). Unstained tissue sections were captured from the same slides onto different caps, collecting positive-stained fetal-derived colonies and negative-stained surrounding adult host tissue from the same biological replicates. When possible, multiple areas of tissue of the same type were captured onto the same cap. Photographs of each cap were analyzed via ImageJ [10] to calculate total tissue area (Figure 1B).

RNA Preparation & Next Gen Sequencing

Isolation of total RNA from adult and immunopurified fetal hepatocytes was accomplished using pellets of approximately 1 million cells and the RNeasy Mini kit (QIAGEN, Hilden, DE). Quality was assessed by NanoDrop One (Thermo Fisher Scientific, Waltham, MA, USA). One sample with a low 260/280 score was passed through the RNA Clean & Concentrator kit (Zymo Research, Irvine, CA, USA). For preparation of total RNA from laser captured tissue samples, tissue on individual laser capture microdissection caps was digested

into extraction buffer and RNA was isolated using the PicoPure RNA Isolation Kit (Applied Biosystems). When the amount of laser captured tissue for each biological replicate was in excess of 24 mm^2, each pooled sample was passed through the RNA Clean & Concentrator kit (Zymo Research). Paired samples from 4 biological replicates were submitted for Next Generation Sequencing at GENEWIZ (South Plainfield, NJ, USA). RNA quality was assessed using a Qubit 2.0 Fluorometer (Life Technologies, Carlsbad, CA, USA) and Agilent TapeStation 4200 (Agilent Technologies, Palo Alto, CA, USA).

RNA library preparation and sequencing reactions were conducted at GENEWIZ, LLC. (South Plainfield, NJ, USA). Sorted cell RNA sequencing libraries were prepared using the NEBNext Ultra RNA Library Prep Kit for Illumina following manufacturer's instructions (New England Biolabs, Ipswich, MA, USA). Laser-capture microdissected RNA sequencing libraries were prepared using the SMARTer Stranded Total RNA-Seq Kit v2 - Pico Input Mammalian (Takara Bio, Kusatsu, Shiga, JP). Sequencing was performed on an Illumina HiSeq 4000 (Illumina, San Diego, CA, USA). RNA-Seq data for LCM and isolated cell samples were generated by GENEWIZ using their standard methods. Briefly, raw sequence reads were trimmed to remove adapter sequences and nucleotides with poor quality using Trimmomatic v.0.36. Sequences were then aligned to the *Rattus norvegicus* reference genome available on ENSEMBL (Rnor 6.0) using STAR aligner v.2.5.2b. [11,12] Hit counts were calculated by using featureCounts from the Subread package v.1.5.2 and were summarized and reported using the gene_id feature in the annotation file. [13] Unique reads that fell within exon regions were counted, and count tables were transferred to our servers for analysis. The resulting libraries are available in the Gene Expression Omnibus with Accession No. GSE201757.

Histone Extraction and hPTM Mass Spectrometry

Histone modification profiling was performed at Northwestern University Proteomics Core using their Epiproteomic Histone Modification Panel. Histones were extracted from adult

and fetal hepatocyte nuclei as previously described. [14] Briefly, the nuclear pellet was washed twice in Buffer B (15mM HEPES, pH 7.5, 30% sucrose, 60mM KCl, 15mM NaCl, 2mM EDTA, 0.5mM EGTA, 14mM 2-mercaptoethanol with freshly added 10mM sodium butyrate, 10 µg/mL leupeptin, 10 µg/mL aprotinin and 24.4 µg/mL 4-(2-aminoethylbenzenesulfonyl fluoride) hydrochloride then histones were extracted using 0.2N sulfuric acid. Extracted histones were chemically derivatized using propionic anhydride and digested with trypsin. [15] For LCM samples, CapSure caps were nested into empty 0.5 mL microcentrifuge tubes and frozen at -80°C. When total adult and fetal tissue for each replicate collected reached in excess of 24mm^2, the cap membrane with bound tissue was removed and pooled into 1.5 mL microcentrifuge tubes and stored at −80°C until preparation. Histones were extracted directly from tissue with the addition of 0.2N sulfuric acid, chemically derivatized, and digested as previously described. [16] All data were acquired on a Triple-Stage Quadrupole Quantiva mass spectrometer according to previous published methods. [17] Three technical replicates per sample were injected for analysis in Skyline. [18] Quantified hPTM percent relative abundance for all samples was calculated from the total peak area and the results were averaged to produce a single value for each histone mark per sample group. Statistically significant marks were determined via two-tailed ANOVA in R using the limma package. [19]

Bioinformatics Analysis

RNA-Seq and hPTM datasets were further analyzed using R and RStudio. [20,21] Differential gene expression analysis was conducted on our RNA-Seq count tables using edgeR. [22] Raw read counts were normalized using the Trimmed Mean of M method following removal of low-count genes as selected by the filterByExpr function. The significance cutoff for differential gene expression was set to a Benjamini-Hochberg false-discovery rate (FDR or q-value) < 0.05. Visualizations of RNA-Seq data were created with the following R packages: 2D Principal Component Analysis (PCA) plots by ggplot2; [23] 3D PCA plots by plot3D; Volcano plots

by EnhancedVolcano; [24] and Gene Ontology (GO) by GOrilla and RRVGO.[25,26] Visualizations of hPTM data were created with the following R packages: Bar graphs by ggplot2;[23] 3D PCA plots by plot3D; and Dotplot Heatmaps by heatmaply. [27] Transcriptomic data were analyzed with the use of Ingenuity Pathway Analysis [28] (IPA; QIAGEN). For analysis of Upstream Regulators and Canonical Pathways, input consisted of differentially expressed genes (DEGs) with FDRs < 0.05. ComBat-seq was employed to batch correct RNA-Seq libraries generated from polyA-selection and rRNA-depletion. [29,30] The R scripts used to generate these data and figures have been deposited on GitHub at https://github.com/SandersLaboratory.

Results

Fetal-derived Colony and Adult Host Gene Expression

When LCM tissue transcriptome results were subjected to PCA (Figure 2A), RNA-Seq data segregated by adult host (n = 4) versus fetal-derived colony (n = 4) along Principal Component 1 (PC1; 34.8% of variation). We observed no grouping by biological replicate. PCA of sorted hepatocytes (Figure 2B) showed 3 distinct groups of samples: adult hepatocytes (n = 5), LAP+/OC.2+ fetal hepatocytes (n = 5), and a group consisting of both LAP+ and LAP+/OC.2− fetal hepatocytes (n = 10, 5 of each). When our laser-captured and cell isolate RNA-Seq datasets were batch corrected and plotted together by PCA (Figure 2C), the laser capture samples plotted between the cluster of adult hepatocytes and the cluster consisting of LAP+ and LAP+/OC.2− fetal hepatocytes, with the LAP+/OC.2+ cells clustering distinctly from all other groups.

We next identified DEGs that accounted for the separation of these sample clusters. When fetal-derived colonies were compared to adult host tissue, a total of 953 DEGs were detected, with the majority (786) being more highly expressed in the colonies and a smaller group (167) being more highly expressed in adult host tissue (Figure 3A). When fetal and adult hepatocytes were compared (Figure 3B), a higher number of significant DEGs were found

between LAP+/OC.2+ and adult hepatocytes (10,698) than between LAP+/OC.2− and adult hepatocytes (8,109). When these cellular DEGs were examined for the presence of DEGs found in the LCM comparison, a larger total number were found to be shared with LAP+/OC.2+ fetal hepatocytes (313) than LAP+/OC.2− hepatocytes (240), reflecting the same proportion of LCM DEGs to cellular DEGs (2.9%). The majority (90.7%) of these overlapping significant genes had the same pattern of expression in adult or fetal hepatocytes as in post-transplant adult host or fetal-derived colony tissue.

To test the hypothesis that these DEGs are relevant to the competitive growth advantage of the transplanted fetal cells, significant LCM DEGs were analyzed by Gene Ontology. The input for this analysis consisted of two sets of significant genes (FDR ≤ 0.05), corresponding to genes with higher expression in either fetal-derived colony (logFC > 0) or adult host tissue (logFC < 0). The output was distinct GO term profiles for each set (Figure 3C, Supplemental Table 1, Supplemental Figure 1). Adult host DEGs showed significant ($P < 10^{-7}$) enrichment of GO terms in the category “metabolic process”. The most significant ($P < 10^{-11}$) subterms were “oxoacid metabolic process” and “lipid metabolic process”. Fetal-derived colony DEGs showed significant ($P < 10^{-7}$) enrichment of terms related to ion transport and transmembrane transport, with the most significant ($P < 10^{-17}$) being “ion transmembrane transport,” “transmembrane transport,” and “inorganic ion transmembrane transport.” A separate category of highly significant ($P < 10^{-10}$) terms included “nervous system process” and “sensory perception.” We performed additional gene set exploration by using Ingenuity Pathway Analysis (IPA) on the same significant DEGs from fetal-derived colonies (Supplemental Table 2). This yielded a number of significant Upstream Regulators, including the ion transporter KCNK9 (p value of overlap = 9.36×10^{-4}). IPA also identified significant Canonical Pathways, with the two most significant being Gustation Pathway ($p = 7.75 \times 10^{-11}$, z-score = 4.426) and Calcium Signaling ($p = 2.75 \times 10^{-9}$, z-score = 4.243). The Calcium Signaling pathway was flagged as

activated due to 26 associated molecules having increased fold change in the fetal-derived colony DEGs. The 10 most significant of these were voltage-gated calcium channels (VGCCs), such as subunits of CACNA1, CACNA2, CACNG3 and CACNG7. Genes more highly expressed in the surrounding adult liver tissue did not yield any notable IPA results.

Histone Post-Translational Modification Quantification by Mass Spectrometry

Given the role of histone PTMs in regulating chromatin structure and subsequently gene expression and cell phenotype, we hypothesized that histone PTMs would differ between fetal and adult hepatocytes and the profile would be maintained post-transplant. When raw hPTM abundance data from LCM and cell samples (Supplemental Table 3) were plotted by PCA for abundance of all detected marks in common (Figure 4A), results were distinctly segregated into 4 groups: adult host (n = 5), fetal-derived colony (n = 5), isolated adult hepatocytes (n = 3), and isolated fetal hepatocytes (n = 9, 3 each of LAP+, LAP+/OC.2+, and LAP+/OC.2−). A separation between LCM and cellular sample groups occurred on PC1 (43.44% of variation), and a separation occurred along Principal Component 2 (PC2; 19.5% of variation) related to adult or fetal status. By examining the Euclidean Distance of Group Centroids for the 4 groups across PCs 1-3 (76.28% of variation), we found that the fetal-derived colony cluster was closer to adult host (d = 8.56) than all fetal hepatocytes (d = 12.62), but least like adult hepatocytes (d = 13.65). When examining the centroids of specific subgroups, fetal-derived colonies were closest to LAP+ (d = 11.11) than LAP+/OC.2− (d = 12.66) or LAP+/OC.2+ (d = 14.17) fetal hepatocytes. Samples in 3 of the 4 groups were tightly clustered, while post-transplant fetal-derived colony samples plotted in a continuum from near the cluster of post-transplant adult host samples up PC2 in the direction of the pre-transplant fetal hepatocyte cluster.

In order to identify the specific hPTMs that are responsible for the distinctive PCA profile of fetal-derived colonies, we examined significant abundance differences of specific hPTMs for the following comparisons: fetal-derived colonies versus surrounding adult liver, and pre-transplant

adult versus LAP+, LAP+/OC.2−, or LAP+/OC.2+ fetal hepatocytes (Figure 4B). A total of 92 hPTMs were quantitated, but due to the lower quality of samples derived from LCM, only 69 of these marks could be confidently differentiated from background noise. Of those, 33 were found to be significantly different in abundance between fetal-derived colonies and adult host (Supplemental Table 4); 13 of those were significant in both our pre- and post-transplant data sets. The majority (11/13) of these hPTMs had a similar abundance pattern pre- and post-transplant; 4 (H3.1:K27un, H3.3:K27un, H3.3:K36me2, H3.1:K27me1) were more abundant in fetal-derived colony or fetal hepatocytes, and 7 (H3:K18me1, H3.3:K27me3, H3.1:K27me2, H3.3:K27me2, H3.3:K36me1, H3.1:K27me3, H3.1:K36me1) were more abundant in adult host or adult hepatocytes. The 2 remaining marks (H3:K9un, H3.1:K36un) were unmodified histones that had higher abundance in fetal hepatocytes than adult hepatocytes, but also higher abundance in adult host than fetal-derived colonies.

Discussion

Our previous studies established that fetal hepatocytes formed colonies that persisted for at least 10 months following transplantation. [7] The present studies establish that these fetal hepatocyte-derived colonies retain transcriptomic characteristics of fetal hepatocytes, as indicated by the pattern of gene expression. We interpret the persistence of a fetal phenotype for such a long period in the adult liver milieu as suggesting that epigenetic factors maintain this phenotype. Indeed, our analysis of histone post-translational modifications is consistent with persistence of a fetal histone code. We speculate that the retained transcriptomic and epigenomic features of the transplanted fetal cells are connected to specific cellular processes that may enable colonies derived from fetal hepatocytes to sustain a growth advantage relative to the surrounding adult hepatocytes.

The differential expression analysis of our RNA-Seq results found almost a thousand DEGs comparing the fetal-derived colonies and adult host tissue. Hundreds of these were found

to also be differentially expressed between fetal and adult hepatocytes: 261 in LAP+/OC.2− vs. adult hepatocytes and 340 in LAP+/OC.2+ vs. adult hepatocytes. The most significant GO terms resulting from the DEGs expressed higher in adult host tissue were related to a variety of metabolic processes. This finding is consistent with a previous report that found transplanted fetal hepatocytes to be metabolically immature compared to adult hepatocytes. [31] In the larger set of overexpressed fetal-derived colony genes, the most significant GO terms were related to ion transport across the plasma membrane. Ion channels and transporters have well established regulatory roles for the cell cycle and other aspects of cell physiology related to both normal cell proliferation and malignant growth. [32,33] Ion-mediated effects include controlling cell pH and volume, the release of growth factors, and interactions with extracellular matrix. An independent examination of this gene set by IPA confirmed a number of ion transporters as activated Upstream Regulators. IPA also identified Calcium Signaling as a highly significant canonical pathway in the fetal-derived colonies. Calcium plays a central role in cell signaling that relates to cellular growth and development.[32] Previous literature has demonstrated the relevance of calcium in both normal and malignant cell growth and proliferation, and has identified a number of the same VGCCs that we identified in fetal-derived colonies as being upregulated in a variety of cancer types. [34]

The second largest GO term category for fetal-derived colony DEGs is “visual perception.” Identification of this GO term was accounted for by the differential expression of genes such as sodium/calcium channels and receptors that are relevant to this GO term but reflect significant expression of target genes that are involved in transporter activity. We see reinforcing evidence for this when looking at the same data via IPA, such as the detection of significant ion channels among the Upstream Regulators, as well as activated (z-score > 2) canonical pathways identified as Gustation Pathway and Calcium Signaling. While gustation may be a pathway with no functional relevance to liver, inspection of the result reveals that the

pathway was identified due to differential expression of calcium, potassium, and sodium voltage-gated channel subunits in the dataset. Several other unexpected canonical pathways, such as neurological and muscular processes, similarly reflect the higher expression of genes related to ion transport in the dataset.

A larger number of total DEGs were found during differential expression analysis between fetal and adult hepatocytes than between laser-captured fetal-derived colonies and surrounding adult tissue. This may reflect the maturation of transplanted ED19 cells to a more adult-like phenotype. However, a caveat to this interpretation is that it may also be accounted for by differences in sample preparation; our laser-captured RNA went through rRNA-depletion library preparation while cell pellets went through a polyA-selection library preparation. Our histochemical DPPIV stain and the laser capture process had to be performed at room temperature and resulted in smaller volumes of collected tissue than our cell isolations. LCM samples had a lower quantity of total RNA as well as lower integrity when assessed prior to sequencing. Since rRNA-depletion library preparation is known to provide better sequencing results for degraded RNA, [35] we employed this technique for our LCM samples. However, rRNA-depletion typically results in a smaller number of detected protein-coding genes than polyA-selection techniques. [36] The SMARTer Stranded library preparation kit used for our LCM samples was found to result in 55% fewer DEGs than a polyA-selection library preparation; however, consistent results between preparation techniques were observed for pathway enrichment. [37]

Our previous studies have identified a subpopulation of ED19 LAP+ fetal hepatocytes which express the ducal marker OC.2 and found that these cells have a distinct gene expression profile from LAP+ cells that lack ductal marker expression. These LAP+/OC.2+ cells may comprise a residual population of bipotential progenitor cells that are less differentiated than LAP+/OC.2− fetal hepatocytes. Due to cellular stress incurred during immunopurification,

dual-sorted populations of fetal hepatocytes were not found to be suitable for transplantation. This restricted us to transplanting cells that had only been sorted for LAP positivity. PCA indicates that the transplanted population that derives from these cells retains fetal gene expression patterns 10 months post-transplant. However, when we compared the LCM DEGs to the sorted fetal and adult hepatocytes, we saw greater similarities in gene set overlap between the post-transplant fetal-derived colony gene expression and the LAP+/OC.2+ fetal hepatocytes than with LAP+/OC.2− hepatocytes. This may indicate that the fetal-derived colonies are derived from the subpopulation of transplanted LAP+ hepatocytes that are also OC.2+. Simper-Ronan et al. used the DPPIV model to transplant liver cells based on the presence of certain ductal markers, including OC.2, and demonstrated that these cells were able to repopulate the liver. [5] This lends credence to the speculation that LAP+/OC.2+ fetal cells may have disproportionately contributed to the repopulation.

Our lab had previously used the suppression subtractive hybridization (SSH) technique to identify genes that are overexpressed in ED19 liver compared with adult liver. [38] This early PCR-based technique identified six genes that were potentially growth-regulating in fetal hepatocytes (Grb10, Eps15, nuc2+ [Cdc27], Cdc25b, Ppara, and dUTPase [Dut]). We have examined gene expression of these genes in our RNA-Seq datasets (Figure 5) to determine their potential role in the fetal colony proliferative advantage. We found that 4 of the 6 genes (Grb10, Cdc25b, Ppara, and Dut) were expressed significantly higher in LAP+ and LAP+/OC.2− cells relative to adult hepatocytes. The same 4 were significantly expressed in LAP+/OC.2+ cells, but with Ppara having a lower expression in fetal than adult cells. While these genes may play an important role in regulating growth and proliferation of fetal hepatocytes, we found that the post-transplant fetal colonies did not have significant expression of any of these genes. Regulation of the fetal phenotype is likely due to broader epigenetic regulatory mechanisms.

Our hPTM results indicate that after 10 months, post-transplant fetal-derived colonies have a global histone profile that has shifted towards the abundance pattern seen in surrounding adult host tissue. However, they also retain certain marks in common with the pre-transplant fetal hepatocyte profile. Thirteen PTMs were found to have significantly different relative abundance between fetal-derived colonies and adult host tissue as well as between fetal and adult hepatocytes, with the majority of these marks having consistent abundance trends in both comparisons. We speculate that these retained differences may be drivers of the competitive growth advantage seen in fetal hepatocytes post-transplant. These differentially abundant hPTMs are all on Histone H3, which has documented associations with gene transcription activity. Specifically, H3K36me2 and H3K27me1 are both found to be more abundant in fetal-derived colonies and hepatocytes, and has annotations associated with promoting gene transcription. [39,40] Investigating the specific genes that are positively regulated by these marks will allow us to explore their associations with the significant pathways such as ion transporters which were identified in our transcriptomics analysis. In addition to those two marks, all unmodified histones (K9, K27, and K36) were found to be more abundant in fetal hepatocytes, with the majority of these (H3.1 and H3.3 K27un, H3.3 K36me2, and H3.1 K27me1) also more abundant in fetal-derived colonies. Unmodified histones typically reflect the synthesis of new histones, indicating a relationship between their abundance and cellular proliferation. [41] All of the other significant marks are methylation of sites which have documented relationships with repression of gene transcription. [42,43] Together, we see evidence for a histone profile in fetal-derived colony tissue with upregulation of marks that promote gene expression and downregulation of repressive marks relative to adult host.

Unlike other types of transplanted fetal cells, such as cells of neuronal origin, which are understood to typically continue to terminally differentiate along committed lineages,[44–46] our transplanted ED19 fetal hepatocytes retain aspects of the fetal transcriptome and epigenome for

10 months following transplantation. Due to their unique regenerative behavior, hepatocytes are known to be particularly plastic; they are poised to re-enter the cell cycle upon liver injury, they are capable of dedifferentiation and transdifferentiation, and they consist of subpopulations particularly suited for increased proliferation. [47] This plasticity may enable fetal hepatocytes to engraft and repopulate an injured adult liver while still retaining a competitive proliferative advantage. A greater understanding of the mechanisms underlying the retention of this phenotype may help to improve HCT outcomes and inform induced pluripotent stem cell (iPSC) differentiation techniques to prime hepatocytes for optimal transplantation. We hypothesize that the differential activity of ion channels in the transplanted fetal hepatocytes may be responsible for their long-term competitive growth advantages over adult hepatocytes, and these pathways could be regulated by the retained histone marks we see in the fetal-derived colonies. This could open avenues for therapeutic induction prior to cell transplantation, to better prime hepatocytes for long-term survival. Our future work will explore the link between specific DEGs and the differentially abundant hPTMs that may be regulating them via CUT&Tag analysis of these specific histone marks.

Figures

A

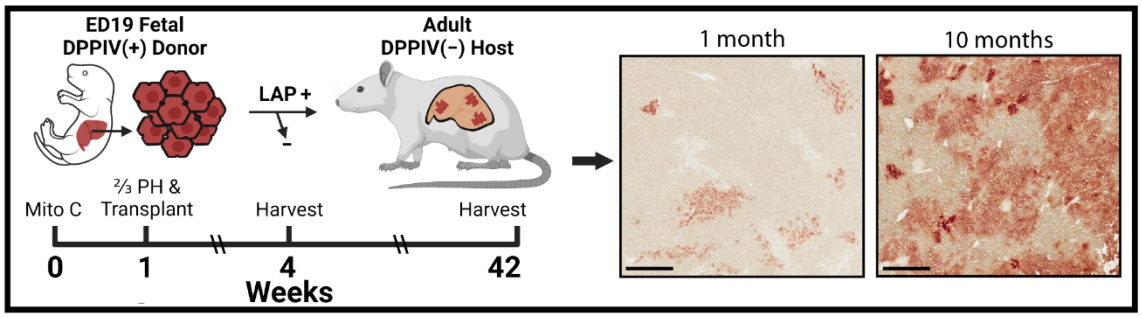

B

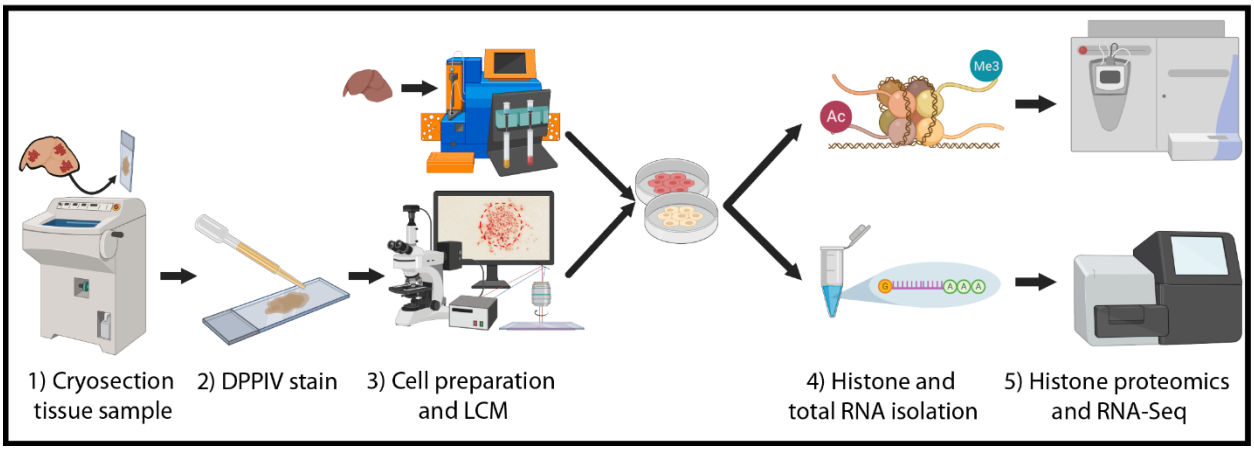

Figure 1. Diagram of the DPPIV transplant model and sample processing pipeline. (A) DPPIV+ ED19 fetal livers were harvested and digested with collagenase. Fetal hepatocytes were immunopurified using an anti-LAP antibody. LAP+ fetal hepatocytes were transplanted via splenic injection into a partial hepatectomized DPPIV- adult rat that had been pretreated with mitomycin C. Livers were harvested at 4 and 42 weeks post-transplant. Histochemical staining for DPPIV activity revealed a significant increase in the proportion of DPPIV+ fetal-derived colonies over time. Scale bar = 500µm. (B). Cryosectioned liver blocks obtained 42 weeks post-transplant were stained for DPPIV activity prior to undergoing laser capture microdissection to isolate fetal-derived colonies and surrounding adult host hepatocytes. Freshly isolated adult hepatocytes and immunopurified fetal cell populations along with microdissected tissue were processed for RNA-Seq and hPTM analysis by mass spectrometry. Created with BioRender.com

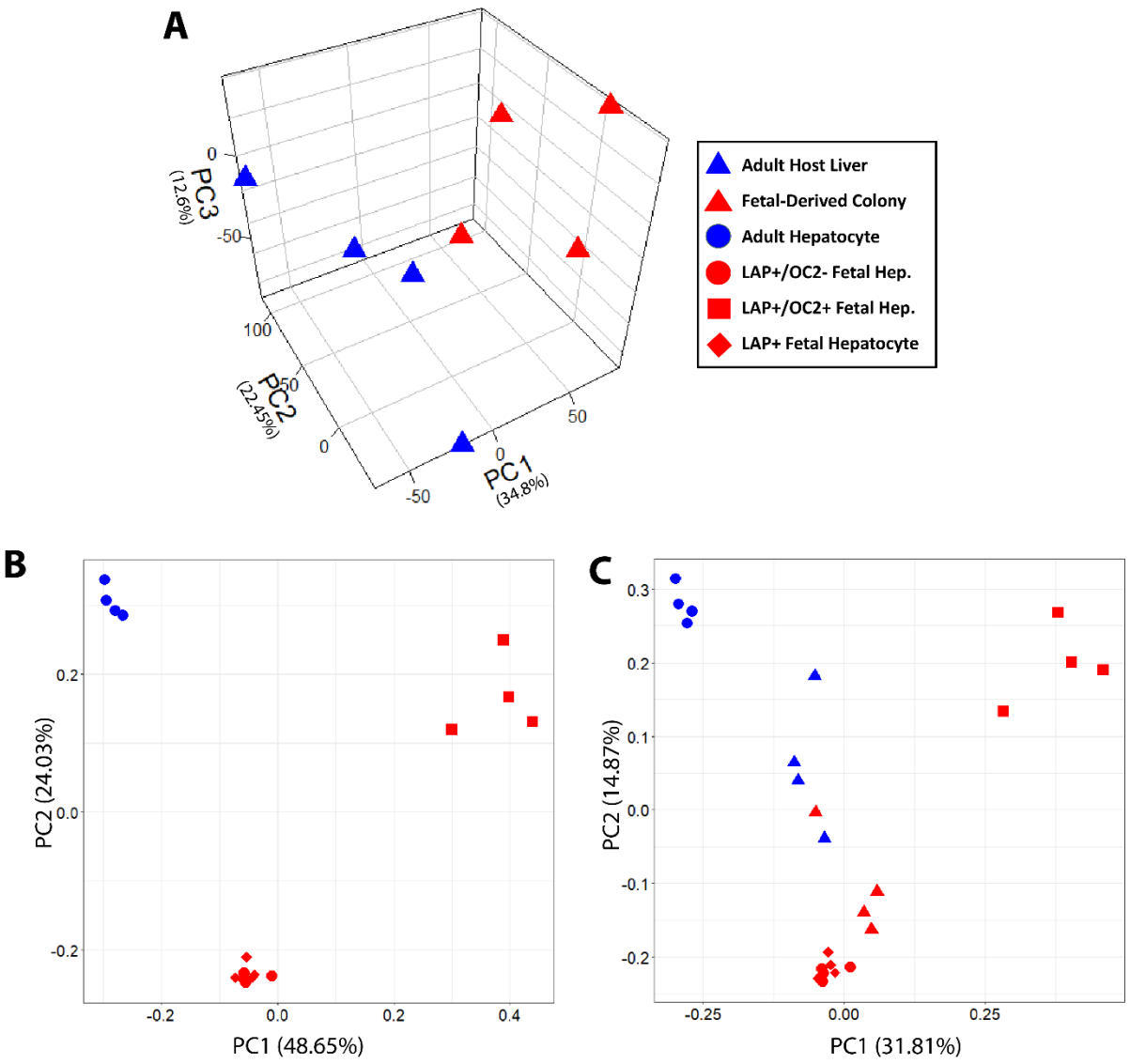

Figure 2. RNA-Seq Principal Component Analyses show that the transcriptome profile of fetal-derived colony samples was distinct from all other sequenced groups. (A) 3D PCA of paired host/colony libraries from four biological replicates. (B) 2D PCA of four biological replicates of freshly isolated adult hepatocytes and LAP+, LAP+/OC.2− and LAP+/OC.2+ fetal hepatocyte subpopulations. Adult and LAP+/OC.2− fetal hepatocytes clustered distinctly, while LAP+ and LAP+/OC.2− fetal hepatocytes clustered closely together. (C) 2D PCA of batch-corrected cellular and LCM data, showing integration of LCM data between the adult hepatocyte and the LAP+ and LAP+/OC.2− fetal hepatocyte clusters.

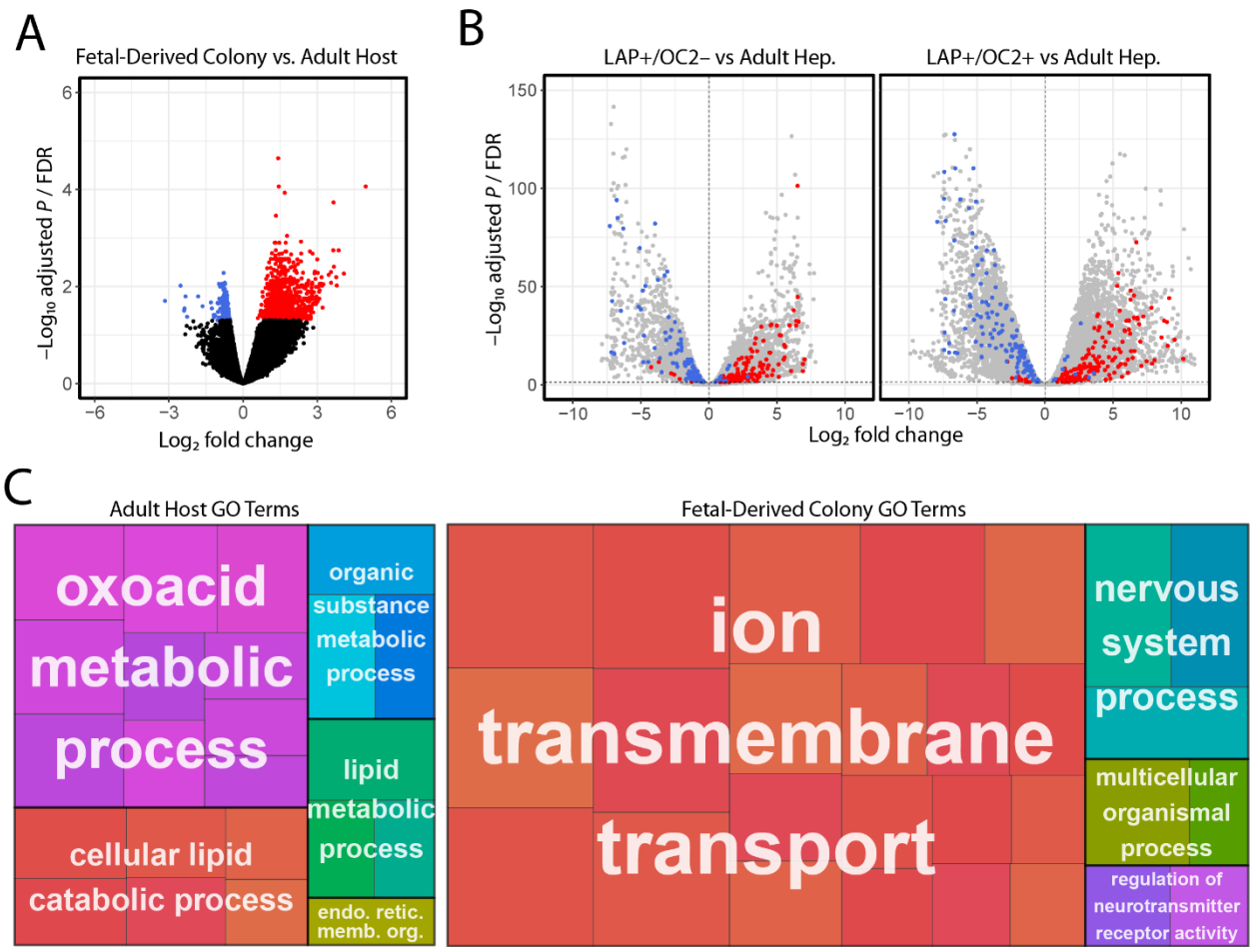

Figure 3. RNA-Seq Differential Expression Analysis and Gene Ontology revealed distinct sets of genes and biological processes expressed in fetal-derived colonies compared to adult host. (A) Volcano plot of differentially expressed genes (DEGs) in LCM fetal-derived colonies and surrounding adult host tissue. 953 significant (FDR < 0.05) differences existed 10 months after transplant, with the majority of these found in fetal-derived colonies. Blue dots indicate significant DEGs which were expressed higher in adult host tissue, while red dots were expressed higher in fetal-derived colony. Black dots were non-significant genes. (B) Volcano plots of DEGs in adult hepatocytes and LAP+/OC.2− (left) and LAP+/OC.2+ (right) fetal hepatocytes, with LCM DEGs superimposed. Red dots represent significant DEGs with higher expression in fetal-derived colonies, blue dots represent significant DEGs with higher expression in adult host tissue, and gray dots represent DEGs in the cellular analyses that were not significantly differentially expressed in the LCM analysis. (C) Gene Ontology analysis of significant DEGs. Distinct patterns were found in the two gene sets, with metabolic processes enriched in host tissue and ion transmembrane transport enriched in the fetal-derived colonies.

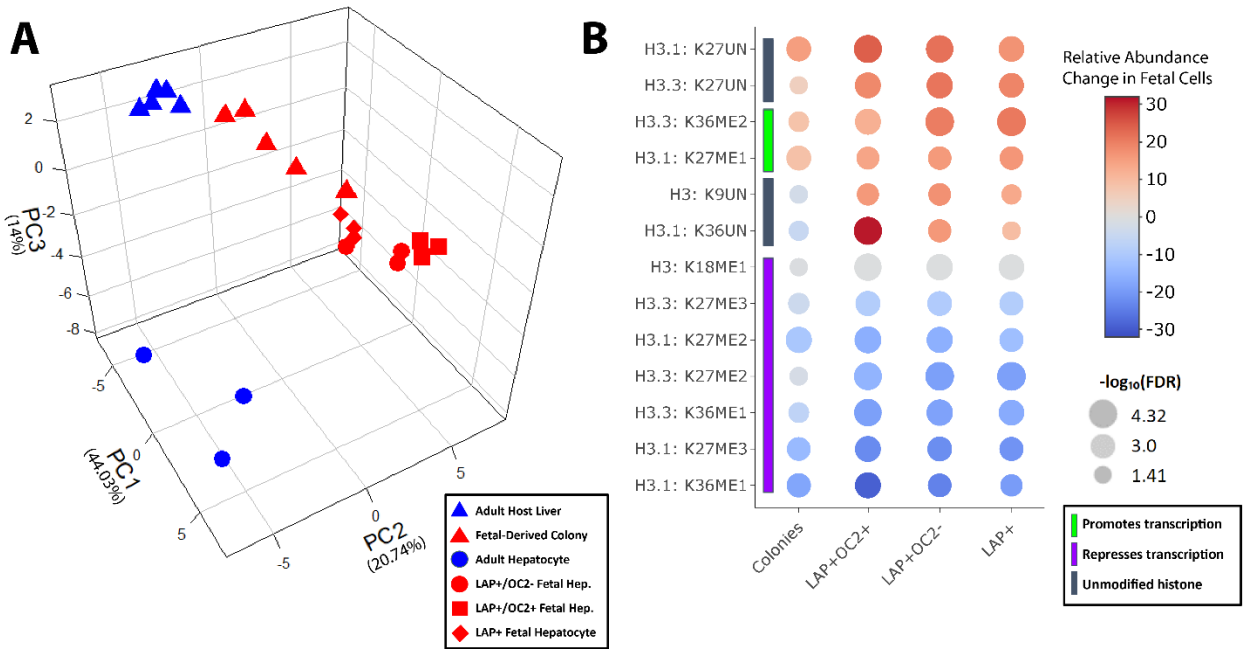

Figure 4. hPTM results show that the unique plotting of fetal-derived colony samples by PCA is driven by retention of fetal hepatocyte histone mark abundance profiles. (A) 3D PCA plot of relative histone post-translational modification (hPTM) abundance for isolated adult and immunopurified fetal hepatocytes as well as post-transplant host tissue and fetal-derived colonies. Distinct clusters emerged for all groups, with colonies being observed in a heterogeneous, intermediate state between fetal hepatocytes and adult host tissue. (B) Clustered dotplot of the 13 hPTMs that are significantly different between freshly isolated adult and immunopurified fetal hepatocytes and adult host and fetal-derived colonies. The majority of hPTMs that were significantly different at both pre- and post-transplant had consistent abundance patterns in both states, with the exception of two unmodified histone marks.

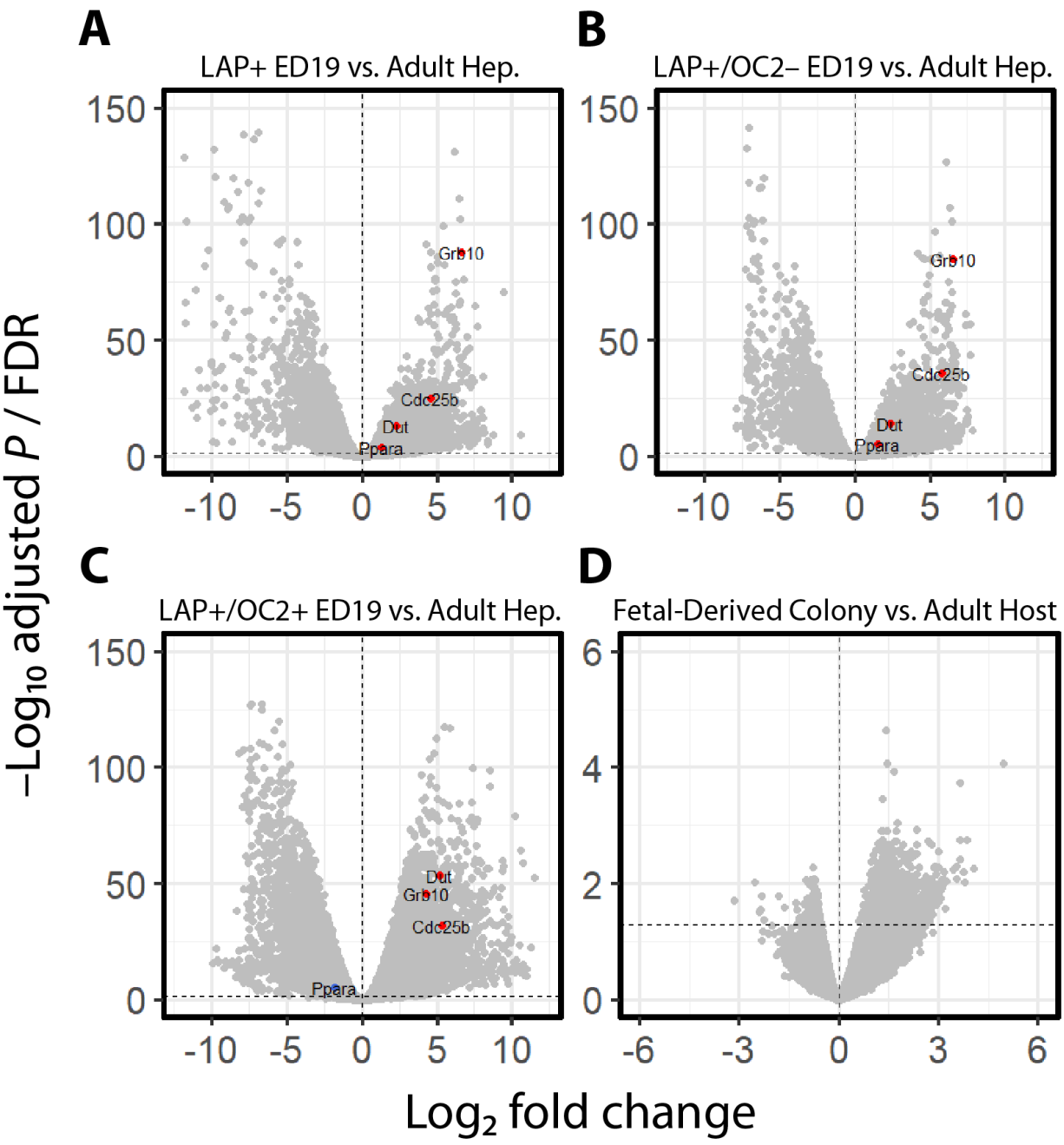

Figure 5. Verification of putative growth regulating genes. Volcano plots of our RNA-Seq data showing the presence of 6 genes that were previously identified by SSH as being overexpressed in late gestation fetal rat liver. When compared to adult hepatocytes, LAP+ (A) and LAP+/OC.2− (B) fetal hepatocytes had significant upregulation of 4 of the 6 SSH genes. LAP+/OC.2+ (C) cells had upregulation of 3 SSH genes and downregulation of 1, while post-transplant fetal-derived colonies (D) had no significant expression of these 6 genes relative to adult host. Red dots represent significant DEGs with higher expression in fetal cells or colonies, blue dots represent significant DEGs with higher expression in adult cells or host tissue.

Supplemental Information

Supplemental data tables are available on the Brown Digital Repository at: https://doi.org/10.26300/6ghh-jc29.

Supplemental Table 1. Gene Ontology results. GOrilla (Gene Ontology enRIchment anaLysis and visuaLizAtion tool) was utilized for organism Rattus norvegicus. The input files were two unranked lists of genes by ENSEMBL ID, with the target set being the significant DEGs from Adult Host or Fetal-Derived Colony, and the background set being the entire gene set following trimming by the filterByExpr function of edgeR. The P-value threshold was set to 10^-6. Full table of GO term results for Biological Processes were exported as Excel files and combined, with separate tabs for the results from the Adult Host or Fetal-Derived Colony input.

Supplemental Table 2. Ingenuity Pathway Analysis results. IPA (Ingenuity Pathway Analysis) was utilized to perform a Core Expression Analysis on significant DEGs from Adult Host or Fetal-Derived Colonies. The species was set to Rat and the False Discovery Rate (q-value) cutoff was set to 0.05, otherwise all settings were set to default options. Full tables of IPA Canonical Pathway and Upstream Regulator results were exported as Excel files and combined, with separate tabs for the results from the Adult Host or Fetal-Derived Colony input, and by Canonical Pathway (CP) or Upstream Regulator (UR).

Supplemental Table 3. Histone PTM Raw Data. Percent relative abundance for all histone post-translational modifications detected by mass spectrometry. The first tab contains abundance data for laser-capture microdissected Adult Host and Fetal-Derived Colony from 5 paired biological replicates (animal numbers 242, 243, 246, 248, and 249), excluding lower abundance modifications whose peaks could not be differentiated from background noise. The second tab contains abundance data for isolated adult hepatocytes, and immunopurified fetal hepatocytes from 3 distinct groups (LAP+, LAP+/OC2-, and LAP+/OC2+) with 3 biological replicates per group.

Supplemental Table 4. ANOVA Results for hPTMs. Results from a two-tailed ANOVA test using input data from Supplemental Table 3. The first tab contains only the 33 hPTMs that were found to be significantly different (FDR < 0.05) between Fetal-Derived Colony and Adult Host. The second tab contains the full ANOVA results for Fetal-Derived Colony vs. Adult Host, including those that did not meet the significance cutoff. The third through fifth tabs contain the ANOVA results for Adult Hepatocytes vs. each of the 3 immunopurified Fetal Hepatocyte populations: LAP+; LAP+/OC2-; and LAP+/OC2+.

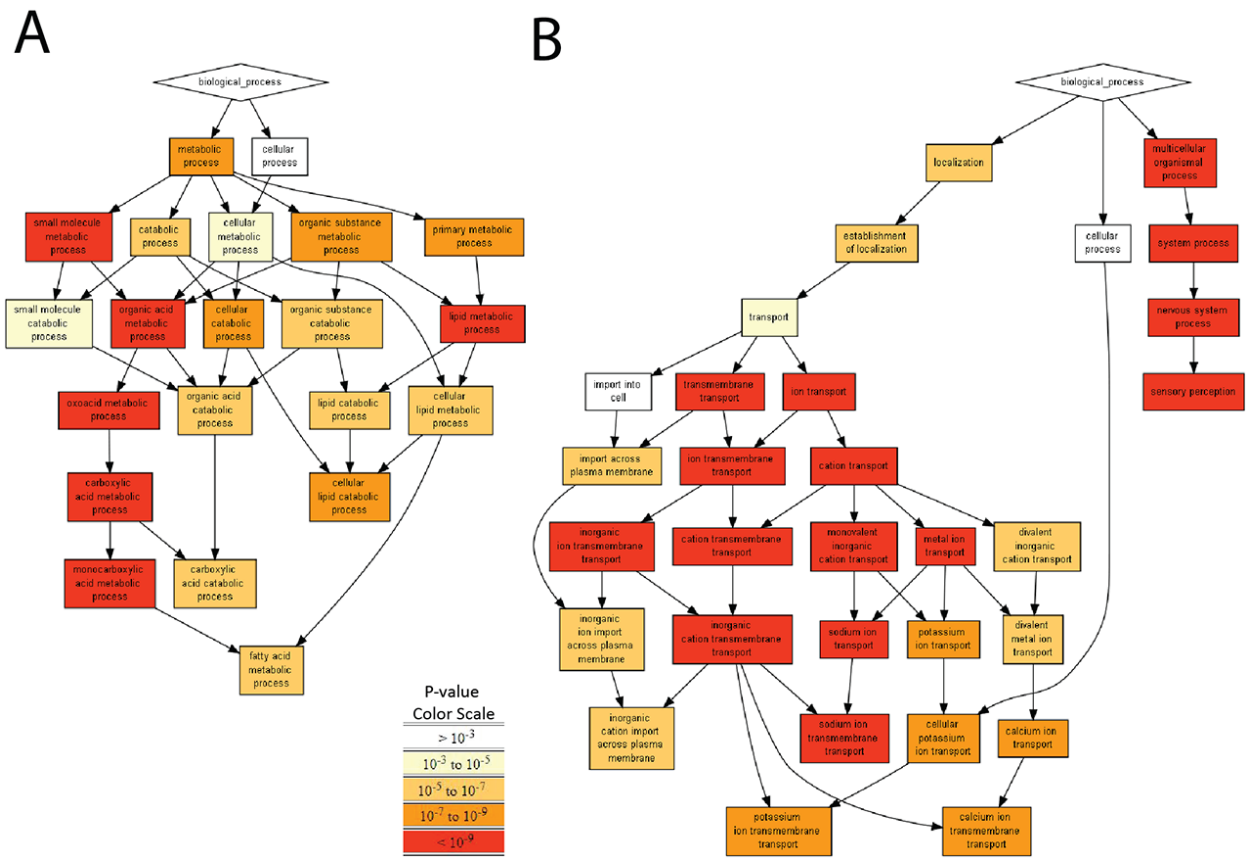

Supplemental Figure 1. Gene Ontology directed acyclic graphs. The Gene Ontology Biological Process results from Supplementary Table 1 were visualized by GOrilla as directed acyclic graphs (DAGs) for either Adult Host (A) or Fetal-Derived Colony (B) input genes. Significance of each GO term is denoted by node color, with the most significant terms ($P<10^{-9}$) rendered in red.

References

1. Iansante V, Mitry RR, Filippi C, Fitzpatrick E, Dhawan A. Human hepatocyte transplantation for liver disease: Current status and future perspectives. *Pediatr Res*. 2018;83(1-2):232-240. doi:10.1038/pr.2017.284

2. Pietrosi G, Vizzini G, Gerlach J, et al. Phases I–II matched case-control study of human fetal liver cell transplantation for treatment of chronic liver disease. *Cell Transplant*. 2015;24(8):1627-1638. doi:10.3727/096368914X682422

3. Oertel M. Fetal liver cell transplantation as a potential alternative to whole liver transplantation? *J Gastroenterol*. 2011;46(8):953-965. doi:10.1007/s00535-011-0427-5

4. Oertel M, Menthena A, Dabeva MD, Shafritz DA. Cell Competition Leads to a High Level of Normal Liver Reconstitution by Transplanted Fetal Liver Stem/Progenitor Cells. *Gastroenterology*. 2006;130(2):507-520. doi:10.1053/J.GASTRO.2005.10.049

5. Simper-Ronan R, Brilliant K, Flanagan D, et al. Cholangiocyte marker-positive and -negative fetal liver cells differ significantly in their ability to regenerate the livers of adult rats exposed to retrorsine. *Development*. 2006;133(21):4269-4279. doi:10.1242/dev.02589

6. Gruppuso PA, Sanders JA. Regulation of liver development: implications for liver biology across the lifespan. *J Mol Endocrinol*. 2016;56(3):R115-R125. doi:10.1530/jme-15-0313

7. Boylan JM, Francois-Vaughan H, Gruppuso PA, Sanders JA. Engraftment and Repopulation Potential of Late Gestation Fetal Rat Hepatocytes. *Transplantation*. 2017;101(10):2349-2359. doi:10.1097/TP.0000000000001882

8. Sanders JA. Late gestation fetal hepatocytes for liver repopulation in the rat. *Methods in Molecular Biology*. 2017;1506:45-60. doi:10.1007/978-1-4939-6506-9_3

9. Seglen PO. Preparation of rat liver cells. I. Effect of Ca2+ on enzymatic dispersion of isolated, perfused liver. *Exp Cell Res*. 1972;74(2):450-454. doi:10.1016/0014-4827(72)90400-4

10. Schneider CA, Rasband WS, Eliceiri KW. NIH Image to ImageJ: 25 years of image analysis. *Nature Methods 2012 9:7*. 2012;9(7):671-675. doi:10.1038/nmeth.2089

11. Bolger AM, Lohse M, Usadel B. Genome analysis Trimmomatic: a flexible trimmer for Illumina sequence data. 2014;30(15):2114-2120. doi:10.1093/bioinformatics/btu170

12. Dobin A, Davis CA, Schlesinger F, et al. STAR: Ultrafast universal RNA-seq aligner. *Bioinformatics*. 2013;29(1):15-21. doi:10.1093/BIOINFORMATICS/BTS635

13. Liao Y, Smyth GK, Shi W. Sequence analysis featureCounts: an efficient general purpose program for assigning sequence reads to genomic features. 2014;30(7):923-930. doi:10.1093/bioinformatics/btt656

14. Gruppuso PA, Boylan JM, Zabala V, et al. Stability of histone post-translational modifications in samples derived from liver tissue and primary hepatic cells. *PLoS One*. 2018;13(9):1-14. doi:10.1371/journal.pone.0203351

15. Garcia BA, Mollah S, Ueberheide BM, et al. Chemical derivatization of histones for facilitated analysis by mass spectrometry. *Nat Protoc*. 2007;2(4):933-938. doi:10.1038/nprot.2007.106

16. Abshiru NA, Sikora JW, Camarillo JM, et al. Targeted detection and quantitation of histone modifications from 1,000 cells. *PLoS One*. 2020;15(10). doi:10.1371/JOURNAL.PONE.0240829

17. Camarillo JM, Swaminathan S, Abshiru NA, Sikora JW, Thomas PM, Kelleher NL. Coupling fluorescence-activated cell sorting and targeted analysis of histone modification profiles in primary human leukocytes. *J Am Soc Mass Spectrom*. 2019;30(12):2526. doi:10.1007/S13361-019-02255-X

18. MacLean B, Tomazela DM, Shulman N, et al. Skyline: an open source document editor for creating and analyzing targeted proteomics experiments. *Bioinformatics*. 2010;26(7):966. doi:10.1093/BIOINFORMATICS/BTQ054

19. Ritchie ME, Phipson B, Wu D, et al. limma powers differential expression analyses for RNA-sequencing and microarray studies. *Nucleic Acids Res*. 2015;43(7):e47-e47. doi:10.1093/NAR/GKV007

20. RStudio Team(2015). RStudio: Integrated Development for R. *RStudio, Inc, Boston, MA*. Published online 2015:http://www.rstudio.com/.

21. Core Development Team R. A Language and Environment for Statistical Computing. *R Foundation for Statistical Computing*. 2020;2:https://www.R-project.org.

22. Robinson MD, McCarthy DJ, Smyth GK. edgeR: a Bioconductor package for differential expression analysis of digital gene expression data. *Bioinformatics*. 2010;26(1):139-140. doi:10.1093/BIOINFORMATICS/BTP616

23. Valero-Mora PM. *Ggplot2: Elegant Graphics for Data Analysis* . Vol 35. Springer-Verlag; 2010. doi:10.18637/jss.v035.b01

24. Blighe K, Rana S, Lewis M. EnhancedVolcano: Publication-ready volcano plots with enhanced colouring and labelin. *R-Package*. Published online 2019:1-8.

25. Eden E, Navon R, Steinfeld I, Lipson D, Yakhini Z. GOrilla: A tool for discovery and visualization of enriched GO terms in ranked gene lists. *BMC Bioinformatics*. 2009;10(1):1-7. doi:10.1186/1471-2105-10-48/TABLES/1

26. Sayols S. rrvgo: a Bioconductor package to reduce and visualize Gene Ontology terms. Published online 2020.

27. Galili T, O'Callaghan A, Sidi J, Sievert C. Heatmaply: An R package for creating interactive cluster heatmaps for online publishing. *Bioinformatics*. 2018;34(9):1600-1602. doi:10.1093/bioinformatics/btx657

28. Krämer A, Green J, Pollard J, Tugendreich S. Causal analysis approaches in Ingenuity Pathway Analysis. *Bioinformatics*. 2014;30(4):523-530. doi:10.1093/BIOINFORMATICS/BTT703

29. Zhang Y, Parmigiani G, Johnson WE. ComBat-seq: batch effect adjustment for RNA-seq count data. *NAR Genom Bioinform*. 2020;2(3). doi:10.1093/NARGAB/LQAA078

30. Chen LL, Yang R, Kwan T, et al. Paired rRNA-depleted and polyA-selected RNA sequencing data and supporting multi-omics data from human T cells. *Scientific Data 2020 7:1*. 2020;7(1):1-7. doi:10.1038/s41597-020-00719-4

31. Tolosa L, Pareja-Ibars E, Teresa Donato M, et al. Neonatal livers: A source for the isolation of good-performing hepatocytes for cell transplantation. *Cell Transplant*. 2014;23(10):1229-1242. doi:10.3727/096368913X669743

32. Becchetti A, Munaron L, Arcangeli A. The role of ion channels and transporters in cell proliferation and cancer. *Front Physiol*. 2013;4. doi:10.3389/FPHYS.2013.00312

33. Hoffmann EK, Lambe IH. Ion channels and transporters in the development of drug resistance in cancer cells. *Philosophical Transactions of the Royal Society B: Biological Sciences*. 2014;369(1638). doi:10.1098/RSTB.2013.0109

34. Wang CY, Lai MD, Phan NN, Sun Z, Lin YC. Meta-Analysis of Public Microarray Datasets Reveals Voltage-Gated Calcium Gene Signatures in Clinical Cancer Patients. Published online 2015. doi:10.1371/journal.pone.0125766

35. Schuierer S, Carbone W, Knehr J, et al. A comprehensive assessment of RNA-seq protocols for degraded and low-quantity samples. *BMC Genomics*. 2017;18(1):1-13. doi:10.1186/S12864-017-3827-Y/TABLES/1

36. Sun Z, Asmann YW, Nair A, et al. Impact of Library Preparation on Downstream Analysis and Interpretation of RNA-Seq Data: Comparison between Illumina PolyA and NuGEN Ovation Protocol. *PLoS One*. 2013;8(8):e71745. doi:10.1371/JOURNAL.PONE.0071745

37. Sarantopoulou D, Tang SY, Ricciotti E, et al. Comparative evaluation of RNA-Seq library preparation methods for strand-specificity and low input. *Sci Rep*. 2019;9(1):1-10. doi:10.1038/s41598-019-49889-1

38. Gruppuso PA, Boylan JM, Vaslet CA. Identification of candidate growth-regulating genes that are overexpressed in late gestation fetal liver in the rat. *Biochimica et Biophysica Acta - Gene Structure and Expression*. 2000;1494(3):242-247. doi:10.1016/S0167-4781(00)00244-X

39. Yuan S, Natesan R, Sanchez-Rivera FJ, et al. Global Regulation of the Histone Mark H3K36me2 Underlies Epithelial Plasticity and Metastatic Progression. *Cancer Discov*. 2020;10(6):854-871. doi:10.1158/2159-8290.CD-19-1299

40. Cheeseman K, Jannot G, Lourenço N, et al. Dynamic methylation of histone H3K18 in differentiating Theileria parasites. *Nature Communications 2021 12:1*. 2021;12(1):1-14. doi:10.1038/s41467-021-23477-2

41. Völker-Albert M, Bronkhorst A, Holdenrieder S, Imhof A. Histone Modifications in Stem Cell Development and Their Clinical Implications. *Stem Cell Reports*. 2020;15(6):1196-1205. doi:10.1016/j.stemcr.2020.11.002

42. Ferrari KJ, Scelfo A, Jammula SG, et al. Polycomb-Dependent H3K27me1 and H3K27me2 Regulate Active Transcription and Enhancer Fidelity. *Mol Cell*. 2014;53(1):49-62. doi:10.1016/J.MOLCEL.2013.10.030

43. Wagner EJ, Carpenter PB. Understanding the language of Lys36 methylation at histone H3. *Nat Rev Mol Cell Biol*. 2012;13(2):115. doi:10.1038/NRM3274

44. Fortin JM, Azari H, Zheng T, et al. Transplantation of Defined Populations of Differentiated Human Neural Stem Cell Progeny. *Scientific Reports 2016 6:1*. 2016;6(1):1-13. doi:10.1038/srep23579

45. Beattie GM, Otonkoski T, Lopez AD, Hayek A. Functional beta-cell mass after transplantation of human fetal pancreatic cells: differentiation or proliferation? *Diabetes*. 1997;46(2):244-248. doi:10.2337/DIAB.46.2.244

46. McLelland BT, Lin B, Mathur A, et al. Transplanted hESC-Derived Retina Organoid Sheets Differentiate, Integrate, and Improve Visual Function in Retinal Degenerate Rats. *Invest Ophthalmol Vis Sci*. 2018;59(6):2586-2603. doi:10.1167/IOVS.17-23646

47. Li W, Li L, Hui L. Cell Plasticity in Liver Regeneration. *Trends Cell Biol*. 2020;30(4):329-338. doi:10.1016/J.TCB.2020.01.007

Chapter 3:
Activation of autophagy during normothermic machine perfusion of discarded livers is associated with improved hepatocellular function

Activation of autophagy during normothermic machine perfusion of discarded livers is associated with improved hepatocellular function

Anders Ohman, [1*] Siavash Raigani, [2,3*] John C. Santiago, [1] Megan G. Heaney, [1] Joan M. Boylan, [1] Nicola Parry, [4] Cailah Carroll, [2] Sofia G. Baptista, [2] Korkut Uygun, [3] Philip A. Gruppuso, [1] Jennifer A. Sanders, [1*] and Heidi Yeh [2*]

[1] Department of Pediatrics, Rhode Island Hospital and Brown University, Providence, Rhode Island; [2] Division of Transplant Surgery, Massachusetts General Hospital, Boston, Massachusetts; [3] Center for Engineering in Medicine and Surgery, Massachusetts General Hospital and Harvard Medical School, Boston, Massachusetts; and [4] Section of Pathology, Cummings School of Veterinary Medicine at Tufts University, North Grafton, Massachusetts

[*] These authors contributed equally to this work.

Originally published in *Am J Physiol Gastrointest Liver Physiol* 322: G21–G33, 2022.
DOI: 10.1152/ajpgi.00266.2021

Introduction

Liver injury can be caused by a variety of sources and results in disastrous consequences for the body. Liver disease is one of the leading causes of death in the United States. As liver injury can compound and easily progress to irreversible end-stage liver disease (ESLD), the number of patients in need of transplant is expected continue to grow alongside the rates of precursor conditions such as non-alcoholic fatty liver disease (NAFLD). While treatment modalities such as artificial liver devices and hepatocyte transplantation have been under investigation and development, ESLD currently has no other effective option for long-term clinical treatment besides orthotopic liver transplantation (OLT). There is currently a much larger need for donor livers than there are available organs for transplantation. In the United States, deceased donor livers allow for approximately 5,000 transplantations per year, but there are 17,000 patients in need of transplantation, leading to mortality on the transplantation waitlist.

An exacerbating obstacle to meeting the needs of the large transplant waitlist with the low organ supply is that many donor livers are discarded prior to transplantation for a number of reasons, all of which are related to factors likely to cause impairment to organ function and potentially causing injury or death of the recipient. [1] However, the scarcity of ideal transplants has led to the careful evaluation of these compromised organs for potential use, leading to the classification of “extended-criteria donors” which may be suitable for use in some situations, and carefully quantifying the spectrum of risks caused by various factors like ischemic time. [2] This is a particular factor in livers that were donated after circulatory death (DCD) instead of donated after brain death (DBD), as removal from the circulatory system increases warm ischemic time, resulting in rates of discard up to 30%. [3]

While the risks to the patient are real and an understandable reason to err on the side of caution, it is possible that many of the discarded livers could have resulted in successful transplantation. New analysis suggests that older extended-criteria donors could be

transplanted to age-matched patients to extend the donor pool without significantly affecting the survival of older recipients. [4] Another approach is the use of normothermic machine perfusion (NMP) to maintain the health of donor organs *ex situ* prior to transplant by providing more physiological conditions for preservation than cold ischemia. While decisions to discard livers prior to transplant are generally the result of a visual assessment of the liver (by gross anatomy or histology), NMP also offers the ability to quantitatively assess relevant functional metrics to determine if the liver is capable of performing its myriad functions. [1,5,6] This could allow for more accuracy than the standard assessment techniques, and potentially minimize discard by revealing that some injured or steatotic donor livers are still viably functional for transplant. [7]

One exciting potential for NMP beyond improved preservation of organs *ex situ* is the ability to improve liver function or rehabilitate donor livers with marginal function. [8,9] While previous work has explored transcriptional changes in viable DBD livers after NMP and found enrichment of repair and regenerative pathways, [10,11] we wanted to explore transcriptional changes during the NMP process itself in a more likely population of livers for discard: DCD donor livers deemed nonviable for transplant. By thoroughly interrogating the transcriptomic and proteomic characteristics of these livers at multiple stages of the NMP process, we sought to identify the mechanisms that characterize the liver's biological response to the perfusion process. By simultaneously measuring functional characteristics at the same time points, we are also able to categorize the livers into viably functional for transplantation or nonviable and correlate those outcomes with the activity of injury and repair mechanisms during NMP. Our major goal is to determine if there are avenues to provide therapeutic adjuvants during the NMP process to target nonviable livers and affect molecular mechanisms to induce viability and expand the donor liver pool by revitalizing organs that would otherwise be discarded.

Materials and Methods

Donor Livers

Six human donor livers with similar donor demographics were chosen for further analysis from a previously reported research cohort of machine-perfused discarded human livers. [7] All six livers were DCD livers without significant steatosis and were rejected for transplant by all transplant centers in the respective donor service area. Reasons for discard included a combination of DCD status, donor age, and length of warm ischemic time. Human livers were procured in standard fashion through two organ procurement organizations (OPOs): New England Donor Services (Waltham, MA) and LiveOnNewYork (New York, NY). Informed consent was obtained from donors by the OPOs. Table 1 describes the donor demographics for each organ. The Massachusetts General Hospital and Lifespan Institutional Review Boards, as well as the two OPOs, approved this study (No. 2011P001496). No organs were procured from prisoners and no vulnerable populations were included in this study.

Six similar discarded DCD livers were selected for supplemental analysis which had high scoring for micro- and macrosteatosis, defined as small droplet steatosis without nuclear displacement or large droplet steatosis with nuclear displacement, respectively. These livers had microsteatosis in an average of 30% of the tissue field evaluated and macrosteatosis in 33%, vs. 3.9% and 1.3% respectively in the cohort of lean livers.

Procurement of Grafts

Procurement techniques based on donation after circulatory death followed standard methods. Donor livers were flushed in situ with University of Wisconsin solution. Total warm ischemic time (WIT) was defined as the period from extubation to cold flush. Functional WIT was defined as the period from asystole to cold flush. Cold ischemic time was defined from cold flush to initiation of machine perfusion. After transport to the laboratory under static cold storage, livers underwent standard back bench preparation for machine perfusion (Figure 1A). [12]

Machine Perfusion

Grafts were perfused on the Liver Assist device (Organ Assist, Groningen, Netherlands) using a previously described protocol. [7] Briefly, perfusate composition consisted of Oþ packed red blood cells, human albumin, lactated Ringer solution, and heparin. Bile salts (taurocholate) and lipid-free parenteral nutrition were continuously infused. Perfusate, bile, and tissue biopsies were collected and analyzed at multiple time points (Figure 1B). Grafts were deemed to demonstrate adequate hepatocellular function if they satisfied the criteria reported by Mergental et al., [1] namely, perfusate lactate ≤ 2.5 mmol/L and two or more of the following minor criteria within 4 h of starting perfusion: 1) perfusate pH ≥ 7.30 without supplemental bicarbonate, 2) arterial flow ≥ 150 mL/min and portal flow ≥ 500 mL/min, 3) evidence of glucose metabolism, 4) bile production, and 5) visually assessed homogenous perfusion. Cholangiocellular (biliary) functional metrics according to van Leeuwen [9] were measured but not used for functional stratification due to technical issues with bile collection in two livers.

Perfusate Analysis and Plasma Proteomics

Perfusate collected at the indicated time points was centrifuged at 5,000 *g* and the plasma collected and stored at −80°C for later analysis. Enzyme-linked immunosorbent assays (ELISAs) were performed for various proteins according to manufacturers' guidelines (Supplemental S1 Methods; all Supplemental Methods and Figs. are available at https://doi.org/10.5281/zenodo.5206547).

Proteomic profiling of trypsinized perfusate proteins was performed following albumin depletion in collaboration with the University of Arkansas Medical Sciences Proteomics Core. The equipment used, protein processing, and analysis are detailed in the Supplemental S2 Methods.

Total RNA Purification, Sequencing, and Analysis

Core needle biopsies taken immediately before perfusion and after 3 and 6 h of perfusion were used for transcriptome sequencing on an Illumina HiSeq 4000 using nine PCR cycles by GENEWIZ (South Plainfield, NJ). Tissue collection, purification, and bioinformatic analysis are detailed in the Supplemental S3 Methods. The differential gene expression threshold for significance was set to a Benjamini–Hochberg false discovery rate (FDR) of <0.05. Raw sequence data have been deposited in the Gene Expression Omnibus with Accession No. GSE165568 and GSE202565.

Histology and immunohistochemistry

Core needle biopsies taken from the right liver lobe at indicated intervals were fixed in formalin and embedded in paraffin. Hematoxylin and eosin (H&E) staining was performed on all biopsies to assess the degree of necrosis and inflammatory cell infiltrate. A pathologist evaluated and scored all slides in a blinded manner using a semiquantitative scoring scheme (Supplemental S4 Methods). Immunohistochemistry methods and antibodies used are available in the Supplemental S5 Methods.

Western Blots

Sequential wedge biopsies from the right lobe of each liver were performed at indicated intervals, flash frozen in liquid nitrogen, and stored at −80°C. Tissue samples (20 mg) were homogenized and Western immunoblots performed as previously described. [13] A full list of antibodies used is provided in the Supplemental S6 Methods.

Statistical analysis

Categorical data are presented as median with interquartile range (IQR) and frequency data as percentages. For statistical tests not related to RNA sequencing or proteomic analysis, the Wilcoxon rank-sum test (Mann–Whitney *U*) and Fisher's exact test were used for group

comparisons. A two-way analysis of variance (ANOVA) was used for comparisons between groups with repeated measures over time. The threshold for statistical significance was set at <0.05. Analyses were conducted using GraphPad Prism 8 (San Diego, CA) and Stata 15 (College Station, TX).

Results

Assessment of Hepatocellular Function during Normothermic Perfusion

Donor demographics for the six study livers are provided in Table 1. Machine perfusion criteria used to determine whether each liver demonstrated adequate (functional) or inadequate (nonfunctional) hepatocellular function are shown in Figure 1C and Supplemental Figure S1. Functional livers (F1–F3) demonstrated evidence of increased glucose metabolism and increased urea synthesis over time (Supplemental Figure S1). Although some nonfunctional livers (N1–N3) were able to meet minor criteria, all failed to meet the perfusate lactate threshold. Aspartate aminotransferase (AST) and alanine aminotransferase (ALT) levels (Supplemental Figure S1) were higher for the functional livers than for the nonfunctional livers at 1 and 3 h of perfusion, though levels plateaued thereafter. In comparison, nonfunctional livers demonstrated AST and ALT levels that increased but were, in general, lower than the levels seen with the functional livers. Bile volume and cholangiocellular functional metrics are presented in Supplemental Figure S2, though statistical comparisons were limited by technical errors with bile collection in two functional livers. Similar heterogeneity between livers was observed in the steatotic liver set as well (Figure 2). Functional steatotic livers performed similarly to functional lean livers in arterial lactate clearance, while having lower ALT levels comparable to lean nonfunctional livers. H&E staining demonstrated an increase in percent necrosis after initiation of NMP in both functional and nonfunctional groups in lean livers, with all lean livers demonstrating up to 30% histologic necrosis by 12 h of perfusion (Figure 1D).

Principal Component Analysis of the Transcriptomic Analyses Discriminates Functional from Nonfunctional Livers

Principal component analysis (PCA) demonstrated distinct changes in gene expression at 0 h (preperfusion), 3 h, and 6 h of NMP among individual livers. The preperfusion gene expression profiles clustered together by hepatocellular function then diverged further once perfusion was initiated. Functional livers continued to cluster together after 3 and 6 h of NMP, whereas the nonfunctional livers demonstrated dissimilar profiles with respect to one another (Figure 3A). Principal component 1 (PC1), which accounted for 28.3% of the variation in differentially expressed genes (DEG), captured the time-dependent changes in gene expression. The functional livers demonstrated a consistent transcriptional shift at each 3-h interval compared with lower magnitude changes in the nonfunctional livers. Analysis of the top 10% of genes contributing to PC1 revealed enrichment of gene ontology (GO) terms related to gene transcription and protein synthesis. Detailed examination of the temporal response of these genes revealed a marked increase in expression by 6 h of perfusion in the functional compared with nonfunctional livers (Figure 3B).

Principal component 2 did not distinguish any notable cellular processes despite accounting for 13.5% of the variation in DEG. Conversely, principal component 3 (PC3), representing 10.0% of the variation, was able to effectively discriminate functional from nonfunctional livers. The top 10% of genes contributing to PC3 were involved in GO cellular components related to extracellular vesicles and exosomes, endoplasmic reticulum, and membrane components, though none of the individual genes met the FDR cutoff for significance (Supplemental Figure S3).

Transcription shifts captured by principal components were remarkably reflective of each liver's hepatocellular functional profile. For example, the nominal transcriptional shift in nonfunctional livers after initiation of NMP appeared to correspond with a delay in lactate

clearance and perfusate pH stability in the first several hours of NMP. Furthermore, liver N2 demonstrated minimal changes in principal components compared with other livers, consistent with that liver's poor functional profile (lowest vascular flows, no evidence of lactate clearance, persistent metabolic acidosis, rising AST/ ALT). Interestingly, liver N1 demonstrated changes over time most similar to the functional livers based on PC1 and PC2 but diverged with the addition of PC3 (Supplemental Figure S4).

When all RNA-Seq libraries were plotted together by PCA, we saw that steatotic and lean livers had a significant degree of overlap (Figure 4A). The most significant principal component (PC1) still appears to reflect duration of NMP time, with the majority of all samples showing a progression from 0hr of NMP at the left, 3hr in the middle, and 6hr at the right. Functional and nonfunctional samples tended to cluster closely together regardless of if they came from a lean or steatotic liver, with both sets segregating vertically on PC2 with all functional livers at the top. When lean and steatotic sets were examined separately by independent PCA, time and functionality still appeared to determine the top contributors of variation in each dataset, and the sample sets strongly resembled each other (Figure 4B-E).

Overview of Differential Gene Expression

Although individual livers clustered according to function with PCA, this was less apparent with comparison of time-static gene sets between groups. Of the ~14,000 transcripts sequenced, only two genes (ARL16, NLGN2) were significantly different (FDR < 0.05) between functional and non-functional livers at the preperfusion time point. No genes were significant at 3 h. In contrast, 53 genes were differentially expressed at 6 h of perfusion (Supplemental Data Set S1; all Supplemental Data Sets are available at https://doi.org/10.5061/dryad.f7m0cfxx0). However, Ingenuity Pathway Analysis (IPA) did not reveal significant enrichment of any canonical pathways (CPs) or upstream regulators (URs) related to this gene set.

Analyses based on the temporal changes in gene expression during NMP relative to the preperfusion baseline were more informative of the physiological differences between functional and nonfunctional livers during perfusion. Volcano plots showed that functional livers responded to NMP at 3h with a robust and statistically significant upregulation of genes (Figure 3C). This was followed by both upregulation and downregulation of numerous genes at 6h. In contrast, nonfunctional livers upregulated expression of only a handful of genes at 3h. This was followed with a greater degree of change in gene expression (both upregulation and downregulation) at 6h. When examining the transcriptome by differential expression analysis in edgeR, we found that the gene expression profiles of functional and nonfunctional livers at both 3h and 6h of perfusion were similar to each other in DEG number and scale of expression, regardless of originating from lean or steatotic livers (Figure 5). Upregulation of genes was seen to have begun by 3hr, with a higher degree of significant up- and down-regulation of genes by 6hr.

Using IPA, we identified canonical pathways and URs associated with the temporal differential gene expression unique to the two experimental groups. In functional livers, over 25 pathways related to inflammation and innate immunity were enriched at 3 h, whereas nonfunctional livers only had four significant pathways and many fewer genes in each pathway (Supplemental Figure S5). By 6 h, there was a shift in significant pathways to those associated with survival, protein ubiquitination, and growth in functional livers. The significant pathways in the nonfunctional livers were similar to those seen in the functional livers at 3 h of perfusion. The URs displayed similar temporal shifts (Supplemental Figure S5). Activation Z-scores of significant URs related to innate immunity were higher in functional compared with non-functional livers after 3 h of NMP, indicating more marked induction of downstream gene targets in the early perfusion phase in the functional livers. By 6 h of NMP, active URs in the nonfunctional livers more closely resembled those of the functional livers (Figure 3D). Despite this, when the top four URs were examined for downstream signaling, the two groups differed

greatly in activation of their gene targets (Figure 3E). Results using CiiiDER [14] to identify enriched transcription factor binding sites in the promoter regions of the differentially expressed genes were very similar to those obtained using IPA (Supplemental Data Set S2).

When all datasets were included in IPA analysis for Upstream Regulators (Figure 6A) and Canonical Pathways (Figure 6B), we saw that functional livers from both the lean and steatotic cohorts had highly activated canonical pathways for innate immune responses after 3hr of NMP that nonfunctional livers did not, including Toll-like receptor, IL-10, and IL-6 ($P < 10E{-}07$). By contrast, we found that lean and steatotic nonfunctional livers both had delayed activation of these pathways until 6hr of perfusion. This could indicate a delay in activation of these critical pathways in nonviable livers, with a consistent delay in both the lean and steatotic groups. We saw a high degree of overlap in the Upstream Regulators identified for all groups, however the significance and number of identified downstream targets were both considerably higher in functional livers, the lean cohort, and the 6hr NMP time point, with the highest levels at the intersection of those 3 groups.

Ischemia-Reperfusion Injury and Innate Immune Activation

As noted earlier, the changes in gene expression that occurred during NMP suggested activation of innate immunity based on canonical pathways identified using pathway analysis (Figure 7A). Functional livers demonstrated early enrichment of Toll-like receptor, high mobility group box 1, and interleukin-6 (IL-6) signaling pathways, among several others. Nonfunctional livers demonstrated activation of only the IL-6 canonical pathway after 3 h of NMP. However, after 6 h of perfusion, the nonfunctional livers displayed an expression profile that resembled that of the functional group at 3 h, whereas the functional group revealed pathway activation indicative of cell turnover and survival. These findings indicated that nonfunctional livers during NMP are distinguished by delayed onset of innate immune signaling. Examination of H&E

stained liver biopsies supported these findings, with significantly more lobular and portal inflammatory cell infiltrates seen in nonfunctional livers (Figure 7, B and C).

Given the findings related to immune activation, we analyzed damage-associated molecular patterns (DAMPs; Figure 7D) and cytokines (Figure 7E) in the circulating perfusate. Results were similar between groups at multiple time points when analyzed by ELISA, and these results were similar between lean and steatotic livers at the same time points (Figure 8A). This was unexpected given the divergent expression profiles of the downstream gene targets noted earlier (Figure 3E), which was also an effect seen in steatotic livers (Figure 8B).

To determine the presence of proteins differentiating functional from nonfunctional livers, we also performed untargeted plasma proteomics to further assess the DAMP and cytokine response to NMP. This revealed numerous enriched proteins varying between groups after 1, 3, and 6 h of perfusion, though only eight proteins remained statistically significant when a stringent FDR cutoff of <0.05 was applied (all at 3 h of NMP; Supplemental Figure S6). Within this subset, none was directly related to DAMP or cytokine signaling (Supplemental Data Set S3).

Role of the Unfolded Protein Response and Autophagy in Hepatocellular Function

Given the notable injury profile differences between functional and nonfunctional livers, we next examined repair responses to the accrued injuries. Accumulation of unfolded and misfolded proteins in the endoplasmic reticulum (ER) during ischemia activates the cellular stress mechanism referred to as the unfolded protein response (UPR). [15] Misfolded proteins bind to and activate protein kinase RNA- activated-like ER kinase (PERK) on the ER membrane, resulting in phosphorylation of eukaryotic initiation factor 2α (eIF2α). The phosphorylation of eIF2α leads to global inhibition of translation, initiation of antioxidant mechanisms, and induction of autophagy, the cell's repair and homeostasis mechanism. [16]

Analysis of eIF2α by Western immunoblot demonstrated increased phosphorylation ratios of eIF2α in preperfusion biopsies in both groups [functional = 0.54 (IQR: 0.46–0.74) vs. nonfunctional = 0.69 (0.40–0.82), P = 0.83] (Figure 9A). After initiation of perfusion, both groups demonstrated a significant time-dependent decrease in phosphorylated eIF2α (two-way ANOVA time factor P = 0.0012), with negligible activation in functional livers after 6 h of perfusion [0.0084 (0.0067–0.030)], potentially indicating resolution of ER stress. Qualitatively, there was a trend toward higher levels of eIF2α phosphorylation in the non-functional livers [0.10 (0.010–0.13), P =0.13], with liver N1 representing the outlier with the lowest ratio at 6 h. As noted previously, nonfunctional liver N1 was most transcriptionally similar to the functional group in PCA.

With respect to activation of autophagy, functional livers demonstrated a more robust response, with the majority of associated genes significantly increasing in expression after initiation of NMP compared with nonfunctional livers (Figure 9B). The mechanistic Target of Rapamycin (mTOR) pathway plays a key role in regulating autophagy; active mTOR complex 1 inhibits autophagy through regulation of autophagy-related proteins and lysosome biogenesis. [17] To assess mTOR complex 1 activation, we performed Western immunoblotting for phosphorylation of its downstream substrate p70 S6 kinase (p70S6K). Phospho-p70S6K was barely detectable before perfusion in both groups. In the functional livers, phosphorylation was increased at 3 h of perfusion and decreased by 6 h. In contrast, nonfunctional livers had high levels of phospho-p70S6K at both 3 and 6 h of perfusion (Figure 9C). Comparisons between groups were nonsignificant due to an outlier, again nonfunctional liver N1. This liver had the lowest activated p70S6K protein ratio at 6 h (0.02) among the nonfunctional group despite having the highest ratio at 3 h (1.21), a pattern similar to the functional livers. In contrast, liver N2, the worst functioning nonfunctional liver, had a low ratio at 3 h (0.03) that greatly increased

at 6 h (0.81). Despite not reaching statistical significance, the temporal pattern of p70S6K phosphorylation appeared consistent with sustained mTOR activation in nonfunctional livers.

Next, we investigated protein components involved in autophagic flux to determine if activation of autophagy was associated with liver function. The microtubule-associated protein 1 light chain 3 (LC3) family is vital to autophagosome formation. Posttranslational modification of LC3 generates LC3-I, which is subsequently conjugated with phosphatidylethanolamine to generate LC3-II, the active protein necessary for elongation of the autophagosome membrane. Both functional and nonfunctional livers demonstrated a time-dependent increase in LC3-II:LC3-I ratio (two-way ANOVA time factor P = 0.0398), indicating autophagosome assembly in response to initiation of NMP (Figure 9C). However, functional livers were found to have a significantly higher ratio after 6 h of NMP compared with nonfunctional livers [2.18 (1.82–3.09) vs. 1.05 (0.98–1.29), P = 0.0495], consistent with the counterregulatory action of p70S6K. Determination of P62 content by Western blot did not demonstrate protein buildup in either group. We further confirmed the LC3 results using immunohistochemistry. Preperfusion biopsies demonstrated hepatocyte LC3 staining in a pan-cytosolic pattern in both groups. In functional livers, LC3 staining changed to demonstrate a granule-type staining pattern at 3 and 6 h of NMP, indicating autophagosome formation in the functional livers. By 12 h of NMP, functional livers again demonstrated pan-cytosolic LC3 staining. In contrast, nonfunctional livers displayed persistent pan-cytosolic and scant granule-type staining after 3 and 6 h, with more apparent granular staining by 12 h of NMP (Figure 9D).

The final step in autophagy involves fusion of the autophagosome with lysosomes to form the autolysosome. Examination of the perfusate proteomic analysis results revealed that nonfunctional livers had significantly higher concentrations of the lysosomal components cathepsin D [log2 fold change (log_2FC) = −2.36 compared with functional livers, FDR = 0.043], prosaposin (log_2FC = −1.95, FDR = 0.016), and hexosaminidase subunit-b (log_2FC = −3.02,

FDR = 0.033) compared with functional livers at 3 h of NMP. A fourth protein, carboxypeptidase vitellogenic like, putatively involved in lysosomal function, [18] was also enriched in nonfunctional liver perfusates ($log_2FC = -4.12$, FDR =0.0014) (Supplemental Figure S7). Confirmatory ELISA reinforced the proteomic analysis, demonstrating a fivefold greater abundance of cathepsin D in the perfusate of nonfunctional compared with functional livers [13,440 ng/mL (10,619–18,416) vs. 2,474 (1,514–2,946) at 3 h, P = 0.0495; Supplemental Figure S7]. Numerous additional lysosomal components, including other cathepsins, demonstrated a trend toward enrichment in the perfusate of nonfunctional livers ($log_2FC < -1$ compared with functional livers) but failed to meet the FDR cutoff (Supplemental Data Set S3).

Prosurvival Signaling Is More Active in Functional Livers

Finally, we investigated the relevance of prosurvival signaling in response to reperfusion injury during NMP. Our transcriptome analysis revealed abundant prosurvival and early regenerative signals in functional relative to nonfunctional livers. Of note, several prosurvival pathways were concurrently involved in innate immune signaling, highlighting the bridge between injury and recovery. In functional livers, pathway analysis showed enrichment of components of the IL-6 and phosphatidylinositol-4,5-bisphosphate 3-kinase/AKT serine/threonine kinase (PI3K/AKT) canonical pathways by 3 h. Transcriptomic profiling and pathway analysis also showed activation by 6 h of downstream effectors: nuclear factor-κβ subunit (NF-κB), mitogen-activated protein kinase (ERK/MAPK), Janus kinase/signal transducer and activator of transcription (JAK/STAT), and hepatocyte growth factor (HGF) (Figure 10A). In contrast, nonfunctional livers appeared to have limited enrichment of IL-6 signaling at 3 h and only subsequent activation of PI3K/AKT and NF-κB pathways by 6 h. To further examine the effects of prosurvival signaling, we assessed ERK1/2 activation by phospho-specific Western immunoblotting. There was a time-dependent increase in ERK activation in both groups after initiation of NMP (two-way ANOVA time factor P=0.014), though without significant differences

between groups (attributable to marked sample-to-sample variability; Figure 10B). Interestingly, examination of gene expression downstream of ERK revealed fewer differentially expressed target genes in nonfunctional compared with functional livers, similar to the pattern seen in innate immune and autophagy signaling (Figure 10C).

With respect to regenerative signaling, we again observed more robust downstream HGF target gene expression in functional compared with nonfunctional livers (Figure 10D). Despite this, no significant difference was seen between groups in the perfusate concentration of HGF after 6 or 12 h of NMP (Figure 10E). The 12-h plasma sample was used in this case given that regenerative pathways are activated in delayed fashion. Similar to the pattern seen in innate immune responses, prosurvival and regenerative signaling in nonfunctional livers lagged behind those seen in functional livers. Consistently, gene expression in nonfunctional livers at 6 h resembled gene expression at 3 h in functional livers. Of note, we did not find any evidence of hepatocellular regeneration as indicated by significant expression of genes involved in cell cycle entry (Supplemental Figure S8), although the 6-h perfusion timeframe may have been too early to detect these changes.

Discussion

Given the shortage of donor livers available to transplant, minimizing discard is a critical step to meeting the needs of the large number of patients on the waitlist. One way of doing so is to provide transplant surgeons clear, quantitative metrics about liver function rather than erring on the side of caution based on anatomic observation or cause of donor death. NMP offers a platform to assess liver function over the duration of perfusion. Here we have shown that half of the rejected DCD livers in our cohort ultimately met several physiological metrics of viability criteria, and by utilizing omics techniques at multiple time points throughout the perfusion process we were able to examine the potential mechanistic reasons behind these responses. We found that livers meeting viability criteria had a transcriptomic signature indicating an early

innate immune response giving way to the activation of autophagy and pro-survival mechanisms; conversely livers that did not meet viability criteria had a delayed response relative to the viable livers along with more innate immune signaling and less autophagy. This utilization of NMP to assess not only viability metrics but also the underlying transcriptome of DCD livers is a novel application to determine the causes behind donor liver viability.

While NMP has been established to allow the assessment of liver function to determine probably viability for transplant, it may also offer the potential to actually improve the donor liver function itself. Previous work has shown that discarded DCD donor livers which have undergone NMP show transcriptomic and proteomic signals of activation of innate immunity, which is also characteristic of the elevated cytokines and inflammatory signals seen in ischemia reperfusion injury during orthotopic liver transplantation. [19,20] These tissue-damaging inflammatory effects can adversely affect donor liver function and thereby the transplantation viability of the organ, so it is critical to assess how the liver balances inflammatory signals with counteracting cellular repair and survival responses. Consistent with this, we saw that the functional livers activated injury response pathways at 3hr earlier than nonfunctional livers, and then pivoted to activating repair and survival signaling by 6hr. By contrast, the nonfunctional livers had delayed and sustained activation of innate immune responses, even though they had comparable levels of cytokines and DAMPs in their perfusate. It is possible that the nonfunctional livers are capable of being rehabilitated by NMP but require a longer duration of perfusion, or that they require a modification of the perfusion solution to trigger robust activation of the same pathways seen in the functional livers, but this was not evaluated in this present study. As the presence of steatosis is one of the primary reasons for discarding of donor livers based on the prediction of poor expected transplant function, we were also curious about the potential for the use of NMP as outlined previously to evaluate these high-risk steatotic donor organs and to examine if they truly perform differently to lean livers on a functional and transcriptional level.

If the major difference between functional and nonfunctional livers is that functional livers are able to balance the effects of damaging inflammation with cell survival processes, we wanted to explore these mechanisms to determine which are most responsible for improving function. The endoplasmic reticulum (ER) has a key role in sensing cell stress via the unfolded protein response (UFP), as well as activating autophagy. [21] Reperfusion following cold ischemia is known to trigger this system, [15,22] so we speculated that the liver response to autophagy may play a role in the functionality difference observed. After NMP begins, we detected a decreasing amount of phosphorylated eIF2α, relaxing inhibition of protein synthesis. This effect was seen disproportionately in the functional livers, which suggested a resolution of ER stress corresponds to a more positive phenotype. Transcriptomic analysis validates this interpretation by showing that functional livers had a higher degree of upregulation of genes in the ontological category of protein biosynthesis compared with nonviable livers (Figure 3B). The UFP also has known beneficial downstream mechanisms such as antioxidant and autophagic effects, although too much stress can also trigger cell death. [16] Thus, a careful balance has to be struck to activate UPR at the right times and for the proper duration to trigger cell repair mechanisms.

We suspected that a more regulated autophagic process was occurring in the functional livers, and validated this by looking at protein levels in both histological and perfusate samples, as well transcriptomic signatures. Functional liver histology had a higher ratio of LC3-II:LC3-I after 6hr, indicating autophagosome formation, [23] as well as a lower level of lysosomal acid hydrolases in perfusate than in nonfunctional livers, indicating that functional livers had less cellular injury and lysosomal damage – as well as lower amounts of downstream activation of cellular death pathways that could impair liver function when overactivated, such as apoptosis. [17] Apoptosis activation from lysosomal enzymes has also been indicted as a key driver of hepatic IRI in a cathepsin knockout mouse, [24] while decreased autophagy also is found to exacerbate damage. [25,26] Previous work in mouse models and human cell lines have shown that

restoration of healthy homeostasis is achievable by inhibiting apoptosis and increasing autophagy, [27] so future efforts at achieving this same balance in the liver during NMP may lead to recovery of function in suboptimal donor livers. We also observed that sustained pro-survival signaling is correlated with liver function. While IL-6 was activated following NMP in functional and nonfunctional livers, activation of non-injurious survival signaling persisted into the 6hr time point exclusively in functional livers. We also see earlier activation of IPA Upstream Regulators corresponding to cell growth and survival in functional livers. While we didn't observe signs characteristic of hepatocyte regeneration, 6hr of NMP may be insufficient in potency or duration to induce cell cycle entry as occurs following partial hepatectomy. [28,29]

Ultimately, we found a high degree of heterogeneity between these livers, even within the subgroups that met or failed functional criteria, and across both lean and steatotic backgrounds. Most notably, in the nonfunctional group, one liver (N1) more closely resembled the functional livers than its peer nonfunctional livers in gene expression patterns by PCA as well as analysis of eIF2α and p70S6K (Figures 1; 2; 4). Meanwhile, nonfunctional liver N2 had the worst viability metrics and almost no transcriptional changes observed over 6hr of NMP. Based on the pattern of transcriptional response, it is possible that some livers like N1 that did not meet functional metrics could have been induced into a functional state over additional time, reinforcing the utility of longer perfusions as typically done in clinical practice. [30] We also observed variability in IRI severity in the functional livers despite their meeting viability criteria, highlighting that current clinical metrics cannot fully capture how a liver will respond following transplantation.

Our study did have three important limitations. First, while the liver is composed of multiple cell types including stellate cells, Kupffer cells, sinusoidal endothelial cells, and biliary ductal cells, our viability metrics were optimized to assay the primary parenchymal cell of the liver, hepatocytes. Examining the contributing factors to graft viability by these other cell types is

beyond the scope of this study, but important in context to the elevated risk of post-transplant ischemic cholangiopathy seen from DCD donors. [31] Secondly, we were not able to carry the livers meeting functional metrics through to transplantation following NMP in order to assess their true viability in a patient. At the time of this study, no machine perfusion device had regulatory approval outside the scope of a clinical trial, making such a follow-up impossible as part of this study, though we hope to implement this in future work following regulatory approval. Finally, our study had a small sample size that may have masked nuanced factors involved in the response to NMP. This is in part due to the scarcity of available human donor livers available for experimentation, as well as our decision to limit the study to non-steatotic DCD livers to minimize sample heterogeneity. [7] However, we were nevertheless able to identify multiple potential biomarkers and therapeutic targets using our multiomics approach.

This study offers insight into the physiological responses of discarded DCD human livers during normothermic machine perfusion, as well as the underlying transcriptomic changes that drive them. We identify differential activation of injury and repair mechanisms correlating with liver functionality metrics, where more functional livers were able to activate autophagy and cellular repair processes in response to reperfusion injury, while nonfunctional livers had unregulated innate immunity, inflammation, and apoptosis responses. Targeting these pathways to balance this response may restore homeostasis, and thereby rehabilitation of nonfunctional donor livers. Importantly, our analysis of the analysis of livers scored for micro- and macrosteatosis reveals similar responses as seen in lean livers. This implies that targeted interventions to improve lean liver function are also applicable to steatotic livers. We also observe that the presence of steatosis does not necessarily mean worse performance in physiological viability metrics than in lean donor livers. NMP could be an important tool for making an accurate assessment of donor liver function, maximizing the ability to make the most of the donor liver pool.

Figures

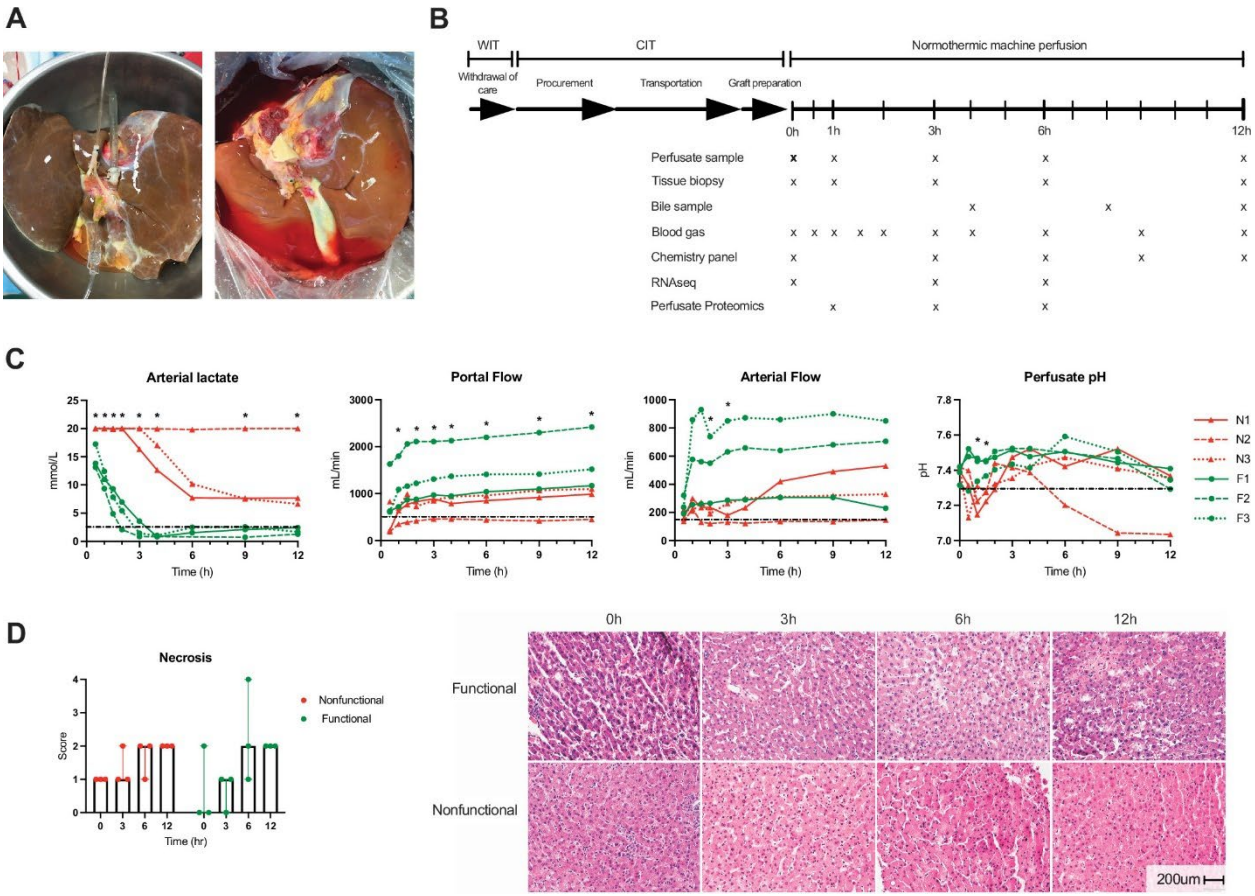

Figure 1. Study schematic and perfusion metrics. *A:* representative images of two human livers being prepared for machine perfusion. *B:* study schematic indicating periods of warm and cold ischemia during procurement followed by normothermic machine perfusion. Data and sample collection time points are indicated by "x" under the perfusion time bar. *C:* criteria used to determine hepatocellular function are shown for individual livers (red: non-functional, green: functional). Functional livers are primarily characterized by the ability to clear lactate below the 2.5 mmol/L threshold. Dotted black line indicates criteria thresholds. **P* < 0.05 for group comparison at indicated time point. Lactate assay upper limit is 20 mmol/L. *D:* hepatocellular necrosis scores at individual time points demonstrate no significant difference between groups. Representative H&E images of functional and nonfunctional livers are shown. Scale bar: 200 microns. CIT, cold ischemic time; H&E, hematoxylin and eosin; F, functional liver; N, nonfunctional liver; WIT, warm ischemic time.

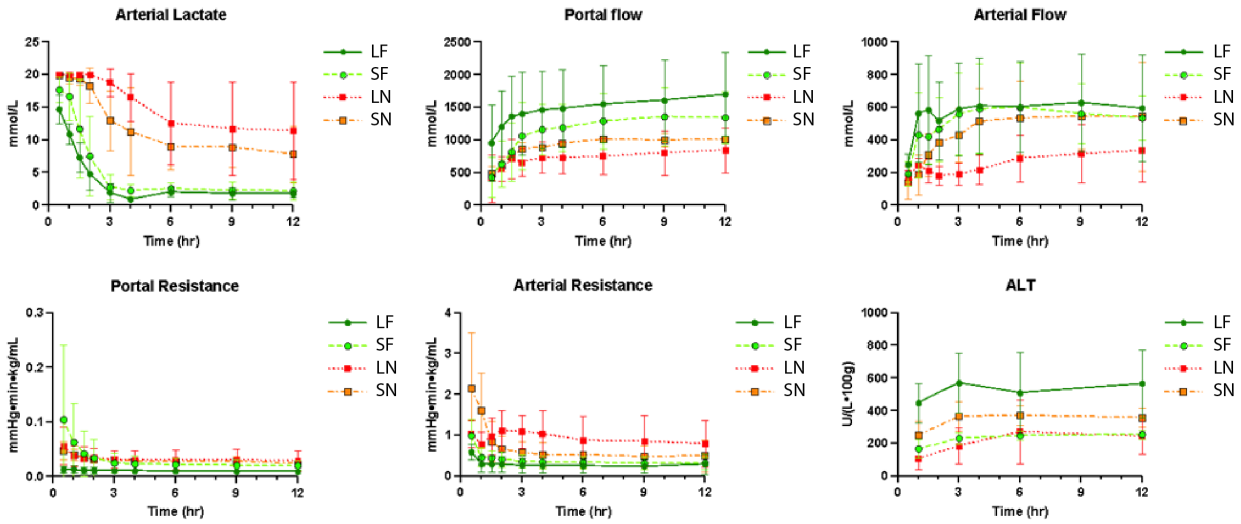

Figure 2. Physiological metrics of Lean and Fatty livers, Viable and Nonviable. Similar to the lean liver metrics in Figure 1C, the set of steatotic livers demonstrated highly variable physiological responses to NMP, with half meeting some viability metrics after perfusion. Both lean and steatotic livers were segregated into functional and nonfunctional groups, and performance tended to look similar between functional groups regardless of steatotic origin.

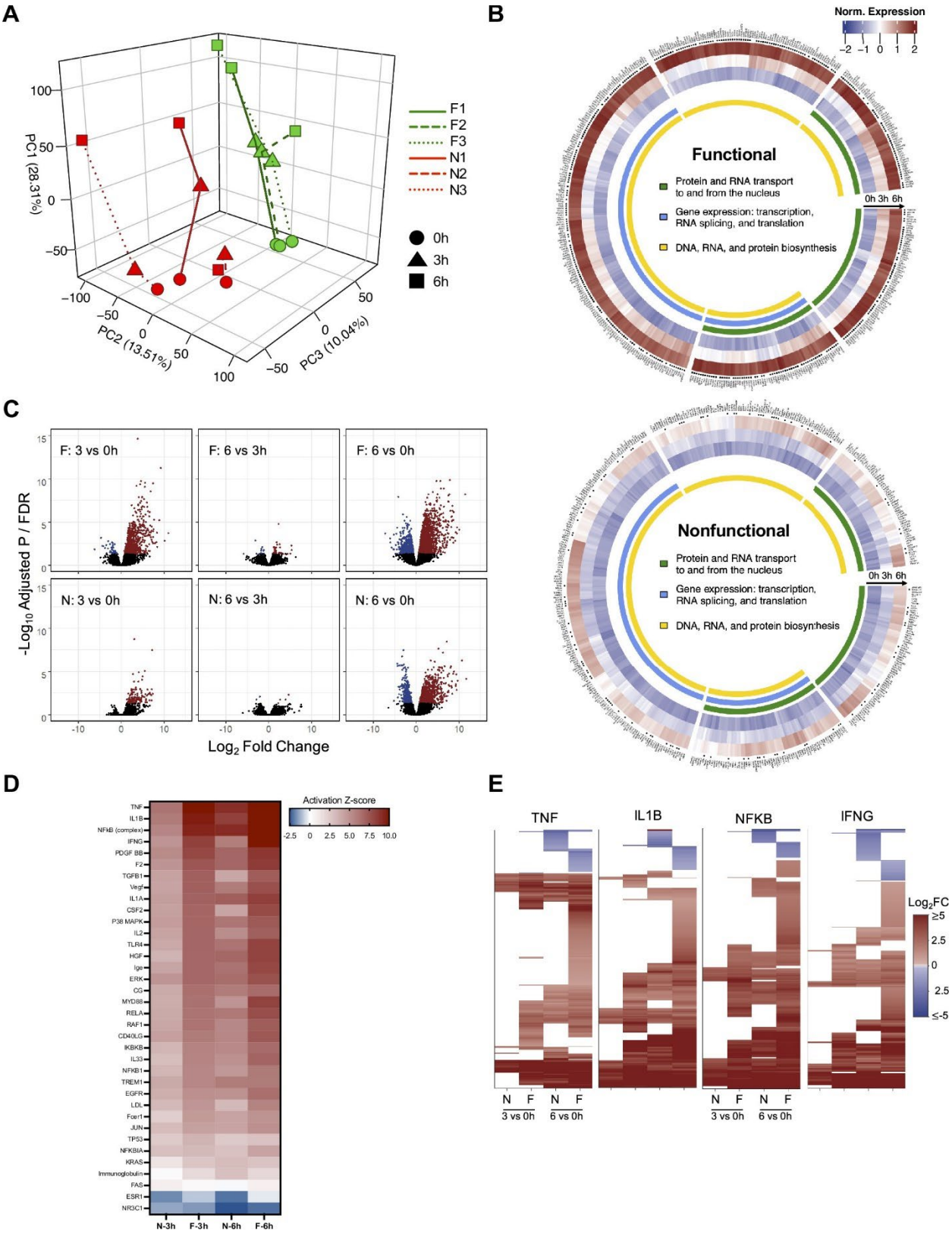

Figure 3. Comparison of differential gene expression patterns in functional and nonfunctional livers. *A:* three-dimensional (3-D) PCA plot demonstrates clustering of individual livers at 0, 3,

and 6 h of perfusion (red: nonfunctional, green: functional). *B:* circular heatmaps for each group represent the top 10% of genes accounting for the variance in PC1. *FDR < 0.05 for either 3 h vs. 0 h or 6 h vs. 0 h comparison. *C:* volcano plots (FDR vs. fold change) comparing gene expression between time points in functional and nonfunctional livers. Genes meeting the FDR cutoff <0.05 are shown in red (upregulated) and blue (downregulated); nonsignificant genes are shown in black. *D:* activation *Z*-scores of the top significant ($P < 10^{-14}$) upstream regulators from IPA enriched in both functional and nonfunctional groups at 3 and 6 h relative to preperfusion (0 h). *E:* heatmaps show differential expression of downstream gene targets for the top four upstream regulators (log_2FC shown for 3 h vs. 0 h and 6 h vs. 0 h comparisons, FDR cutoff <0.05); nonsignificant expression indicated by white space). F, functional livers; FDR, false discovery rate; IPA, ingenuity pathway analysis; N, nonfunctional livers; PC1, principal component 1; TNF, tumor necrosis factor; IL1β, interleukin 1β; NF-κB, nuclear factor-κβ subunit; IFNγ, interferon γ.

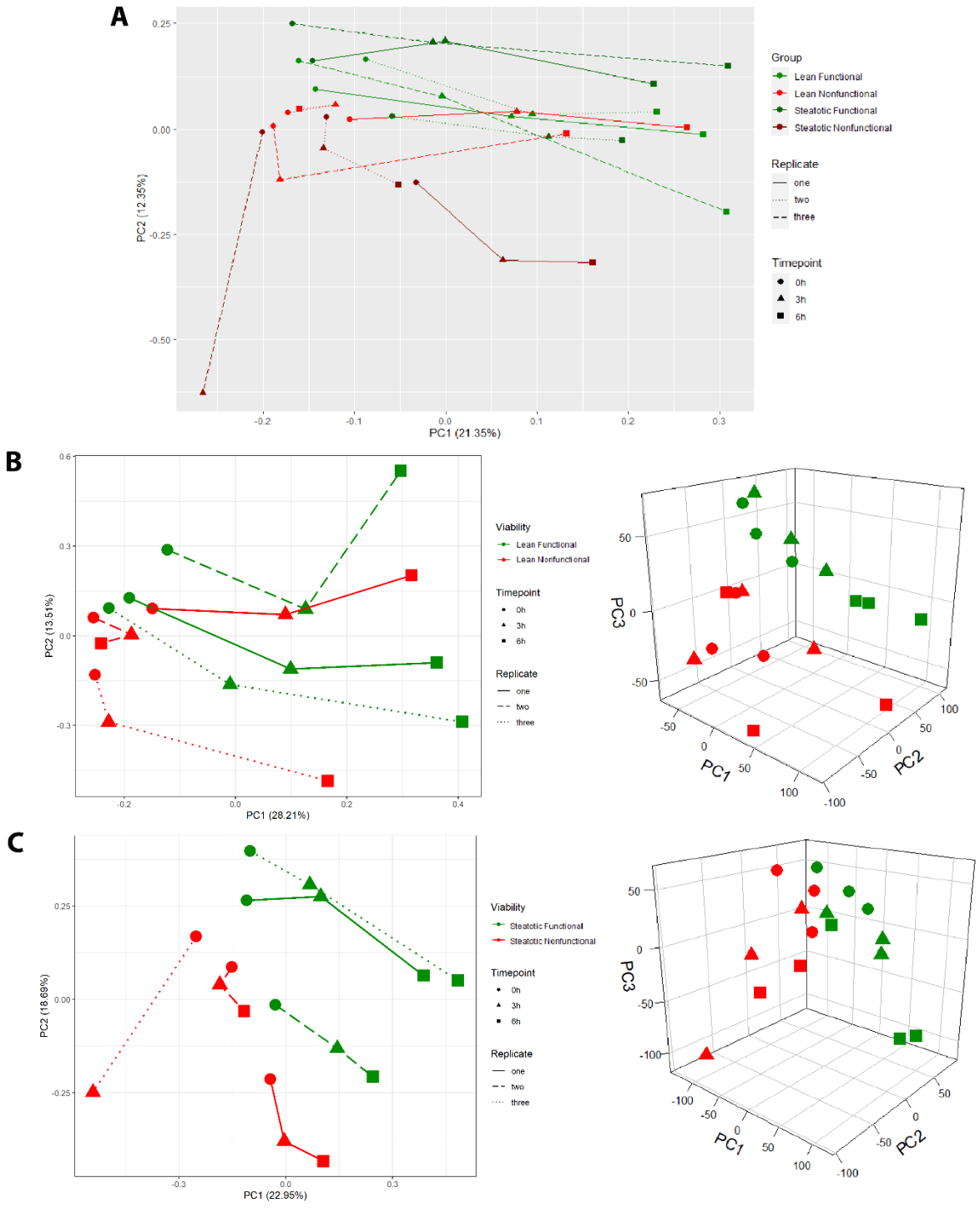

Figure 4. PCAs of Lean and Steatotic sample gene expression. PCAs of *A:* all samples (Lean and Steatotic) plotted together shows a strong degree of overlapping expression between functional and nonfunctional samples. PCAs of *B:* Lean livers in 2D and 3D and *C:* Steatotic livers in 2D and 3D show that in both Lean and Steatotic livers, the transcriptomics over the NMP time course clearly segregates Function and Nonfunctional livers into distinct groups, and shows the changes in gene expression progressing from 0h to 3h and 6h of NMP.

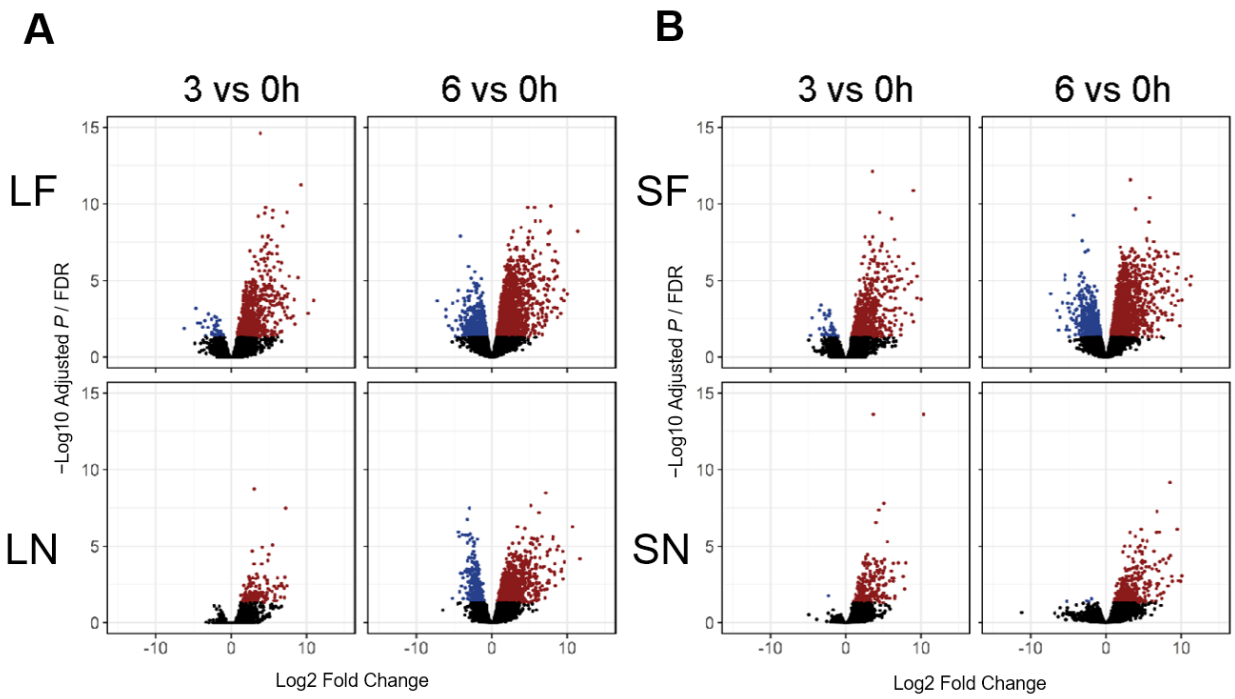

Figure 5. Volcano Plots of *A:* Lean and *B:* Steatotic DEGs across 3 and 6h of NMP. Steatotic livers had overall similar gene expression profiles at 3h and 6h to Lean livers, potentially indicating a shared response to NMP and rehabilitation of functionality.

A

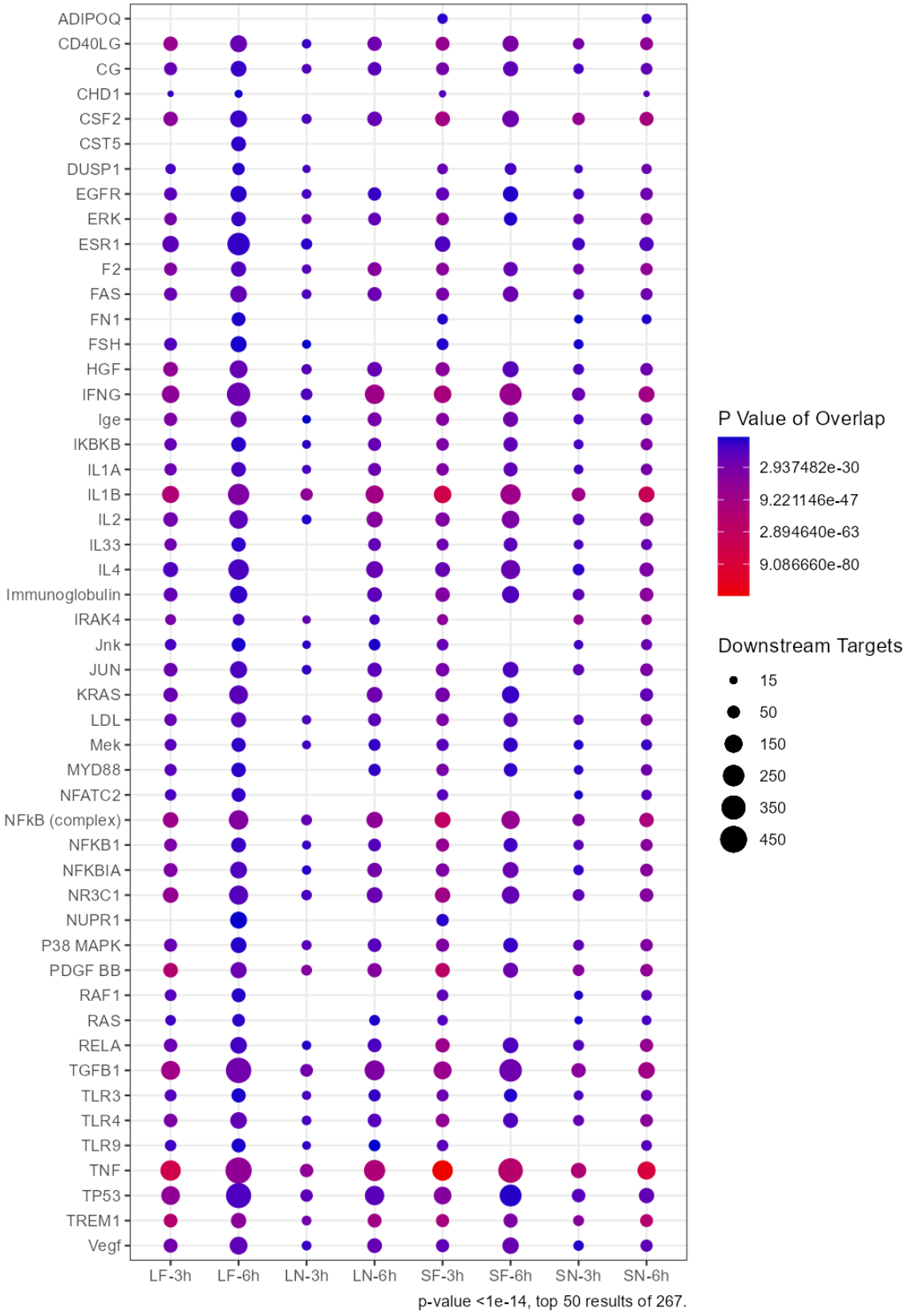
ADIPOQ
CD40LG
CG
CHD1
CSF2
CST5
DUSP1
EGFR
ERK
ESR1
F2
FAS
FN1
FSH
HGF
IFNG
Ige
IKBKB
IL1A
IL1B
IL2
IL33
IL4
Immunoglobulin
IRAK4
Jnk
JUN
KRAS
LDL
Mek
MYD88
NFATC2
NFkB (complex)
NFKB1
NFKBIA
NR3C1
NUPR1
P38 MAPK
PDGF BB
RAF1
RAS
RELA
TGFB1
TLR3
TLR4
TLR9
TNF
TP53
TREM1
Vegf
LF-3h
LF-6h
LN-3h
LN-6h
SF-3h
SF-6h
SN-3h
SN-6h
p-value <1e-14, top 50 results of 267.
P Value of Overlap
2.937482e-30
9.221146e-47
2.894640e-63
9.086660e-80
Downstream Targets
15
50
150
250
350
450

B

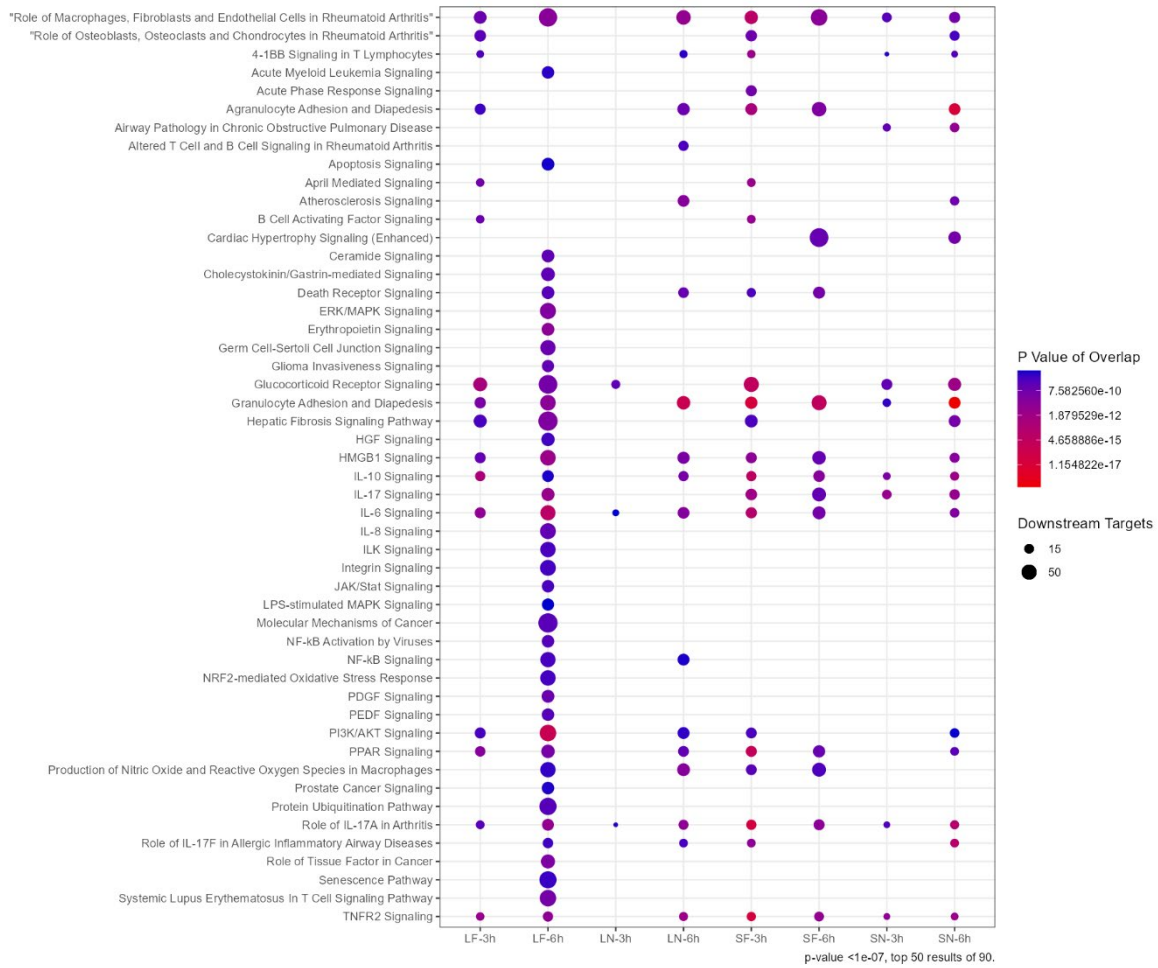

Figure 6. IPA Results for Lean and Steatotic samples. Dotplots show the top 50 most significant results in the Lean Functional group for *A:* Upstream Regulators and *B:* Canonical Pathways. Many of the most significant activated regulators in functional livers were shared between lean and steatotic groups, and similar pattern of lowered activation is seen in nonfunctional livers from both groups, indicating similar pathways play a role in positive and negative responses to NMP. Dot size corresponds to the number of activated Downstream Targets. Dot color corresponds to the P Value of Overlap.

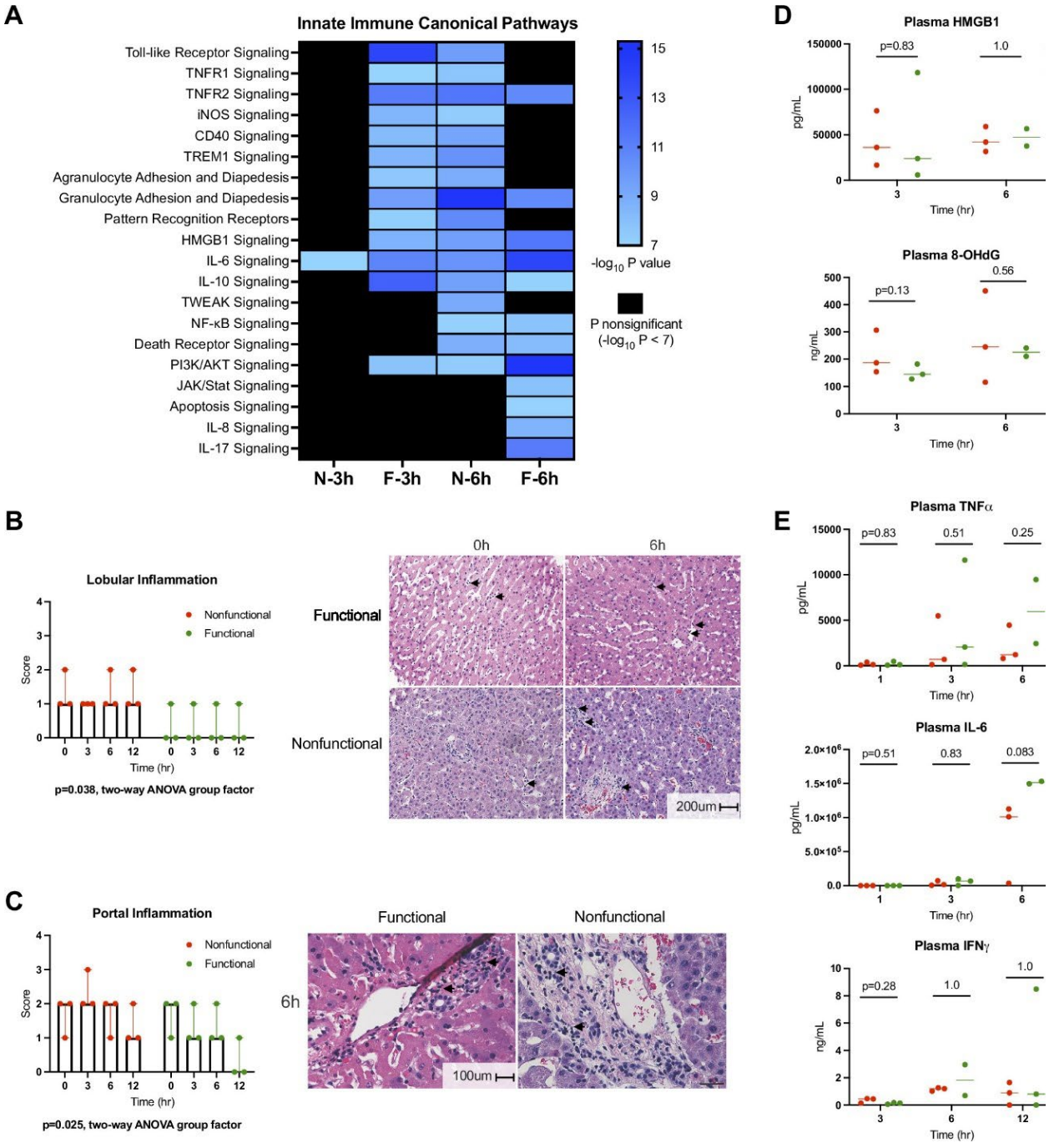

Figure 7. Ischemia-reperfusion injury and innate immunity in functional and nonfunctional livers. *A:* heatmap displays enrichment of canonical pathways related to innate immunity derived from IPA. The significance threshold was set to $-\log_{10}$ *P* value > 7 for comparisons of 3- and 6-h gene sets to preperfusion (0 h) baseline for each group. Lobular (*B*) and portal (*C*) inflammatory infiltrate as scored by a blinded pathologist. Representative H&E images for functional and nonfunctional livers are displayed. Scale bars: 200 μm (lobular), 100 μm (portal). *D:* damage-associated molecular pattern (HMGB1) and oxidative stress (8-OHdG) levels in circulating perfusate. Liver F2 6-h perfusate sample not available. *E:* perfusate levels of cytokines involved in IRI response. Liver F2 6-h perfusate sample not available. F, functional livers (green); H&E;

hematoxylin-eosin; HMGB1, high mobility group box 1; IFNγ, interferon γ; IL-6, interleukin-6; IPA, ingenuity pathway analysis; JAK/STAT, Janus kinase/signal transducer and activator of transcription; N, nonfunctional livers (red); NF-κB, nuclear factor-κβ subunit; 8-OHdG, 8-hydroxy-2′deoxyguanosine; TNFα, tumor necrosis factor α.

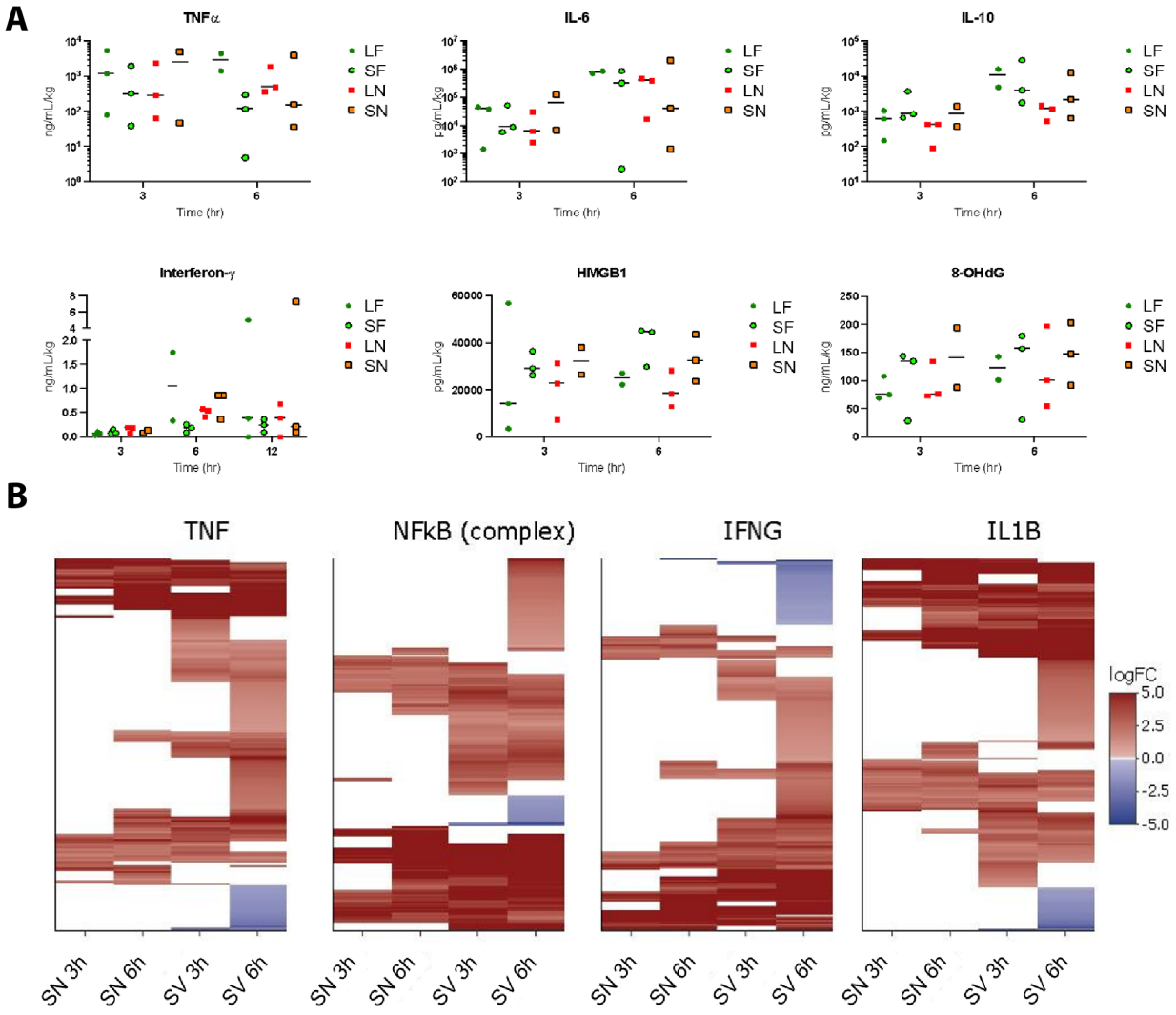

Figure 8. Measurements of perfusate and downstream activation in all groups. *A:* Expression level of selected molecules in perfusate in Lean and Steatotic livers, Functional and Nonfunctional. DAMP and cytokine levels were similar at each time point regardless of lean or steatotic status. *B:* Downstream target activation of IPA Upstream Regulators for Steatotic samples. As with lean samples, we see more downstream target expression in the functional livers and at 6hr, with the most expression at the intersection of those groups.

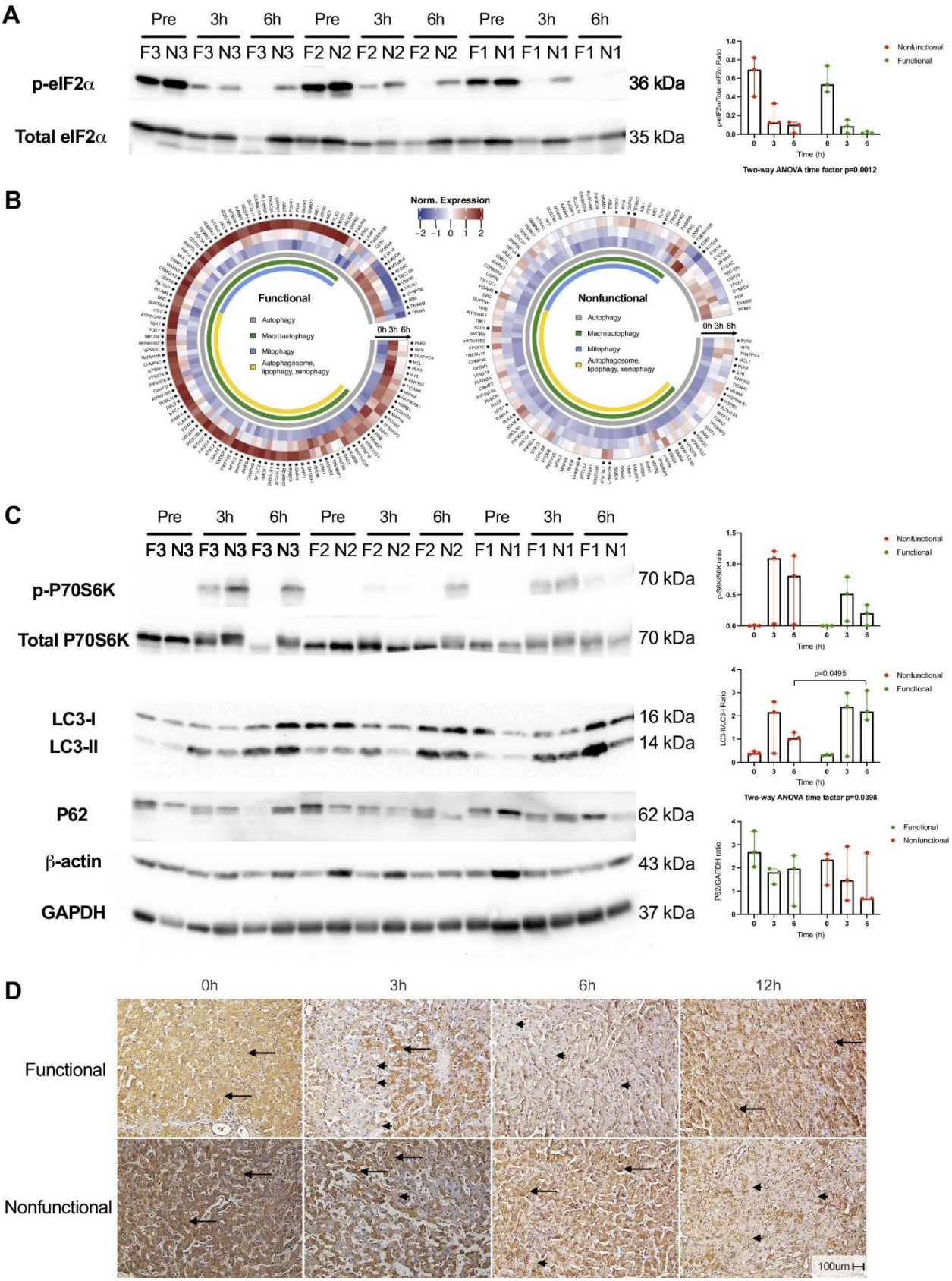
A
Pre 3h 6h Pre 3h 6h Pre 3h 6h
F3 N3 F3 N3 F3 N3 F2 N2 F2 N2 F2 N2 F1 N1 F1 N1 F1 N1
p-eIF2α
Total eIF2α
36 kDa
35 kDa
Nonfunctional
Functional
p-eIF2α/Total eIF2α Ratio
Time (h)
Two-way ANOVA time factor p=0.0012
B
Norm. Expression
−2 −1 0 1 2
Functional
Autophagy
Macroautophagy
Mitophagy
Autophagosome, lipophagy, xenophagy
0h 3h 6h
Nonfunctional
Autophagy
Macroautophagy
Mitophagy
Autophagosome, lipophagy, xenophagy
0h 3h 6h
C
Pre 3h 6h Pre 3h 6h Pre 3h 6h
F3 N3 F3 N3 F3 N3 F2 N2 F2 N2 F2 N2 F1 N1 F1 N1 F1 N1
p-P70S6K
Total P70S6K
70 kDa
70 kDa
Nonfunctional
Functional
p-S6K/S6K ratio
Time (h)
LC3-I
LC3-II
16 kDa
14 kDa
p=0.0495
Nonfunctional
Functional
LC3-II/LC3-I Ratio
Time (h)
Two-way ANOVA time factor p=0.0398
P62
62 kDa
β-actin
43 kDa
GAPDH
37 kDa
Functional
Nonfunctional
P62/GAPDH ratio
Time (h)
D
0h 3h 6h 12h
Functional
Nonfunctional
100um

Figure 9. Activation of autophagy in response to injury and stress during NMP. *A:* Western blot of phosphorylated and total eIF2α with densitometry ratios. *B:* circular heatmaps demonstrating differential expression of genes associated with the GO term “autophagy” in functional and nonfunctional livers. Asterisk (*) next to gene names indicates FDR < 0.05 for either 3 h vs. 0 h or 6 h vs. 0 h comparison. *C:* phospho-/total P70S6K, LC3-I/-II, and P62 Western blots for both groups with densitometry ratios. b-Actin and GAPDH levels are shown as control and demonstrate variability between human livers. *D:* representative images of LC3 immunohistochemistry shown for both groups. Scale bar: 100 μm. eIF2α, eukaryotic initiation factor 2α; FDR, false discovery rate; F, functional livers (green); GO, gene ontology; LC3-I/-II, light chain 3-I/II; N, nonfunctional livers (red); NMP, normothermic machine perfusion.

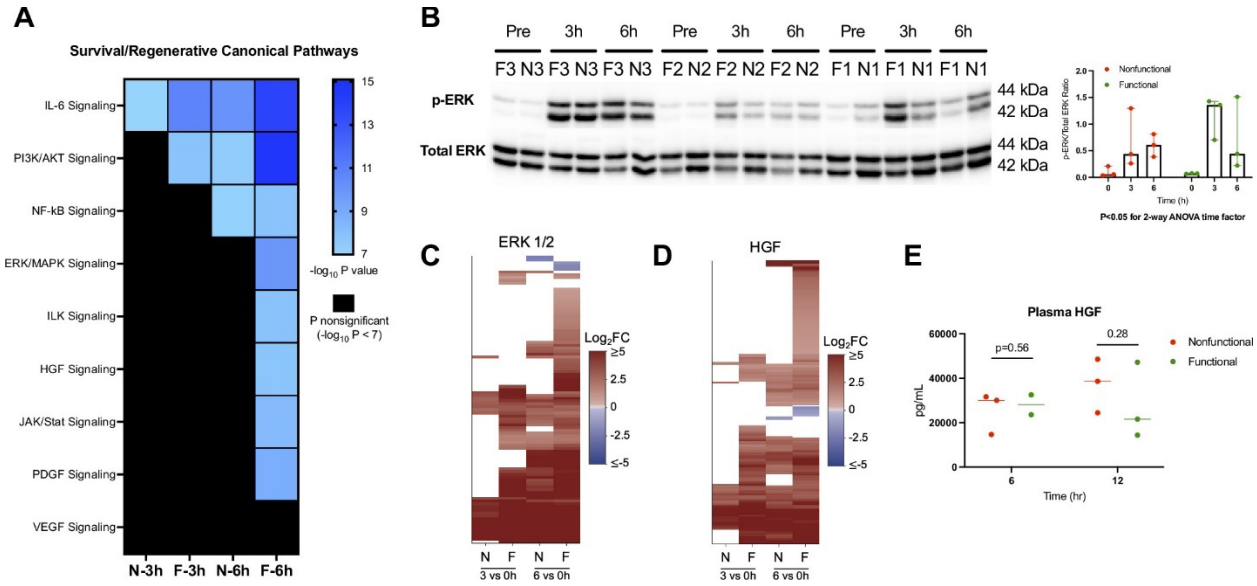

Figure 10. Prosurvival and regenerative signaling during NMP. *A:* heatmap displays enrichment of canonical pathways related to prosurvival and regenerative signaling derived from IPA. The significance threshold was set to $-\log_{10} P$ value > 7 for comparison of 3- and 6-h gene sets to the preperfusion (0 h) baseline for each group. *B:* Western blot of phosphorylated and total ERK (*top*) with densitometry ratios (*bottom*). *C:* heatmap displaying differential expression of downstream ERK targets in functional and nonfunctional livers ($\log_2$FC shown for 3 h vs. 0 h and 6 h vs. 0 h comparisons, FDR cutoff <0.05); nonsignificant expression indicated by white space). Target list derived from upstream regulator analysis in IPA. *D:* perfusate concentration of HGF in both groups after 6 and 12 h of NMP. Liver F2 6-h perfusate sample not available. *E:* heatmap of downstream gene target differential expression for HGF. F, functional livers; FDR, false discovery rate; HGF, hepatocyte growth factor; IPA, ingenuity pathway analysis; JAK/STAT, Janus kinase/signal transducer and activator of transcription; $\log_2$FC, log2 fold change; N, nonfunctional livers; NF-κB, nuclear factor-κβ subunit; NMP, normothermic machine perfusion.

Supplemental Data

Supplemental Data Sets S1, S2, and S3: https://doi.org/10.5061/dryad.f7m0cfxx0.
Supplemental Methods and Figs. S1–S8: https://doi.org/10.5281/zenodo.5206547.

Supplemental Methods

S1. Enzyme-linked immunosorbent assay (ELISA) kits

Protein	Manufacturer	Product Number
Tumor necrosis factor-alpha (TNFα)	Sigma-Millipore	RAB0476
Interleukin-6 (IL-6)	Sigma-Millipore	RAB0306
High mobility group box 1 (HMGB1)	Aviva Systems Biology	OKCD04074
Interferon-gamma (IFNγ)	Abcam	ab174443
8-hydroxy 2-deoxyguanosine (8OHdG)	Abcam	ab201734
Hepatic growth factor (HGF)	Abcam	ab100534
Cathepsin D	Abcam	ab213470

Abcam (Waltham, MA, USA), Aviva Systems Biology (San Diego, CA, USA), Sigma-Millipore (Waltham, MA, USA).

S2. Perfusate Proteomics

Mass Spectrometry Data-Independent Acquisition (DIA)

Following depletion of abundant proteins from serum samples using High Select Top 14 resin (Thermo Fisher, Waltham, MA, USA), remaining serum proteins were reduced, alkylated, and purified by chloroform/methanol extraction prior to digestion with sequencing grade modified porcine trypsin (Promega, Madison, WI, USA). Tryptic peptides were then separated by reverse phase XSelect CSH C18 2.5 micrometer resin (Waters, Milford, MA, USA) on an in-line 150 x 0.075 mm column using an UltiMate 3000 RSLCnano system (Thermo Fisher). Peptides were eluted using a 60 min gradient from 98:2 to 65:35 buffer A:B ratio (Buffer A, 0.1% formic acid, 0.5% acetonitrile; Buffer B, 0.1% formic acid, 99.9% acetonitrile). Eluted peptides were ionized by electrospray (2.2 kV) followed by mass spectrometric analysis on an Orbitrap Exploris 480 mass spectrometer (Thermo Fisher). To assemble a chromatogram library, six gas-phase fractions were acquired on the Orbitrap Exploris with 4 m/z DIA spectra (4 m/z precursor isolation windows at 30,000 resolution, normalized automatic gain control (AGC) target 100%, maximum inject time 66 ms) using a staggered window pattern from narrow mass ranges using optimized window placements. Precursor spectra were acquired after each DIA duty cycle, spanning the m/z range of the gas-phase fraction (i.e. 496-602 m/z, 60,000 resolution, normalized AGC target 100%, maximum injection time 50 ms). For wide-window acquisitions,

the Orbitrap Exploris was configured to acquire a precursor scan (385-1015 m/z, 60,000 resolution, normalized AGC target 100%, maximum injection time 50 ms) followed by 50x 12 m/z DIA spectra (12 m/z precursor isolation windows at 15,000 resolution, normalized AGC target 100%, maximum injection time 33 ms) using a staggered window pattern with optimized window placements. Precursor spectra were acquired after each DIA duty cycle.

Data Analysis

Following data acquisition, we searched the data using an empirically-corrected library and performed a quantitative analysis to obtain a comprehensive proteomic profile of the *Homo sapiens* proteome. Proteins were identified and quantified using EncyclopeDIA [32] and visualized with Scaffold DIA using 1% false discovery thresholds at both the protein and peptide level.

Protein exclusive intensity values were assessed for quality using our in-house ProteiNorm app, a user-friendly tool for a systematic evaluation of normalization methods, imputation of missing values and comparisons of different differential abundance methods. [33] Popular normalization methods were evaluated including log2 normalization (Log2), median normalization (Median), mean normalization (Mean), variance stabilizing normalization (VSN), [34] quantile normalization (Quantile) (R software preprocessCore), cyclic loess normalization (Cyclic Loess), [35] global robust linear regression normalization (RLR), [36] and global intensity normalization (Global Intensity). [36] The individual performance of each method was evaluated by comparing the following metrices: total intensity, Pooled intragroup Coefficient of Variation (PCV), Pooled intragroup Median Absolute Deviation (PMAD), Pooled intragroup estimate of variance (PEV), intragroup correlation, sample correlation heatmap (Pearson), and log2-ratio distributions.

The data was normalized using Cyclic Loess and differential abundance analysis was performed using Linear Models for Microarray Data (limma) with empirical Bayes (eBayes) smoothing to the standard errors. [36] Proteins with an FDR adjusted p-value < 0.05 and a fold change > 2 were considered to be significant.

S3. Total RNA purification, sequencing, and analysis

RNA Purification and Sequencing

Tissues samples from livers taken immediately prior to perfusion and after 3 and 6 hours of perfusion were used for transcriptome sequencing. Core needle biopsies from the right liver lobe were collected in RNAlater solution (Sigma-Millipore, Waltham, MA, USA) and stored overnight at 4°C. Tissue samples were then removed from solution and stored at -80°C. Total RNA was isolated using the RNeasy Mini Kit (Qiagen, Germantown, MD, USA) according to manufacturer guidelines. 500ng of each sample was sequenced on an Illumina HiSeq 4000 using 9 PCR cycles by GENEWIZ (South Plainfield, NJ, USA). Data files were aligned to the human genome build 38 and transferred to servers at Brown University via sFTP.

Bioinformatic analysis

Raw read counts were normalized using the Trimmed Mean of M method following removal of low-count genes (fewer than 10 reads in the smallest library). Differential gene expression

analysis was conducted in R [37] using edgeR. [38] The significance cutoff for differential gene expression was set to a Benjamini-Hochberg false-discovery rate (FDR or q-value) < 0.05. Canonical pathway and upstream regulator enrichment analysis was generated through Ingenuity Pathway Analysis (IPA, Qiagen). [39] IPA categories were considered significant when the P value was below the P values obtained from 5 similarly sized sets of randomly selected genes with a fold-change in expression ≤1. [40] In this study, the threshold for significance was P<10E-7 for canonical pathways and P<10E-14 for upstream regulators.

Principal component analysis (PCA), volcano plots, Venn diagrams, and heatmaps were created using the following R packages: ggplot2 (2D PCA), plot3D/plot3Drgl (3D PCA), EnhancedVolcano (volcano plots), VennDiagram (Venn diagrams), and heatmaply (heatmaps).

Transcription factor binding site enrichment analysis was conducted using the software package CiiiDER. The total number of genes with putative transcription factor binding site motifs were compared between differentially expressed gene sets and the background gene set used in the differential expression analysis. Significance for transcription factor binding site enrichment is determined using a Fisher's exact test and a P value cutoff of 0.05. The analysis was performed using the lists of differentially expressed genes identified for the four individual perfusion conditions relative to their corresponding pre-perfused state (Dataset S2).

Gene ontology (GO) enrichment analysis was performed using the R package GOseq. A Benjamini-Hochberg FDR adjusted p-value of < 0.05 was used for determining significant GO term enrichment. [41] The genes with the highest amount of variance explained by principal component 1 or 3 cumulatively totaling to 10% of the total variance explained by PC1/PC3 were further analyzed. The proportion of variance explained for a gene by PC1/PC3 was calculated using the squared loading values generated by the prcomp function in R. GO term analysis was performed on the genes from this subset that positively correlated with PC1/PC3. The significantly enriched GO terms in the biological processes category for PC1 and cellular components category for PC3 were organized in hierarchal networks and parsed in to three independent 'regions' of categories that best captured the majority of GO term nodes. These clusters were characterized by a parental GO term and included all sub-categories of that node found significantly enriched in our gene set (Parental and sub-categories are listed in Dataset S4). For PC1, the resulting individual sub-networks of significantly enriched GO terms were then functionally generalized in to “Protein and RNA transport to and from the nucleus”, “Gene expression: transcription, RNA splicing, and translation” and “DNA, RNA, and protein biosynthesis”. For PC3, the resulting individual sub-networks of significantly enriched GO terms were then functionally generalized in to “Extracellular vesicle/exosome”, “Intrinsic component of membrane” and “Endoplasmic reticulum”. Circular heatmaps were generated with the circlize package in R (6) [42] using the means of biological replicates from the normalized counts per million read data then scaled by row to show relative gene expression across the 6 conditions (2 groups, 3 time points). Only genes associated with these GO terms were used in the heatmaps. The genes were clustered according to their association with the three GO term sub-networks, and the clusters were denoted by colored concentric rings inside the center of the circular heatmaps. The rows are labeled with the gene symbol and the columns are oriented from innermost to outermost as 0 hour (pre-perfusion), 3 hour, and 6 hour time points. Genes with

significant differential expression FDR of < 0.05 at 3 or 6 hours perfusion compared to pre-perfusion are indicated with a *.

Raw sequence data have been deposited in the Gene Expression Omnibus (GEO) with accession no. GSE165568.

S4. H&E Scoring System

i) Necrosis
0=None
1=Few scattered cells
2=Mild (anything from “few” up to 30% of the section affected)
3=Moderate (31% to 60%)
4=Severe (61% +)

ii) Lobular Inflammation
0=None
1=Minimal (up to four scattered small foci of a few cells; or one/two cells seen multifocally)
2=Mild (anything from “minimal” up to 25% of section affected)
3=Moderate (26% to 60%)
4=Severe (61% or greater)

iii) Portal Inflammation:
0=None
1=Minimal (focal; few scattered cells in one to ‘a few’ portal areas)
2=Mild (focal, most portal areas affected)
3=Moderate (inflammation beginning to expand portal tracts and/or beginning to become continuous/surround up to 50% of portal tracts/septa, +/- extending to interface)
4=Severe (inflammation continuous and around 50% or more portal tracts/septa)

S5. Immunohistochemistry antibodies and methods

Antibody	Manufacturer	Product Number
LC3B	Novus Biologicals (Littleton, CO, USA)	NB100-2220

Immunohistochemistry was performed using antibodies directed toward LC3B (see above). Paraffin sections (6 μm) were deparaffinized with xylene and rehydrated with graded ethanol. Antigen retrieval was performed by sub-boiling in 1X-diluted Dako Target Retrieval Solution for 10 min (DakoCytomation, Inc., Carpinteria, CA). Slides were then quenched in 3% H_2O_2 and blocked in 2.5% Normal Horse Serum (Vector Labs, Burlingame, CA) before overnight incubation in primary antibody (1:200 dilution) at 4°C. Slides were incubated with a horseradish-peroxidase conjugated secondary rabbit antibody (Vector Laboratories) for 1 hr prior to staining with DAB (Vector Laboratories). Slides were counterstained with hematoxylin. Omission of the primary antibody served as a negative control.

S6. Western immunoblot antibodies

Antibody	Manufacturer	Product Number
eIF2α	Santa Cruz Biotechnology	sc-11386
Phospho-eIF2α	Cell Signaling Technology	9721
p70 S6 Kinase	Cell Signaling Technology	2708
Phospho-p70 S6 Kinase (Thr389)	Cell Signaling Technology	9234
MAP Kinase 1/2	Sigma-Millipore	06-182
Phospho-p44/42 MAPK (Erk1/2) (Thr202/Tyr204)	Cell Signaling Technology	4370
LC3B	Cell Signaling Technology	2775
β-actin	Santa Cruz Biotechnology	sc-47778
GAPDH	Cell Signaling Technology	5174
P62	Cell Signaling Technology	39749

Cell Signaling Technology (Danvers, MA, USA), Santa Cruz Biotechnology (Dallas, TX, USA), Sigma-Millipore (Waltham, MA, USA).

To compare target protein expression, densitometry quantification was conducted. Blots for β-actin and GAPDH are shown in Figure 4. Both proteins varied across samples and the changes were not consistent between the two proteins, with the variation representing the biologic variability in the human liver.

Supplemental Figures

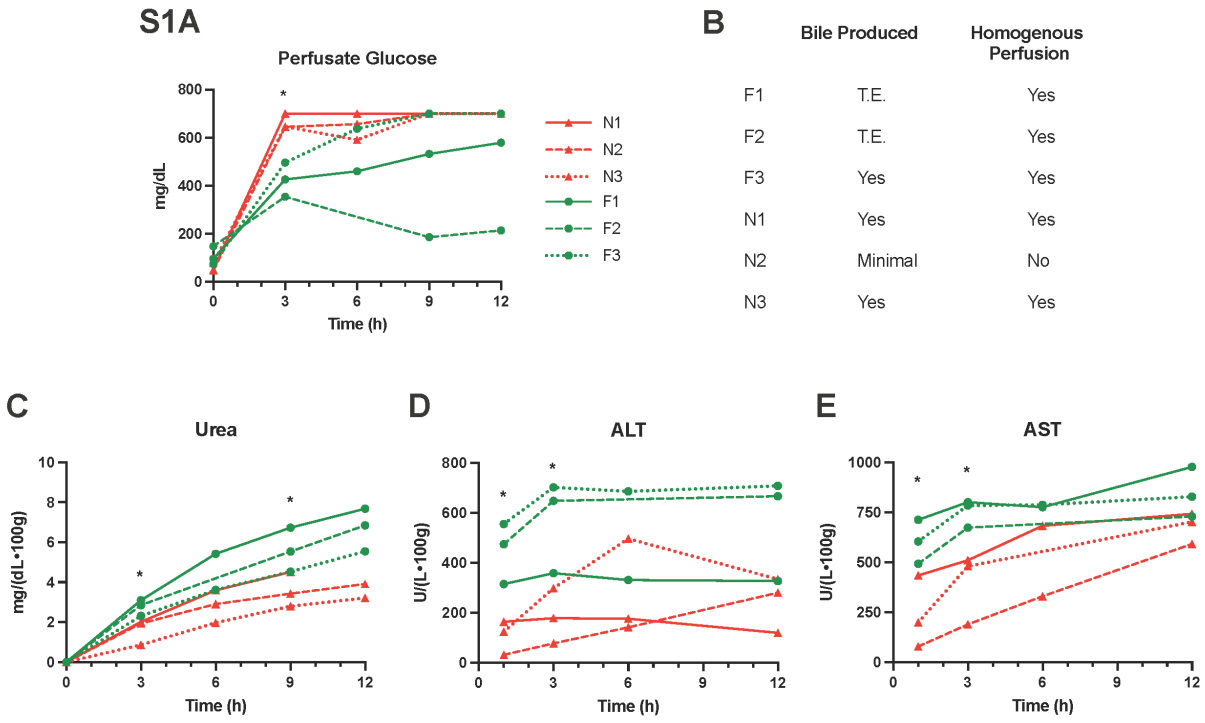

Figure S1. Additional functional metrics for individual livers during NMP. (A) Perfusate glucose concentrations during NMP. * indicates P<0.05 for group comparison; assay upper limit 700 mg/dL. (B) Bile production and visually homogenous liver perfusion of individual livers. (C) Perfusate urea concentration indicating urea synthesis in individual livers. * indicates P<0.05 for group comparison. Liver F2 6-hour perfusate sample not available. (D) ALT and (E) AST levels after initiation of NMP. * indicates P<0.05 for group comparison. N, nonfunctional liver; F, functional liver; T.E., technical error.

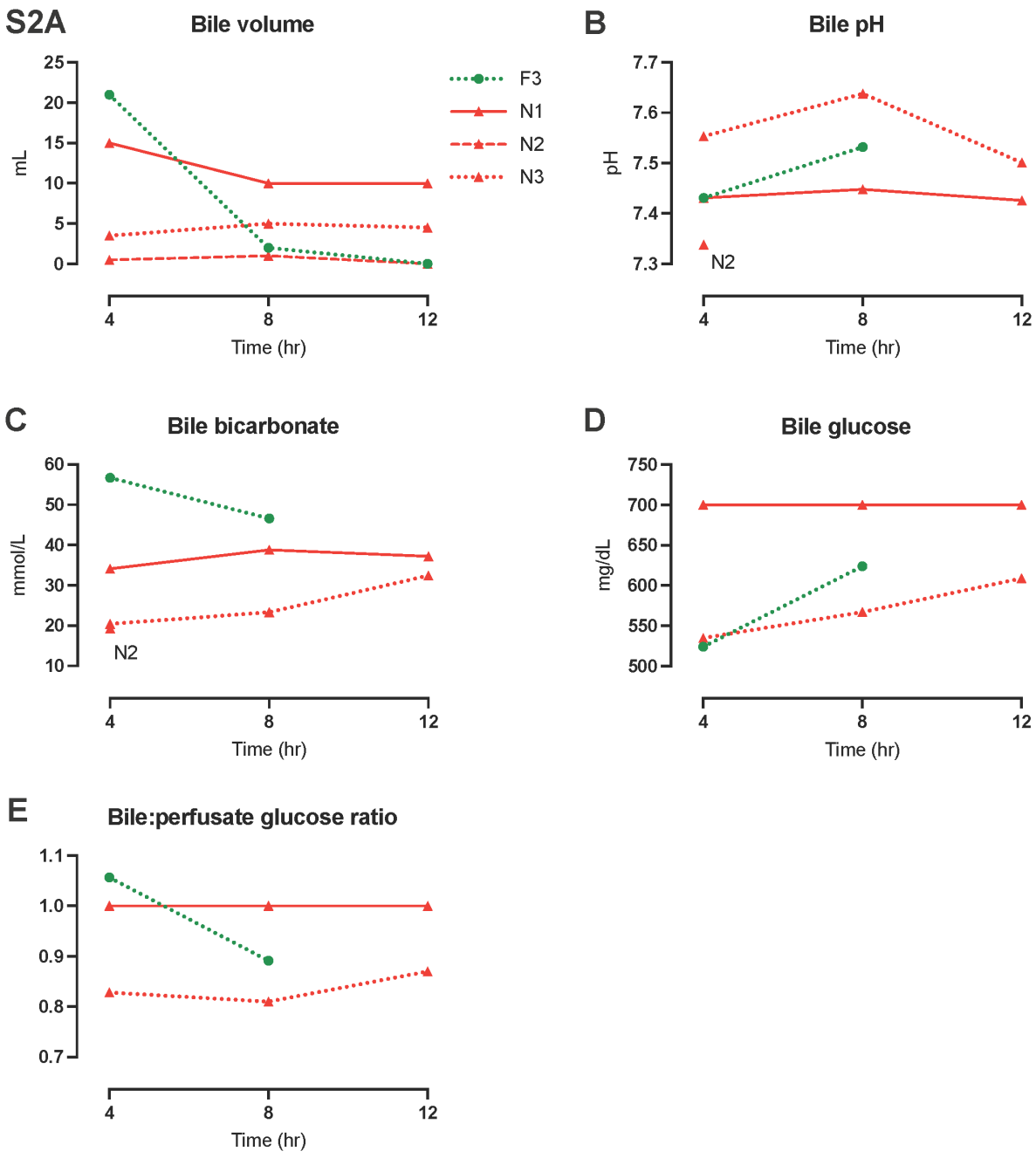

Figure S2. Additional cholangiocellular functional metrics. Bile volume (A) and quality metrics (B-E) after 4, 8, and 12 hours of NMP are shown. Liver N2 produced <1 mL of bile within the time intervals, limiting testing for some metrics. Bile collection was not possible in two livers due to technical errors. Liver F1 demonstrated persistent hemobilia after core needle biopsy, limiting accurate bile sampling. Liver F2 did not produce any bile owing to an unrecognized ductal obstruction due to the biliary cannula. N, nonfunctional liver; F, functional liver.

Fig. S3

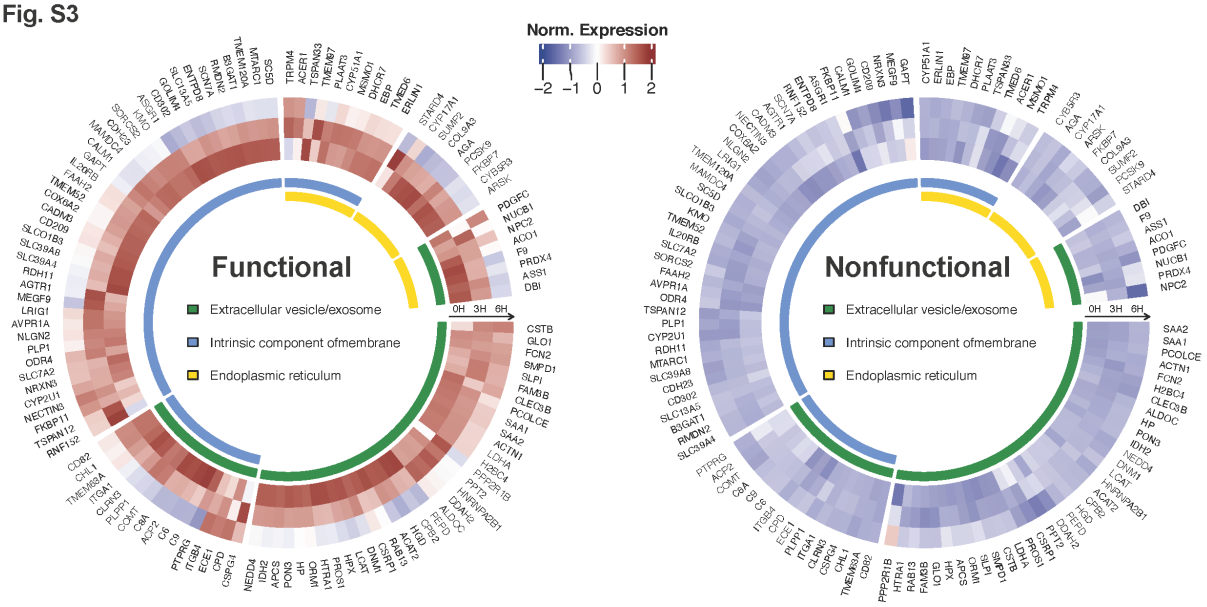

Figure S3. Top 10% of genes accounting for variation in principal component 3. Circular heatmaps display normalized expression of the genes accounting for the top 10% of variation in principal component 3 (PC3) from PCA. GO parental terms are used to categorize genes into 3 major subcategories. Differential expression did not reach significance (FDR<0.05) for any genes when compared within groups at 3h vs 0h or 6h vs 0h. GO, gene ontology.

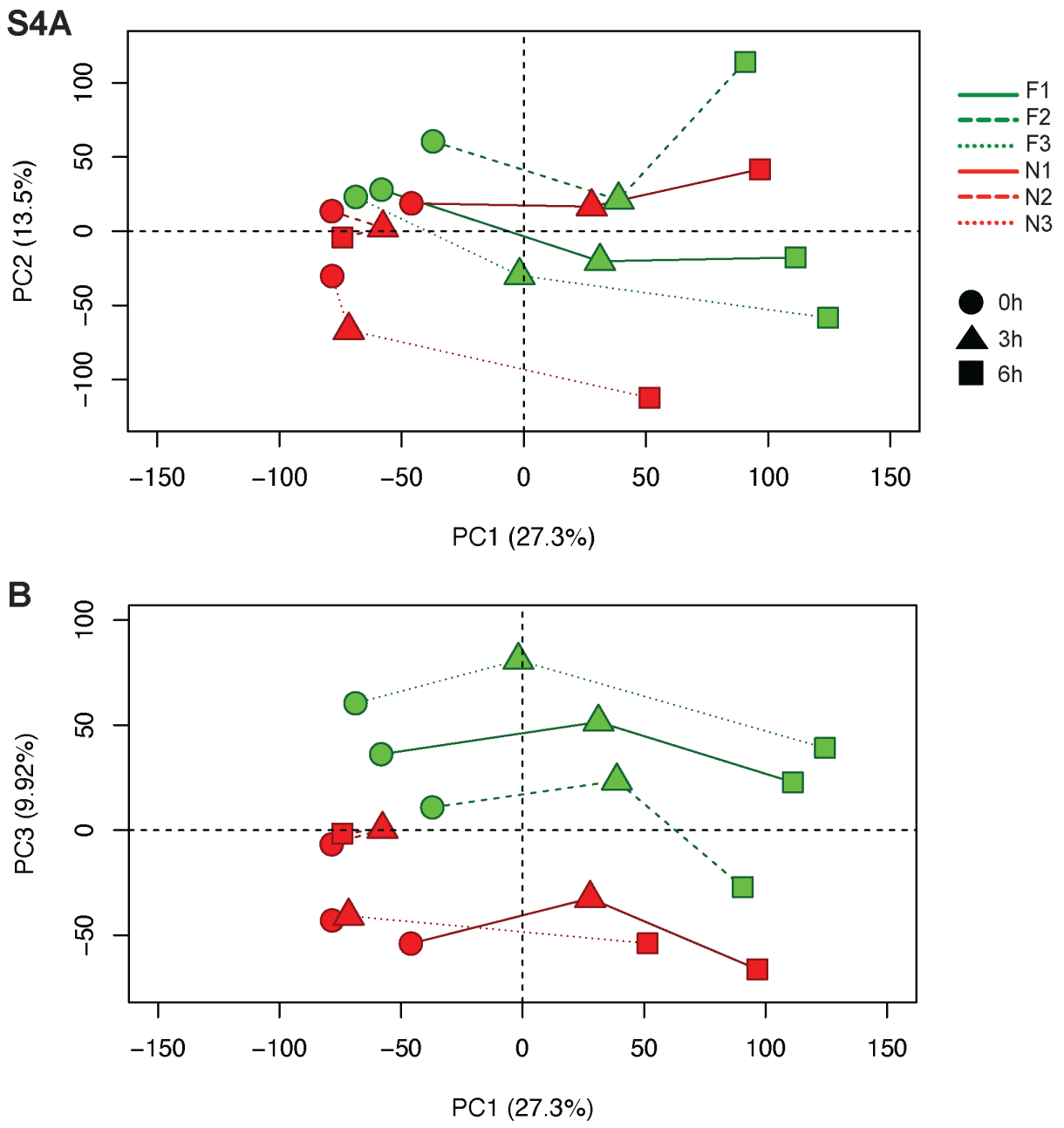

Figure S4. Two-dimensional principal component analysis plots. (A) 2D plot of PC1/PC2 demonstrates close clustering of pre-perfusion (0 hour) gene sets of individual livers. Functional livers tend to cluster together after initiation of perfusion. Nonfunctional liver N1 demonstrates a similar shift in gene expression to the functional livers. (B) 2D plot of PC1/PC3 more effectively discriminates differences in the expression sets between functional and nonfunctional livers. Functional livers again cluster together, though nonfunctional livers demonstrate divergent patterns relative to one another. N, nonfunctional liver; F, functional liver.

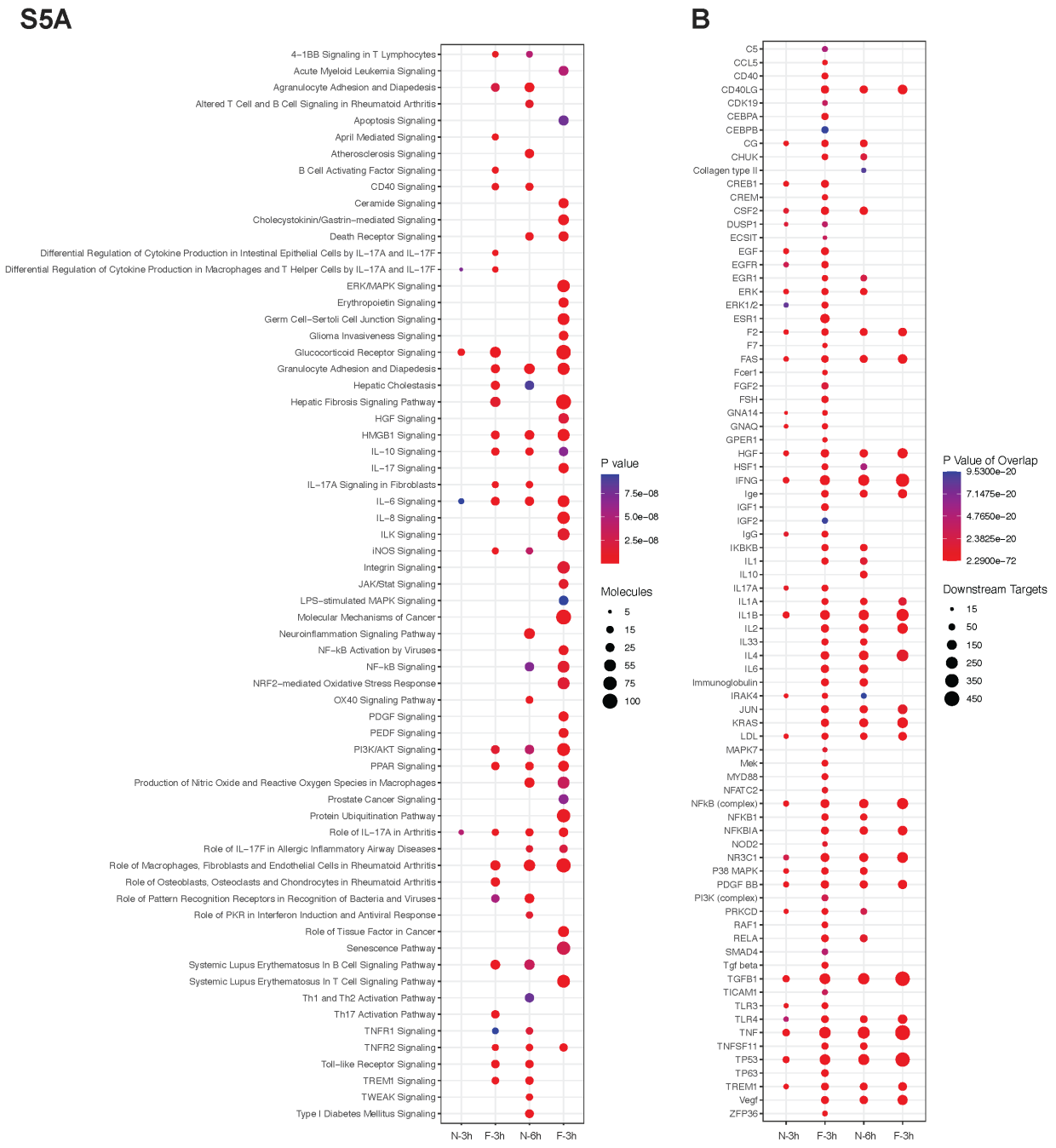

Figure S5. Ingenuity Pathway Analysis of differentially expressed genes (FDR<0.05) at 3h and 6h of perfusion versus 0h in nonfunctional and functional livers. Dot plots contains significant canonical pathways (A) and upstream regulators (B) for the arbitrary P value cut-off indicated in the legend (10-7 for CPs and 10-19 for URs). The size of each dot represents the number of downstream targets gene in our gene set that were in the IPA gene set for that CP or UR. The color of each dot represents the P value for the CP or UR. N, nonfunctional livers; F, functional livers.

Fig. S6

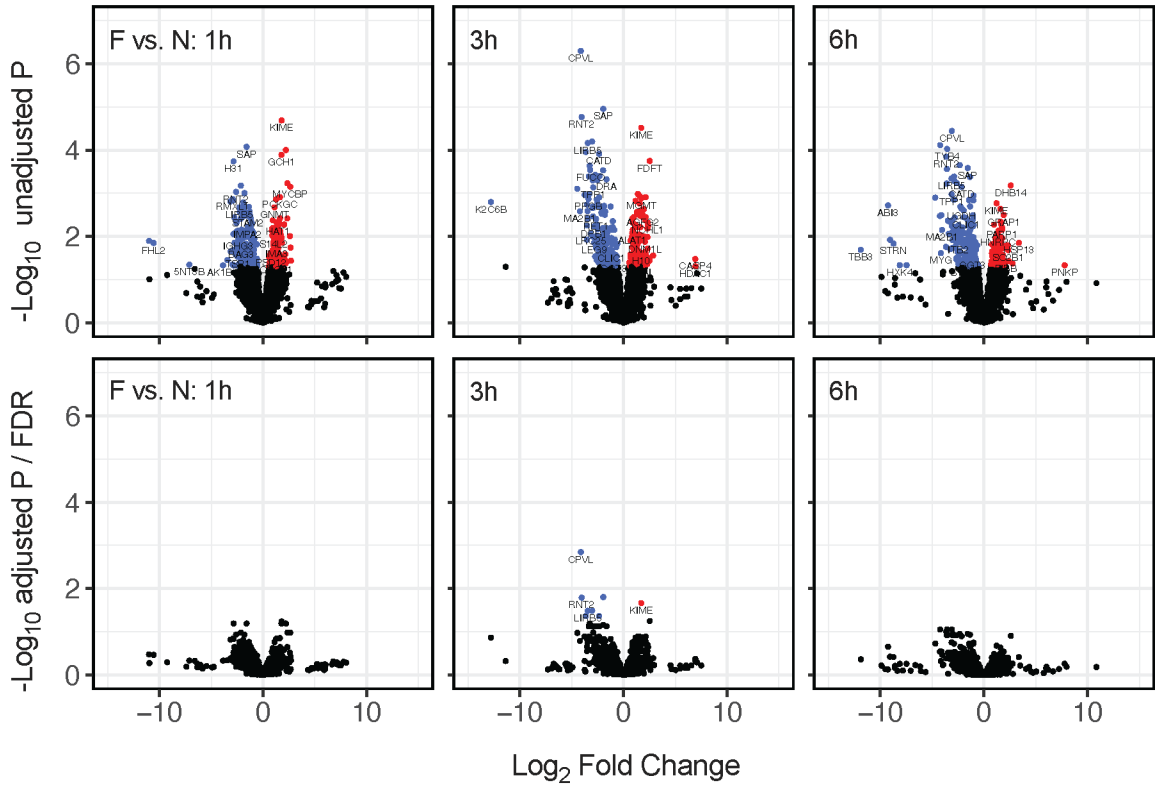

Figure S6. Volcano plots for untargeted perfusate proteomics. Top row: Unadjusted P-value vs. fold change for functional compared to nonfunctional livers at 1h, 3h, and 6h of normothermic machine perfusion. Bottom row: Adjusted P-value (FDR) vs. fold change for the same time point comparisons. FDR cutoff < 0.05 was used. Red dots indicate protein enriched in perfusate of functional relative to nonfunctional livers. Blue dots indicate protein enriched in perfusate of nonfunctional relative to functional livers. N, nonfunctional livers; F, functional livers; FDR, false discovery rate.

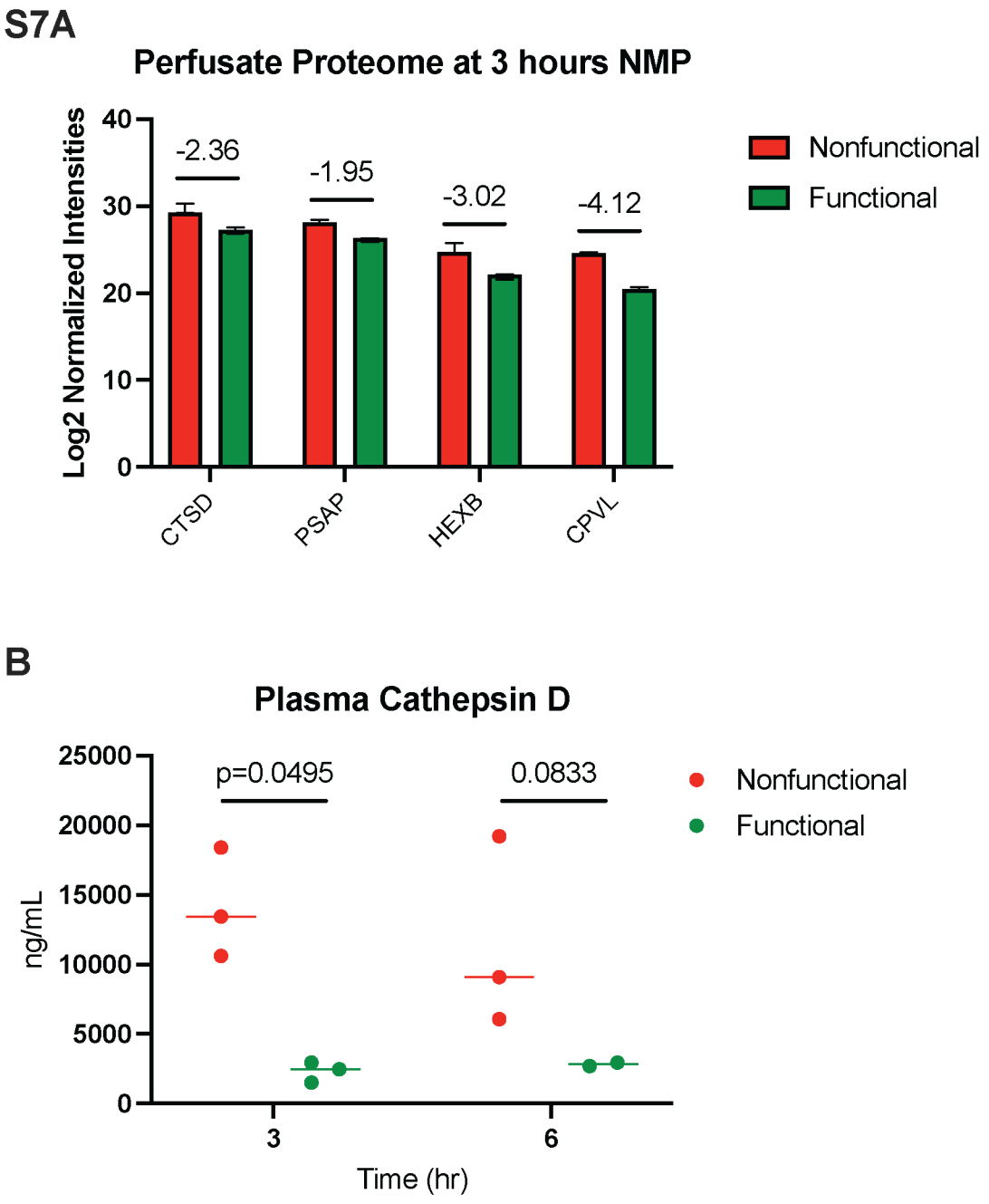

Figure S7. Nonfunctional livers demonstrate higher perfusate concentrations of lysosomal protein components. (A) Significantly enriched perfusate proteins from proteomic analysis with FDR<0.05 after 3 hours of NMP displayed. Column bars indicate log2FC between functional and nonfunctional groups. (B) Circulating levels of cathepsin D are significantly higher after 3 hours of perfusion in the nonfunctional compared to functional livers (P=0.0495), confirming results from perfusate proteomic analysis. After 6 hours of perfusion, cathepsin D levels remain qualitatively higher, though did not reach significance due to a missing sample for liver F2. Concentrations derived by ELISA.

Fig. S8

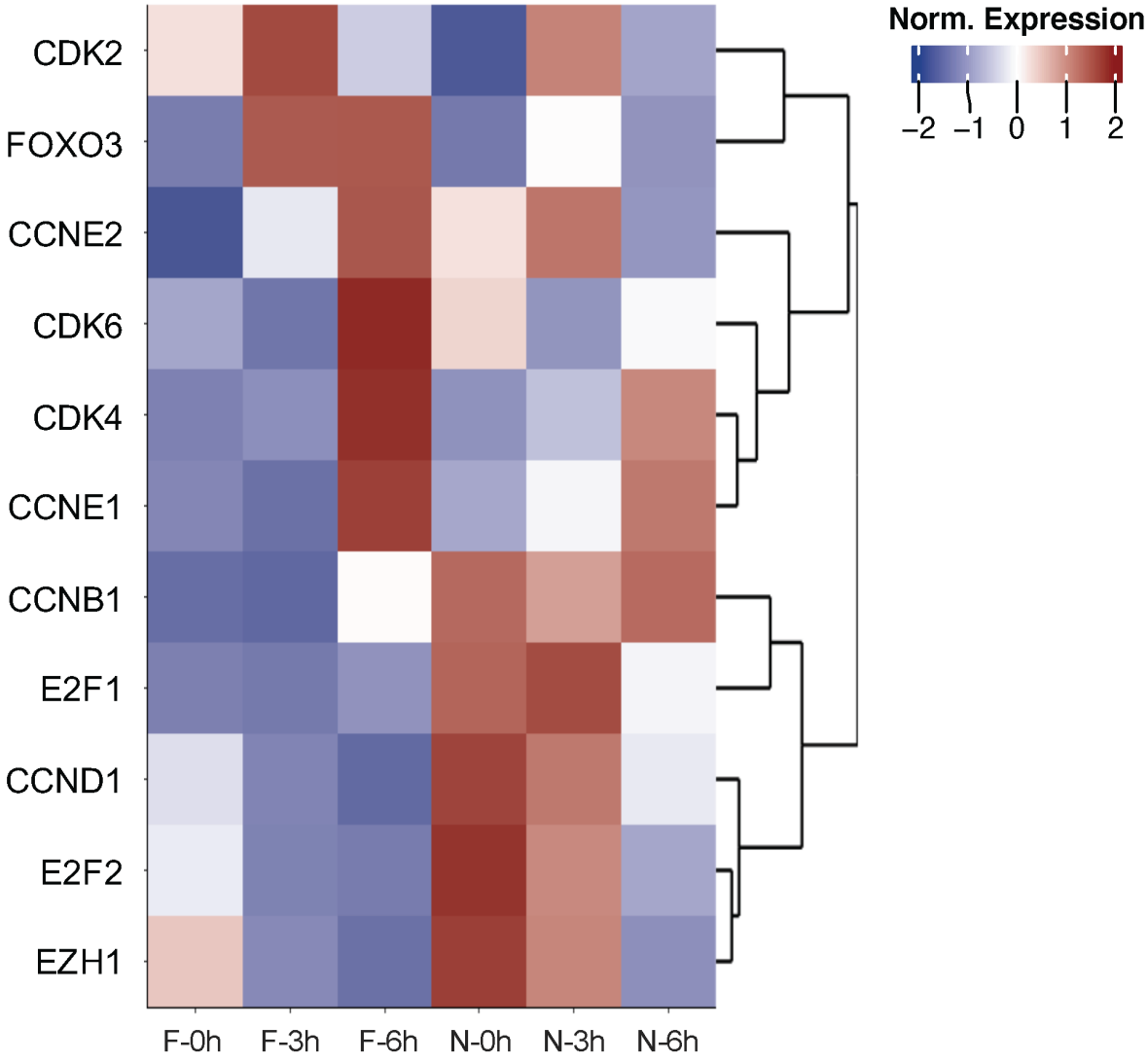

Figure S8. Expression heatmap of genes involved in cell cycle entry. Normalized expression of genes involved in cell cycle entry (manually curated) in functional and nonfunctional livers. No gene reached the significance cutoff (FDR<0.05) in either group for comparisons of 3h vs 0h or 6h vs 0h. N, nonfunctional livers; F, functional livers.

References

1. Mergental H, Laing RW, Kirkham AJ, et al. Transplantation of discarded livers following viability testing with normothermic machine perfusion. *Nat Commun*. 2020;11(1):2939. doi:10.1038/s41467-020-16251-3

2. Vodkin I, Kuo A. Extended Criteria Donors in Liver Transplantation. *Clin Liver Dis*. 2017;21(2):289-301. doi:10.1016/j.cld.2016.12.004

3. Scientific Registry of Transplant Recipients (SRTR). https://www.srtr.org/reports-tools/opo-specific-reports/

4. Durand F, Levitsky J, Cauchy F, Gilgenkrantz H, Soubrane O, Francoz C. Age and liver transplantation. *J Hepatol*. 2019;70(4):745-758. doi:10.1016/j.jhep.2018.12.009

5. Nasralla D, Coussios CC, Mergental H, et al. A randomized trial of normothermic preservation in liver transplantation. *Nature*. 2018;557(7703):50-56. doi:10.1038/s41586-018-0047-9

6. Yeh H, Uygun K. *Increasing Donor Liver Utilization Through Machine Perfusion*. Vol 70. John Wiley and Sons Inc.; 2019:431-433. doi:10.1002/hep.30523

7. Raigani S, de Vries RJ, Carroll C, et al. Viability testing of discarded livers with normothermic machine perfusion: Alleviating the organ shortage outweighs the cost. *Clin Transplant*. 2020;34(11):e14069. doi:10.1111/ctr.14069

8. di Francesco F, Pagano D, Martucci G, Gruttadauria S. Normothermic Machine Perfusion Using an Air/Oxygen Mixer for Reconditioning a Liver From a Marginal Brain Death Donor. *Artif Organs*. 2017;41(7):E66-E68. doi:10.1111/AOR.12964

9. Van Leeuwen OB, De Vries Y, Fujiyoshi M, et al. Transplantation of High-risk Donor Livers After Ex Situ Resuscitation and Assessment Using Combined Hypo- and Normothermic Machine Perfusion: A Prospective Clinical Trial. *Ann Surg*. 2019;270(5):906-914. doi:10.1097/SLA.0000000000003540

10. Jassem W, Xystrakis E, Ghnewa YG, et al. Normothermic Machine Perfusion (NMP) Inhibits Proinflammatory Responses in the Liver and Promotes Regeneration. *Hepatology*. 2019;70(2):682-695. doi:10.1002/hep.30475

11. Schlegel A, Dutkowski P. Letter to Editor: Repair or Prevent: What Is the Real Impact of Normothermic Machine Perfusion in Liver Transplantation? *Hepatology*. 2019;70(6):2231-2232. doi:10.1002/hep.30567

12. Karimian N, Matton APM, Westerkamp AC, et al. Ex Situ Normothermic Machine Perfusion of Donor Livers. *JoVE (Journal of Visualized Experiments)*. 2015;2015(99):e52688. doi:10.3791/52688

13. Sanders JA, Lakhani A, Phornphutkul C, Wu KY, Gruppuso PA. The effect of rapamycin on DNA synthesis in multiple tissues from late gestation fetal and postnatal rats. *Am J Physiol Cell Physiol*. 2008;295(2):C406-13. doi:10.1152/ajpcell.00450.2007

14. Gearing LJ, Cumming HE, Chapman R, et al. CiiiDER: A tool for predicting and analysing transcription factor binding sites. *PLoS One*. 2019;14(9):e0215495. doi:10.1371/JOURNAL.PONE.0215495

15. Emadali A, Nguyên DT, Rochon C, Tzimas GN, Metrakos PP, Chevet E. Distinct endoplasmic reticulum stress responses are triggered during human liver transplantation. *J Pathol*. 2005;207(1):111-118. doi:10.1002/path.1798

16. Almanza A, Carlesso A, Chintha C, et al. Endoplasmic reticulum stress signalling - from basic mechanisms to clinical applications. *Febs j*. 2019;286(2):241-278. doi:10.1111/febs.14608

17. Zhu SY, Yao RQ, Li YX, et al. Lysosomal quality control of cell fate: a novel therapeutic target for human diseases. *Cell Death Dis*. 2020;11(9):817. doi:10.1038/s41419-020-03032-5

18. Behrends C, Sowa ME, Gygi SP, Harper JW. Network organization of the human autophagy system. *Nature 2010 466:7302*. 2010;466(7302):68-76. doi:10.1038/nature09204

19. Sosa RA, Zarrinpar A, Rossetti M, et al. Early cytokine signatures of ischemia/reperfusion injury in human orthotopic liver transplantation. *JCI Insight*. 2016;1(20):e89679. doi:10.1172/jci.insight.89679

20. Zhai Y, Petrowsky H, Hong JC, Busuttil RW, Kupiec-Weglinski JW. Ischaemia-reperfusion injury in liver transplantation--from bench to bedside. *Nat Rev Gastroenterol Hepatol*. 2013;10(2):79-89. doi:10.1038/nrgastro.2012.225

21. Chipurupalli S, Samavedam U, Robinson N. Crosstalk Between ER Stress, Autophagy and Inflammation. *Front Med (Lausanne)*. 2021;8:2125. doi:10.3389/FMED.2021.758311/BIBTEX

22. Liu X, Green RM. Endoplasmic reticulum stress and liver diseases. *Liver Res*. 2019;3(1):55-64. doi:10.1016/j.livres.2019.01.002

23. Tanida I, Ueno T, Kominami E. LC3 and autophagy. *Methods in Molecular Biology*. 2008;445:77-88. doi:10.1007/978-1-59745-157-4_4/COVER

24. Baskin-Bey ES, Canbay A, Bronk SF, et al. Cathepsin B inactivation attenuates hepatocyte apoptosis and liver damage in steatotic livers after cold ischemia-warm reperfusion injury. *Am J Physiol Gastrointest Liver Physiol*. 2005;288(2):G396-402. doi:10.1152/ajpgi.00316.2004

25. Boteon YL, Laing R, Mergental H, et al. Mechanisms of autophagy activation in endothelial cell and their targeting during normothermic machine liver perfusion. *World J Gastroenterol*. 2017;23(48):8443-8451. doi:10.3748/wjg.v23.i48.8443

26. Shen Y, Malik SA, Amir M, et al. Decreased Hepatocyte Autophagy Leads to Synergistic IL-1β and TNF Mouse Liver Injury and Inflammation. *Hepatology*. 2020;72(2):595-608. doi:10.1002/hep.31209

27. Xu D, Zhao H, Jin M, et al. Modulating TRADD to restore cellular homeostasis and inhibit apoptosis. *Nature*. Published online 2020. doi:10.1038/s41586-020-2757-z

28. Cho H, Lim IK, Lee JH. Changes in the expression of cell cycle regulators during rat liver regeneration after partial hepatectomy. *Exp Mol Med*. 1996;28(4):187-191. doi:10.1038/emm.1996.29

29. Michalopoulos GK, Bhushan B. Liver regeneration: biological and pathological mechanisms and implications. *Nat Rev Gastroenterol Hepatol*. Published online 2020. doi:10.1038/s41575-020-0342-4

30. Eshmuminov D, Becker D, Bautista Borrego L, et al. An integrated perfusion machine preserves injured human livers for 1 week. *Nat Biotechnol*. 2020;38(2):189-198. doi:10.1038/s41587-019-0374-x

31. Chan EY, Olson LC, Kisthard JA, et al. Ischemic cholangiopathy following liver transplantation from donation after cardiac death donors. *Liver Transpl*. 2008;14(5):604-610. doi:10.1002/LT.21361

32. Searle BC, Pino LK, Egertson JD, et al. Chromatogram libraries improve peptide detection and quantification by data independent acquisition mass spectrometry. *Nature Communications 2018 9:1*. 2018;9(1):1-12. doi:10.1038/s41467-018-07454-w

33. Graw S, Tang J, Zafar MK, et al. proteiNorm - A User-Friendly Tool for Normalization and Analysis of TMT and Label-Free Protein Quantification. *ACS Omega*. 2020;5(40):25625-25633. doi:10.1021/ACSOMEGA.0C02564/SUPPL_FILE/AO0C02564_SI_002.ZIP

34. Huber W, von Heydebreck A, Sültmann H, Poustka A, Vingron M. Variance stabilization applied to microarray data calibration and to the quantification of differential expression. *Bioinformatics*. 2002;18(suppl_1):S96-S104. doi:10.1093/BIOINFORMATICS/18.SUPPL_1.S96

35. Ritchie ME, Phipson B, Wu D, et al. limma powers differential expression analyses for RNA-sequencing and microarray studies. *Nucleic Acids Res*. 2015;43(7):e47-e47. doi:10.1093/NAR/GKV007

36. Chawade A, Alexandersson E, Levander F. Normalyzer: A tool for rapid evaluation of normalization methods for omics data sets. *J Proteome Res*. 2014;13(6):3114-3120. doi:10.1021/PR401264N/SUPPL_FILE/PR401264N_SI_003.PDF

37. Core Development Team R. A Language and Environment for Statistical Computing. *R Foundation for Statistical Computing*. 2020;2:https://www.R-project.org. http://www.r-project.org

38. Robinson MD, McCarthy DJ, Smyth GK. edgeR: a Bioconductor package for differential expression analysis of digital gene expression data. *Bioinformatics*. 2010;26(1):139-140. doi:10.1093/BIOINFORMATICS/BTP616

39. QIAGEN Inc. Ingenuity Pathway Analysis (IPA). Published online 2016. https://www.qiagenbioinformatics.com/products/ingenuity-pathway-analysis

40. Lamming DW, Demirkan G, Boylan JM, et al. Hepatic signaling by the mechanistic target of rapamycin complex 2 (mTORC2). *FASEB Journal*. 2014;28(1):300-315. doi:10.1096/FJ.13-237743

41. Young MD, Wakefield MJ, Smyth GK, Oshlack A. Gene ontology analysis for RNA-seq: accounting for selection bias. *Genome Biol*. 2010;11(2):1-12. doi:10.1186/GB-2010-11-2-R14/TABLES/4

42. Gu Z, Gu L, Eils R, Schlesner M, Brors B. circlize implements and enhances circular visualization in R. *Bioinformatics*. 2014;30(19):2811-2812. doi:10.1093/BIOINFORMATICS/BTU393

Chapter 4:
Pan-caspase inhibition during normothermic machine perfusion of discarded livers mitigates ex situ innate immune responses

Pan-caspase inhibition during normothermic machine perfusion of discarded livers mitigates ex situ innate immune responses

Siavash Raigani [1,2], John Santiago [3], Anders Ohman [3], Megan Heaney [3], Sofia Baptista [1,2], Taylor M. Coe [1], Reinier J. de Vries [2], Ivy Rosales [4], Angela Shih [4], James F. Markmann [1,2], Philip Gruppuso [2], Korkut Uygun [1,2], Jennifer Sanders [3*†] and Heidi Yeh [1*†]

[1] Division of Transplant Surgery, Massachusetts General Hospital, Boston, MA, United States, [2] Center for Engineering in Medicine and Surgery, Massachusetts General Hospital and Harvard Medical School, Boston, MA, United States, [3] Department of Pediatrics, Rhode Island Hospital and Brown University, Providence, RI, United States, [4] Department of Pathology, Massachusetts General Hospital, Boston, MA, United States

[†] These authors have contributed equally to this work and share senior authorship

Originally published in *Front. Immunol.* 13:940094

DOI: 10.3389/fimmu.2022.940094

Introduction

End-stage liver disease (ESLD) is the final outcome of a number of different progressive liver diseases and can ultimately be a fatal condition if the patient is unable to receive an orthotopic liver transplantation (OLT). However, patients in need of organs dramatically exceed the number of available donor organs. As a result, it is critical to make the most out of this limited organ pool. Techniques currently being explored to accomplish this include using *ex situ* normothermic machine perfusion (NMP) on donor organs. This process allows for surveying quantifiable metrics of organ functionality and transplant viability rather than relying on less-accurate physical assessment. It also may help to prime donor livers to recover from ischemia-reperfusion injury prior to transplantation into a recipient. This has helped to facilitate the use of extended-criteria or marginal grafts, which would have been discarded otherwise out of concern for patient safety, [1,2] though more information is needed to understand the physiological changes induced by NMP before it can be safely and consistently applied to the riskiest donor organs, such as damaged livers.

We have recently published a study resulting from a collaboration between the Sanders Laboratory at Brown University and the Organ Reengineering Group at Massachusetts General Hospital designed to examine the transcriptomic and hepatocellular functional changes that occurred in discarded DCD donor livers throughout a six hour time course of NMP. [3] We found that donor livers that were able to achieve functional metrics for transplantation had activation of early innate immune signaling followed by activation of autophagy, while nonfunctional livers had a delayed response, more innate immune signaling, and less autophagy. This suggests there may be the potential to target these systems with adjuvant therapies in order to induce a more functional signature in nonfunctional livers during the NMP process, thereby converting a nonviable graft into a viable one.

Based on our previous study, we suspected that more positive outcomes would result from reestablishing homeostasis after ischemia-reperfusion injury (IRI) by increasing autophagy via targeting stress-responsive cell death mechanisms like apoptosis. [4–6] This and other cell death mechanisms have beneficial properties in normal conditions by offsetting production of new cells with the clearance of damaged or senescent cells, but can also have pathological effects including inflammation and fibrosis if not counterbalanced by proliferation. [7] Most importantly, previous work has identified that IRI in the context of liver transplantation has a pathologic apoptosis component. Since inhibiting apoptosis helps to mitigate the damage from IRI, [8–13] restoration of healthy homeostasis is achievable by inhibiting apoptosis and increasing autophagy. [14] Resulting from our observations of the relevance of autophagy in the functional response to NMP, we hypothesized that inhibition of apoptosis during NMP may shift the balance of response to injury in donor livers that would otherwise remain nonfunctional. By modifying our perfusion solution to deliver an irreversible pan-caspase inhibitor, emricasan, we explored if apoptosis inhibition during NMP could indeed improve hepatocyte function in a similar cohort of discarded livers. We utilized similar physiological metrics and transcriptomic analyses in order to back-compare the emricasan-treated donor livers to the functional and nonfunctional livers we previously studied.

Materials and Methods

Human liver perfusions

Sixteen human livers from donation after circulatory death, with consent for research, were included in this study after being turned down by all transplant centers in the respective region of procurement. Eleven livers had been previously described in a research cohort of machine perfused discarded human livers [15] and comprised the control groups. Additional details regarding procurement, enrollment, and bench preparation are provided in the supplemental methods. Donor risk index (DRI) was calculated according to Feng et al. [16]

Grafts were perfused on the Liver Assist device (Organ Assist, Groningen, Netherlands) using a previously described protocol [15]. Briefly, perfusate composition consisted of O+ packed red blood cells, human albumin, Lactated Ringer's solution, and heparin. Bile salts (taurocholate) and lipid-free parenteral nutrition were continuously infused. Perfusate, bile, and tissue biopsies were collected and analyzed at multiple time points. Grafts were assessed for adequate hepatocellular and cholangiocellular function. Hepatocellular function was defined as the ability to clear lactate below a threshold of 2.5 mmol/L, in addition to demonstrating stable vascular flow and pH without sustained bicarbonate supplementation. Cholangiocellular (biliary) viability metrics were measured according to van Leeuwen. [17]

Of the 11 livers comprising the control groups, six demonstrated adequate hepatocellular function (AHF) and five did not (inadequate hepatocellular function, IHF). With respect to the experimental group (emricasan, EM), five consecutive human livers turned down for transplant were enrolled. Emricasan, also known as IDN-6556 (MedChemExpress, Monmouth Junction, NJ), dissolved in DMSO was added to the circulating perfusate prior to initiation of liver perfusion at a dose of 5mg/kg liver weight (1mL total volume, 0.05% v/v total perfusate). Vehicle control (1mL DMSO) was previously incorporated in the control liver perfusions (Figure 1).

RNA sequencing

Core need biopsies taken immediately prior to perfusion and after 3 and 6 hours of perfusion were used for transcriptome sequencing. Methods of tissue collection, purification, and bioinformatic analysis have been previously described [3] and are detailed in the Supplemental Methods. The differential gene expression threshold for significance was set to a Benjamini-Hochberg false discovery rate (FDR) < 0.05. Raw sequence data have been deposited in the Gene Expression Omnibus with accession no. GSE202565 and no. GSE165568 (open access).

Protein analysis

Perfusate collected at the indicated time points was centrifuged at 5000g and the plasma collected and stored at −80°C for later analysis. Enzyme-linked immunosorbent assays (ELISA) were performed for various proteins according to manufacturers' guidelines (Supplemental Methods).

Sequential wedge biopsies from the right lobe of each liver were performed at indicated intervals, flash frozen in liquid nitrogen, and stored at −80°C. Tissue samples (20mg) were homogenized and Western immunoblots performed as previously described. [18] A full list of antibodies used is provided in the Supplemental Methods.

Histology and immunohistochemistry

Core needle biopsies taken from the right liver lobe at indicated intervals were fixed in formalin and embedded in paraffin. Hematoxylin and eosin (H&E) stains were performed on all biopsies to assess the degree of necrosis, inflammatory cell infiltrate, and reperfusion injury using a validated scoring system. [19] Immunohistochemistry for LC3 was performed as previously described. [3]

Statistical analysis

Categorical data are presented as median with interquartile range (IQR) and frequency data as percentages. For statistical tests not related to RNA sequencing, the Kruskal-Wallis test was used to compare multiple groups. The Wilcoxon rank-sum test (Mann-Whitney U) and Fisher's exact test were used for two-group comparisons. A two-way analysis of variance (ANOVA) was used for comparisons between groups with repeated measures over time. The threshold for statistical significance was set at <0.05. Analyses were conducted using GraphPad Prism 8 (San Diego, CA, USA) and Stata 15 (College Station, TX, USA).

Results

Donor demographics and functional assessment

Eleven discarded DCD livers were included in the control cohort and stratified using predefined criteria for demonstrating adequate hepatocellular function. Table 1 displays donor and liver characteristics between 6 livers demonstrating adequate hepatocellular function (AHF) and five livers with inadequate hepatocellular function (IHF). No significant differences were found between groups, though there was a trend toward longer cold ischemic time in the AHF group and higher donor body mass index in the IHF group. Median donor risk index (DRI) was 2.4 [2.2,2.4] in IHF livers compared to 2.05 [1.9,2.2] in AHF livers (p=0.14). Donor demographics for the five emricasan-treated livers are also shown. Livers EM1 and EM2 were from young DCD donors with relatively low DRIs turned down due to logistic reasons and inability to find a suitable recipient. Livers EM3-5 were from older donors with extended warm and cold ischemic times, and therefore had notably high DRIs.

With respect to hepatocellular function (Figure 2), four emricasan-treated livers demonstrated adequate hepatocellular function, including EM3 and EM4 (DRI 3.56 and 3.04, respectively). Low DRI livers EM1 and EM2 rapidly cleared lactate in similar fashion to AHF livers. Livers EM3 and EM4 initially displayed delayed lactate clearance within the first two hours of NMP similar to IHF livers, but subsequently were able to demonstrate adequate lactate clearance by 6 hours of NMP. Liver EM5, with the longest WIT, demonstrated IHF and failed to meet the lactate threshold despite a steady decrease in perfusate lactate throughout NMP (Figure 2A). Like AHF livers, EM1-4 livers demonstrated stable vascular flows and perfusate pH (Figure 2B-D). Only liver EM5 required bicarbonate supplementation after 2 hours of NMP to maintain pH above 7.3 (Figure 2E). Bile production was similar between the three groups (Figure 2F).

Analysis of cholangiocellular metrics demonstrated relatively adequate function in EM1 and EM2, which had the shortest ischemic times compared to EM3-5. Comparison of EM livers to the control groups was limited by differences in collection times and lack of corresponding perfusate chemistries (Figure S1).

Principal component analysis (PCA) and gene expression

PCA demonstrated notable transcriptional trends among the 3 groups (Figures 3A, B). Principal component 1 (PC1) captured the time-dependent changes in gene expression. Livers with AHF demonstrated consistent large transcriptional shifts at 3 and 6 hours of perfusion while these changes were dampened in the IHF and emricasan-treated livers especially at the 3h timepoint. Analysis of the top 10% of genes accounting for the variation in PC1 revealed Gene Ontology (GO) processes related to RNA transcription, RNA processing, and protein translation. Compared to AHF and IHF livers, EM livers demonstrated muted upregulation of genes within the PC1 subset (Figure 3C). On the other hand, PC2 appeared to distinguish AHF from IHF livers. EM livers clustered closer to AHF livers on the PC2 axis. Analysis of the top 10% of genes accounting for PC2 revealed marked differences between groups both prior to initiation of and during NMP. This gene subset demonstrated functional enrichment of GO processes related to immune response activation, immune cell migration, and the mitochondrial membrane. The gene expression heatmap demonstrates strong upregulation of genes categorized under the immune response phenotype in the IHF group after initiation of perfusion. In contrast, AHF and EM livers demonstrate more robust activation of genes associated with the mitochondrial membrane phenotype and minimal immune response (Figure 3D). Transcriptional changes accounting for PC3 were enriched for GO processes related to mitosis and microtubule organization (Figure S2). Analysis of the canonical pathways and upstream regulators obtained from Ingenuity Pathway Analysis (IPA) are shown in Figure S3.

Volcano plots of differentially expressed genes after 3 and 6 hours of NMP compared to pre-perfusion biopsies demonstrated robust up- and down-regulation of genes in the AHF livers. In comparison, IHF livers demonstrated significant expression of a smaller number of genes. Emricasan-treated livers displayed a markedly smaller set of DEGs compared to both control groups (Figure 4A). To further detail differences between AHF and EM livers, volcano plots comparing gene expression after 6 hours of NMP between the two groups were annotated for select GO processes. Compared to EM livers, the AHF group demonstrated more robust activation of genes associated with oxidative stress, cytokine-mediated signaling, programmed cell death, and leukocyte migration (Figures 4B-F). Similar patterns were seen when comparing EM and IHF livers. No significant differences were noted between AHF and IHF groups given equally robust expression of genes within the GO processes of interest (Figure S4).

Adjunct delivery of caspase inhibitor mitigates IRI during liver NMP

Analysis of perfusate plasma samples for apoptosis biomarkers showed significantly higher circulating levels of cleaved cytokeratin 18 and caspase-3/7 activity after 6 hours of NMP in IHF compared to AHF livers. Addition of emricasan significantly decreased evidence of apoptosis after both 3 and 6 hours of NMP. Circulating cell-free DNA, a damage-associated molecular pattern (DAMP), was also significantly reduced in the EM livers compared to control groups (Figures 5A-C).

To determine the consequences of emricasan treatment on extracellular signaling proteins, plasma levels of numerous pro-inflammatory cytokines were evaluated. EM livers demonstrated significantly lower levels of interleukin-6 (IL-6), interleukin-8 (IL-8), and interferon-γ (IFNG) compared to AHF and IHF groups (Figures 5D-F). Circulating tumor necrosis factor-α (TNFα) and interleukin-1β (IL-1β) were qualitatively lower but failed to meet statistical significance (Figures 5G, H). Histopathologic analysis demonstrated a significant time-dependent increase in inflammatory cell infiltrate and necrosis among the three groups but no

difference between groups. Qualitatively, EM livers did not demonstrate an increase in inflammatory cells over time compared to IHF livers (Figure S5).

Given the decreased pro-inflammatory cytokine profile in the perfusate of EM livers, Ingenuity Pathway Analysis was used to evaluate the downstream signaling effect of this finding. EM livers demonstrated minimal enrichment of IRI canonical pathways associated with innate immunity and sinusoidal endothelial cell activation (Figure 5I). IHF livers also demonstrated a pattern of delayed activation of these CPs at 6 hours of NMP whereas AHF livers appeared to show early activation at 3 hours. Moreover, downstream gene target expression analysis of the above pro-inflammatory upstream regulators revealed categorically fewer differentially expressed genes in EM livers compared to AHF and IHF groups (Figure S6).

Stress response mechanisms in the setting of caspase inhibition

We have previously shown that functional livers demonstrate a more robust homeostatic stress response including activation of autophagy compared to inadequately functioning livers. However, when the cellular stress response is overwhelmed, crosstalk between autophagy and apoptosis initiates programmed cell death. [4] We hypothesized that caspase inhibition would bolster cell survival and upregulate autophagy, thereby improving hepatocellular function. Therefore, we performed Western immunoblotting for key proteins involved in regulation of these processes. Eukaryotic initiation factor 2α (eIF2α) is phosphorylated in response to misfolded proteins accumulating in the endoplasmic reticulum (ER). This phosphorylation of eIF2α leads to initiation of antioxidant signaling, repression of global protein translation and induction of autophagy. Western immunoblotting revealed high levels of phospho-eIF2α pre-perfusion in all groups. After initiation of perfusion all groups demonstrated a significant time-dependent decrease in phosphorylation. After 6 hours of perfusion, AHF livers had lower phospho:total-eiF2α ratios (0.21, IQR 0.14-0.31) compared to IHF (0.78, IQR 0.69-1.58, P<0.01 vs. AHF) and EM livers (1.22, IQR 0.73-.78, P<0.01 vs. AHF) (Figure 6A). The mechanistic

Target of Rapamycin (mTOR) pathway also plays a key role in regulation of autophagy with activation of mTORC1 leading to suppression of autophagy. Phosphorylation of ribosomal protein S6 kinase (P70S6K), a downstream target of mTORC1, was not detectable pre-perfusion. NMP resulted in a significant time-dependent increase in phospho:total-P70S6K ratios in all groups (Figure 6B). There was a trend toward higher levels in the IHF compared to AHF and emricasan treated livers. However, this did not reach significance due to the variation in individual livers. Proteins directly involved in autophagic flux were investigated next. Beclin, a marker of autophagy induction, demonstrated a time-dependent decrease during perfusion. Beclin protein content in IHF livers after 3 hours of NMP was significantly lower compared to AHF and EM groups (Figure 6C). This difference was qualitatively apparent at 6hr although it was no longer statistically significant. Following initiation of autophagy, microtubule-associated protein 1 light chain 3 beta (LC3B) is converted from its inactive form LC3B-I to LC3B-II through lipidation by the autophagy machinery. LC3B-II then associates with the lipid membranes of the phagophore to form the autophagosome. LC3B-II:I ratios were significantly higher in AHF livers (1.33, IQR 0.99-1.57) at 3hr compared to IHF (0.96, IQR 0.64-1.29, $P<0.05$ vs. AHF) and emricasan livers (0.85, IQR 0.51-0.89, $P<0.01$ vs. AHF). The ratio increased in the IHF livers at 6hr such that there was no difference between IHF and AHF livers (Figure 6D). We confirmed the LC3B results using immunohistochemistry for LC3B (Figure S7). Pre-perfusion biopsies demonstrated pan-cytosolic staining in all groups. In AHF livers, LC3B was localized to a granule staining pattern at 3 and 6hr indicative of LCB-II association with the autophagosome. This shift in staining pattern was not observed in the IHF group and variable in emricasan livers. p62 content was investigated to determine whether autophagy was potently inhibited in IHF or EM livers (Figure 6E). A trend toward lower levels of p62 was observed in all groups at 3hr compared to pre-perfusion. However, there was a notable divergence in p62 expression at 6hr of perfusion with IHF livers maintaining very low expression compared to EM livers.

Finally, we sought to determine if pan-caspase inhibition resulted in off-target activation of other cell death pathways such as necroptosis. [6,20] To assess whether treatment with emricasan resulted in compensatory activation of necroptosis, we probed for phosphorylation of mixed lineage kinase domain-like (MLKL). MLKL is the terminal kinase in the necroptotic cell death program. Phosphorylation of MLKL is believed to lead to its oligomerization, transport to the membrane, and membrane destruction. Phospho-MLKL was below the limit of detection in all groups before and during perfusion, suggesting that treatment with emricasan did not lead to induction of necroptosis (Figure S8).

Discussion

While apoptosis is an important process to clear injured or senescent cells from the body, it must be balanced with proliferation of replacement cells or it can become pathologic. [7] During the apoptotic process, cell contents are released into the microenvironment, which can include damage-signaling molecules like cell-free DNA, which self-perpetuate a cycle of cell death. We have previously found that during NMP, discarded donor livers that eventually met adequate functional transplant criteria (AHF) had activation of autophagy, while those that ended up nonfunctional (IHF) showed evidence of inflammation and autophagy. [21] In the current study, we confirmed that IHF livers had a lower level of autophagy and more sustained apoptosis and innate immunity than AHF livers, and found that addition of emricasan in the perfusate solution helped to ameliorate the levels of these self-destructive pathways, leading to better performance by physiological metrics. Transcriptomic analysis confirmed that this improvement is driven by a suppression of pathways related to inflammatory cytokine signaling and innate immune activation suppressing apoptosis.

Emricasan treatment has previously shown the potential for clinical benefits in the context of liver transplantation in both rodent models and human trials, resulting increased survival in rodents [10–12] and improved AST and ALT levels in humans. [8] However, it is not

currently used in clinical practice, which may reflect the difficulty of incorporating novel drug administration to an already-complicated organ procurement and transplantation pipeline. As two NMP devices have recently been approved by the FDA following clinical trials, [22] the Organ Care System (OCS) Liver and the OrganOx metra, the use of perfusion devices prior to transplantation is likely to become more common and enable the implementation of pre-treatment adjuvants that have been demonstrated to improve liver function. [23] We demonstrate here that treatment of discarded DCD livers with emricasan can lead to improved functional metrics and this outcome is linked to transcriptomic and proteomic changes related to emricasan mitigating IRI. As many caspases, including 2, 3, 6, 7, 8, 9, and 10 have established links to apoptosis, [24] it is possible that inhibition of this form of cell death is responsible for the healthier liver phenotype we observe. However, as emricasan is a pan-caspase inhibitor, its effects at lowering IRI may be due to direct inhibition of inflammatory caspase signaling. This is driven by caspases 1, 4, and 5, and results in pyroptosis, a form of inflammatory cell death characterized by activation of inflammasomes and interleukin-1β (IL-1β). [6,20] If this is indeed the case, specific inhibitors of these caspases may have similar effects while reducing unintended off-target effects. Inflammasome inhibitors have been researched in the context of cancer and other conditions like rheumatoid arthritis, and multiple inhibitors of caspase-1 and/or IL-1β are under active investigation. [25] While clinical trials of many caspase inhibitors have been hindered by undesirable side effects, [26] the short duration and *ex situ* use case in pre-transplantation NMP could provide an optimal use case. Future studies using more specific inhibitors in NMP may elucidate the important nuances responsible for emricasan's beneficial effects. Regardless of the cause of cell death, preventing or lowering the release of DAMPs should result in a corresponding lower activation of immune cell responders, preventing a cycle of inflammatory signaling from resulting. This relationship between increased DAMP release resulting in increased apoptosis has been demonstrated in rat models of NMP [27] and a similar cytokine signature to what we associated primarily with IHF livers was also observed in human transplant

recipients. [19] The effect of inappropriate damage sensing resulting in cycles of damaging immune response resembles the “cytokine storm” seen following certain infections and administration of some cancer immunotherapies. [28] The emricasan-treated livers in this study had a suppressed proinflammatory cytokine signature, suggesting that immunomodulatory therapies proposed to mitigate cytokine release syndrome may be able to more specifically minimize IRI and improve liver function during NMP.

As previous studies have shown that a disruption of autophagy activity can drive apoptosis, [4] we had hypothesized that an imbalance between these two factors is responsible for the IHF phenotype. We therefore examined the ER stress response in EM livers as was done in our previous NMP study. [21] While the AHF livers had a high level of autophagy activation as assessed by a low phospho-eiF2α level and a high LC3B-II:I ratio, the EM liver p-eiF2α levels were at an intermediate state between IHF and AHF livers and a lower increase in LC3B-II:I ratios, reflecting a more moderate level of autophagy than in AHF livers. This is not unexpected, as many caspase inhibitors block the activity of apoptosis, but do not stimulate autophagy. [14] New compounds such as TRADD inhibitors have shown dual effect at simultaneously activating autophagy and inhibiting apoptosis, and may result in more favorable rehabilitation of IHF livers. In the present study, emricasan resulted in heterogeneous rehabilitation outcomes, with some livers like EM-3 and EM-4 meeting some functional metrics like high lactate clearance. However, due to lack of NMP device approval until the recent OCS Liver and the OrganOx metra devices, our study was unable to assess real-world post-transplantation function. Additionally, emricasan treatment in our study did not result in improved cholangiocyte functional metrics, which reflects a limitation of the current end-ischemic NMP and requires changes to the perfusion process to include a modified sequential hypo- and normothermic perfusion. [2,29,30] Without this process, bile duct function can remain inhibited.

Our study shows that the administration of emricasancan during NMP can lead to hepatic rehabilitation in some discarded DCD donor livers and this effect can be assessed by protein measurements in the perfusate. Now that multiple NMP devices have been FDA approved, emricasan administration in NMP could then be taken to a clinical trial with human liver transplant. Further work, such as determining the specific caspases driving cell death, utilizing compounds that not only inhibit apoptosis but also stimulate autophagy, and perfusing in a way that improves cholangiocyte function, can improve upon the effects we observed. As our work demonstrates that perfusion adjuvant interventions can recover the function of discarded human livers, this offers the exciting potential to prevent unnecessary organ discard and maximize utilization of donor livers.

Tables and Figures

	Emricasan N=5					AHF N=6	IHF N=5	AHF *vs.* IHF P-value
Liver #	EM1	EM2	EM3	EM4	EM5			
DCD?	Y	Y	Y	Y	Y	6 (100%)	5 (100%)	
tWIT	22	23	32	23	53	27.5 (24–28)	24 (23-34)	0.93
fWIT	9	8	7	12	13	8.5 (8-10)	11 (9-11)	0.36
CIT	347	553	758	703	679	625.5 (458-697)	358 (357-367)	0.082
Age	28	26	60	50	59	58.5 (40-60)	56 (55-59)	0.85
Gender	M	M	F	F	F	5M, 1F	2M, 3F	0.24
BMI	38.7	19.8	31.2	28.3	31.9	26 (24.5-28.3)	32.9 (29.9-40.2)	0.068
Weight (kg)	129.5	61.7	90.5	74.9	84.8	80.6 (77.6-87)	90.9 (74.1-100)	0.86
Macrosteatosis	30	0	2	0	0	3.5 (0-5)	35 (0-40)	0.35
Microsteatosis	10	5	0	30	0	3.8 (0-50)	5 (0-55)	0.85
AST	32	38	134	78	27	41.5 (39-57)	98.5 (41.5-366)	0.39
ALT	22	27	40	47	32	32.5 (22-58)	100.5 (25.5-317.5)	0.52
Total bilirubin	1.2	0.8	0.6	0.2	0.2	0.75 (0.4-1)	0.35 (0.25-0.45)	0.086
ALP	72	48	76	104	83	58 (36-95)	99 (94-494)	0.12
DRI	1.74	1.47	3.56	3.04	2.83	2.05 (1.9-2.2)	2.4 (2.2-2.4)	0.14

Median with interquartile range shown for continuous data. Wilcoxon rank-sum test or Fisher's exact test used for group comparisons. AHF, adequate hepatocellular function group; IHF, inadequate hepatocellular function group; DCD, donation after circulatory death; tWIT, total warm ischemic time (extubation to cold flush) in minutes; fWIT, functional warm ischemic time (asystole to cold flush) in minutes; CIT, cold ischemia time in minutes; BMI, body mass index (kg/m^2); steatosis expressed in percentages; DRI, donor risk index. Terminal values prior to procurement shown for AST (aspartate aminotransferase), ALT (alanine aminotransferase), ALP (alkaline phosphatase).

TABLE 1 Discarded liver donor demographics.

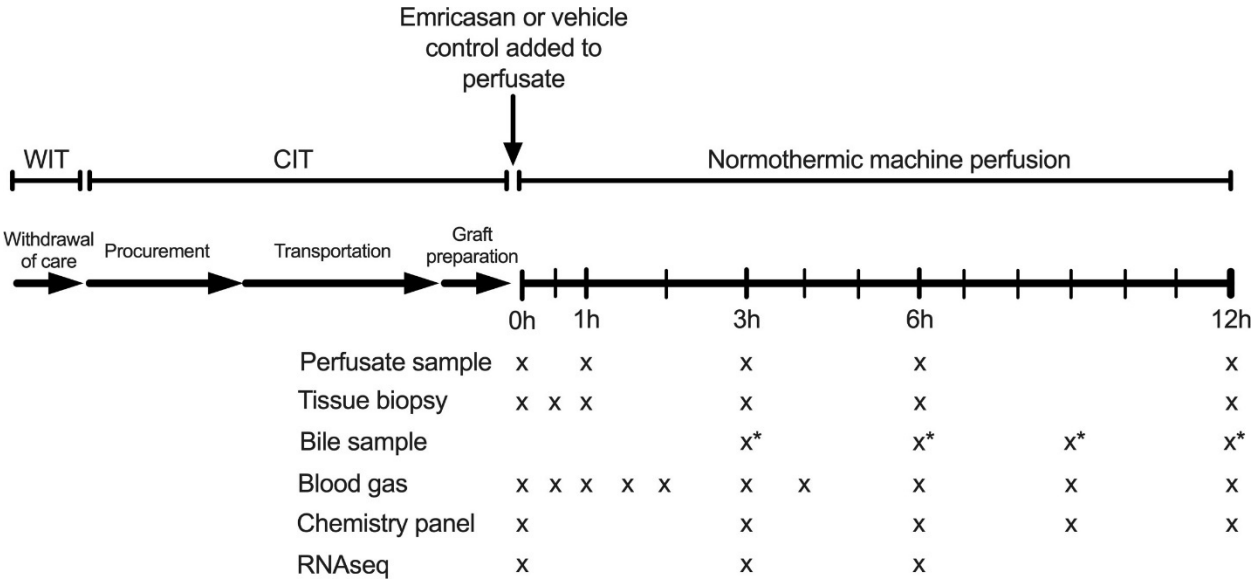

FIGURE 1 Liver preservation and NMP protocol. Emricasan (5mg/kg liver) or vehicle control (1mL DMSO) was added to the circulating perfusate immediately prior to connection of the liver to the NMP device. Serial tissue biopsies and perfusate samples were taken at indicated time points for subsequent analysis. * indicates a discordance between EM perfusions (bile samples taken at 3, 6, 9, and 12 hours) and control perfusions (bile samples taken at 4, 8, and 12 hours). NMP, normothermic machine perfusion; WIT, warm ischemic time; CIT, cold ischemic time; RNAseq, bulk RNA sequencing.

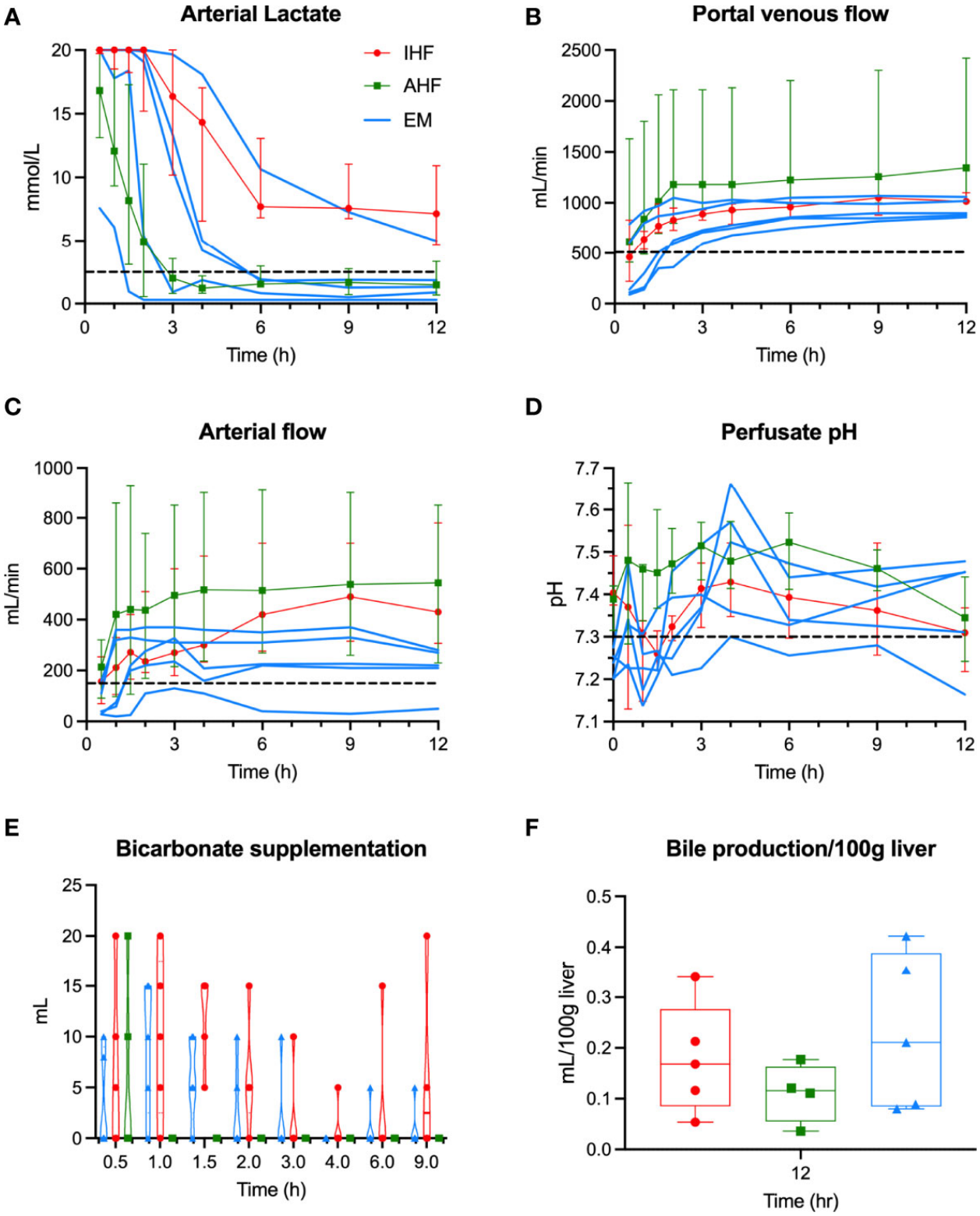

FIGURE 2 Hepatocellular perfusion metrics during NMP. Individual liver data for emricasan-treated livers (EM) shown in blue. Median and interquartile ranges shown for AHF (green) and IHF (red) groups. Dashed black line shows the cutoff used to determine adequate hepatocellular function for (A) arterial lactate, (B) portal flow, (C) arterial flow, and (D) perfusate pH. (E)

Volume of bicarbonate supplementation required to maintain pH>7.3 show. Only the inadequate functioning EM liver continued to require bicarbonate after 2 hours of NMP. (F) Bile production shown for each group. No significant difference was seen though to livers in the AHF group were omitted due to technical issues with bile collection. NMP, normothermic machine perfusion; AHF, adequate hepatocellular function; IHF, inadequate hepatocellular function; EM, emricasan.

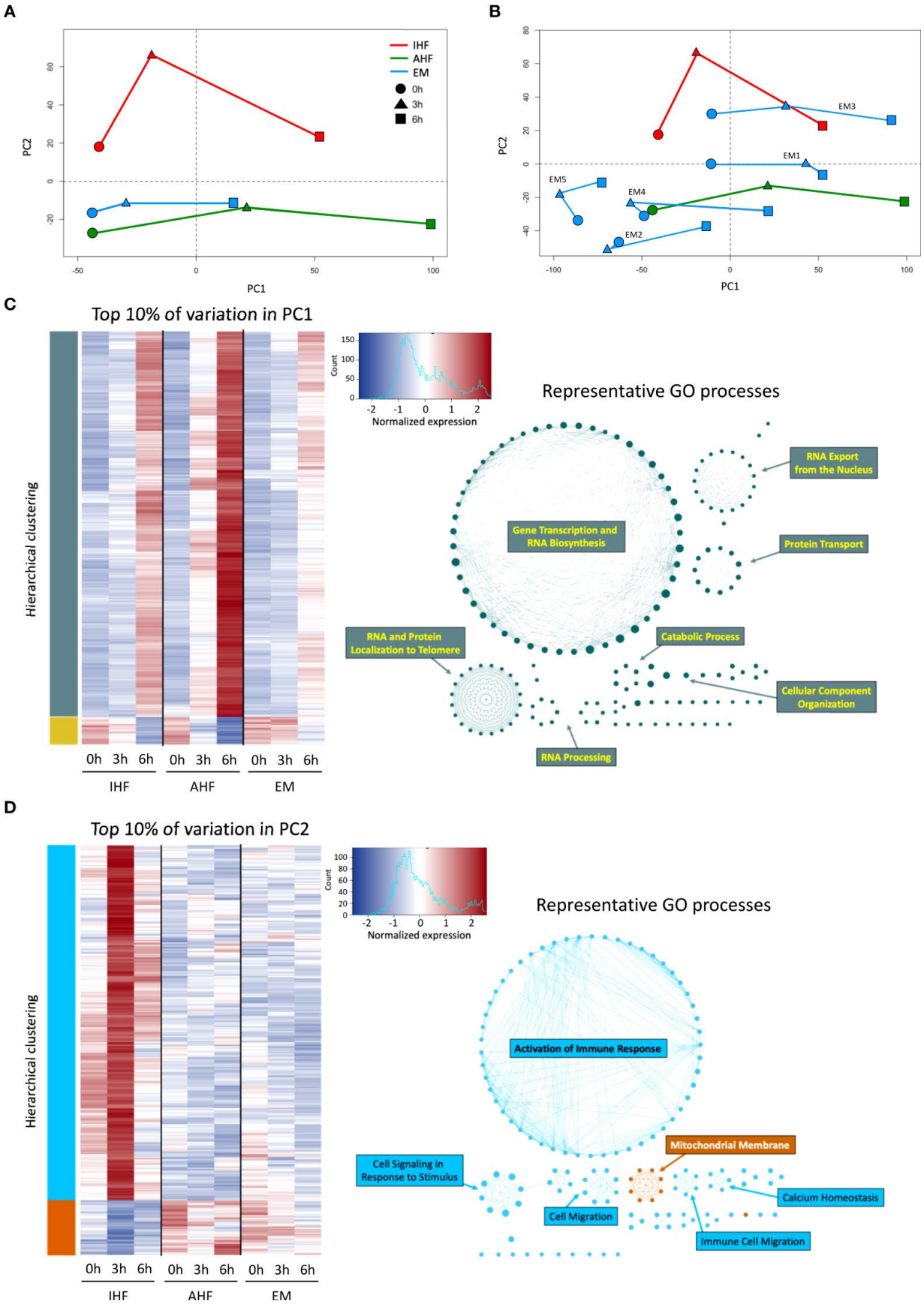
A
IHF
AHF
EM
0h
3h
6h
PC2
PC1
B
EM1
EM2
EM3
EM4
EM5
PC2
PC1
C
Top 10% of variation in PC1
Count
Normalized expression
Hierarchical clustering
0h 3h 6h 0h 3h 6h 0h 3h 6h
IHF
AHF
EM
Representative GO processes
RNA Export from the Nucleus
Gene Transcription and RNA Biosynthesis
Protein Transport
RNA and Protein Localization to Telomere
Catabolic Process
Cellular Component Organization
RNA Processing
D
Top 10% of variation in PC2
Count
Normalized expression
Hierarchical clustering
0h 3h 6h 0h 3h 6h 0h 3h 6h
IHF
AHF
EM
Representative GO processes
Activation of Immune Response
Mitochondrial Membrane
Cell Signaling in Response to Stimulus
Calcium Homeostasis
Cell Migration
Immune Cell Migration

FIGURE 3 Principal component and gene ontology analysis of transcriptional changes during NMP. PCA of EM, AHF, and IHF groups for PC1 and PC2 at 0 (pre-perfusion), 3, 6 hours of NMP shown in (A) composite form and (B) with individual EM livers. PC2 clearly distinguishes AHF from IHF livers, whereas PC1 captures time-dependent transcriptional changes. The worst functioning liver (EM5) demonstrates the least transcriptional change during NMP. (C) Hierarchical clustering heatmap of the top 10% of genes accounting for the variation in PC1. GO network analysis indicates PC1 is enriched for gene expression accounting for DNA transcription and RNA translation (teal networks), which is upregulated in all three groups during NMP. D) The top 10% of genes accounting for the variation in PC2 show remarkable differences between the three groups. GO network analysis indicates significant upregulation of genes involved in immune response activation and cell migration (light blue networks) in the IHF group compared to AHF and EM groups. AHF and EM groups demonstrated comparatively increased expression of genes related to mitochondrial membrane integrity (orange network) compared to IHF livers. AHF, adequate hepatocellular function; IHF, inadequate hepatocellular function; EM, emricasan; PC, principal component.

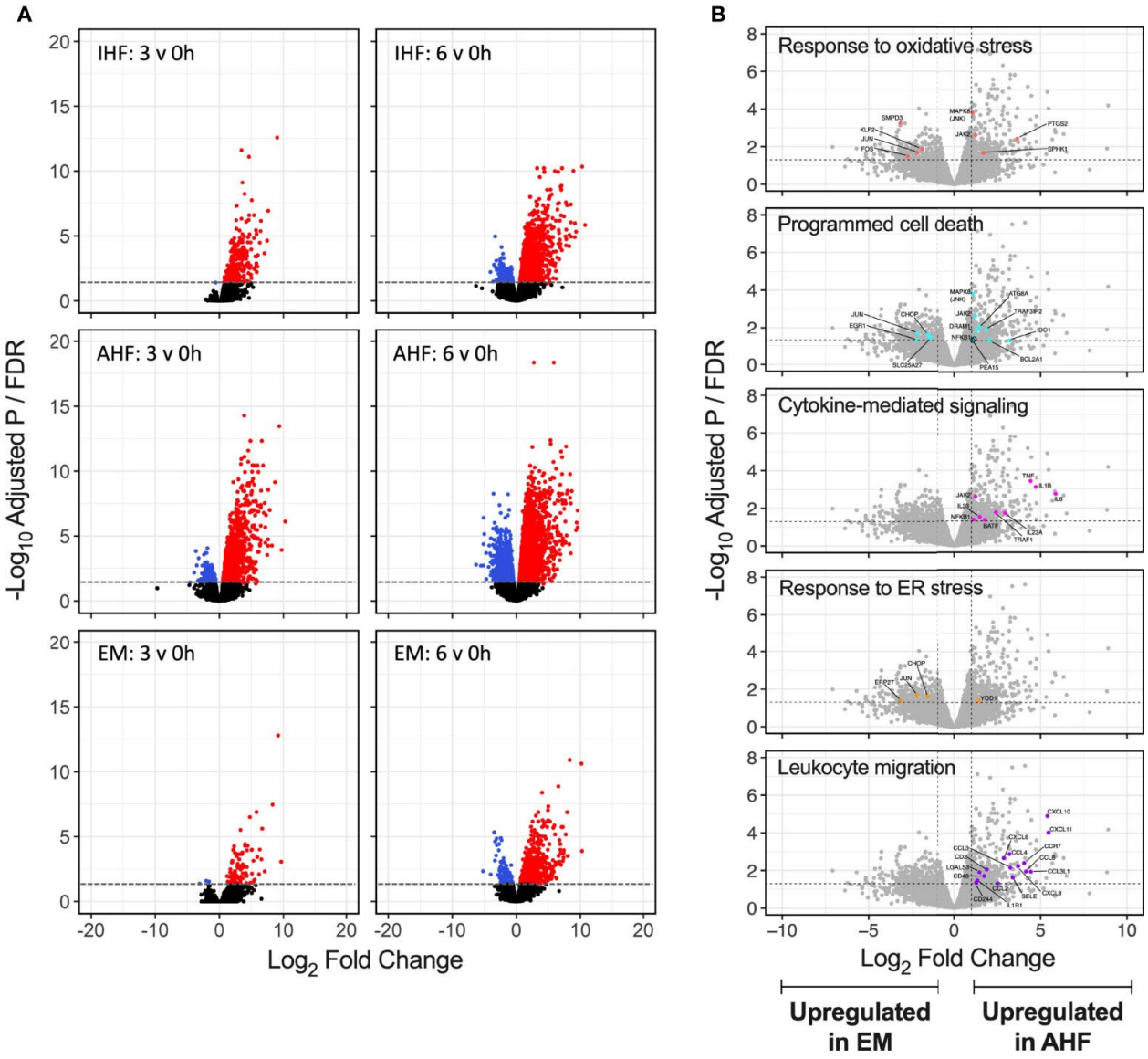

FIGURE 4 Volcano plots of differentially expressed genes during NMP. (A) Significant upregulated (red) and downregulated (blue) genes shown for each group at 3 and 6 hours of NMP compared to pre-perfusion. The absolute number of differentially expressed genes appeared lower in the EM compared to AHF and IHF groups. (B) Select GO term volcano plots shown for comparison of EM to AHF groups at 6 hours of NMP. Significant differentially expressed genes within each GO term are shown in color and labelled. Genes related to inflammatory signaling and leukocyte migration were significantly upregulated in AHF compared to EM livers. Horizontal dashed line indicates the adjusted P value (false discovery rate) cutoff of 0.05. Vertical dashed lines indicate the log2 fold change cutoff -1 and 1. NMP, normothermic machine perfusion; GO, gene ontology; AHF, adequate hepatocellular function; IHF, inadequate hepatocellular function; EM, emricasan; ER, endoplasmic reticulum.

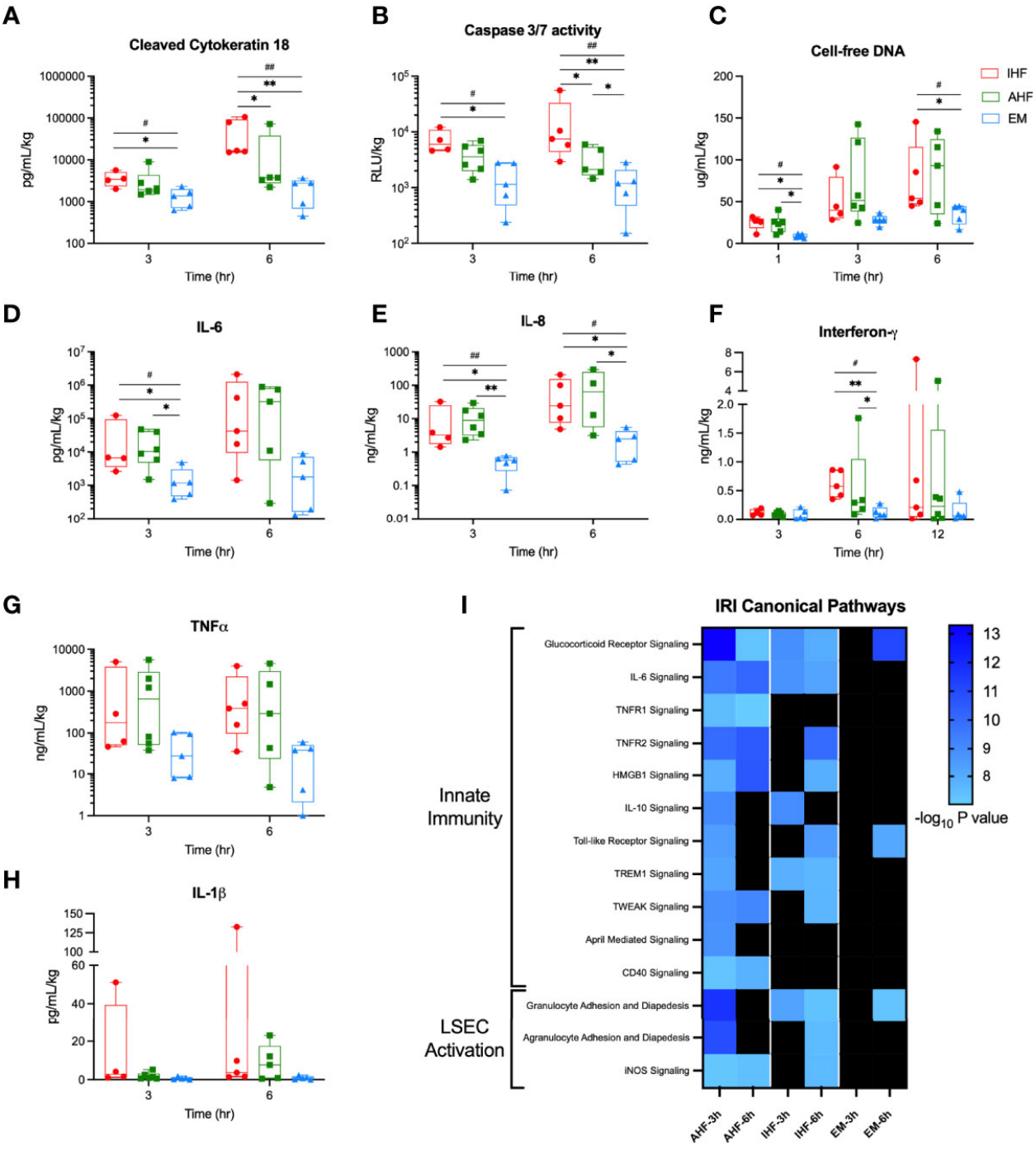

FIGURE 5 Perfusate cell death and cytokine analysis. Addition of emricasan to NMP resulted in significantly lower perfusate levels of the apoptosis biomarkers (A) cleaved cytokeratin 18 and (B) caspase-3/7 enzyme activity. (C) Cell-free DNA, a DAMP, was significantly lower in the perfusate of EM livers at 1 and 6 hours. Levels of pro-inflammatory cytokines (D) interleukin-6 (IL-6), (E) interleukin-8 (IL-8), and (F) interferon-γ were also significantly lower in EM livers compared to control groups. Perfusate levels of (G) tumor necrosis factor-α (TNF-α) and (G) interleukin-1β (IL-1 β) were qualitatively lower but did not reach significance. I) Heatmap of canonical pathways involved in ischemic-reperfusion injury (IRI). The significance threshold was

set to -log10 P value > 7 for comparison of 3- and 6-hour gene sets to the pre-perfusion (0 hour) baseline for each group. Kruskal-Wallis test: ## P<0.01, # P<0.05; Wilcoxon ranksum test: ** P<0.01, * P<0.05. NMP, normothermic machine perfusion; AHF, adequate hepatocellular function; IHF, inadequate hepatocellular function; EM, emricasan.

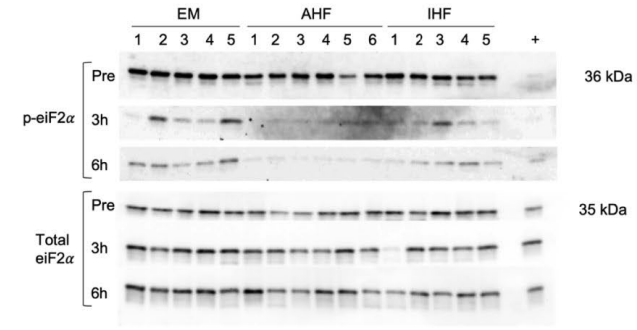

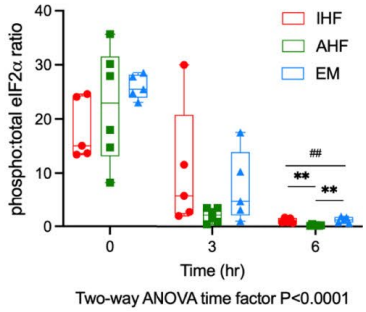

Two-way ANOVA time factor P<0.0001

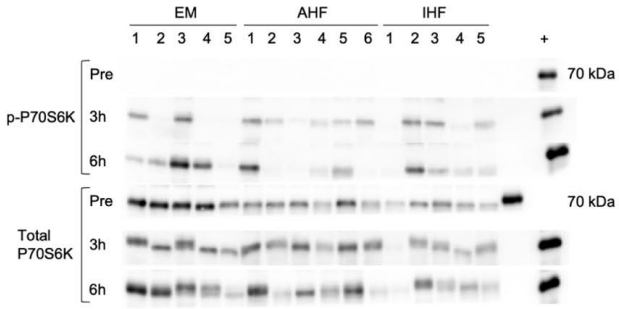

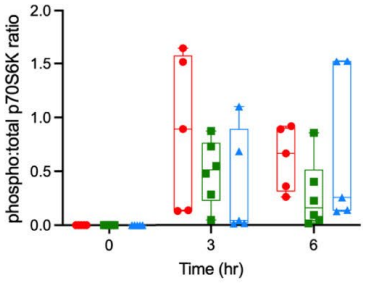

Two-way ANOVA time factor P<0.0001

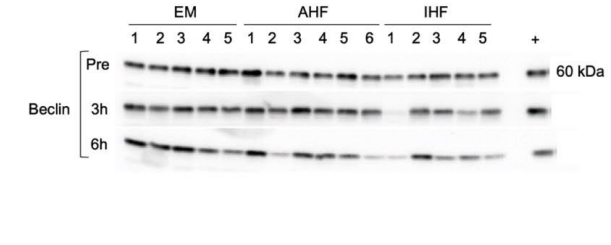

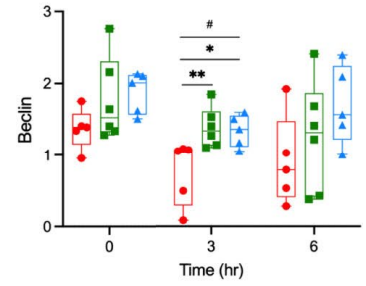

Two-way ANOVA time factor P<0.01

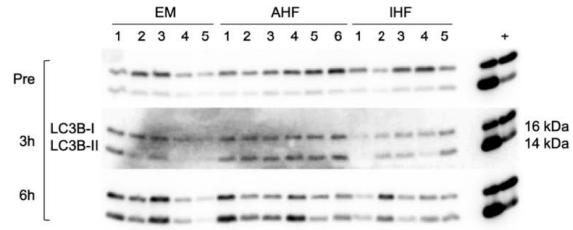

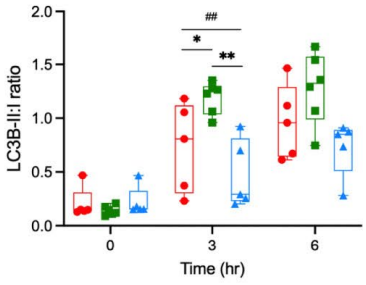

Two-way ANOVA time factor P<0.0001, group factor <0.01

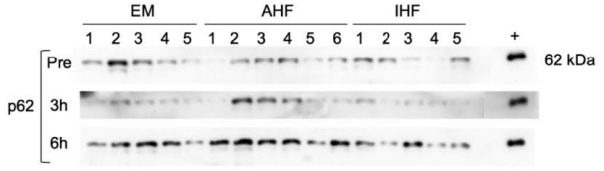

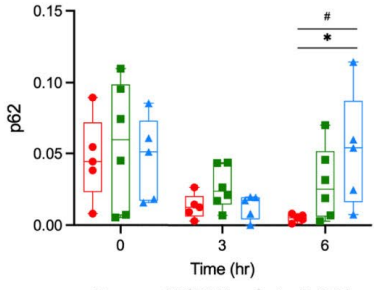

Two-way ANOVA time factor P<0.01

FIGURE 6 Autophagy and the unfolded protein response during liver NMP. Western immunoblots of (A) phosphorylated to total protein ratio of eiF2α, (B) phosphorylated to total protein ratio P70S6K, (C) Beclin, (D) LC3B-II to LC3B-I ratio, and (E) p62. Kruskal-Wallis test: ## P<0.01, # P<0.05; Wilcoxon ranksum test: ** P<0.01, * P<0.05. NMP, Normothermic machine perfusion; AHF, adequate hepatocellular function; IHF, inadequate hepatocellular function; EM, emricasan; eiF2α, eukaryotic initiation factor 2α; P70S6K, P70 S6 kinase; LC3B, microtubule-associated protein 1 light chain 3 beta.

Supplemental Material

The Supplementary Material for this article can be found online at: https://www.frontiersin.org/articles/10.3389/fimmu.2022.940094/full#supplementary-material

Supplementary Data Sheet 1 | Full list of gene ontology (GO) processes demonstrating enrichment used to create the network diagrams for principal component 1-3 in and Figure S2.

Supplemental Methods

S1. Human liver perfusions

Discarded human livers

Human livers were procured in standard fashion through two Organ Procurement Organizations (OPO): New England Donor Services (Waltham, MA, USA) and LiveOnNewYork (New York, NY, USA). In addition, one liver was obtained through the International Institute for the Advancement of Medicine (IIAM, Edison, NJ, USA), which originated from the Gift of Life Donor Program (Philadelphia, PA, USA). Informed consent was obtained from donors by the OPO. The Massachusetts General Hospital and Lifespan Institutional Review Boards, as well as the two OPOs and IIAM, approved this study (No. 2011P001496). No organs were procured from prisoners and no vulnerable populations were included in this study.

Procurement of Grafts

Procurement techniques based on donation after circulatory death followed standard methods. Donor livers were flushed in situ with University of Wisconsin solution. Total warm ischemic time was defined as the period from extubation to cold flush. Functional WIT was defined as the period from asystole to cold flush. Cold ischemic time was defined from cold flush to initiation of machine perfusion. All livers were transported via ground courier. After arrival to the laboratory under static cold storage, livers underwent standard back bench preparation for machine perfusion.

S2. Total RNA purification, sequencing, and analysis

RNA Purification and Sequencing

Tissues samples from livers taken immediately prior to perfusion and after 3 and 6 hours of perfusion were used for transcriptome sequencing. Core needle biopsies from the right liver lobe were collected in RNAlater solution (Sigma-Millipore, Waltham, MA, USA) and stored overnight at 4°C. Tissue samples were then removed from solution and stored at -80°C. Total RNA was isolated using the RNeasy Mini Kit (Qiagen, Germantown, MD, USA) according to manufacturer guidelines. 500ng of each sample was sequenced on an Illumina HiSeq 4000 using 9 PCR cycles by GENEWIZ (South Plainfield, NJ, USA). Raw RNA-Seq data files were transferred to the Brown University computing cluster via sFTP and aligned to the human genome build 38 using STAR 2.7.3a. [31] While sequencing was performed in two batches, the alignment was performed on all samples simultaneously using the same settings. To quantify any batch effect in our aligned data, we utilized MBatch 1.7.1 [32] to generate a Dispersion Separability Criterion (DSC) value for the pre-treatment (0hr) timepoints from the two batches,

resulting in a DSC of 0.197 (p = 0.671). Due to this low batch effect severity score and insignificant p-value, we did not apply a batch correction to our data.

Bioinformatic analysis

Raw read counts were normalized using the Trimmed Mean of M method following removal of low-count genes (fewer than 10 reads in the smallest library). Differential gene expression analysis was conducted in R [33] using edgeR. [34] The significance cutoff for differential gene expression was set to a Benjamini-Hochberg false-discovery rate (FDR or q-value) < 0.05. Canonical pathway and upstream regulator enrichment analysis was generated through Ingenuity Pathway Analysis (IPA, Qiagen). [35] IPA categories were considered significant when the P value was below the P values obtained from 5 similarly sized sets of randomly selected genes with a fold-change in expression ≤1. [36] In this study, the threshold for significance was P<10E-7 for canonical pathways and P<10E-14 for upstream regulators.

Principal component analysis (PCA), volcano plots, Venn diagrams, and heatmaps were created using the following R packages: ggplot2 (2D PCA), plot3D/plot3Drgl (3D PCA), EnhancedVolcano (volcano plots), VennDiagram (Venn diagrams), and heatmaply (heatmaps).

Gene ontology (GO) enrichment analysis was performed using the R package GOseq. [37] A Benjamini-Hochberg FDR adjusted p-value of < 0.05 was used for determining significant GO term enrichment. The genes with the highest amount of variance explained by principal component 1, 2, or 3 cumulatively totaling to 10% of the total variance explained by the specified PC were further analyzed. The proportion of a gene's variance explained by a PC was calculated using the squared loading values generated by the prcomp function in R. GO term analysis was performed on these gene subsets and the significantly enriched GO terms in the biological processes category for each PC were summarized in 75% similarity networks generated in Cytoscape. [38] For each PC, the enriched GO terms in each hub of their networks can be found in Dataset S1.

Raw sequence data have been deposited in the Gene Expression Omnibus with accession no. GSE202565 and no. GSE165568 (open access).

S3. Enzyme-linked immunosorbent assay (ELISA) kits

Protein	**Manufacturer**	**Product Number**
Tumor necrosis factor-alpha (TNFα)	Sigma-Millipore	RAB0476
Interleukin-6 (IL-6)	Sigma-Millipore	RAB0306
Interferon-gamma (IFNγ)	Abcam	ab174443
Cleaved cytokeratin 18	Abcam	ab254515
Caspase 3/7	Promega	G8091
Cell-free DNA	Sigma-Millipore	11774425001
Interleukin-8 (IL-8)	Abcam	ab214030
Interleukin-1 Beta (IL-1B)	Sigma-Millipore	RAB0273

Abcam (Waltham, MA, USA), Aviva Systems Biology (San Diego, CA, USA), Sigma-Millipore (Waltham, MA, USA).

S4. Western immunoblot antibodies

Antibody	Manufacturer	Product Number
eIF2α	Santa Cruz Biotechnology	sc-11386
Phospho-eIF2α	Cell Signaling Technology	9721
p70 S6 Kinase	Cell Signaling Technology	2708
Phospho-p70 S6 Kinase (Thr389)	Cell Signaling Technology	9234
LC3B	Cell Signaling Technology	2775
β-actin	Santa Cruz Biotechnology	sc-47778
GAPDH	Cell Signaling Technology	5174
P62	Cell Signaling Technology	39749
Beclin	Cell Signaling Technology	3738
MLKL	Cell Signaling Technology	14993
Phospho-MLKL	Cell Signaling Technology	91689

Cell Signaling Technology (Danvers, MA, USA), Santa Cruz Biotechnology (Dallas, TX, USA), Sigma-Millipore (Waltham, MA, USA).

To compare target protein expression, densitometry quantification was conducted. Blots for β-actin and GAPDH are shown in Figure S6. Both proteins varied across samples and the changes were not consistent between the 2 proteins, with the variation representing the biologic variability in the human liver. As a result, target relative protein was expressed as a ratio of active to inactive protein intensity (or phosphorylated protein to total protein intensity).

S5. Immunohistochemistry antibodies and methods

Antibody	Manufacturer	Product Number
LC3B	Novus Biologicals (Littleton, CO, USA)	NB100-2220

Immunohistochemistry was performed using antibodies directed toward LC3B (see above). Paraffin sections (6 μm) were deparaffinized with xylene and rehydrated with graded ethanol. Antigen retrieval was performed by sub-boiling in 1X-diluted Dako Target Retrieval Solution for 10 min (DakoCytomation, Inc., Carpinteria, CA). Slides were then quenched in 3% H2O2 and blocked in 2.5% Normal Horse Serum (Vector Labs, Burlingame, CA) before overnight incubation in primary antibody (1:200 dilution) at 4°C. Slides were incubated with a horseradish-peroxidase conjugated secondary rabbit antibody (Vector Laboratories) for 1 hr prior to staining with DAB (Vector Laboratories). Slides were counterstained with hematoxylin. Omission of the primary antibody served as a negative control.

Supplemental Figures

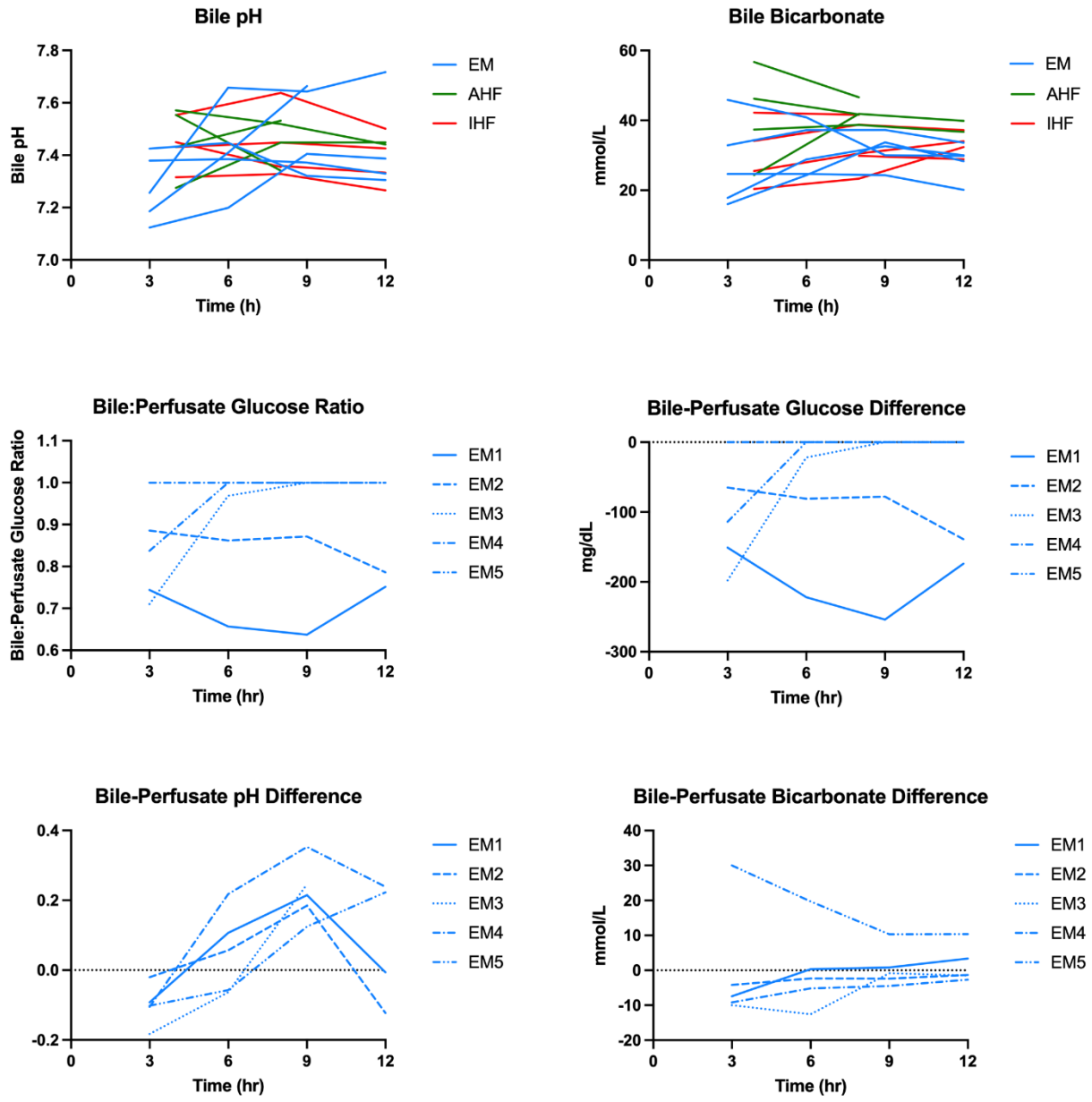

Supplementary Figure 1 | Cholangiocellular functional criteria during liver NMP. Various cholangiocellular functional criteria demonstrated. Technical issues with bile collection prevented accurate measurement of bile in two livers from the AHF group. Bile pH and bicarbonate is shown collectively for all available livers. Additional functional data comparing bile and perfusate glucose, pH, and bicarbonate is shown only for EM livers as equivalent data points were not available for the control livers. NMP, normothermic machine perfusion; AHF, adequate hepatocellular function; IHF, inadequate hepatocellular function; EM, emricasan.

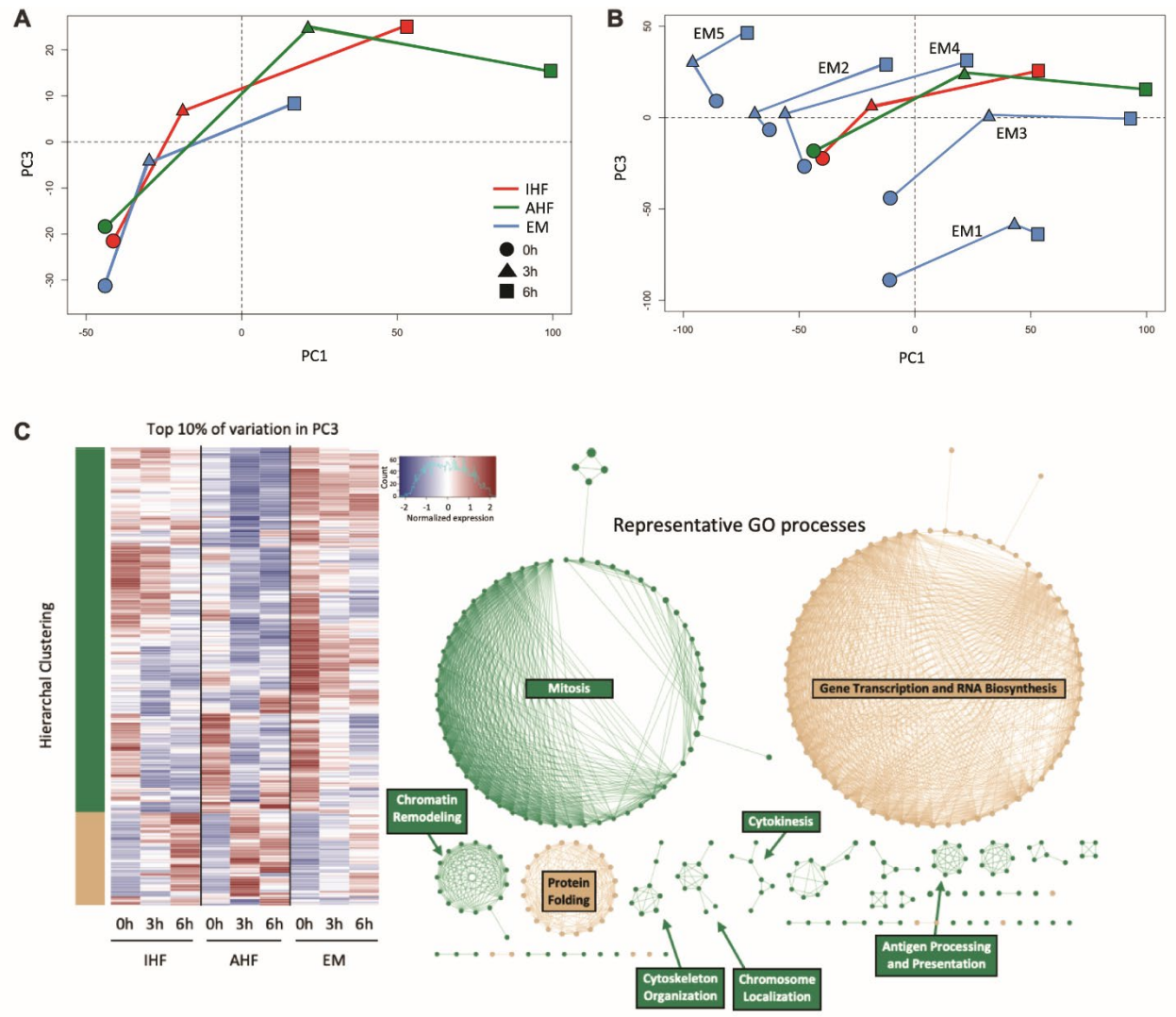

Supplementary Figure 2 | Gene expression and ontology analysis of principal component 3 (PC3). (A) Combined and (B) individual principal component plots for PC3 across PC1. (C) Hierarchical clustering heatmap of the top 10% of genes accounting for the variation in PC3. GO network analysis indicates PC3 is enriched for gene expression accounting for mitosis (forest green networks) and DNA transcription (beige networks). In contrast to AHF and IHF livers, EM livers appear to demonstrate overall upregulation of mitosis-related genes. AHF, adequate hepatocellular function; IHF, inadequate hepatocellular function; EM, emricasan.

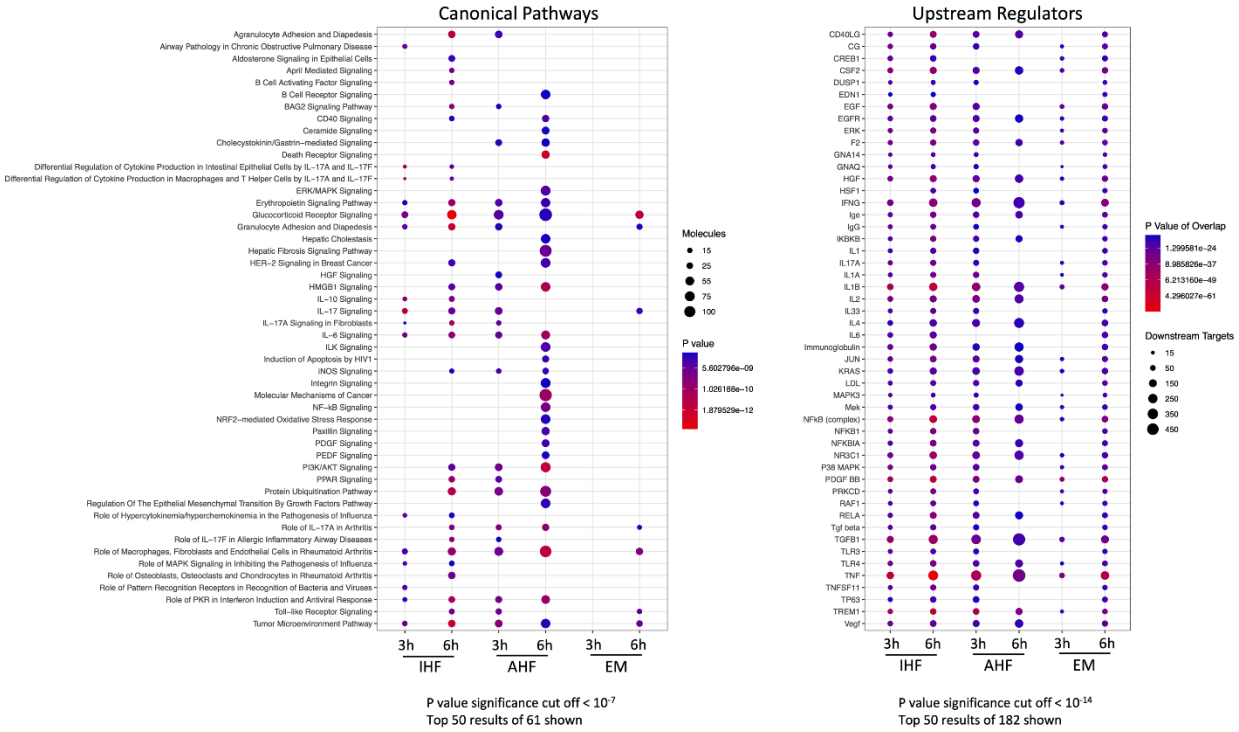

Supplementary Figure 3 | Ingenuity Pathway Analysis (IPA) of differentially expressed genes. Dot plots contain significant (A) canonical pathways (CP) and (B) upstream regulators (UR) for the arbitrary P value cut-off indicated in the legend (10-7 for CPs and 10-14 for URs). Results are shown for differentially expressed genes at 3 and 6 hours of NMP compared to the pre-perfusion (0 hour) baseline. The size of each dot represents the number of downstream target genes in our gene set that were in the IPA gene set for that CP or UR. The color of each dot represents the P value for the CP or UR. NMP, normothermic machine perfusion; AHF, adequate hepatocellular function; IHF, inadequate hepatocellular function; EM, emricasan.

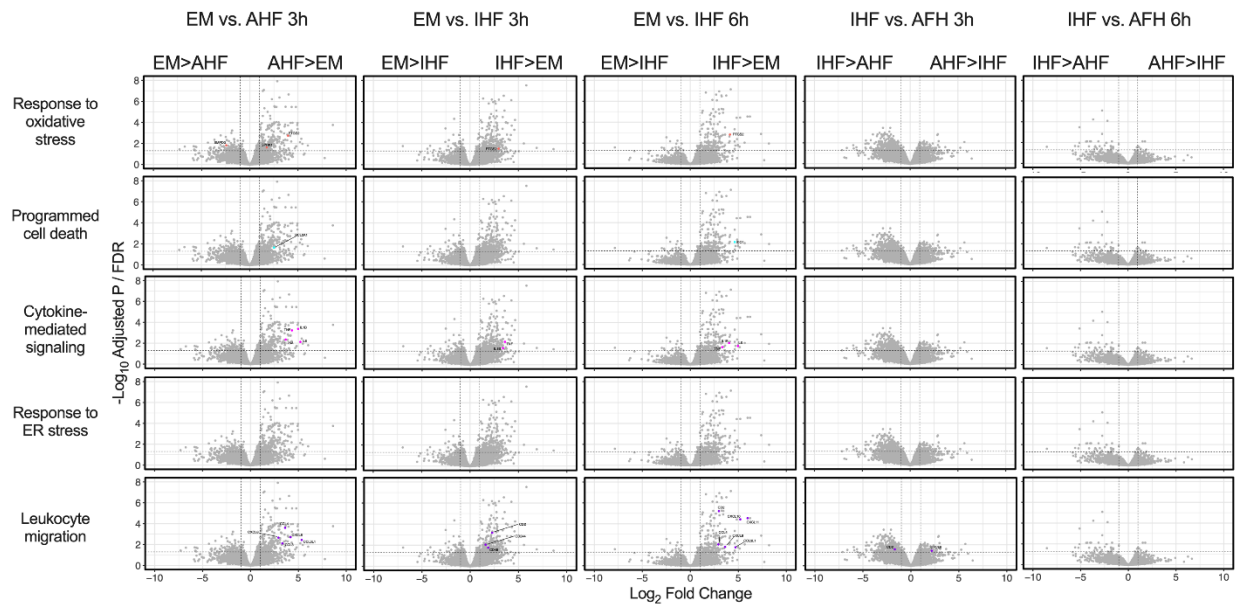

Supplementary Figure 4 | Selective volcano plots for all group comparisons. Individual time-point comparisons at 3 and 6 hours of NMP among all groups are demonstrated for the select gene ontology processes demonstrated in Figure 4B. Differentially expressed genes meeting the false discovery rate (FDR) > 0.05 threshold are shown in color and labeled. NMP, normothermic machine perfusion; AHF, adequate hepatocellular function; IHF, inadequate hepatocellular function; EM, emricasan.

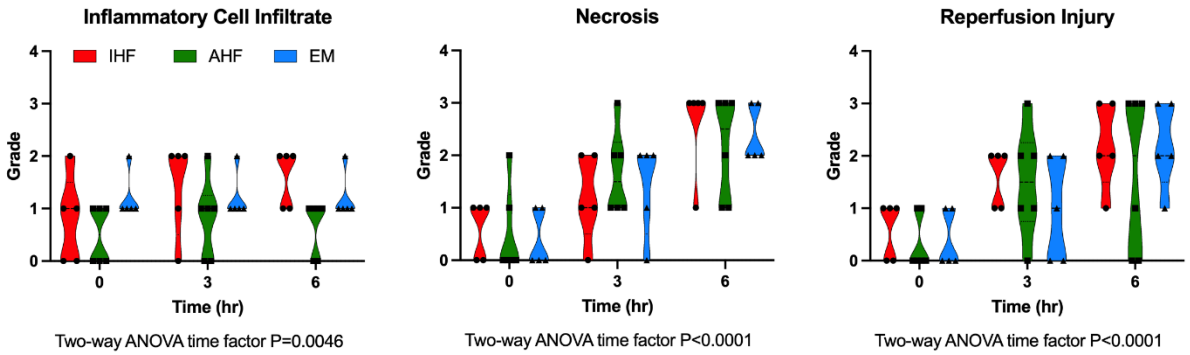

Supplementary Figure 5 | Histopathologic reperfusion injury during NMP. Blinded pathologists scored 0, 3, and 6 hours biopsy samples for (A) inflammatory cell infiltrate, (B) necrosis, and (C) reperfusion injury (a composite of A and B). The two-way ANOVA time factor was statistically significant for all three evaluated histologic markers. No significant differences were seen between groups. NMP, normothermic machine perfusion; AHF, adequate hepatocellular function; IHF, inadequate hepatocellular function; EM, emricasan; ANOVA, analysis of variance.

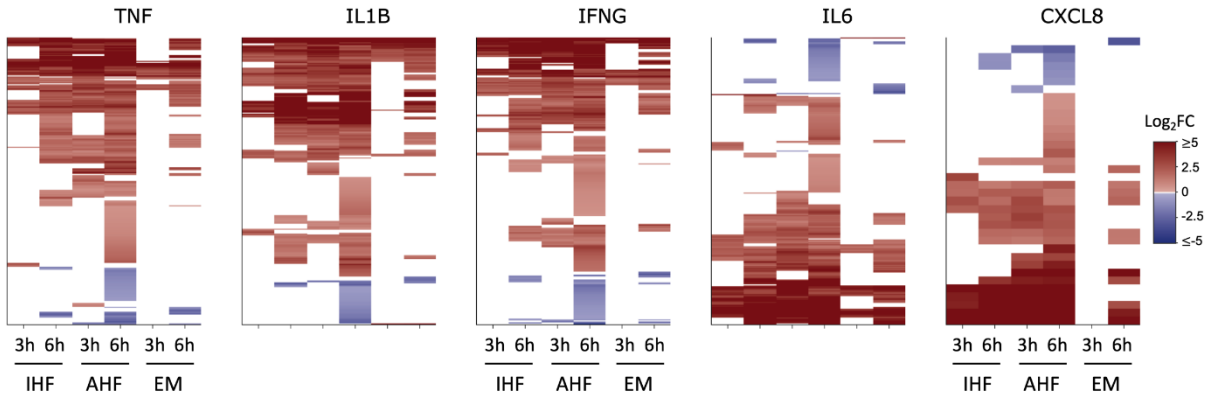

Supplementary Figure 6 | Downstream target gene expression for selected proinflammatory cytokine. Proinflammatory cytokines from were analyzed as upstream regulators in IPA for downstream target gene expression. EM livers demonstrate categorically lower enrichment of target genes compared to IHF and AHF groups. NMP, normothermic machine perfusion; AHF, adequate hepatocellular function; IHF, inadequate hepatocellular function; EM, emricasan; IPA, Ingenuity Pathway Analysis; TNF, tumor necrosis factor; IL1B, interleukin-1 β; IFNG, interferon-γ; CXCL8, C-X-C motif chemokine ligand 8 (also known as interleukin-8).

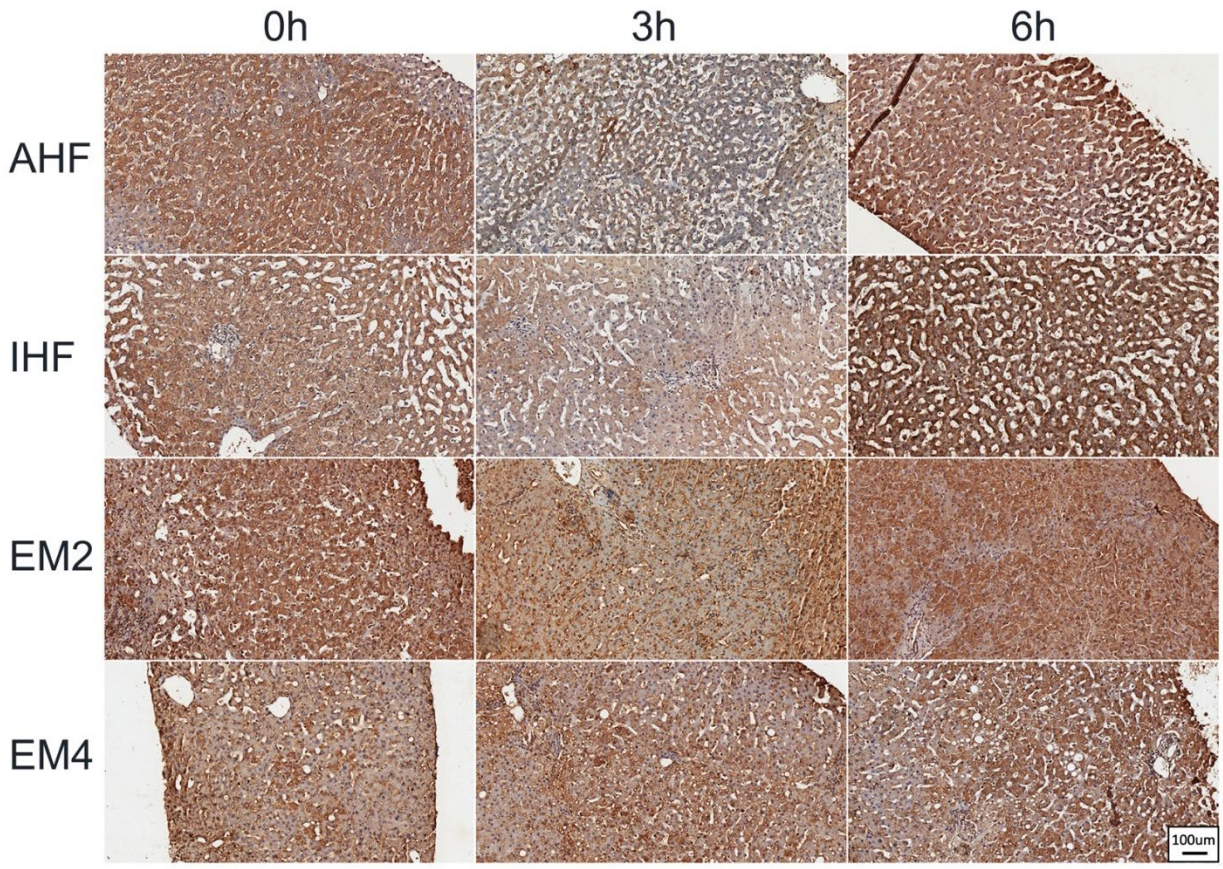

Supplementary Figure 7 | LC3B Immunohistochemistry. Immunohistochemistry for LC3B demonstrating patterns of autophagosome assembly during perfusion among the three groups. AHF livers demonstrate active autophagy at 3 and 6 hours of NMP as indicated by the transition from pancytosolic to granular LC3B staining pattern. In contrast, IHF livers demonstrated more sporadic granular LC3B staining after initiation of NMP. EM livers had variable staining with some livers demonstrating granular LC3B staining after 3 hours with return to pancytosolic staining by 6 hours of NMP. 100 micron scale bar shown. NMP, Normothermic machine perfusion; AHF, adequate hepatocellular function; IHF, inadequate hepatocellular function; EM, emricasan; LC3B, microtubule-associated protein 1 light chain 3 beta.

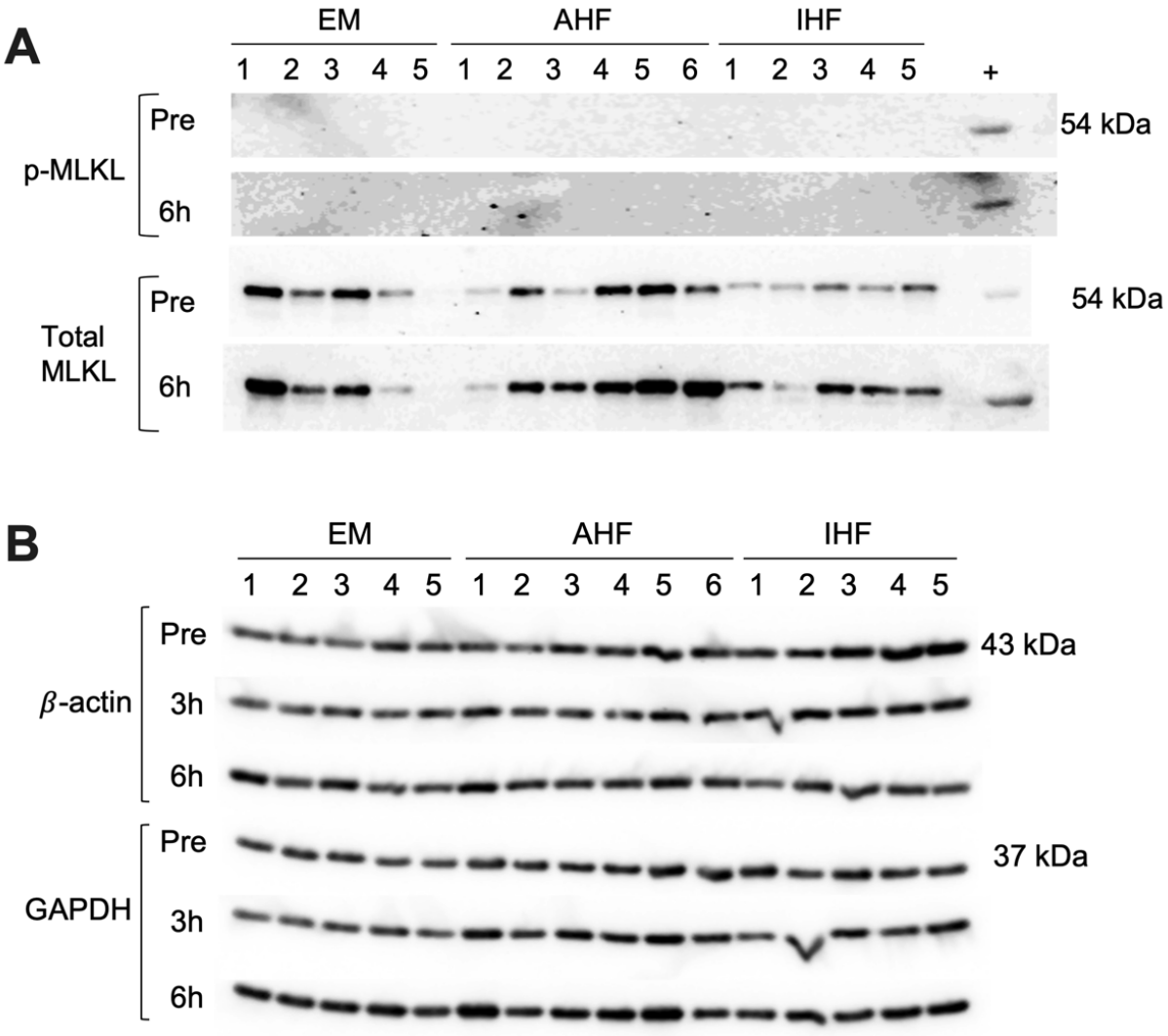

Supplementary Figure 8 | Necroptosis and protein controls during NMP. (A) Western immunoblot analysis of phosphorylated and total levels of the necroptosis marker mixed lineage kinase domain-like (MLKL). Phosphorylated MLKL protein was below the level of detection at pre-perfusion and after 6 hours of NMP. (B) β-actin and glyceraldehyde-3-phosphate dehydrogenase (GAPDH) levels for all three groups. NMP, normothermic machine perfusion; AHF, adequate hepatocellular function; IHF, inadequate hepatocellular function; EM, emricasan.

References

1. Nasralla D, Coussios CC, Mergental H, et al. A randomized trial of normothermic preservation in liver transplantation. *Nature*. 2018;557(7703):50-56. doi:10.1038/s41586-018-0047-9

2. van Rijn R, Schurink IJ, de Vries Y, et al. Hypothermic Machine Perfusion in Liver Transplantation - A Randomized Trial. *N Engl J Med*. 2021;384(15):1391-1401. doi:10.1056/NEJMoa2031532

3. Ohman A, Raigani S, Santiago JC, et al. Activation of autophagy during normothermic machine perfusion of discarded livers is associated with improved hepatocellular function. *Am J Physiol Gastrointest Liver Physiol*. Published online 2021. doi:10.1152/ajpgi.00266.2021

4. Fairlie WD, Tran S, Lee EF. Crosstalk between apoptosis and autophagy signaling pathways. *Int Rev Cell Mol Biol*. 2020;352:115-158. doi:10.1016/bs.ircmb.2020.01.003

5. Brenner C, Galluzzi L, Kepp O, Kroemer G. Decoding cell death signals in liver inflammation. *J Hepatol*. 2013;59(3):583-594. doi:10.1016/j.jhep.2013.03.033

6. Galluzzi L, Lopez-Soto A, Kumar S, Kroemer G. Caspases Connect Cell-Death Signaling to Organismal Homeostasis. *Immunity*. 2016;44(2):221-231. doi:10.1016/j.immuni.2016.01.020

7. Guicciardi ME, Gores GJ. Apoptosis: a mechanism of acute and chronic liver injury. *Gut*. 2005;54(7):1024-1033. doi:10.1136/gut.2004.053850

8. Baskin-Bey ES, Washburn K, Feng S, et al. Clinical Trial of the Pan-Caspase Inhibitor, IDN-6556, in Human Liver Preservation Injury. *Am J Transplant*. 2007;7(1):218-225. doi:10.1111/j.1600-6143.2006.01595.x

9. Guicciardi ME, Malhi H, Mott JL, Gores GJ. Apoptosis and necrosis in the liver. *Compr Physiol*. 2013;3(2):977-1010. doi:10.1002/cphy.c120020

10. Hoglen NC, Anselmo DM, Katori M, et al. A caspase inhibitor, IDN-6556, ameliorates early hepatic injury in an ex vivo rat model of warm and cold ischemia. *Liver Transpl*. 2007;13(3):361-366. doi:10.1002/lt.21016

11. Mueller TH, Kienle K, Beham A, Geissler EK, Jauch KW, Rentsch M. Caspase 3 inhibition improves survival and reduces early graft injury after ischemia and reperfusion in rat liver transplantation. *Transplantation*. 2004;78(9):1267-1273. doi:10.1097/01.tp.0000141095.06273.10

12. Natori S, Higuchi H, Contreras P, Gores GJ. The caspase inhibitor IDN-6556 prevents caspase activation and apoptosis in sinusoidal endothelial cells during liver preservation injury. *Liver Transpl*. 2003;9(3):278-284. doi:10.1053/jlts.2003.50019

13. Natori S, Selzner M, Valentino KL, et al. Apoptosis of sinusoidal endothelial cells occurs during liver preservation injury by a caspase-dependent mechanism. *Transplantation*. 1999;68(1):89-96. doi:10.1097/00007890-199907150-00018

14. Xu D, Zhao H, Jin M, et al. Modulating TRADD to restore cellular homeostasis and inhibit apoptosis. *Nature*. Published online 2020. doi:10.1038/s41586-020-2757-z

15. Raigani S, de Vries RJ, Carroll C, et al. Viability testing of discarded livers with normothermic machine perfusion: Alleviating the organ shortage outweighs the cost. *Clin Transplant*. 2020;34(11):e14069. doi:10.1111/ctr.14069

16. Feng S, Goodrich NP, Bragg-Gresham JL, et al. Characteristics Associated with Liver Graft Failure: The Concept of a Donor Risk Index. *American Journal of Transplantation*. 2006;6(4):783-790. doi:10.1111/J.1600-6143.2006.01242.X

17. van Leeuwen OB, de Vries Y, Fujiyoshi M, et al. Transplantation of High-risk Donor Livers After Ex Situ Resuscitation and Assessment Using Combined Hypo- and Normothermic Machine Perfusion: A Prospective Clinical Trial. *Ann Surg*. 2019;270(5):906-914. doi:10.1097/SLA.0000000000003540

18. Sanders JA, Lakhani A, Phornphutkul C, Wu KY, Gruppuso PA. The effect of rapamycin on DNA synthesis in multiple tissues from late gestation fetal and postnatal rats. *Am J Physiol Cell Physiol*. 2008;295(2):C406-13. doi:10.1152/ajpcell.00450.2007

19. Sosa RA, Zarrinpar A, Rossetti M, et al. Early cytokine signatures of ischemia/reperfusion injury in human orthotopic liver transplantation. *JCI Insight*. 2016;1(20):e89679. doi:10.1172/jci.insight.89679

20. Orning P, Lien E. Multiple roles of caspase-8 in cell death, inflammation, and innate immunity. *J Leukoc Biol*. 2021;109(1):121-141. doi:10.1002/JLB.3MR0420-305R

21. Ohman A, Raigani S, Santiago JC, et al. Activation of autophagy during normothermic machine perfusion of discarded livers is associated with improved hepatocellular function. *Am J Physiol Gastrointest Liver Physiol*. 2022;322(1):G21-G33. doi:10.1152/AJPGI.00266.2021

22. Markmann JF, Abouljoud MS, Ghobrial RM, et al. Impact of Portable Normothermic Blood-Based Machine Perfusion on Outcomes of Liver Transplant: The OCS Liver PROTECT Randomized Clinical Trial. *JAMA Surg*. 2022;157(3):189. doi:10.1001/JAMASURG.2021.6781

23. Raigani S, De Vries RJ, Uygun K, Yeh H. Pumping new life into old ideas: Preservation and rehabilitation of the liver using ex situ machine perfusion. *Artif Organs*. 2020;44(2):123-128. doi:10.1111/aor.13579

24. Li J, Yuan J. Caspases in apoptosis and beyond. *Oncogene 2008 27:48*. 2008;27(48):6194-6206. doi:10.1038/onc.2008.297

25. Xu S, Li X, Liu Y, Xia Y, Chang R, Zhang C. Inflammasome inhibitors: promising therapeutic approaches against cancer. *Journal of Hematology & Oncology 2019 12:1*. 2019;12(1):1-13. doi:10.1186/S13045-019-0755-0

26. Dhani S, Zhao Y, Zhivotovsky B. A long way to go: caspase inhibitors in clinical use. *Cell Death & Disease 2021 12:10*. 2021;12(10):1-13. doi:10.1038/s41419-021-04240-3

27. Scheuermann U, Zhu M, Song M, et al. Damage-Associated Molecular Patterns Induce Inflammatory Injury During Machine Preservation of the Liver: Potential Targets to Enhance a Promising Technology. *Liver Transplantation*. 2019;25(4):610-626. doi:10.1002/LT.25429

28. Fajgenbaum DC, June CH. Cytokine Storm. *New England Journal of Medicine*. 2020;383(23):2255-2273. doi:10.1056/NEJMRA2026131/SUPPL_FILE/NEJMRA2026131_DISCLOSURES.PDF

29. de Vries Y, Matton APM, Nijsten MWN, et al. Pretransplant sequential hypo- and normothermic machine perfusion of suboptimal livers donated after circulatory death using a hemoglobin-based oxygen carrier perfusion solution. *American Journal of Transplantation*. 2019;19(4):1202-1211. doi:10.1111/AJT.15228

30. Mergental H, Laing RW, Kirkham AJ, et al. Transplantation of discarded livers following viability testing with normothermic machine perfusion. *Nat Commun*. 2020;11(1):2939. doi:10.1038/s41467-020-16251-3

31. Dobin A, Davis CA, Schlesinger F, et al. STAR: ultrafast universal RNA-seq aligner. *Bioinformatics*. 2013;29(1):15-21. doi:10.1093/BIOINFORMATICS/BTS635

32. MD Anderson Cancer Center. MD-Anderson-Bioinformatics/BatchEffectsPackage: The MBatch R package and Docker image are designed to help assess and correct for batch effects. Accessed October 11, 2022. https://github.com/MD-Anderson-Bioinformatics/BatchEffectsPackage

33. Core Development Team R. A Language and Environment for Statistical Computing. *R Foundation for Statistical Computing*. 2020;2:https://www.R-project.org. http://www.r-project.org

34. Robinson MD, McCarthy DJ, Smyth GK. edgeR: a Bioconductor package for differential expression analysis of digital gene expression data. *Bioinformatics*. 2010;26(1):139-140. doi:10.1093/BIOINFORMATICS/BTP616

35. QIAGEN Inc. Ingenuity Pathway Analysis (IPA). Published online 2016. https://www.qiagenbioinformatics.com/products/ingenuity-pathway-analysis

36. Lamming DW, Demirkan G, Boylan JM, et al. Hepatic signaling by the mechanistic target of rapamycin complex 2 (mTORC2). *FASEB Journal*. 2014;28(1):300-315. doi:10.1096/FJ.13-237743

37. Young MD, Wakefield MJ, Smyth GK, Oshlack A. Gene ontology analysis for RNA-seq: accounting for selection bias. *Genome Biol*. 2010;11(2):1-12. doi:10.1186/GB-2010-11-2-R14/TABLES/4

38. Shannon P, Markiel A, Ozier O, et al. Cytoscape: A Software Environment for Integrated Models of Biomolecular Interaction Networks. *Genome Res*. 2003;13(11):2498-2504. doi:10.1101/GR.1239303

Chapter 5:
Conclusions and Future Directions

Conclusions

This dissertation's goal was to explore possible novel improvements to the current standard of orthotopic liver transplantation (OLT). Specifically, we characterized the underlying mechanisms behind what happens in fetal hepatocytes following hepatic cellular transplantation (HCT), as well as in livers undergoing normothermic machine perfusion (NMP). We hope a more detailed understanding of these processes will allow for optimization of these techniques as clinical advancements over current techniques. Our methodology utilized several modern omics techniques. Transcriptomics via RNA sequencing allowed us to examine gene expression patterns in fetal and adult hepatocytes, pre- and post-transplantation in a rat model of liver regeneration. It also allowed us to explore gene expression changes in human livers over multiple time points before and during the NMP process, and match gene expression to physiological viability criteria at these same time points. Utilizing bioinformatics tools such as Ingenuity Pathway Analysis (IPA), we were able to take this large dataset of differentially expressed genes (DEGs) and determine putative relationships and networks of gene expression that may reflect upstream regulators and activated pathways. We also explored aspects of the epigenome by way of histone proteomics, where post-translational modifications of histone tails that are associated with gene expression or repression were analyzed to find patterns common to fetal or adult samples. Proteomic analysis of the perfusate during NMP allowed us to quantify functional dynamics and assess liver transplant viability.

Fetal Hepatocyte Cellular Transplantation

In our analysis of fetal- and adult-derived hepatocytes in Chapter 2, we hypothesized that there would be retained epigenetic differences following fetal HCT that retained fetal transcriptomic characteristics and promoted a proliferative advantage. We found that there are approximately 1,000 significant DEGs in post-transplant fetal-derived colonies compared to surrounding adult host tissue, with the majority of genes expressed higher in the fetal-derived

colonies. These changes resulted in clustering of post-transplant samples by colony or host identity, rather than with their counterpart sample from the same paired biological replicate. When compared to pre-transplant fetal and adult hepatocytes, the post-transplant fetal-derived colonies plot closely to single-sorted leucine aminopeptidase-positive (LAP+) fetal hepatocytes and dual-sorted LAP+/OC.2− fetal hepatocytes, and further from adult hepatocytes and dual-sorted LAP+/OC.2+ fetal hepatocytes. Additionally, we saw an overlap of hundreds of genes that are significantly different between adult and fetal hepatocytes both pre- and post-transplant. The significant post-transplant genes corresponded to distinct gene ontology and pathway analysis results between adult and fetal-derived samples, where fetal-derived colonies had enriched terms related to ion transmembrane transport and activated signaling pathways. We also found multiple histone post-translational modifications (hPTMs) that were significantly different both pre- and post-transplant with similar patterns of relative abundance between fetal and adult samples at both time points. Of these, all of the hPTMs that were associated with gene transcription repression were more abundant in adult samples, and the majority of those that were unmodified or associated with gene transcription promotion were found to be more abundant in fetal samples. Overall, we found retained significant differences between fetal and adult samples, in both gene expression and histone PTM abundance, from pre-transplantation to at least 10 months following transplantation.

Normothermic Machine Perfusion

Our collaboration with the Organ Reengineering Group at Massachusetts General Hospital and Harvard Medical School set out to characterize and understand the effect of NMP on human livers. Post-perfusion, two different groups emerged: one set of livers that met predefined hepatocellular viability criteria, and one that did not. We performed genomic sequencing on tissue samples taken from both of these groups during perfusion. By use of principal component analysis (PCA), we were able to plot a time course trajectory from pre-

perfusion to 3 and 6 hours of NMP. We see samples begin with similar patterns of gene expression and diverge as early as 3 hours of perfusion into clear “functional” and “nonfunctional” groups. When these groups were examined by differential expression analysis, we found that the nonfunctional groups featured less gene activation at each time point than the functional groups. When categories of annotated genes were examined, a stronger expression pattern was detected in the functional group. When the top canonical pathways and upstream regulators identified by IPA were examined, the functional group was found to have significantly more activation of pathways related to inflammation and innate immunity at 3 hours, which shifted to enrichment of survival and growth by 6 hours. Histological examination of biopsies confirmed that the nonfunctional livers had a delayed activation of innate immune signaling. We also found a larger number of downstream target genes of top IPA upstream regulators were significantly expressed in functional groups and at later time points in the perfusion course. Based on the gene expression data, protein expression was measured by Western blot and confirmed that functional groups had disproportionate indicators of autophagy activation (eIF2α and LC3), potentially identifying a link between cellular repair mechanisms and liver functionality suitable for transplantation.

With this mechanistic understanding, our study in Chapter 4 aimed to apply adjuvant pre-treatment to improve liver functionality during NMP. We found that functional livers undergoing NMP had increased levels of autophagy, which can be protective against apoptosis. We hypothesized that the addition of the irreversible pan-caspase inhibitor emricasan to the perfusate may have the effect of mitigating pathologic apoptosis in nonfunctional livers, which could contribute to liver injury and lack of viability for transplantation. Discarded donation after cardiac death (DCD) livers, similar to the untreated control livers described in Chapter 3, were perfused with the addition of emricasan and underwent similar physiological, transcriptomic, and proteomic analysis to the analytical process described in Chapter 3. By physiological metrics

and gene expression PCA, the majority of emricasan-treated livers more closely resembled AHF donor livers than IHF ones. The strongest outlier by these metrics had the longest warm ischemic time of all the treated samples. Treated livers had distinct gene expression profiles from both adequate and inadequate donor livers, with fewer total differentially expressed genes at each time point of perfusion. However, both adequate and emricasan-treated livers had a lower expression of genes related to innate immunity than seen in inadequate livers. When the perfusate of all 3 groups were measured for apoptosis biomarkers (cleaved cytokeratin 18, caspase-3/7) the lowest levels were found in the emricasan-treated livers. In addition, the perfusate was surveyed for pro-inflammatory cytokines (IL-6, IL-8, Interferon-γ) and again the lowest levels were found in the emricasan-treated livers.

Taken together, Chapters 2, 3, and 4 demonstrate that using omics toolsets to investigate the molecular drivers of hepatocyte function is critical for making meaningful improvements to liver transplantation techniques. Associations drawn between optimal physiological characteristics and transcriptomic, epigenomic, and proteomic data may be used in the future to induce those desirable phenotypes in the scarce liver cell and organ populations that are available to leverage for transplantation.

Future Directions

Total proteomics analysis

In addition to our study of the epigenetic profile using histone proteomics by mass spectrometry (MS), we also explored using MS-based proteomic analysis in order to investigate differences in the total protein complement between fetal colony and adult host laser capture microdissection (LCM) tissue. Transcriptomics assesses mRNA levels which act as the template for protein synthesis and can therefore be considered a proxy for expected protein levels. [1] However, a variety of factors including differing decay rates and alternative RNA splicing make it

so that the connection between mRNA and protein levels is inexact. As a result, we also attempted to assess proteomic differences between our sample groups via MS, in order to integrate that perspective into our analysis. We utilized bottom-up proteomics, which is the most commonly utilized technique as a result of it having a simple peptide preparation pipeline via proteolytic enzyme digestion as well as a plethora of compatible instruments and analysis software. [2] Our collaborators at the IDeA National Resource for Quantitative Proteomics performed filter aided sample preparation (FASP) [3] followed by tandem mass tag (TMT) isobaric labeling, [4] based on their previous successful use of these techniques with LCM proteomics. FASP is able to utilize strong detergents for solubilization followed by ultrafiltration in order to remove detergents and retain only purified peptides. TMT involves labeling the resulting peptides with isobaric tags, which allows multiplexing several samples at a time in a single liquid chromatography (LC)-MS run.

We collected paired fetal-derived colony and adult host LCM samples for proteomic analysis from 5 rats collected from the same set of biological replicates used in Chapter 2 via a similar laser capture protocol. A quality control assessment found usable results in 4 of these samples, resulting in approximately 2100 to 2200 detected protein IDs each. The 5th sample only had approximately 200 detected proteins and may reflect technical issues with collection from that particular PEN Membrane slide. The 4 high-quality samples were carried through to TMT-MS.

When the raw protein expression data was plotted by PCA, we found no strong correlation between colony and host groups, nor a strong association between paired replicates (Figure 1A). When analyzed by ANOVA and visualized by volcano plot, only 9 proteins were significant by *P* value and only the Dpp4 protein was significant by FDR (Figure 1B). We also looked at the raw protein expression data by hierarchically clustered heatmap using the MORPHEUS matrix visualization and analysis software (Broad Institute, Cambridge MA) and

saw no strong clustering by fetal or adult samples or by paired replicate (Figure 1C). We finally sought to integrate this proteomic expression data alongside transcriptomic expression data in a process called 2D annotation enrichment (Figure 1D). [5] Due to the low number of significant proteins between the highly variable samples, we adjusted the significance cutoff threshold for the proteomic component of the analysis to a non-significant adjusted *P* value of < 0.6 for the purposes of hypothesis generation and data exploration. We found that the 5 results in the upper-right quadrant (indicating positive association between higher mRNA and higher protein expression) all had links to transporters (Mcpt1, Npc1l1) or other cell membrane interactions with the microenvironment (Spta1, Ank1, Abcb9), indicating a plausible relationship with cell proliferation.

What we found from this proteomic exploration on LCM tissue was inconclusive and indicates that such a sensitive technique may not be ideal to investigate highly variable samples such as ours, with high biological heterogeneity and possibly substantial technical effects on protein stability throughout the capture process. However, the detection of slight but significant changes in Dpp4 expression in the adult host tissue (likely reflective of the amino acid sequence differences of the inactivated enzyme in the German Fischer 334 rats not being recognized as a protein match) indicates that this technique is extremely sensitive for consistent changes in expression, and our preliminary assessment by 2D enrichment analysis shows that this could be a valuable method to integrate multiomics data. It may be important to perform future LCM proteomic studies on a more homogeneous sample set and under more rigid capture conditions in order to minimize biological and technical replicate variability in protein level.

Tissue validation of transporters

Our transcriptomic data identified several highly expressed genes that have known roles in ion transmembrane transport and may relate to the highly proliferative phenotype of post-transplant fetal hepatocytes. However, given the unreliability of our total proteomic dataset, it

will be important for us to verify the activation and cellular localization of these transporters to confirm that the elevated mRNA levels for detected ion transport pathways in fetal colonies and metabolic enzymes in adult host correspond to meaningful functional physiological changes. We can do so using a variety of techniques, the most obvious being Western blot to assess total protein levels, as well as immunofluorescence (IF) and immunohistochemistry (IHC) to identify the exact cellular localization of relevant proteins.

We went on to examine significant DEGs and enriched IPA molecules to assess feasibility of targets for these validation techniques. Our goal was to identify proteins that were significantly different between our fetal colony and adult host tissue with a substantial enough fold change to suggest there would be a detectable protein level difference, which also were flagged as being relevant core components or downstream targets of enriched GO pathways and activated IPA upstream regulators and canonical pathways, and which had available antibodies for techniques like Western blotting and IF/IHC with rat tissue reactivity. We identified several compelling potential targets including calcium and potassium channels (CACNA1B, KCNJ12), sodium/phosphate contransporters (SLC34A3), transmembrane channel proteins (TMC7), and signaling receptor binding proteins (WNT3A). Upon literature review, all of these proteins were found to have relevance in cancer and general cell proliferation, implying important roles in cellular metabolism and growth. Interestingly, many of these specific genes and pathways were not found to be significantly elevated in pre-transplant fetal hepatocytes, indicating potential distinct activation in the fetal cells after transplantation into the adult host microenvironment. Alternatively, the sheer number of significant pre-transplant DEGs may be masking these genes if they are not as significantly expressed in a pre-transplantation context.

While we have not observed tumor development in any of our rat transplant studies following the 10 month length of the prior experiments, the relevance of some of these pathways in cancer also prompts us to explore potential biomarkers of cancer. These include markers for

double-strand breaks such as γ-H2AX, as well as potential early makers of hepatocellular carcinoma, such as heat shock proteins HSP70 and HSP27. [6] We will also be probing for broader metabolic markers, as well as markers of cell proliferation and cell cycle entry in both tumor and normal cells such as Ki-67 and PCNA.

Methyltransferase and polycomb repressive complex expression

Trimethylation of histone 3 lysine 27 (H3K27me3) is associated with repressive marks of gene transcription and has significantly higher abundance in our adult cells and host, while monomethylation of this same mark (H3K27me1) is associated with active transcription at highly transcribed gene bodies and has significantly higher abundance in our fetal cells and colonies. Methylation of H3K27 is carried out by polycolmb group repressive complex 2 (PRC2) primarily via its methyltransferase subunit Enhancer of Zeste Homolog 2 (EZH2) and to a lesser degree its paralog EZH1. [7,8] This activity is critical in the differentiation of embryonic stem cells (ESCs) to adult cells by its repression of stem-like marks to maintain cell identity. Conversely, deregulation of EZH2 in cancer can lead to repression of tumor-suppressive marks and result in promoted tumor growth, [9] highlighting an important pleiotropic effect in different contexts. In a study of H3K27 during hepatic differentiation, it was found that inhibition of EZH2 caused upregulation of hepatic markers and downregulated cell cycle inhibitors, while the inhibition of H3K27 demethylases JMJD3 and UTX conversely decreased hepatic markers and induced proliferation. [10] One caveat is that the bulk of this work was performed on HepaRG cells, which is a human hepatoma-derived cell line, and the authors limited their verification of results in cultured primary hepatocytes to measuring levels of albumin and CyP3A4.

In our post-transplant LCM RNA-Seq dataset, we found that expression of both EZH1 and EZH2 mRNA are very slightly lower in fetal colonies than adult host but without any statistical significance (EZH1 logFC = −0.013, FDR = 0.976; EZH2 logFC = −0.073, FDR = 0.879). Since significant expression of the methyltransferases themselves was not detected, we

ran our RNA-Seq data through gene set enrichment analysis (GSEA). GSEA is a computational method developed by UC San Diego and the Broad Institute which can be used to compare two biological states against a predefined gene set to detect statistically significant differences. [11,12] We utilized an available gene set for PRC2 targets identified by ChIP-on-chip analysis of ESCs. [13] The enrichment plot (Figure 2) shows that polycomb-regulated gene expression is heavily weighted towards fetal colonies (enrichment score = 0.54525995, normalized enrichment score = 2.0435662), indicating relaxed repression of target genes by PRC2 in the fetal colonies, and reinforcing our hPTM data showing a higher abundance of H3K27me3 and H3K36me1 in adult host and hepatocytes. The top 15 enriched genes from the leading edge subset prominently feature ion channels (CACNA1B, KCNQ3, CACNA1E), carriers (SLC6A1, SLC24A4, SLC6A5), and receptors (ROBO3, GRIK1). This suggests that the ion transport phenotype we observed in the fetal colonies may relate to a retained proliferative signature reminiscent of attributes of stem or progenitor cells. We can confirm the activation of polycomb targets in our samples by using antibodies for common sets such as the Polycomb Group or Polycomb Group 2 Antibody Kits by Cell Signaling Technologies (CST #9788 and #62083). Exploring additional markers of stem-like pathways can help confirm phenotypic markers of stemness phenotypes in 10-month post-transplant fetal-derived hepatocyte colonies.

CUT&Tag on significant fetal hPTM marks

In our post-transplant fetal HCT epigenomic data, we found 13 significant hPTMs that were differentially abundant between adult and all 3 populations of fetal hepatocytes, as well as adult host and fetal derived colonies (Figure 3A). Along with our transcriptomic results, the 11 that had a consistent abundant pattern pre- to post-transplantation supported our hypothesis that aspects of the fetal phenotype are retained in fetal-derived colonies following transplantation into the adult host microenvironment. We are planning a follow-up study to integrate our epigenomic and transcriptomic results by determining what genes are being

regulated by which hPTMs. This can be performed by chromatin immunoprecipitation sequencing (ChIP-Seq), where an antibody against a protein of interest, such as an hPTM, is used to pull down fragmented genomic DNA and sequence surrounding DNA. [14] CUT&Tag is a more recent evolution of this technique which simplifies the sample preparation protocol and is ideal for high-quality results from small sample quantities, such as our LCM tissue. [15] Similar to ChIP-Seq, an antibody is bound against a histone target. However, in CUT&Tag, pA-Tn5 transposase is tethered at the site, which generates DNA fragments with simultaneous ligation of next-gen sequencing adapters. This leads to an efficient generation of sequencing libraries.

As discussed previously, H3K27 mono-, di-, and trimethylation has important implications for gene transcription, cell identity, and stemness. Given that all 3 of these PTMs are significantly differentially abundant pre- and post-transplant, they present obvious targets of interest to understand the regulation of gene expression in fetal and adult hepatocytes. While validated antibodies exist for H3K27 monomethylation and trimethylation, H3K27 dimethylation antibodies have problematic cross-reactivity with trimethylation, disfavoring its use in our initial experiments. We hope that probing the genes associated with the fetal-associated H3K27 monomethylation and the adult-associated H3K27 trimethylation will provide insight into critical pathways core to the long-term fetal proliferative advantage. Another significant mark with higher abundance in fetal cells and colonies is H3K26me3, which has a known oppositional relationship with H3K27me3. These two marks help regulate and restrict each other throughout the genome, engaging in boundary-setting. [16] As a result, this histone may provide additional context for how H3K27me3 is restricted on the genomic landscape of fetal cells and colonies.

When looking into activated targets in our transcriptomic dataset for follow-up tissue localization confirmation studies via WB, IHC, IF, and ISH, we observed that many of the most significantly enriched ion transport genes post-transplant did not seem to be consistently activated in pre-transplant fetal cells compared to adult host tissue. To address the possibility

that the gene expression differences we observe are due to epigenetic regulation specific to the post-transplant population, and not the 11 marks shared pre- and post-transplant, we also looked for hPTMs that were significant only after transplant by compiling hPTMs that had a significant difference (FDR < 0.05) between colony and host, but no significance (FDR > 0.05) between adult hepatocytes and any of the pre-transplant fetal hepatocyte groups (Figure 3B).

Most of the histone marks resulting from this analysis were not remarkable. Unlike the 13 hPTMs significant between all groups, the 15 marks that were significant post-transplant but not significant in at least one pre-transplant comparison had generally low average percent relative abundance differences (< 4%) between the host and colony groups, with the exception of H3.1 K36me2, which was expressed 13.81% higher in the fetal colonies. However, the other isoform of this same mark (H3.3 K36me2) was one of the 13 significantly abundant in all groups. As antibodies for PTM pulldown assays do not distinguish based on histone protein isoform, any follow-up experiments outlined above, including CUT&Tag, will probe for this hPTM as well.

Transplantation clinical trial with NMP livers

Our work in Chapters 3 and 4 determined that insufficient autophagy and overactive apoptosis may be an important driver in ischemia reperfusion injury (IRI) of donor livers. Livers unable to restore homeostasis after IRI may fall into a cyclical state of inflammation and injury, ultimately rendering the liver nonfunctional. While NMP may be able to more optimally preserve and even rehabilitate some donor organs prior to transplantation, previous work and our study in Chapter 4 also indicate that pan-caspase inhibition may help this process by minimizing inflammatory injury driven by apoptosis and/or pyroptosis, leading to better functional metrics. [17]

Additional improvements to rehabilitation may be seen by identifying specific caspases driving nonfunctional phenotypes and targeting those for inhibition during NMP rather than using pan-caspase inhibition. This could be accomplished by finding existing inflammasome inhibitors that achieve similar physiological results as emricasan but which may minimize off-target effects

of pan-caspase inhibition. [18,19] Going forward, it will be important to integrate the NMP protocol used in our Chapter 3 and 4 studies, which is optimized to improve hepatocellular activity, with protocols designed to also rehabilitate other liver cell types, such as cholangiocytes. One such protocol involves a sequential dual hypothermic oxygenated machine perfusion (DHOPE), controlled oxygenated rewarming (COR), and finally NMP to improve not only hepatic function but also biliary and mitochondrial activity. [20] Now that NMP devices have clinical approval, [21] a next logical step in our research is to carry through rehabilitated human livers into a transplantation clinical trial, in order to confirm that our observations from perfusate proteomic analysis and transcriptional analysis do correlate to improved clinical outcomes.

Materials and Methods

The data described in this chapter were obtained using the same methods implemented in Chapters 2, 3, and 4, with the exception of total proteomic analysis and GSEA.

Proteomic methods

We thank the IDeA National Resource for Quantitative Proteomics, which is supported by National Institutes of Health Grant Nos. R24GM137786, P20GM121293, and S10OD026736, for their valuable input and for processing our samples. We collected 5 samples of stained paired LCM adult rat liver tissue sections, each approximately 10 mm^2 in area. These were spun into 20 µL of PBS and frozen at −70°C prior to analysis.

Protocol for FASP bHPLC TMT on Orbitrap Eclipse: Purified proteins were reduced, alkylated, and digested using filter-aided sample preparation. [22] Tryptic peptides were labeled using tandem mass tag isobaric labeling reagents (Thermo) following the manufacturer's instructions and combined into two multiplex sample groups with a common reference sample. The labeled peptide multiplexes were separated into 46 fractions on a 100 x 1.0 mm Acquity BEH C18 column (Waters) using an UltiMate 3000 UHPLC system (Thermo) with a 50 min gradient from 99:1 to 60:40 buffer A:B ratio under basic pH conditions, and then consolidated into 18 super-fractions. Each super-fraction was then further separated by reverse phase XSelect CSH C18 2.5 um resin (Waters) on an in-line 150 x 0.075 mm column using an UltiMate 3000 RSLCnano system (Thermo). Peptides were eluted using a 75 min gradient from 98:2 to 60:40 buffer A:B ratio. Eluted peptides were ionized by electrospray (2.2 kV) followed by mass spectrometric analysis on an Orbitrap Eclipse Tribrid mass spectrometer (Thermo) using multi-notch MS3 parameters. MS data were acquired using the FTMS analyzer in top-speed profile mode at a resolution of 120,000 over a range of 375 to 1500 m/z. Following CID activation with normalized collision energy of 35.0, MS/MS data were acquired using the ion trap analyzer in centroid mode and normal mass range. Using synchronous precursor selection, up to 10

MS/MS precursors were selected for HCD activation with normalized collision energy of 65.0, followed by acquisition of MS3 reporter ion data using the FTMS analyzer in profile mode at a resolution of 50,000 over a range of 100-500 m/z. Buffer A = 0.1% formic acid, 0.5% acetonitrile. Buffer B = 0.1% formic acid, 99.9% acetonitrile. Both buffers adjusted to pH 10 with ammonium hydroxide for offline separation.

For data analysis, protein exclusive intensity values were assessed for quality using the in-house ProteiNorm app, a user-friendly tool for a systematic evaluation of normalization methods, imputation of missing values and comparisons of different differential abundance methods. [23] Popular normalization methods were evaluated including log2 normalization (Log2), median normalization (Median), mean normalization (Mean), variance stabilizing normalization (VSN), [24] quantile normalization (Quantile), [25] cyclic loess normalization (Cyclic Loess), [26] global robust linear regression normalization (RLR), [27] and global intensity normalization (Global Intensity). [27] The individual performance of each method was evaluated by comparing the following metrices: total intensity, Pooled intragroup Coefficient of Variation (PCV), Pooled intragroup Median Absolute Deviation (PMAD), Pooled intragroup estimate of variance (PEV), intragroup correlation, sample correlation heatmap (Pearson), and log2-ratio distributions. The data was normalized using Cyclic Loess and differential abundance analysis was performed using Linear Models for Microarray Data (limma) with empirical Bayes (eBayes) smoothing to the standard errors.

Gene set enrichment analysis

We acknowledge our use of the gene set enrichment analysis, GSEA software, and Molecular Signature Database (MSigDB). We utilized a published human gene set of Polycomb Repression Complex 2 (PRC) targets (standard name: BENPORATH_PRC2_TARGETS, systematic name: M8448).

Figures

A

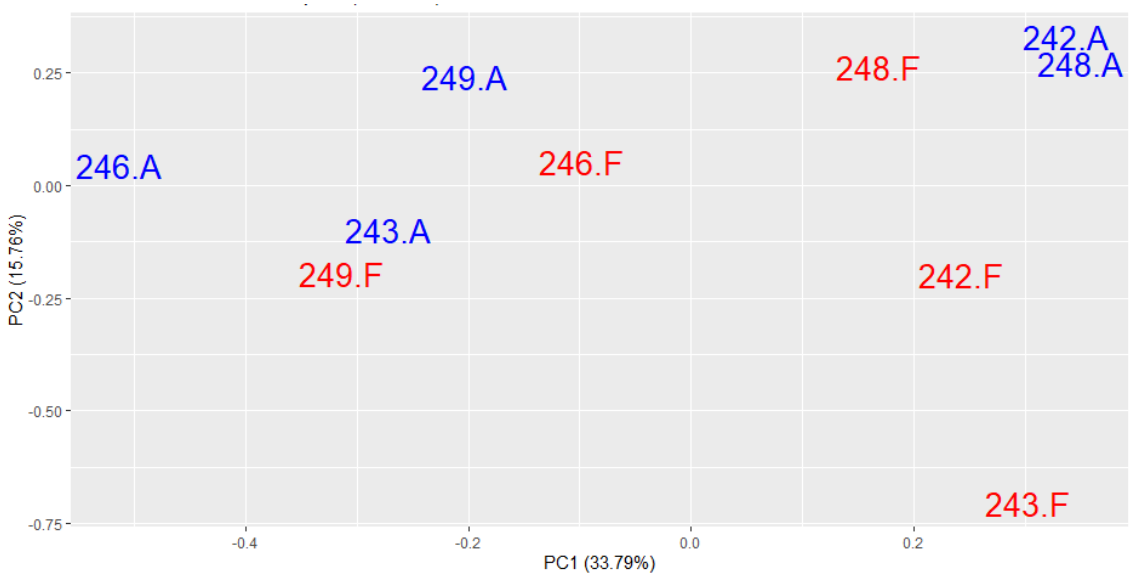
242.A
248.A
248.F
249.A
246.A
246.F
243.A
249.F
242.F
243.F
0.25
0.00
-0.25
-0.50
-0.75
PC2 (15.76%)
-0.4
-0.2
0.0
0.2
PC1 (33.79%)

B

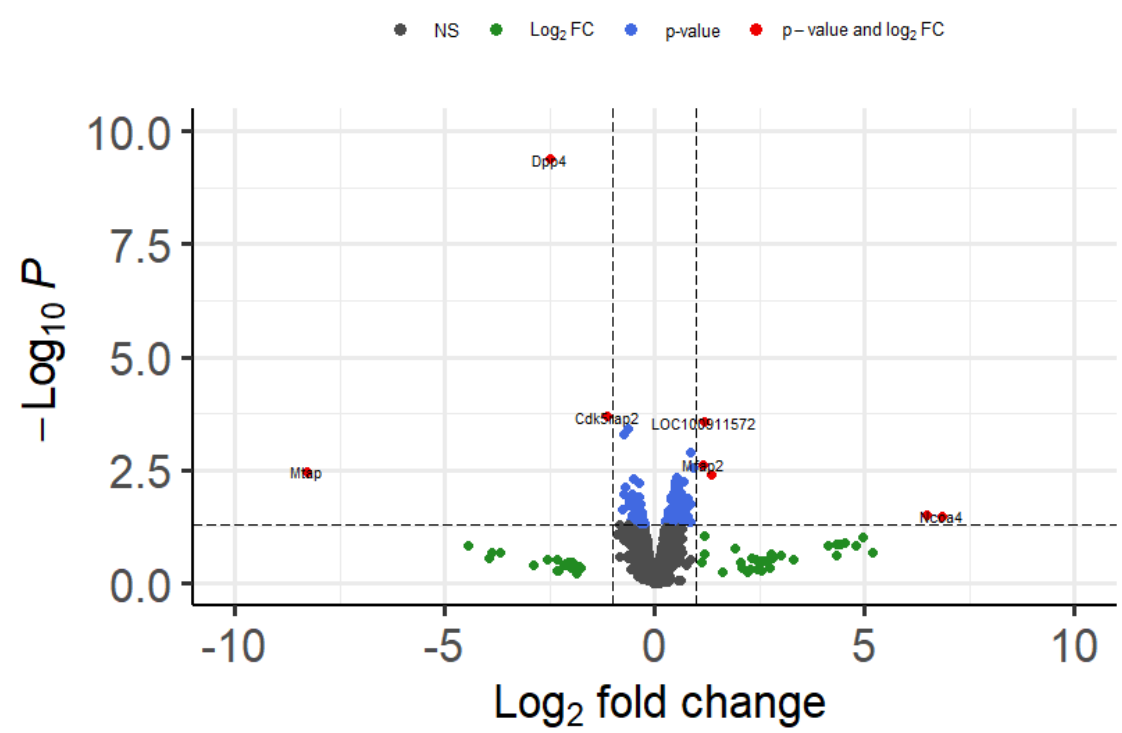
NS
Log2 FC
p-value
p – value and log2 FC
10.0
7.5
5.0
2.5
0.0
−Log10 P
Dpp4
Cdk5rap2
LOC100911572
Mtap2
Mtap
Ncoa4
-10
-5
0
5
10
Log2 fold change

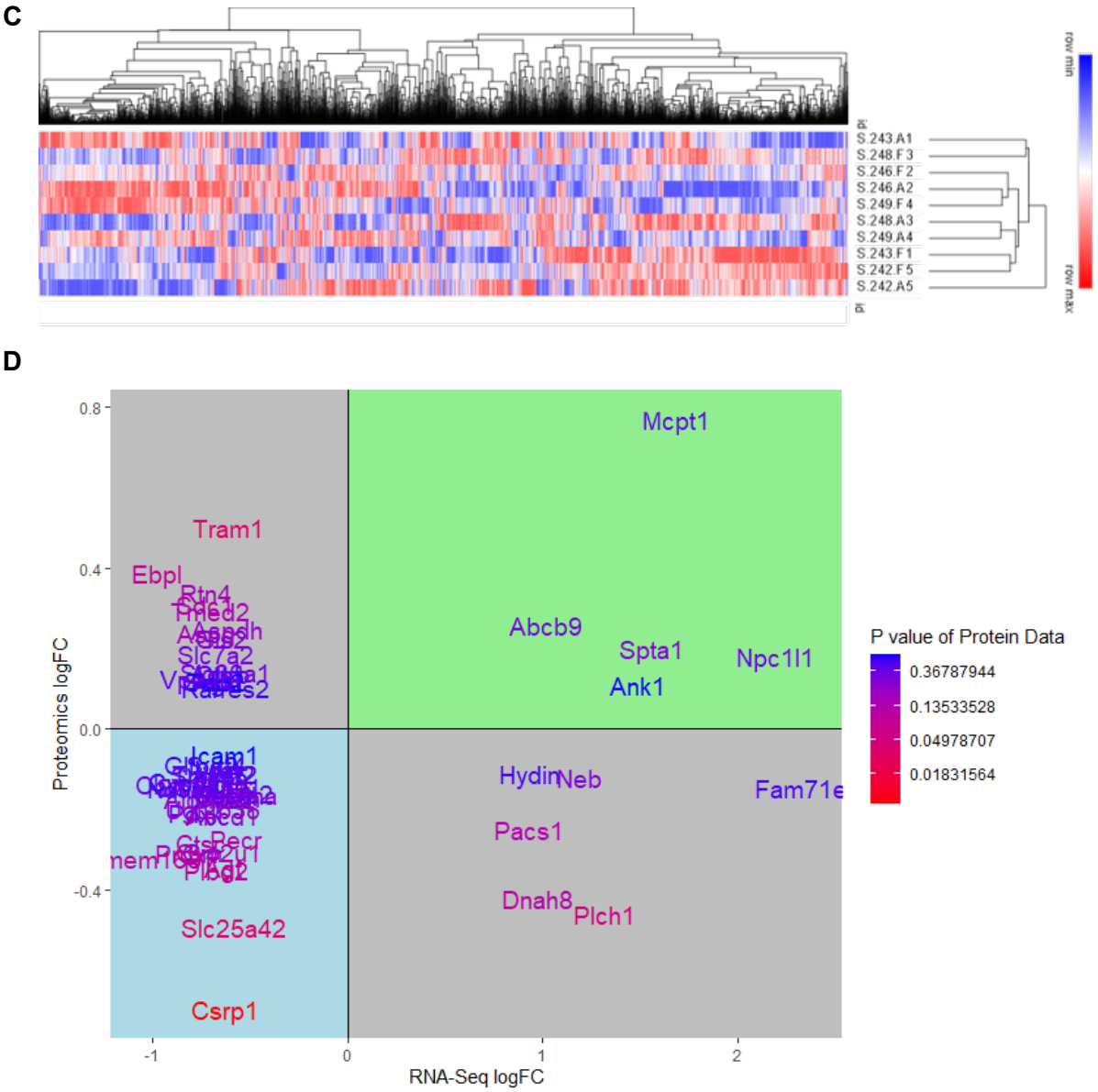

Figure 1. Exploration of TMT Proteomics Data in fetal HCT. **A)** PCA of fetal colony and paired adult host biological replicates show minimal segregation by sample type, with a slight trend towards fetal colony (red) samples on the lower right and adult host (green) on the upper left. **B)** Volcano plot of significantly different quantitated proteins between fetal colony and adult host shows few (9) proteins that are significant by non-adjusted *P* value ($P < 0.05$, horizontal dashed line) and with a logFC > 1 or logFC < −1 (vertical dashed lines). **C)** Clustered heatmap by Morpheus shows minimal clustering of samples by protein expression. **D)** 2D Annotation Enrichment map comparing significant (FDR < 0.05) RNA expression and paired non-significant (0.05 < FDR < 0.6) protein expression. Symbol color represents the *P* value of the protein expression. The green quadrant shows concordant upregulation of mRNA and protein expression, while the blue quadrant shows concordant downregulation. The gray quadrants are both anti-correlating.

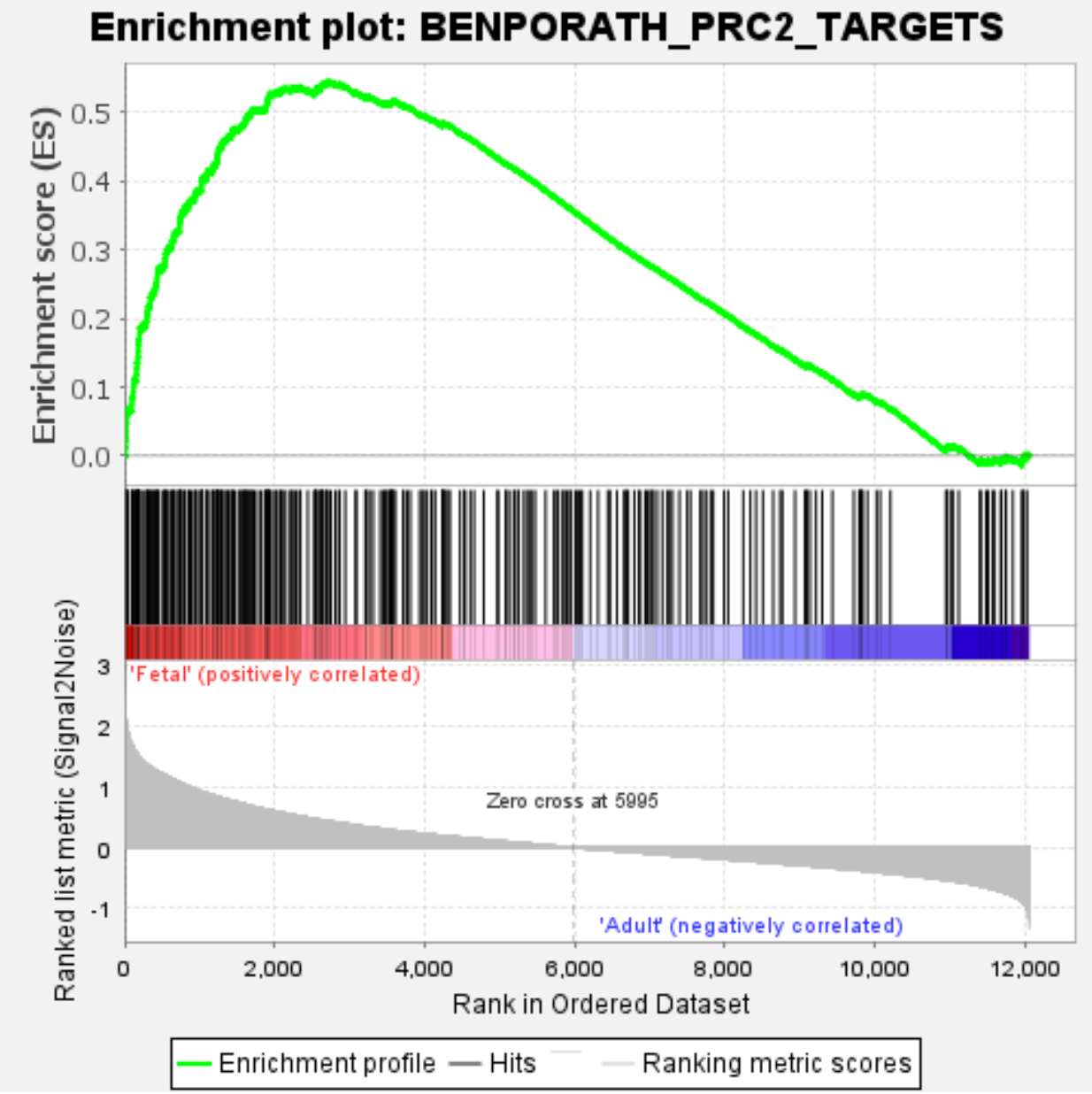

Figure 2. Gene Set Enrichment Analysis of PRC2 targets in fetal-derived colonies. Enrichment Score (ES) = 0.54525995, Normalized Enrichment Score (NES) = 2.0435662. Of the 135 enriched genes out of 289 total genes in the set, many of the top enriched genes prominently feature ion channels (CACNA1B, KCNQ3, CACNA1E), carriers (SLC6A1, SLC24A4, SLC6A5), and receptors (ROBO3, GRIK1). “Fetal” (in red) denotes fetal-derived colonies, while “Adult” (in blue) denotes Adult Host. Full details are available as Supplemental Table 5 on the Brown Digital Repository at: https://doi.org/10.26300/6ghh-jc29.

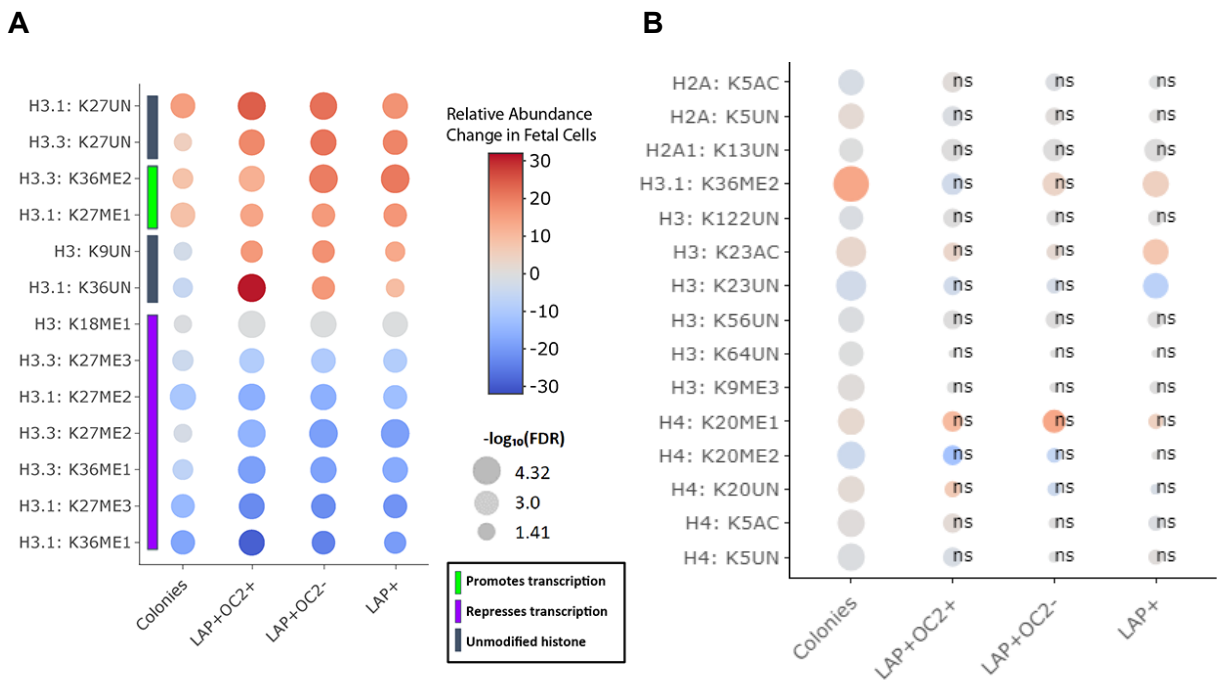

Figure 3. Potential hPTM targets for CUT&Tag follow-up study. **A)** 13 hPTMs that are significantly differentially abundant in pre- and post-transplant fetal/adult comparisons. **B)** 15 hPTMs that are significantly differentially abundant post-transplant but not significant in at least one pre-transplant population. Color scales denote relative change of hPTM abundance in the direction of the fetal element of the comparison. Dot sizes correspond to $-\log_{10}$ of the FDR for that hPTM. "ns" denotes non-significant marks.

References

1. Hegde PS, White IR, Debouck C. Interplay of transcriptomics and proteomics. *Curr Opin Biotechnol*. 2003;14(6):647-651. doi:10.1016/j.copbio.2003.10.006

2. Toby TK, Fornelli L, Kelleher NL. Progress in Top-Down Proteomics and the Analysis of Proteoforms. *Annu Rev Anal Chem (Palo Alto Calif)*. 2016;9(1):499. doi:10.1146/ANNUREV-ANCHEM-071015-041550

3. Wiśniewski JR, Zougman A, Nagaraj N, Mann M. Universal sample preparation method for proteome analysis. *Nature Methods 2009 6:5*. 2009;6(5):359-362. doi:10.1038/nmeth.1322

4. Thompson A, Schäfer J, Kuhn K, et al. Tandem Mass Tags: A Novel Quantification Strategy for Comparative Analysis of Complex Protein Mixtures by MS/MS. *Anal Chem*. 2003;75(8):1895-1904. doi:10.1021/AC0262560

5. Cox J, Mann M. 1D and 2D annotation enrichment: a statistical method integrating quantitative proteomics with complementary high-throughput data. *BMC Bioinformatics*. 2012;13 Suppl 1:S12. doi:10.1186/1471-2105-13-S16-S12

6. Tateishi R, Enooku K, Shiina S, Koike K. Tumor markers for hepatocellular carcinoma. *Mol Clin Oncol*. 2013;1(4):593. doi:10.3892/MCO.2013.119

7. Lavarone E, Barbieri CM, Pasini D. Dissecting the role of H3K27 acetylation and methylation in PRC2 mediated control of cellular identity. *Nature Communications 2019 10:1*. 2019;10(1):1-16. doi:10.1038/s41467-019-09624-w

8. Shen X, Liu Y, Hsu YJ, et al. EZH1 mediates methylation on histone H3 lysine 27 and complements EZH2 in maintaining stem cell identity and executing pluripotency. *Mol Cell*. 2008;32(4):491. doi:10.1016/J.MOLCEL.2008.10.016

9. Yoo KH, Hennighausen L. EZH2 Methyltransferase and H3K27 Methylation in Breast Cancer. *Int J Biol Sci*. 2012;8(1):59. doi:10.7150/IJBS.8.59

10. Pediconi N, Salerno D, Lupacchini L, et al. EZH2, JMJD3, and UTX epigenetically regulate hepatic plasticity inducing retro-differentiation and proliferation of liver cells. doi:10.1038/s41419-019-1755-2

11. Subramanian A, Tamayo P, Mootha VK, et al. Gene set enrichment analysis: A knowledge-based approach for interpreting genome-wide expression profiles. *Proc Natl Acad Sci U S A*. 2005;102(43):15545-15550. doi:10.1073/PNAS.0506580102/SUPPL_FILE/06580FIG7.JPG

12. Mootha VK, Lindgren CM, Eriksson KF, et al. PGC-1α-responsive genes involved in oxidative phosphorylation are coordinately downregulated in human diabetes. *Nat Genet*. 2003;34(3):267-273. doi:10.1038/ng1180

13. Ben-Porath I, Thomson MW, Carey VJ, et al. An embryonic stem cell-like gene expression signature in poorly differentiated aggressive human tumors. *Nat Genet*. 2008;40(5):499-507. doi:10.1038/NG.127

14. O'Geen H, Echipare L, Farnham PJ. Using ChIP-seq technology to generate high-resolution profiles of histone modifications. *Methods in Molecular Biology*. 2011;791:265-286. doi:10.1007/978-1-61779-316-5_20

15. Kaya-Okur HS, Wu SJ, Codomo CA, et al. CUT&Tag for efficient epigenomic profiling of small samples and single cells. *Nature Communications 2019 10:1*. 2019;10(1):1-10. doi:10.1038/s41467-019-09982-5

16. Yuan W, Xu M, Huang C, Liu N, Chen S, Zhu B. H3K36 methylation antagonizes PRC2-mediated H3K27 methylation. *Journal of Biological Chemistry*. 2011;286(10):7983-7989. doi:10.1074/jbc.M110.194027

17. Baskin-Bey ES, Washburn K, Feng S, et al. Clinical Trial of the Pan-Caspase Inhibitor, IDN-6556, in Human Liver Preservation Injury. *Am J Transplant*. 2007;7(1):218-225. doi:10.1111/j.1600-6143.2006.01595.x

18. Xu S, Li X, Liu Y, Xia Y, Chang R, Zhang C. Inflammasome inhibitors: promising therapeutic approaches against cancer. *Journal of Hematology & Oncology 2019 12:1*. 2019;12(1):1-13. doi:10.1186/S13045-019-0755-0

19. Dhani S, Zhao Y, Zhivotovsky B. A long way to go: caspase inhibitors in clinical use. *Cell Death & Disease 2021 12:10*. 2021;12(10):1-13. doi:10.1038/s41419-021-04240-3

20. de Vries Y, Matton APMM, Nijsten MWNN, et al. Pretransplant sequential hypo- and normothermic machine perfusion of suboptimal livers donated after circulatory death using a hemoglobin-based oxygen carrier perfusion solution. *Am J Transplant*. 2019;19(4):1202-1211. doi:10.1111/ajt.15228

21. Markmann JF, Abouljoud MS, Ghobrial RM, et al. Impact of Portable Normothermic Blood-Based Machine Perfusion on Outcomes of Liver Transplant: The OCS Liver PROTECT Randomized Clinical Trial. *JAMA Surg*. 2022;157(3):189. doi:10.1001/JAMASURG.2021.6781

22. Wiśniewski JR, Zougman A, Nagaraj N, Mann M. Universal sample preparation method for proteome analysis. *Nat Methods*. 2009;6(5):359-362. doi:10.1038/nmeth.1322

23. Graw S, Tang J, Zafar MK, et al. proteiNorm - A User-Friendly Tool for Normalization and Analysis of TMT and Label-Free Protein Quantification. *ACS Omega*. 2020;5(40):25625-25633. doi:10.1021/ACSOMEGA.0C02564/SUPPL_FILE/AO0C02564_SI_002.ZIP

24. Huber W, von Heydebreck A, Sültmann H, Poustka A, Vingron M. Variance stabilization applied to microarray data calibration and to the quantification of differential expression. *Bioinformatics*. 2002;18(suppl_1):S96-S104. doi:10.1093/BIOINFORMATICS/18.SUPPL_1.S96

25. Bolstad B. preprocessCore: A collection of pre-processing functions. Published online 2022. https://github.com/bmbolstad/preprocessCore

26. Ritchie ME, Phipson B, Wu D, et al. limma powers differential expression analyses for RNA-sequencing and microarray studies. *Nucleic Acids Res*. 2015;43(7):e47-e47. doi:10.1093/NAR/GKV007

27. Chawade A, Alexandersson E, Levander F. Normalyzer: A tool for rapid evaluation of normalization methods for omics data sets. *J Proteome Res*. 2014;13(6):3114-3120. doi:10.1021/PR401264N/SUPPL_FILE/PR401264N_SI_003.PDF

Appendix I:
Fetal Hepatocyte Transplantation Methods Development

Methods Development

During the fetal hepatocyte transplantation project in Chapter 2, we had to develop and optimize our methods to work with challenging samples. While the post-transplant liver tissue blocks were flash frozen in a hexane-acetone bath and stored at −80°C until cryosectioning, the dipeptidyl peptidase IV (DPPIV) stain and laser capture microdissection (LCM) process introduces several factors that presented obstacles in this project. Because the stain for DPPIV is an enzyme activity stain, the cryosectioned liver tissue must be first thawed to room temperature and then exposed to a stain solution for several minutes prior to LCM. Afterwards, the laser capture session is also performed at room temperature, and requires additional time to assess the slide, select the regions to cut, and then wait for the machine to capture the selected tissue onto a cap. In the process of capture, the tissue is exposed to both UV and IR lasers, in addition to ambient air. While this basic process was used previously in our lab to capture hepatocellular carcinoma samples for proteomic analysis, those were formalin fixed, paraffin embedded (FFPE) and therefore more stable. [1] Using that same protocol with the fresh frozen samples employed here, we found that we had to dynamically adjust our methods in response to issues arising during quality control (QC) validation.

We began by utilizing a similar protocol to the one previously employed, in which the tissue has an application of formalin applied to the slide following the DPPIV stain. This was used in order to stabilize the DPPIV stain onto the tissue, with the goal of preventing the stain from diffusing over time prior to and during LCM. We then isolated total RNA from one batch of captured tissue using a Qiagen kit optimized for FFPE samples, and also submitted identical tissue for mass spectrometry-based peptide quantitation with our collaborators at Northwestern University as done previously. However, initial QC checks for both nucleic acid and peptide workflows raised issues with sample integrity. Prior to attempting RNA-Seq, assessment by Bioanalyzer 2100 (Agilent Technologies, Inc.) resulted in low quality traces with undetectable

28S and 18S rRNA (Figure 1A) and a very low RNA integrity number (RIN) when compared to RNA from fresh liver tissue control (Figure 1B). In QC chromatograms for mass spectrometry, we similarly saw a trend of low signal and loss of detected peaks in samples from fixed tissue not seen in unfixed tissue (Figure 1C).

We attempted to move forward with RNA-Seq after minor boosts to sample QC metrics resulting from scaling up the amount of sample used for RNA isolation. Ultimately, standard polyadenosine (polyA) amplification library preparation was not successful. We hypothesize that the short formalin treatment process, combined with the heated incubations of the Qiagen FFPE kit, may have exacerbated the activity of RNases and thereby the degradation of RNA. Combined with the low amount of starting material, it is likely that the oligo(dT) primer used to amplify mRNA via its 3'-polyA tail could not bind to an intact tail fragment.

Other researchers have mitigated the deleterious effects of oxygen exposure to the tissue during LCM by rigging a stage to deliver an argon gas layer over the sample at all times. [2] However, as the LCM equipment we were using was in a shared core facility at Rhode Island Hospital, this was not a workable solution for us. We attempted to prevent the activity of RNases to the best of our ability using other methods. RNasin Ribonuclease Inhibitor (Promega Corporation) was spiked into our sodium phosphate buffer during thawing as well as into the stain solution, so the only time the sample was at room temperature but did not have RNase inhibitor applied was as soon as laser capture started. The stain time was reduced in half from 30 to 15 minutes, which was the minimum point where it still produced a clearly discernable stain during LCM. The formalin fixation step was omitted, and laser capture sessions were completed as quickly as possible. Samples were kept on dry ice until being thawed for staining, and caps were immediately placed into either 0.1 µL tubes containing Arcturus PicoPure Extraction Buffer to stabilize RNA, or frozen on dry ice for hPTM quantitation by MS.

After these protocol modifications to streamline the process and omit fixation, our quality control metrics improved dramatically for RNA (Figure 1E, 1F) and protein (Figure 1D). While we attempted to minimize the effect of degraded RNA and saw notable improvement in quality, we assumed that the stress the sample is exposed to resulted in some inevitable degradation. In an attempt to maximize our odds of sequencing success, we worked with GENEWIZ to run a pilot study using a low-input library prep kit that also utilized rRNA depletion instead of polyA amplification, which targets abundant rRNA and is more successful in enriching for mRNA in degraded total RNA. [3] Ultimately, these protocol modifications allowed for the successful use of fresh liver samples for both RNA-Seq and mass spectrometry despite the necessary stressors of the DPPIV stain and LCM process.

Following RNA-Seq, we also encountered the challenge of integrating sequencing data from two very distinct batches of samples. Isolated cells were collected in pellets of 1 million cells each and snap-frozen in liquid nitrogen prior to RNA isolation. These could easily be submitted for GENEWIZ's standard sequencing pipeline, which included polyA amplification library preparation. However, the special steps required for the processing of LCM tissue required rRNA depletion in library preparation of these lower quality samples. While both library preparation techniques enrich the mRNA population from total RNA and reduce the population of abundant rRNA, they do so using different underlying methods. While polyA amplification enriches for polyA+ mRNA by using an oligo(dT) primer, rRNA depletion utilizes techniques like hybridization capture or targeting of ribosomal cDNA in order to suppress this RNA population from the library. These techniques therefore result in distinct libraries with different artifacts; for instance, rRNA depletion retains expression of potentially interesting non-mRNA and non-rRNA species such as lncRNAs or polyA− histone transcripts, while also potentially including higher rates of intron read fragments. [4]

We explored options for bioinformatic batch correction to integrate these disparate types of RNA-Seq data, including MBatch by the MD Anderson Cancer Center, [5] as well as Kallisto by the Patcher Lab of Caltech. [6,7] Due to ease of integration with our existing count data, we settled on using a batch effect adjustment R package optimized for RNA-Seq data called ComBat-seq. [8] In a study designed to compare the outcomes of both library preparation techniques, human T cells were sequenced using both methods and then compared by PCA and clustering before and after the use of ComBat. [9] This technique resulted in the pairing of all 40 samples, demonstrating ComBat's ability to integrate RNA-Seq data generated from multiple library preparation techniques and correct for biases. While we considered redoing the cellular sequencing using rRNA depletion as well, we opted to take the approach of performing batch correction when doing limited comparisons between cellular and LCM data such as our PCAs on raw count data (Figure 2), while performing detailed analysis of expression data only from within the two batches, not between them. While rRNA depletion sequencing on the cellular samples may have somewhat reduced the scale of the batch effect, the intrinsic differences between the sets of samples (freshly isolated and frozen cells vs. frozen, thawed, stained, and refrozen liver), the use of different RNA isolation kits required by the LCM process, and the fact that the samples were sequenced in two different groups, made some degree of batch effect inevitable. By restricting our quantitative gene expression analysis to intragroup comparisons, we aimed to minimize the relevance of any present batch effect in normalizing and analyzing our sequencing data. This way, we were able to ensure that each sample group had a reasonable intragroup biological coefficient of variation (BCV) and did not have to apply corrections to our DE analysis based on the effect on BCV of intergroup comingling of count data.

We additionally had to discard one sample outlier for RNA-Seq from the LCM group. Samples for this study began collection just prior to the onset of the COVID-19 pandemic and

the resulting emergency shutdown of operations across institutions. As a result, one paired sample (rat # 246) was fully collected and stored at −80°C prior to the shutdown, while the other samples were collected months later after Brown University and Rhode Island Hospital reopening procedures had been finalized. While all samples were taken through sequencing, we noticed quickly that the paired samples from 246 resulted in read alignment errors on our computing cluster, differed in transcriptomic profile compared with the other samples by PCA and differential expression analysis, and had a noticeably blunted gene expression pattern (Figure 3). Including this sample adversely affected the signal of DEGs, and based on the suspected sample RNA degradation in storage, it was excluded from RNA-Seq analysis.

Figures

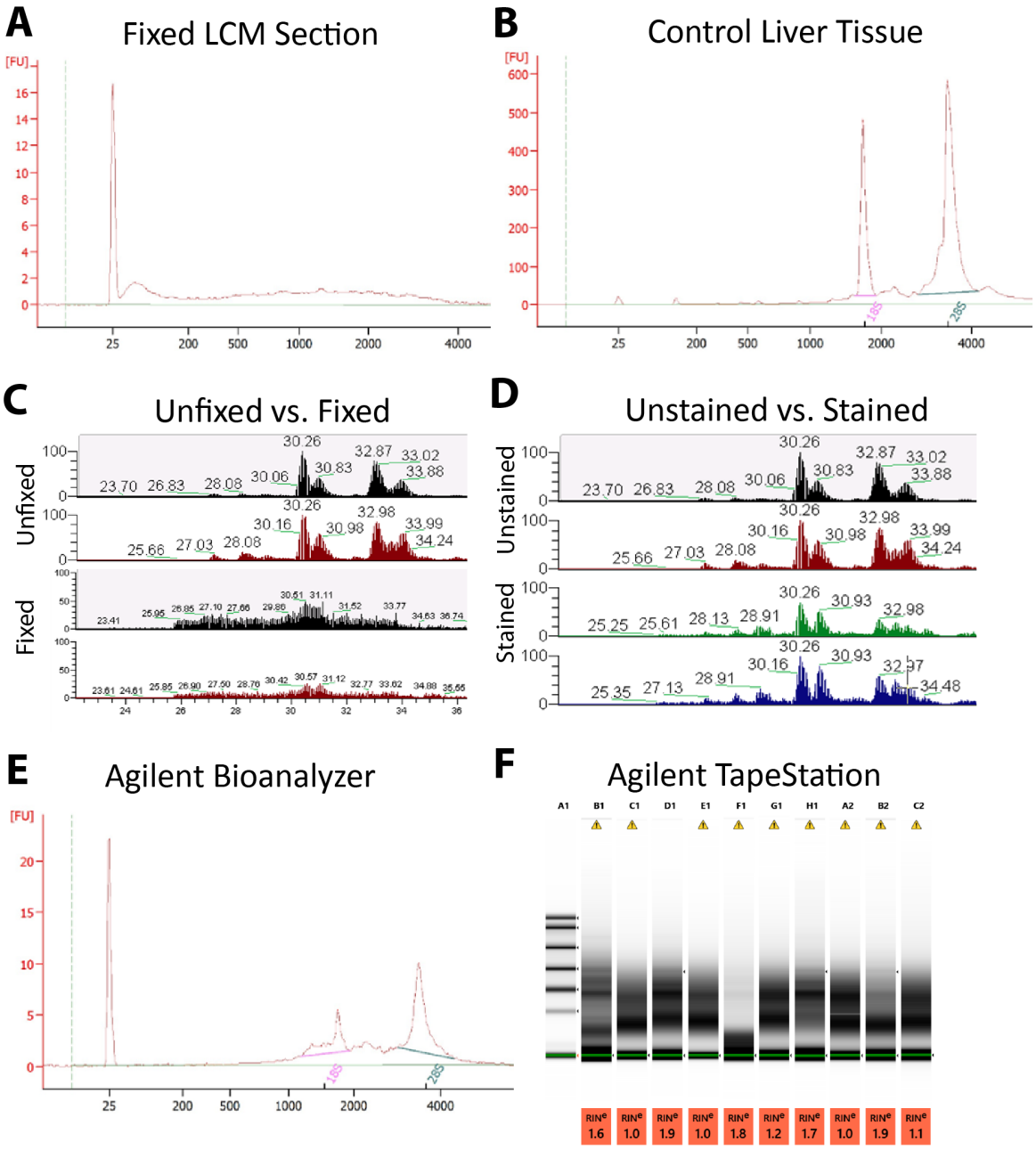

Figure 1. QC Agilent Bioanalyzer electrophoretic traces of total RNA from *A:* fixed LCM tissue and *B:* fresh unfixed liver tissue control. Fixed LCM tissue has lower fluorescence units (FU) and no detectable 18S or 28S rRNA peaks compared to fresh unfixed liver tissue. *C:* QC chromatograms for mass spectrometry for unfixed and fixed LCM tissue also show signal degradation correlating to fixation, while *D:* the effect of the DPPIV stain without fixation does not lead to similar sample loss. Stained but unfixed tissue also led to dramatically improved RNA quality as assessed by **E.** Agilent Bioanalyzer and **F.** low but consistent RNA Integrity Numbers on Agilent TapeStation that were usable with a library preparation kit designed for low-quality RNA.

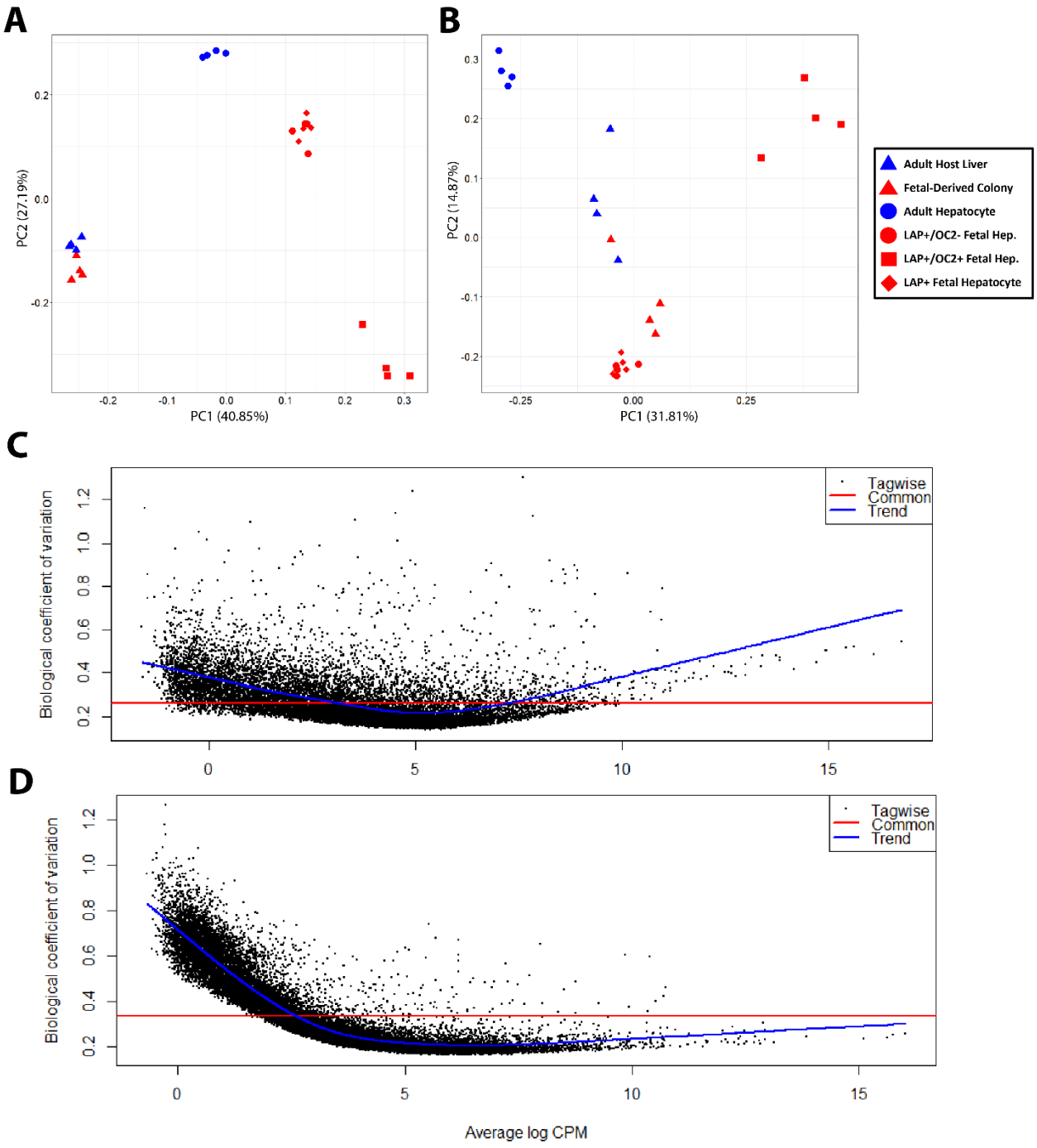

Figure 2. PCAs of combined cellular and LCM RNA-Seq data *A:* before and *B:* after ComBat-seq batch correction. Biological Coefficient of Variations (BCVs) were separately generated for the *C:* cellular and *D:* LCM count data. BCV plots measure the biological variation within a particular condition. Both the cellular and LCM data sets have a common dispersion between 0.2 and 0.4, which is usually considered reasonable to detect sufficient DE genes.

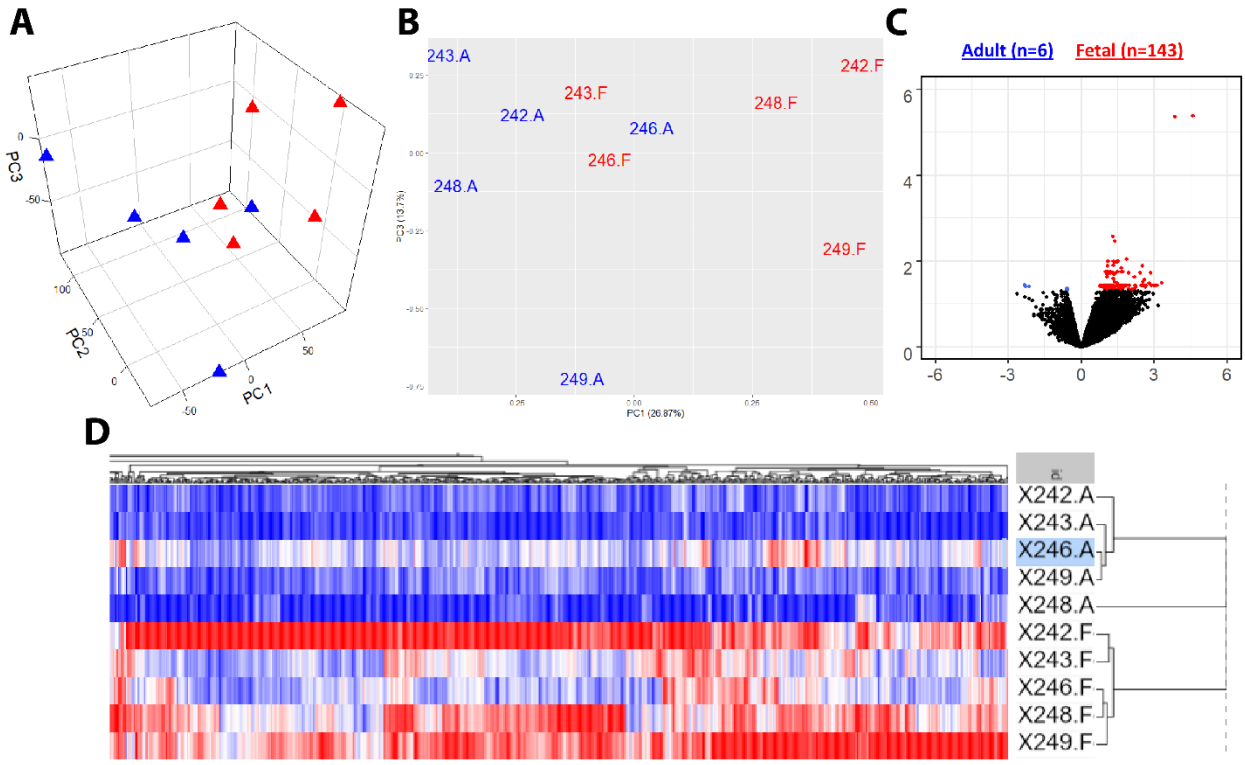

Figure 3. Quality Control metrics for excluding LCM biological replicate #256 (both the adult host and fetal-derived colony samples) from analysis. When PCA (*A:* 3D, PC1-3; and *B:* 2D, PC1 & PC3) was performed including sample 246, we see that replicate's host and colony components have with very little variation from each other compared to all other pairs, and the 246 host sample clusters with the colony samples. *C:* DE Analysis of samples including 246 show hundreds fewer DEGs than when 246 was excluded (Chapter 2, Figure 3A). *D:* A Morpheus heatmap of normalized counts of all LCM samples shows that the adult host component of rat 246 (highlighted with blue) shows a very different gene expression pattern than all other host samples, and the fetal-derived colony component of rat 246 is distinct from most other colony samples.

References

1. Michael AOAA, Ahsan N, Zabala V, et al. Proteomic analysis of laser capture microdissected focal lesions in a rat model of progenitor marker-positive hepatocellular carcinoma. *Oncotarget*. 2017;8(16):26041-26056. doi:10.18632/oncotarget.15219

2. Castro NP, Merchant AS, Saylor KL, Anver MR, Salomon DS, Golubeva YG. Adaptation of Laser microdissection technique for the study of a spontaneous metastatic mammary carcinoma mouse model by NanoString technologies. *PLoS One*. 2016;11(4). doi:10.1371/journal.pone.0153270

3. Schuierer S, Carbone W, Knehr J, et al. A comprehensive assessment of RNA-seq protocols for degraded and low-quantity samples. *BMC Genomics*. 2017;18(1):1-13. doi:10.1186/S12864-017-3827-Y/TABLES/1

4. Zhao S, Zhang Y, Gamini R, Zhang B, Von Schack D. Evaluation of two main RNA-seq approaches for gene quantification in clinical RNA sequencing: PolyA+ selection versus rRNA depletion. 2018;8(1):1-12. doi:10.1038/s41598-018-23226-4

5. MD Anderson Cancer Center. MD-Anderson-Bioinformatics/BatchEffectsPackage: The MBatch R package and Docker image are designed to help assess and correct for batch effects. Accessed October 12, 2022. https://github.com/MD-Anderson-Bioinformatics/BatchEffectsPackage

6. Bush SJ, McCulloch MEB, Summers KM, Hume DA, Clark EL. Integration of quantitated expression estimates from polyA-selected and rRNA-depleted RNA-seq libraries. *BMC Bioinformatics*. 2017;18(1):1-12. doi:10.1186/S12859-017-1714-9/FIGURES/6

7. Bray NL, Pimentel H, Melsted P, Pachter L. Near-optimal probabilistic RNA-seq quantification. *Nature Biotechnology 2016 34:5*. 2016;34(5):525-527. doi:10.1038/nbt.3519

8. Zhang Y, Parmigiani G, Johnson WE. ComBat-seq: batch effect adjustment for RNA-seq count data. *NAR Genom Bioinform*. 2020;2(3). doi:10.1093/NARGAB/LQAA078

9. Chen LL, Yang R, Kwan T, et al. Paired rRNA-depleted and polyA-selected RNA sequencing data and supporting multi-omics data from human T cells. *Scientific Data 2020 7:1*. 2020;7(1):1-7. doi:10.1038/s41597-020-00719-4